STRUCTURAL AND REACTIVITY RELATIONSHIPS IN ARYL- AND ALKYLAMINE BISPHOSPHINE COMPLEXES OF Tc(I) AND Re(I)

by

DUMISANI VINCENT KAMA

Submitted in fulfilment of the requirements in respect of the
Doctoral degree qualification

PHILOSOPHIAE DOCTOR

in the

DEPARTMENT OF CHEMISTRY

in the Faculty of

NATURAL AND AGRICULTURAL SCIENCES

at the

UNIVERSITY OF THE FREE STATE

Supervisor

Prof. Andreas Roodt

Co-Supervisor

Dr. Alice Brink

FEBRUARY 2018

Acknowledgements

First and foremost, none of this would have been possible without the Lord Almighty on my side. I believe with all my heart that the Lord planned all of this. There is no word in this planet that can describe how thankful I am Lord. From the bottom of my heart thank you!

Secondly, I would like to express my sincere gratitude to my supervisors Prof. André Roodt and Dr. Alice Brink for all the guidance, suggestions and the constant motivational talks provided throughout the course of this project. Without you none of this would have been possible.

I also would like to place on record, my sincere gratitude to Prof. Deon Visser, Dr. Marietjie Schutte-Smith, Dr. Johan Venter and Dr Truidie Venter for their constant encouragement and valuable guidance extended to me.

I wish to also express my sincere thanks to Prof. Roger Alberto, Dr. Henrik Braband and Angelo Frei for providing me with the opportunity to work and learn from them throughout the course of this project.

I owe a deep sense of gratitude to my colleagues. You were always available to assist with everything from the beginning of this journey. Rest assured your encouragement did no go unnoticed and is greatly appreciated.

To my friends, thank you for all the fun times, jokes, lab fights and the support. You are the best support system that one could ever ask for.

To the Kama family and my life partner Nthabiseng Mahloane, without your unconditional love and support none of this would have been possible. Thank you for standing by my side through all the tough times.

Financial assistance from The Swiss National Science Foundation (SNF) and the South African National Research Foundation (NRF) is here by also greatly acknowledged.

Table of Contents

TABLE OF CONTENTS

TABLE OF CONTENTS

TABLE OF CONTENTS

TABLE OF CONTENTS

Abbreviations

Label	Definition
α	Alpha
β	Beta
γ	Gamma
MeCN	Acetonitrile
CD_2Cl_2	Deuterated dichloromethane
PNP	Diphosphinoamine
PNPO	Diphosphinoamineoxide
PTA	1,3,5-triaza-7-phosphaadamantane
Å	Angstrom
δ	Chemical shift
ν	Stretching frequency on IR
°C	Degrees Celsius
π	pi
λ	Wavelength
°	Degrees
XRD	X-ray Diffraction
Å	Angstrom
ppm	Units of chemical shift (parts per million)
fac	Facial isomer
Hz	Hertz
s	seconds
T	Temperature
K	Kelvin
g	Gram
M	$Mol.dm^{-3}$
IR	Infrared spectroscopy
RMS	Root mean square

Label	Definition
$\theta_{N\text{-}sub}$	Effective Tolman-based N-substituent steric effect
k_{obs}	Observed *pseudo* first-order constant
K	Equilibrium constant
UV	Ultraviolet
NMR	Nuclear magnetic resonance
Vis	Visible
*p*Tol-PhPNP	*N*,*N*-Bis(diphenylphosphino)-*p*-toluidine
*p*ClPh-PhPNP	*N*,*N*-Bis(diphenylphosphino)-4-chloroaniline
*p*FPh-PhPNP	*N*,*N*-Bis(diphenylphosphino)-4-fluoroaniline
NBoc-PhPNP	*N*,*N*-Bis(diphenylphosphino)-*N*-Boc-ethylenediamine
5-*p*-tolyl-PNP	*N*,*N*-Bis(di-*p*-tolylphosphino)-*p*-toluidine
4-*p*-tolyl-o-tol	*N*,*N*-Bis(di-*p*-tolylphosphino)-*o*-toluidine
Cbutyl-4-*p*-tolyl	*N*,*N*-Bis(di-*p*-tolylphosphino)cyclobutylamine
Chzyl-4-*p*-tolyl	*N*,*N*-Bis(di-*p*-tolylphosphino)cyclohexylamine
*p*Tol-PhPNPO	*N*,*N*-Bis(diphenylphosphineoxide)-*p*-toluidine
*p*ClPh-PhPNPO	*N*,*N*-Bis(diphenylphosphineoxide)-4-chloroaniline
*p*FPh-PhPNPO	*N*,*N*-Bis(diphenylphosphineoxide)-4-fluoroaniline
NBoc-PhPNPO	*N*,*N*-Bis(diphenylphosphineoxide)-*N*-Boc-ethylenediamine
5-p-tolyl-PNPO	*N*,*N*-Bis(di-*p*-tolylphosphineoxide)-*p*-toluidine
4-p-tolyl-*o*-tol-PNPO	*N*,*N*-Bis(di-*p*-tolylphosphineoxide)-*o*-toluidine
Cbutyl-4-*p*-tolyl-PNPO	*N*,*N*-Bis(di-*p*-tolylphosphineoxide)cyclobutylamine
Chzyl-4-*p*-tolyl-PNPO	*N*,*N*-Bis(di-*p*-tolylphosphineoxide)cyclohexylamine

1 Introduction

What to expect!

A story! A grand tale of medicinal organometallic chemistry which includes the complex chemistry of group 7 metals in medicine and a list of aims & objectives which prompted this journey into the depth of radiopharmaceutical models.

1.1 Introduction

Medicinal organometallic chemistry is still considered by many as a very young and complex discipline in natural sciences, even though the use of metals in medicine can be traced back to ancient civilizations found in countries such as China and Egypt. This is partly because drug development in general is highly complex and a difficult task to accomplish, complicated further by the addition of metal ions.[1,2,3,4,5,6]

Common maladies where metals have been widely used as medicine since ancient times for either diagnostic or treatment purposes includes diseases such as cancer and arthritis,[2,7] with the former being one of the leading causes of mortality and morbidity worldwide. According to the World Health Organization (WHO), cancer related deaths in 2015 amounted to about 8.8 million

[1] Thompson, K. H., Orvig, C., *Science*, **2003**, *300*, 936-939.

[2] Magner, L. N., *A History of Medicine*. 2 Ed., Taylor & Francis: Boca Raton, **2005**.

[3] Sigel, A., Sigel, H., *Metal Ions in Biological Systems &Metal Ions in Life Sciences*. Vol 42., CRC Press, Netherlands, **2004**.

[4] Mjos, K. D., Orvig, C., *Chem. Rev.* **2014**, *114*, 4540−4563.

[5] Orvig, C., Abrams, M.J., *Chem. Rev.* **1999**, *99*, 2201-2204.

[6] King, R.B., *Encyclopedia of Inorganic Chemistry and Bioinorganic Chemistry*. 2 Ed., John Wiley & Sons Ltd.: **2011.**

[7] Davis, P., *Can. Fam. Physician.* **1988**, *34*, 445-452.

deaths making it the second leading cause of death globally.[8] To reduce this burden, cancer research studies suggests that this can be accomplished by avoiding risk factors such as unhealthy diet, tobacco use and alcohol abuse or by applying existing evidence-based prevention strategies such as the use of metal mediated radiopharmaceuticals. For the latter reason, the development of new pharmaceuticals that can accurately detect and eliminate cancer cells becomes crucial. More recently, development of metal mediated drugs has become the subject of medicinal research across different scientific disciplines.[4,5]

1.2 Metals in medicine

The use of transition metal complexes can have several advantages when compared to pure organic compounds. For one, it allows for unique chemical results which are sometimes unobtainable with pure organic or biological compounds. The transition metals contain empty *d*-orbitals of appropriate energies required for bond formation between the metal and the ligand (*i.e.* organic or biological compounds).[9] Secondly, most of them are known to be low-valent agents and thus in many cases kinetically inert and therefore will usually not act as oxidants themselves. Thirdly, due to the relatively strong bonds between the metal and the ligand(s), alterations on the periphery of the ligand are sometimes possible which can in most cases be done while keeping the metal and original ligand intact.[10] Finally, when using radioactive metals such as $^{99m}Tc^{I}$, metal-specific reactions starts to play a significant role and this provides an added advantage over pure organic compounds.[11] Various organometallic compounds such as Arsphenamine®, Cardiolite® and Cisplatin® (**Figure 1**) not only indicate the importance of organometallic chemistry in medicinal research but also highlights the significance of interdisciplinary research within the natural sciences.[12,13] These organometallic complexes are used for treatment of syphilis (Arsphenamine®),[12] detection of coronary artery diseases

[8] GBD-2015-Risk-Factors-Collaborators, *Lancet.* **2016**, *388*, 1659-1724.

[9] Cotton F.A., W., G., Murillo, C., Bochmann, M., *Advanced Inorganic Chemistry*. 6 Ed., John Wiley & Sons, INC: USA, **1999**.

[10] Mundwiler, S., Kündig, M., Ortner, K., Alberto, R., *Dalton Trans.* **2004**, 1320-1328.

[11] Zeglis, B. M., Houghton, J. L., Evans, M. J., Viola-Villegas, N., Lewis, J. S., *Inorg. Chem.*, **2014**, *53*, 1880-99.

[12] Jaouen, G., Metzler-Nolte, N., *Medicinal Organometallic Chemistry*. Springer-Verlag Berlin Heidelberg, **2010**.

[13] Lippert, B., *Cisplatin: Chemistry and Biochemistry of a Leading Anticancer Drug*. Ed., Helv Chim Acta. Wiley-VCH Zürich, **1999**.

(Cardiolite®)[12,14] and for treatment of various types of cancers such as testicular, ovarian, and cervical cancers (Cisplatin®).[15]

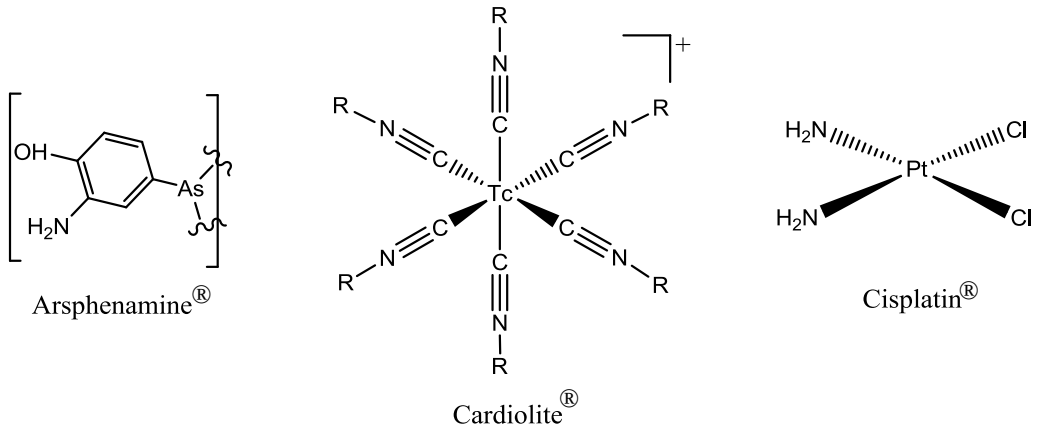

Figure 1 Selected organometallic complexes with biological functions: Cisplatin®, Cardiolite® [R = $CH_2C(CH_3)_2OCH_3$] and Arsphenamine® (also known as Compound no.606).[12]

Other organometallic compounds with biological functions of importance include compounds such as Vitamin B_{12} for treatment of Vitamin B_{12} deficiency anaemia (pernicious anaemia),[6] Auranofin for treatment of rheumatoid arthritis[14] and bismuth subsalicylate for treatment of helicobacter pylori infections.[6] Despite the widespread use of metal ions in drug development, the bio-coordination chemistry for most of these organometallic compounds is still poorly understood. Hence selective drug delivery to targeted organs remains poor, leading to various side-effects.[12,16,17]

1.3 Radiopharmaceuticals

Radiopharmaceuticals are essentially drugs containing radioactive nuclides used as therapeutic and/ or diagnostic agents in nuclear medicine. The development of radiolabelled drugs can be predominantly traced back to the early 19th century when metals such as radium and thorium

[14] Roat-Malone, R. M., *Bioinorganic Chemistry: A Short Course*. John Wiley & Sons, Inc: Hoboken, New Jersey, **2002**, 292-300.

[15] Gottlieb, R., *Can. Med. Assoc. J.* **1932**, *27*, 356-360.

[16] Schaefer, C., Peters, P., Miller, R.K., *Drugs During Pregnancy and Lactation: Treatment options and risk assessment*. 2 Ed., Academic Press, London, **2007**.

[17] Lee, S. P., *Scand. J. Gastroenterol. Suppl.* **1991**, *185*, 1-6.

were used for treatment of various cancer diseases.[15,18] For the past few decades, the number of mortalities caused by cancer has been growing significantly and this led to an increase in a number of cancer related research thrusts, both industrially and academically, to help eradicate this problem.

Recently, extensive studies in medicinal organometallic chemistry, particularly in the field of radiopharmaceuticals have been directed towards increasing the selectivity and effectiveness, while minimizing the side-effects.[19,20] These studies may not only lead to novel therapeutic and diagnostic approaches, but will contribute greatly to the understanding of biological processes. Investigations have been directed towards finding bi- and tridentate chelators with specific electron and steric capabilities to induce appropriate properties for targeting specific organs.[19] Different aspects of organometallic chemistry in aqueous solutions such as the stability and the environmentally friendly reaction medium have also attracted considerable interest throughout the years, particularly in the fields of catalysis and drug design.[21,22,23] For an example, the aqueous tricarbonyl complexes of Group 7 transition elements (Mn, Tc and Re) received particular attention due to the high kinetic stability of the carbonyl ligands in the low-spin d^6 *fac*-$[M(CO)_3]^+$ (M = Mn, Tc or Re) core and the synthesis which is conducted in aqueous medium.[24,25]

Taking into consideration the aforementioned considerations, there has been an increasing interest in investigating the architecture possibility of bidentate diphosphinoamine ligands which can coordinate to ^{188}Re and ^{99m}Tc tricarbonyl complexes and is the central focus point of this

[18] Liniecki, J., Medicine after the Discovery of Radium. *Chemistry Int, IUPAC. Boston*, **2011**, 33, 36-37.

[19] Alberto, R., Pak, J. K., van Staveren, D., Mundwiler, S., Benny, P., *Biopolymers*, **2004**, *76*, 324-333.

[20] Spagnul, C., Alberto, R., Gasser, G., Ferrari, S., Pierroz, V., Bergamo, A., Gianferrara, T., Alessio, E., *J. Inorg. Biochem.* **2013**, *122*, 57-65.

[21] Gan, W., Fellay, C., Dyson, P. J., Laurenczy, G., *J. Coord. Chem.* **2010**, *63*, 2685-2694.

[22] Schubiger, P. A., Alberto, R., Smith, A., *Bioconjugate Chem.* **1996**, *7*, 165-179.

[23] Bahrmann, H.; Bach, H., *Phosphorus, Sulfur Silicon Relat. Elem.* **1987**, *30*, 611-614.

[24] Hoepping, A., Reisgys, M., Brust, P., Seifert, S., Spies, H., Alberto, R., Johannsen, B., *J. Med. Chem.* **1998**, *41*, 4423-4432.

[25] Frei, A., Sidler, D., Mokolokolo, P., Braband, H., Fox, T., Spingler, B., Roodt, A., Alberto, R., *Inorg Chem.* **2016**, *55*, 9352-9360.

study. More topics on the theory concerning this project will be thoroughly discussed in the following chapters.

1.4 Aim of this study

It is without a doubt that mono-, bi- and tri-dentate tertiary phosphine ligands have in the last few decades become widely utilized in organic, inorganic and organometallic chemistry. This is partly due to their ease to coordinate to various metal centers through their lone electron pairs, but most importantly it is due to their tunable steric and electronic properties.[26]

On the other hand, a considerable interest has been shown to the aqueous tricarbonyl complexes, particularly the *fac*-$[M(CO)_3]^+$ of group 7 metals (M = Mn, Tc, Re) due to their high kinetic stability and their labile H_2O/halide ligands for use in radiopharmaceuticals.[27] In most cases rhenium compounds stoichiometrically resemble their technetium counterparts, and studies have shown that some properties such as the size of the complex, the shape of the structure and the charge of the complex can be easily projected from one metal type to the other.[28] Since the *fac*-$[M(CO)_3]^+$ core readily accept ligands of different binding modes, one can coordinate various ligands including biomolecules directly onto the metal.[19]

Based on this, the aim of this study was to investigate various bidentate diphosphinoamine ligands as a potential chelator system for *fac*-$[M(CO)_3]^+$ (M = ^{99m}Tc, ^{99}Tc and Re) and evaluate both the free and the coordinated ligand properties such as steric, electronic and biological characteristics. Therefore, a significant part of this project was focused on the synthesis, characterization and biological evaluation of these ligands and complexes.

Specific objectives for this Ph.D. study on diphosphinoamine ligands can thus be summarized as follows:

- Synthesize various diphosphinoamine (PNP) ligands with systematically altered functionalities to study the effect of different electronic and steric properties on the solid

[26] Appleby, T., Woollins, J.D., *Coord. Chem. Rev.* **2002**, *235*, 121-140.

[27] Alberto, R., Schibli R., Waibel R., Abram U., Schubiger P.A., *Coord. Chem. Rev.* **1999**, *190*, 901-919.

[28] Jürgens, S., Herrmann, W. A., Kühn, F. E., *J. Organomet. Chem.* **2014**, *751*, 83-89.

and solution state as well as the biological activity of both the complexes and the free ligands.

- Synthesize PNP ligands with various functional groups such as –COOH and NH_2 to increase the water solubility and to ensure that complexation can be performed in physiologically favorable media.

- To synthesize complexes of the type *fac*-[$M(CO)_3$(L,L'-Bid)Br] (M = Re(I) or $^{99/99m}$Tc(I); L,L'-Bid = PNP). For technetium complexes, particular interest is to be given to PNP ligands which demonstrate a certain degree of water solubility.

- To characterize both the free and the coordinated ligands using various analytical techniques such as nuclear magnetic resonance (NMR) and infrared (IR) spectroscopy; more importantly to characterize complexes using single crystal X-ray diffraction spectroscopy.

- Determine the mechanism of formation and substitution reactions on *fac*-[$Re(CO)_3$(L,L'-Bid)Br] (L,L'-Bid = PNP) through NMR or UV/Vis kinetic studies. These studies should be very useful when determining the effects introduced by these complexes when performing *in vivo* evaluations.

- Perform preliminary biological evaluations with both the free and the Re(I) coordinated ligands and to correlate the results to the ligand steric and electronic properties.

In the following chapter, a brief overview of the theory related to this study, particularly in the field of radiopharmaceuticals will be presented, followed by the discussion of experimental results.

2 Literature overview related to this study

What to expect!

A critical overview on the discovery and development of medicinal organometallic chemistry, particularly in the field of radiopharmaceuticals. Followed by, a discussion on the fundamental ligand effects, kinetic data and current interesting developments of transition metals in medicine.

2.1 Introduction

Over the last five decades, significant interests in radiopharmaceutical development have involved the investigation of versatile metal cores and ligand systems using simple synthetic approaches. Since the 1980's, considerable interest has included group seven transition metals such as rhenium and technetium due to their nuclear properties and their rich coordination chemistry. A few valuable aspects of radiopharmaceutical developments relevant to this study will be presented in this chapter.

2.2 Radiopharmaceuticals

Radiopharmaceuticals are known medicinal formulations containing radioactive isotopes which are regularly used in nuclear medicine for diagnosis and/or therapeutic treatment of diseases. Photon emitters [gamma (γ) or positron (β^+)] are generally used for imaging (diagnostic), while short range particle emitters [alpha (α), beta (β^-) or Auger] are generally used as therapeutic agents. For imaging, the radiation is normally detected through a camera that uses techniques such as Single-Photon Emission Computed Tomography (SPECT) and Positron Emission Tomography (PET). [1,2,3,4] This radiation is normally short-lived due to rapid radioactive decay.

[1] King, R. B., *Encyclopedia of Inorganic Chemistry and Bioinorganic Chemistry*. 2nd Ed., John Wiley and Sons., **2011**.

[2] Srivastava, S. C., *Braz. Arch. Biol. Technol.* **2007**, *50*, 49-62.

[3] Milenic, E. D., Brady E. D., Brechbiel, M. W., *Nature Reviews.* **2004**, *3*, 488-498.

[4] Unak, P., *Braz. Arch. Biol. Technol.* **2002**, *45*, 97-110.

For therapeutic purposes on the other hand, emitted particles causes cell destruction over a set range. Some of the most common radioactive isotopes used as therapeutic and imaging agents are listed in **Table 1**.

Table 1 Some of the available therapeutic and diagnostic radionuclides used in nuclear medicine.[1,2,3,4]

Radionuclide	Emission	Half-life	E_{max}(MeV)	Therapy	Diagnosis
^{99m}Tc	γ	6.0 hours	0.141		✓
^{111}In	γ	2.8 days	0.245, 0.171		✓
^{68}Ga	γ,β	1.1 hours	0.511		✓
^{67}Ga	γ,β,Auger	3.3 days	0.185, 0.296, 0.388		✓
^{90}Y	β	2.7 days	2.28	✓	
^{131}I	γ,β	8.0 days	0.181	✓	✓
^{177}Lu	γ,β	6.7 days	0.208, 0.497	✓	
^{213}Bi	α	45.7 min	5.87	✓	
^{188}Re	γ,β	17.0 hours	0.137, 2.12	✓	✓
^{18}F	β	110 min	0.51		✓
^{153}Sm	γ,β	2.0 days	0.103, 0.81	✓	✓

Radiopharmaceuticals can be further classified based on their bio-distribution. Firstly, those whose bio-distribution is determined by their physical and chemical properties, while secondly, those whose bio-distributions are determined by their receptor binding capabilities or biological interactions. The second class is often referred to as target-specific radiopharmaceuticals.[5,6,7] These two classes of radiopharmaceuticals will be discussed and the radio-medicinal development of each which has occurred, by highlighting the chemistry of technetium followed by that of rhenium.

2.3 Technetium

2.3.1 A brief history of Technetium

Technetium falls within the transition metal category on the periodic table of elements and lies centrally therein with an atomic number of 43. When coordinated to ligands of different types, it

[5] Liu, S., Edwards, D. S., *Chem. Rev.* **1999**, *99*, 2235-2268.

[6] Jürgens, S., Herrmann, W. A., Kühn, F. E., *J. Organomet. Chem.* **2014**, *751*, 83-89.

[7] Morais, M., Paulo, A., Gano, L., Santos, I., Correia, J. D. G., *J. Organomet. Chem.* **2013**, *744*, 125-139.

can exist in a wide range of oxidation states ranging from -1 to 7 resulting in various coordination geometries.[1,7] The first technetium isotopes that were artificially produced by Perrier and Segrè through molybdenum activation with deuterons were ^{95}Tc and ^{97}Tc.[8] It is highly unlikely that anyone would have envisaged that this element will one day become one of the most significant elements in medicinal chemistry.[9] In 1938 Segrè and Seaborg discovered the first metastable radioactive isotope ^{99m}Tc, which is now one of the most widely used radioactive isotopes in diagnostic nuclear medicine. The versatile ^{99m}Tc has a short but physiological suitable half life ($t_{1/2}$= 6.0 hours) and emits readily detectable gamma rays with E_{max} = 141 keV.[8,9,10,11]

2.3.2 Technetium-99m: The Work-Horse

Often called the "work-horse" of radiopharmaceuticals, ^{99m}Tc is currently by far the most important radionuclide in diagnostic nuclear medicine, representing approximately 85% of clinical administered radiopharmaceuticals. The four paramount reasons why ^{99m}Tc is so successful are listed below:[1,5,6,9,5,12]

1. Half-life ($t_{1/2}$) = 6.0 hours: Ensures practical imaging intervals, allowing enough time for synthesis, purification and administration to patients, with minimal radiation exposure to the patients.
2. E_{max} (γ) = 141 keV: Presenting relatively low radiation dose but capable of penetrating tumor tissues. This energy is in the range of a required window (100 – 250 keV) of current gamma cameras.

[8] Hoffman, D. C., Ghiorso, A., Seaborg, G. T., *The Transuranium People: The Inside Story*. Imperial College Press, London., **2000**.

[9] Alberto, R., *New Organometallic Technetium Complexes for Radiopharmaceutical Imaging*, Springer-Verlag, Berlin, Heidelberg., **2005**.

[10] Icenhower, J. P., Qafoku, N. P., Zachara, J. M., Martin W. J., *Am. J. Sci.* **2010**, *310*, 721–752.

[11] Roat-Malone, R. M., *Bioinorganic Chemistry: A Short Course*. John Wiley and Sons, Hoboken, New Jersey., **2002**.

[12] Johannsen, B., Spies, H., *Isotopenpraxis*, **1988**, *24*, 449-454.

3. The low cost of $^{99}Mo/^{99m}Tc$ generator is advantageous as the cost of living has been increasing over the past few decades. Nowadays the cost of health facilities plays a major role in selection of diagnostic procedures.
4. The readily availability of the ^{99m}Tc generator as the inventors at the Brookhaven National Laboratories did not patent the generator. Therefore, a wide spectrum of companies is able to manufacture $^{99}Mo/^{99m}Tc$ generators.

Due to the above mentioned fact regarding the availability of ^{99m}Tc generators, the method used for producing ^{99m}Tc has been widely reported in literature. ^{99m}Tc is produced from ^{99}Mo as described in **Figure 1** by loading the ^{99}Mo in the form of molybdate $[^{99}MoO_4]^{2-}$ onto an alumina column and allowing it to decay to the meta-stable ^{99m}Tc in the form of pertechnetate $[^{99m}TcO_4]^-$, which is then eluted with ~0.15 M solution of saline from the generator to an "all-in-one-radiopharmaceutical-instant-kit" (**Figure 2**).[13] Nearly all of the available commercial kits in fact obey the "all-in-one" format, which utilize radiopharmaceuticals of significantly low concentrations ranging between 10^{-7} to 10^{-10} M. At the same time it ensures that the incubation at either room temperature or elevated temperatures occurs as fast as possible within a prescribed period of time and leads to a highly radio-chemically pure technetium imaging agent.

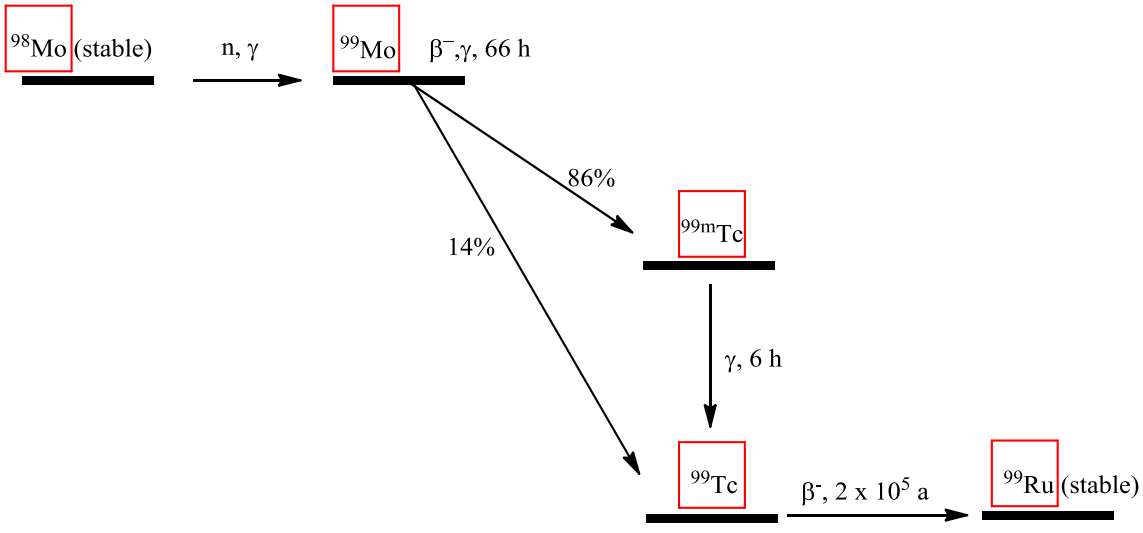

Figure 1 Production of ^{99m}Tc from the $^{99}Mo/^{99m}Tc$ generator, illustrating the decay of ^{99}Mo to ^{99m}Tc.[1,6]

[13] Jaouen, G., Metzler-Nolte, N., *Medicinal Organometallic Chemistry*. Springer-Verlag, Berlin, Heidelberg., **2010**.

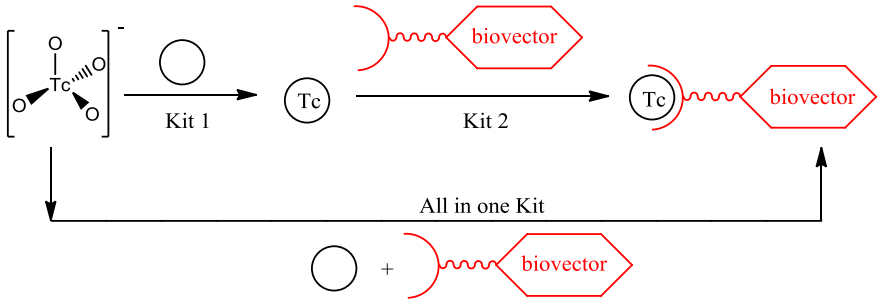

Figure 2 Schematic representation of the two strategies used in producing technetium-99m radiopharmaceuticals. The step below represents the favored "all-in-one" approach.[13]

2.3.3 Technetium-99m: 1st Generation

The first generations of radiopharmaceuticals were prepared via the "all-in-one-radiopharmaceutical-kit" with the permetallate being introduced directly before *in vivo* injections.[6] These radiopharmaceutical kits normally contained a ligand, buffer to control the pH, reducing agents (such as a Sn(II) salt), catalysts and stabilizers.[6,14] Generally, the ligand systems chosen, were on their own biologically inactive, hence they only acted as stabilizers of the metal centers and also aided in determining the biological distribution.[15,16] Most of the commercialized radiopharmaceuticals belong to the first generation of technetium radiopharmaceuticals. This generation led to compounds such as [$^{99m}TcO_4^-$] which was initially used for diagnosis of thyroid diseases but is now used as a source of ^{99m}Tc (e.g. as sodium pertechnetate) for new ^{99m}Tc radiopharmaceuticals.[1,17]

Three of the most widely utilized imaging agents are first generation technetium radiopharmaceuticals. The first complex, ^{99m}Tc-sestamibi (**Figure 3**) (i.e. Cardiolite®) is used as a diagnostic agent in myocardial imaging. It is believed that due to its d^6 configuration of its metal centre, this complex is highly stable towards its isonitrile ligand loss and or oxidation. The second complex, ^{99m}Tc-HMPAO (**Figure 3**) (i.e. Ceretec®) is used in cerebral blood flow

[14] Yang, W., Zhang, X., Wang, X., Tang, Z., *Nucl. Med. Biol.* **2010**, *37*, 710-711.

[15] Vallabhajosula, S., Zimmerman, R. E., Picard, M., Stritzke, P., Mena, I., Hellman, R. S., Tikofsky, R. S., Stabin, M. G., Morgan, R. A., Goldsmith, S. J., *J. Nucl. Med.* **1989**, *30*, 599-604.

[16] International-Atomic-Energy-Agency., *Technetium-99m radiopharmaceuticals: manufacture of kits*. Technical Reports Serieses, IAEAL: Vienna., **2008**.

[17] Braband, H., Benz, M., Tooyama, Y., Alberto, R., *Chem.Commun.* **2014**, *50*, 4126-4129.

imaging, while the third complex, ^{99m}Tc-MAG3 (**Figure 3**) (i.e. Technescan®) is used in renal clearing studies.[1,6]

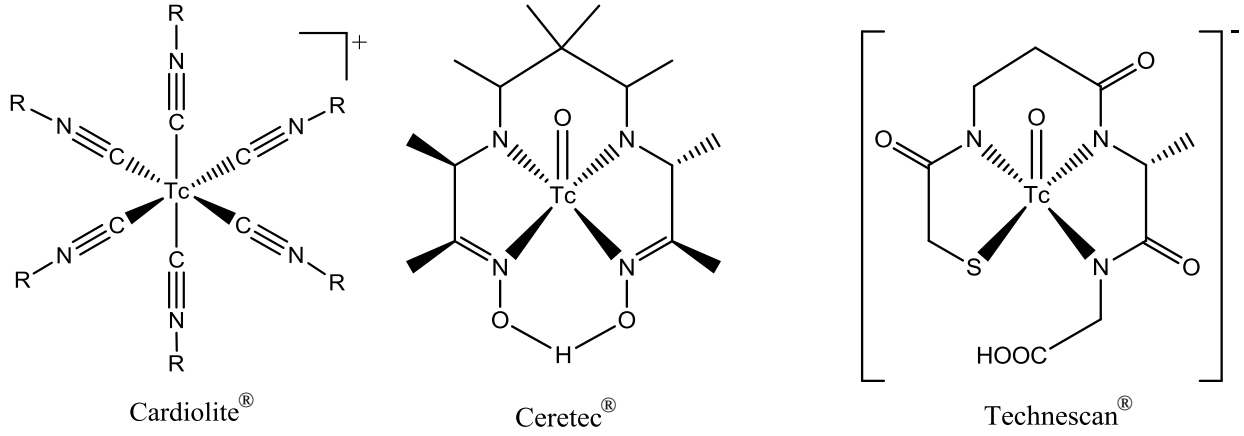

Figure 3 Some of the most widely applied first generation technetium-99m radiopharmaceuticals.[6]

The problem with this generation was that the majority of its complexes are perfusion agents and display no targeting functions; hence a window of opportunity for a new generation of complexes was highly critical.[1,6]

2.3.4 Technetium-99m: 2nd Generation - Bifunctional Approach

Unlike the first generation, the second generation of technetium radiopharmaceuticals are target specific and are derived from well designed synthetic approaches.[6] However, first generation radiopharmaceuticals can be utilized as precursors for second generation radiopharmaceuticals. One example would *e.g*. be to use the carboxylic acid group on the ^{99m}TcMAG3 (Technescan®, **Figure 3**) to further link biomolecules such as proteins, peptides or pharmacophores.[1,6] To ensure that they bind to a specific receptor, the second-generation radiopharmaceuticals are normally prepared via bifunctional chelators (see **Figure 4**).[7,18] The primary application of the bifuntional chelators are: Firstly to form a coordination complex with the radioactive precursor. These ligands are often addressed as a "metal chelator", and secondly, to create a link between the radioactive metal and the targeting vector as illustrated in **Figure 2**. For the past 10 to 15 years, several different macrocyclic and linear aminopolycarboxylic metal chelators have been employed as chelating ligands, with the most common ones shown in **Figure 4**.

[18] Correia, J. D. G., Paulo, A., Santos, I., *Curr. Radiopharm.* **2009**, *2*, 277 – 294.

1,4,7-Triazacyclononane-1,4,7-triacetic acid (NOTA), diethylenetriaminepentacetic acid (DTPA), tetraazamocycle derivative 3,6,10,13,15,18-hexaazabicyclo[6.6.4] octadecane (SAR) and 1,4,7,10-tetraazacyclododecane-1,4,7,10-tetraacetic acid (DOTA) are all part of a list of commonly used bifunctional chelators. These organic ligands are normally activated via common ligand activation methods.[1,6]

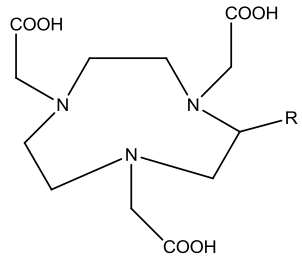

NOTA

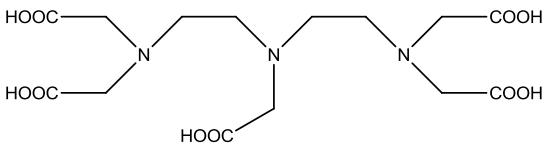

DTPA

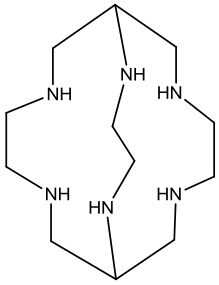

SAR

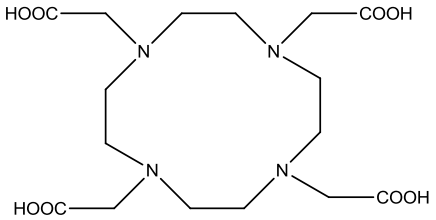

DOTA

Figure 4 Organic ligands that are most commonly used as bifunctional chelators in second generation technetium-99m radiopharmaceuticals.[1]

The general design of second generation radiopharmaceuticals is dictated by (i) the specific location of the receptor in the body and (ii) the receptor structure and how it interacts with the employed ligand. Some of these like somatostatin receptors are located on the peripheral/vascular system and to reach the target receptor they do not have to cross the blood-brain-barrier.[1] In such cases, there is a high degree of freedom towards the size and the charge of the radiopharmaceutical. However, for entities that must cross the blood-brain-barrier such as neurotransmitter receptors, the radiopharmaceutical needs to be small ($M_w \leq 600$ Da), lipophilic,

neutral, stable *in vivo* and must have high affinity for the target. This is to ensure that binding to other receptors and proteins is kept to a minimum.[1,6,19]

A number of ^{99m}Tc labeled tropane systems have shown promising results as target specific brain receptors (**Figure 5)**. These complexes exhibit different levels of binding affinity to the dopamine receptors found in the striatum of the brain and have been evaluated for psychiatric and neurodegenerative diseases such as Schizophrenia, Alzheimer and Parkinson's disease. [1,20] In fact, ^{99m}Tc-TRODAT which is a tropane derivative which is linked via a methylene group to the diaminodithiol ligand, has successfully passed all preclinical tests and was in 2007 clinically accepted.[1,6,20]

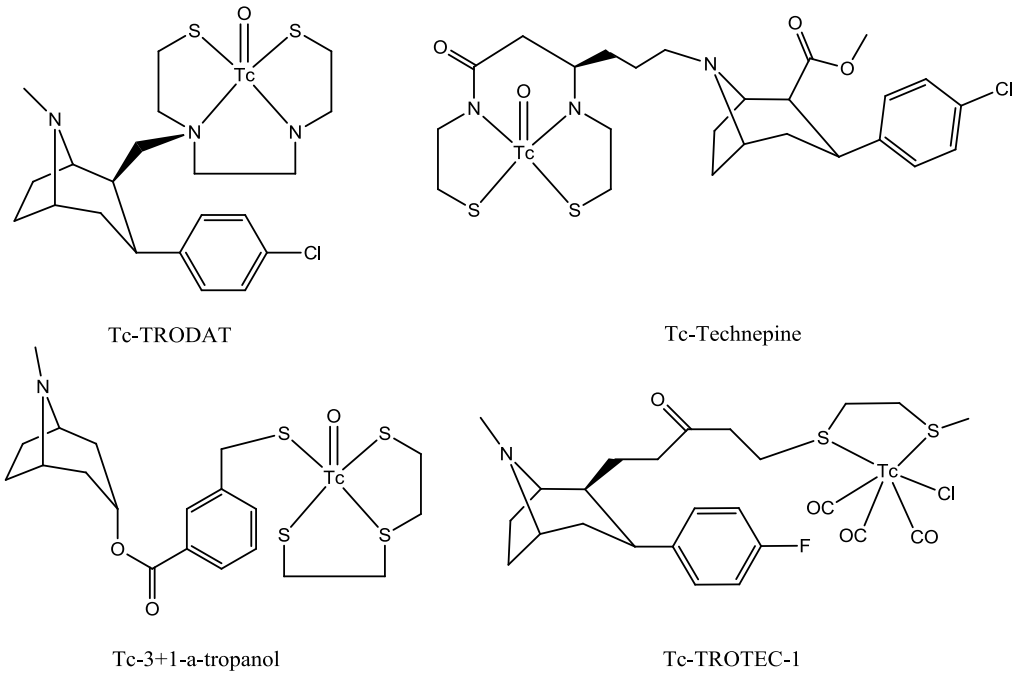

Figure 5 Technetium-99m labeled tropane systems known for imaging the dopamine transporter.[20]

2.3.5 Technetium-99m: 2rd Generation - Integrated Approach

This generation of radiopharmaceuticals is prepared via the so called integrated labeling approach (**Figure 6**). In this labeling approach, biomolecules such as hormones and steroid

[19] Spagnul, C., Alberto, R., Gasser, G., Ferrari, S., Pierroz, V., Bergamo, A., Gianferrara, T., Alessio, E., *J. Inorg .Biochem.* **2013**, *122*, 57-65.

[20] Hoepping, A., Reisgys, M., Brust, P., Seifert, S., Spies, H., Alberto, R., Johannsen, B., *J. Med. Chem.* **1998**, *41*, 4423-4432.

analogs are mimicked, and the technetium complex is merged into the carbon skeleton of these biomolecules. This is done while retaining the receptor biochemical and physiological activities (**Figure 7**). Unlike the bifunction chelator radiopharmaceuticals where the radioactive metal complex couples to a receptor binding biovector via a linker, in the integrated approach the metal complex binds directly to a receptor.[1,6,21,22,23]

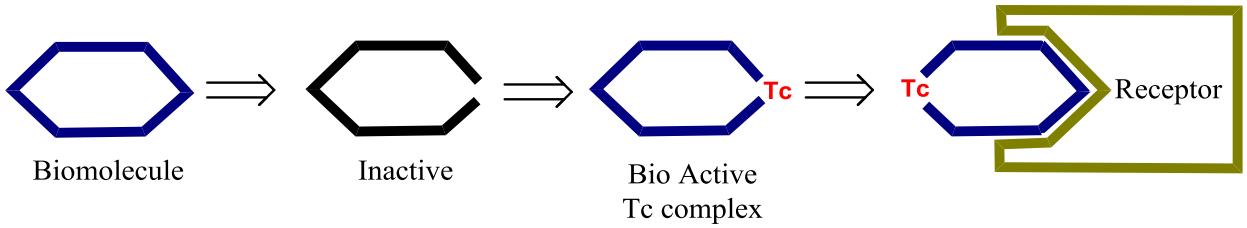

Figure 6 Schematic representation of an integrated technetium labeling approach.[23]

Over-expression of progesterone, estrogen and androgen steroids receptors in prostate, ovarian and breast cancers is well known. For instance, it has been established that progesterone and estrogen receptors exist in about 65% of breast cancers and their presence assists in determining the therapeutic approach that will be more effective in cases of breast carcinoma. Similar to the bifunctional approach, size and lipophilicity of the integrated approach are two of the most critical physiochemical properties, to ensure that the radiopharmaceutical can cross the membrane lipid bilayer of the cells.[1,6]

Extensive analysis of steroids receptor ligands was done by Katzenellenbogen and coworkers. Using the $^{99m}TcO^{3+}$ core containing an N_2S_2 chelating group, they succeeded in coordinating a ^{99m}Tc complex to progestin hormones. Even though their ^{99m}Tc templates showed some degree of an affinity to the progestin receptors, further studies revealed that the complexes were nonspecific leading to significant uptake in non-targeted organs.[24] Miao and coworkers have also utilized the integrated labeling approach to synthesize ^{99m}Tc complexes of melanocyte stimulating hormone analogues for potential melanoma imaging. Similar to what

[21] Casini, A., *J. Inorg. Biochem.* **2012**, *109*, 97-106.

[22] Ferro-Flores, G., de Murphy, C. A., Melendez-Alafort, L., *Curr. Pharm. Anal.* **2006**, *2*, 339 - 352.

[23] Charron, C. L., Hickey, J.L., Nsiama, T. K., Cruickshank, D. R., Turnbulla, W. L., Luyt, L. G., *Nat. Prod. Rep.* **2016**, *33*, 761-800.

[24] Hom, R. K., Katzenellenbogen, J. A., *Nucl. Med. Biol.* **1997**, *24*, 485-498.

Katzenellenbogen and coworkers found, their ^{99m}Tc complexes also displayed high non-specific renal uptake.[25,26,27]

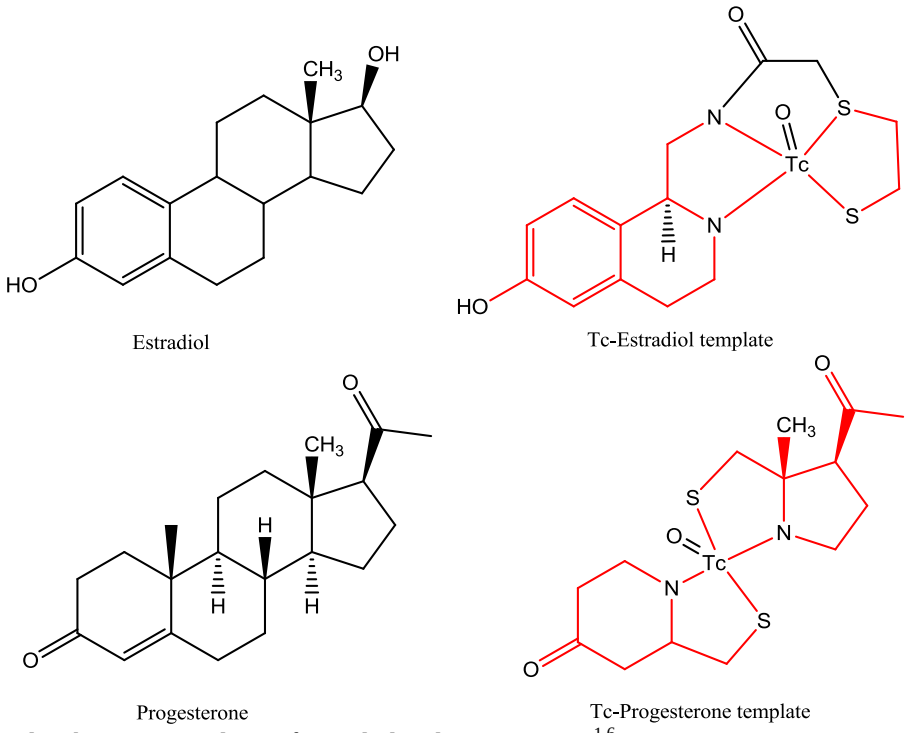

Figure 7 Integrated technetium templates of estradiol and progesterone.[1,6]

Although research developments of technetium radiopharmaceuticals have been intensively studied in the past few decades, there has hardly been any, or very little (pre)clinical trials. However, recent studies on ^{99m}Tc labeled inhibitors of Prostate-Specific Membrane Antigen (PSMA) by Babich and coworkers have shown promising results and in fact some of their compounds are currently undergoing clinical trials. If approved, Babich and coworkers' ^{99m}Tc complexes will further prove the importance of using the integrated technetium labeling approach.[6,28]

[25] Bartholom, M., Valliant, J., Maresca, K. P., Babich, J., Zubieta, J., *Chem. Commun.* **2009**, *5*, 493–512.

[26] Yang, J., Hu, C. -A. A., Miao, Y., *Amino Acids*, **2015**, *47*, 813–823.

[27] Yang, J., Guo, H., Miao, Y., *Nucl. Med. Biol.* **2010**, *37*, 873–883.

[28] Hillier, S. M., Maresca, K. P., Lu, G., Merkin, R. D., Marquis, J. C., Zimmerman, C. N., Eckelman, W. C., Joyal, J. L., Babich, J. W., *J. Nucl. Med.* **2013**, *54*, 1369-1376.

2.3.6 Technetium-99m: Current approaches

Current approaches apply both second generation protocols but focuses mainly on improving the receptors targeting ability. A number of studies have been published were technetium cores were utilized. Presented here are a selection of some relevant ones which will be discussed in detail in the following paragraphs.

2.3.6.1 Hydrazinonicotinyl (HYNIC) approach

Ferro-Flores and coworkers reported a new labeling approach from lyophilized kits for a ^{99m}Tc-tricarbonyl-iPSMA (PSMA = Prostate Specific Membrane Antigen) (**Figure 8**) with high radiochemical purity and obtained auspicious results from their preliminary clinical evaluations. [29] Preliminary images of a patient with metastatic prostate cancer were obtained using ^{68}Ga-PSMA-617 as well as ^{99m}Tc-EDDA/HYNIC-iPSMA and demonstrated the ability of the ^{99m}Tc-based iPSMA to compete with ^{68}Ga-based iPSMA.[30]

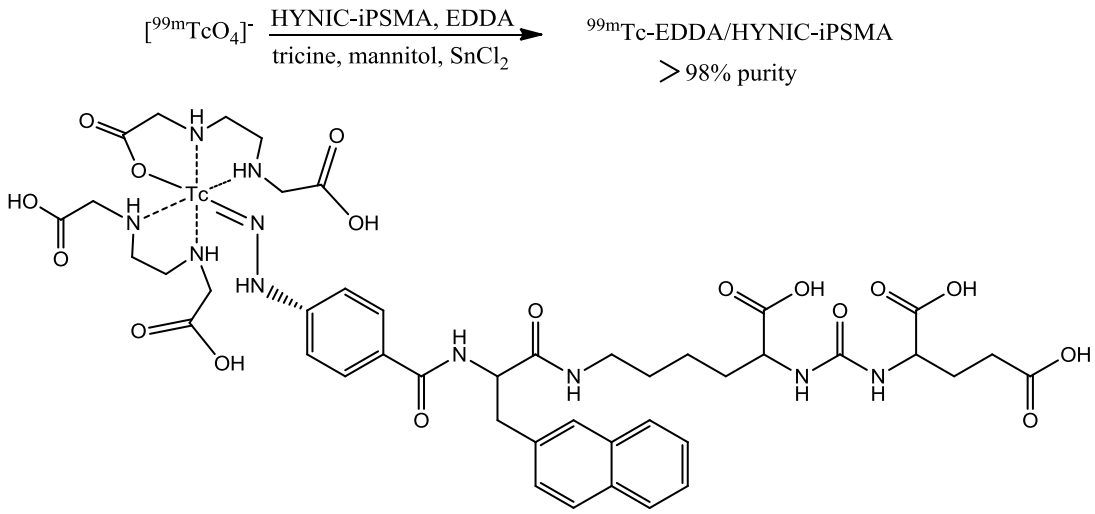

Figure 8 Schematic representation of the synthesis and structure of ^{99m}Tc-EDDA/HYNIC-iPSMA.[29,30]

Zhang and coworkers also recently conducted a study on ^{99m}Tc-based PSMA inhibitor using the HYNIC labeling approach. [31] Using 6-Hydrazinonicotinate-aminocaproic acid-lysine-urea-

[29] Ferro-Flores, G., Luna-Gutiérrez, M., Ocampo-García, B., Santos-Cuevas, C., Azorín-Vega, E., Jiménez-Mancilla, N., Orocio-Rodríguez, E., Davanzo, J., García-Pérez, F. O., *Nucl. Med. Biol.* **2017**, *48*, 36–44.

[30] Santos-Cuevas, C., Davanzo, J., Ferro-Flores, G., García-Pérez, F. O., Ocampo-García, B., Ignacio-Alvarez, E., Gómez-Argumosa, E., Pedraza-López, M., *Nucl. Med. Biol.* **2017**, *52*, 1-6.

[31] Xu, X., Zhang, J., Hu, S., He, S., Bao, X., Ma, G., Luo, J., Cheng, J., Zhang, Y., *Nucl. Med. Biol.* **2017**, *48*, 69-75.

glutamate (HYNIC-ALUG) labeled with ^{99m}Tc (^{99m}Tc-HYNIC-ALUG), they also obtained promising results on the radiation dosimetry and in vivo biological evaluations on mice. Their compound was highly specific to PSMA-positive tumors and had low background levels in non-targeted organs.

2.3.6.2 Mercaptoacetyl triserine (MAS_3) approach

Wester and coworkers successfully synthesized and evaluated 1,4,7,10-tetraazacyclododececane,1-(glutaric acid)-4,7,10-triacetic acid (DOTAGA) as potential PSMA chelator for theranostic and imaging of prostate cancer using ^{68}Ga, ^{111}In and ^{177}Lu metal centers. [32] In addition, they conducted another study were the DOTAGA chelator was replaced by a mercaptoacetyl triserine (MAS_3) using a ^{99m}Tc metal center as illustrated in **Figure 9**. What Wester and coworkers established on the basis of preclinical and first patient data was that the new ^{99m}Tc-based complex was a superior substitute for the ^{111}In-based complex for PSMA-targeted radioguided surgery.[33]

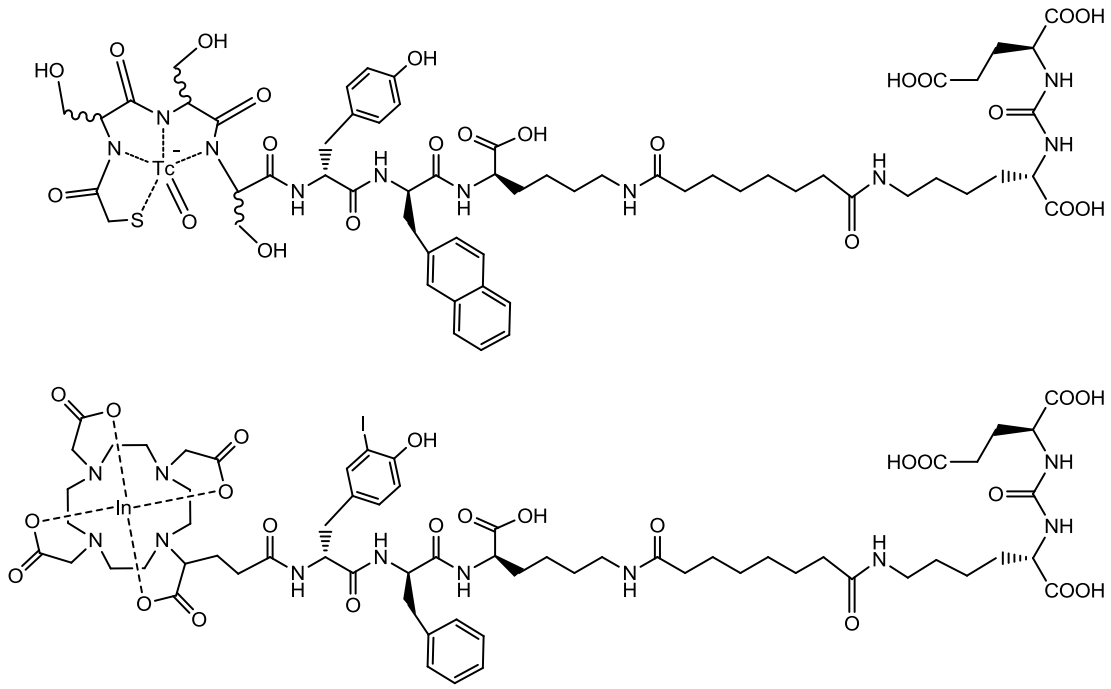

Figure 9 The structures of ^{99m}Tc-PSMA and ^{111}In-PSMA complexes derived from MAS_3 modified and plain DOTAGA ligands.[32,33]

[32] Robu, S., Schottelius, M.., Eiber, M., Maurer, T., Gschwend, J., Schwaiger, M., Wester, H. J., *J. Nuc. Med.* **2017**, *58*, 235-242.

[33] Weineisen, M., Simecek, J., Schottelius, M., Schwaiger, M., Wester, H. J., *EJNMMI Research.* **2014**, *4*, 1-15.

2.3.6.3 Tricarbonyl approach

The synthesis, first introduced by Alberto and coworkers[34] in 1994, described the aqueous tricarbonyl complexes of the Group 7 transition metals (Tc and Re) and received much attention due to the high kinetic stability of the carbonyl ligands in the low-spin d^6 *fac*-$[M(CO)_3]^+$ core (M = Re or Tc) (**Figure 10**).[35] The labile H_2O ligand makes it possible for one to coordinate various mono-, bi- and tridentate ligand systems.[36] Since the discovery of these tricarbonyl systems, a number of complexes have been reported with a variety of ligands and some will be discussed in the following paragraphs.

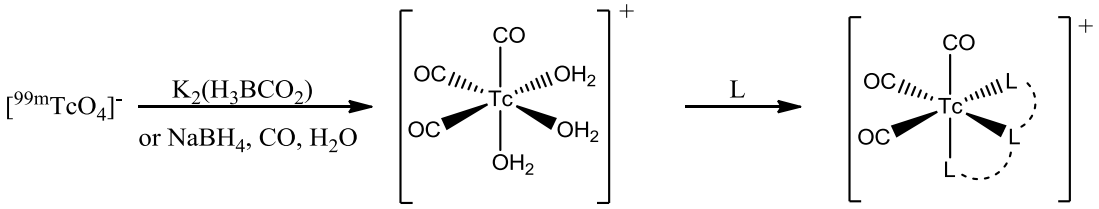

Figure 10 Synthetic pathways for technetium tricarbonyl (*fac*-$[^{99m}Tc(CO)_3(H_2O)_3]^+$) complexes from $[^{99m}TcO_4]^-$ utilizing a tridentate ligand.[35]

Mundwiler, Alberto and coworkers later described a new [2+1] mixed ligand concept for substitution of the three labile aqua ligands in the *fac*-$[^{99m}Tc(CO)_3(H_2O)_3]^+$ complex. This new method was based on the substitution of the aqua ligands with one bidentate and one monodentate ligand, while the biomolecule species was linked to either the monodentate $[2+1_B]$ or the bidentate $[2_B+1]$ as shown in **Figure 11**. For the monodentate $[2+1_B]$ ligand approach, the steric and electronic properties of the entering bidentate ligand should be tuned in such a way that only one bidentate ligand can be coordinated and the remaining 3rd position should be occupied by an aqua ligand before substitution by the monodentate entering nucleophile can occur.[37] The substitution variation of the *fac*-$[^{99m}Tc(CO)_3(H_2O)_3]^+$ core can be blocked by removing all the three aqua ligands simultaneously.

[34] Alberto, R., Egli, A., Abram, U., Hegetschweiler, K., Gramlich V., Schubiger, P. A., *J. Chem. Soc. Dalton Trans.* **1994**, 2815-2820.

[35] Alberto, R., Schibli, R., Egli, A., Schubiger, A. P., *J. Am. Chem. Soc.* **1998**, *120*, 7987-7988.

[36] Alberto, R., Schibli R., Waibel R., Abram U., Schubiger P. A., *Coord. Chem. Rev.* **1999**, *190*, 901-919.

[37] Mundwiler, S., Kündig, M., Ortner K., Alberto, R., *Dalton Trans.* **2004**, 1320-1328.

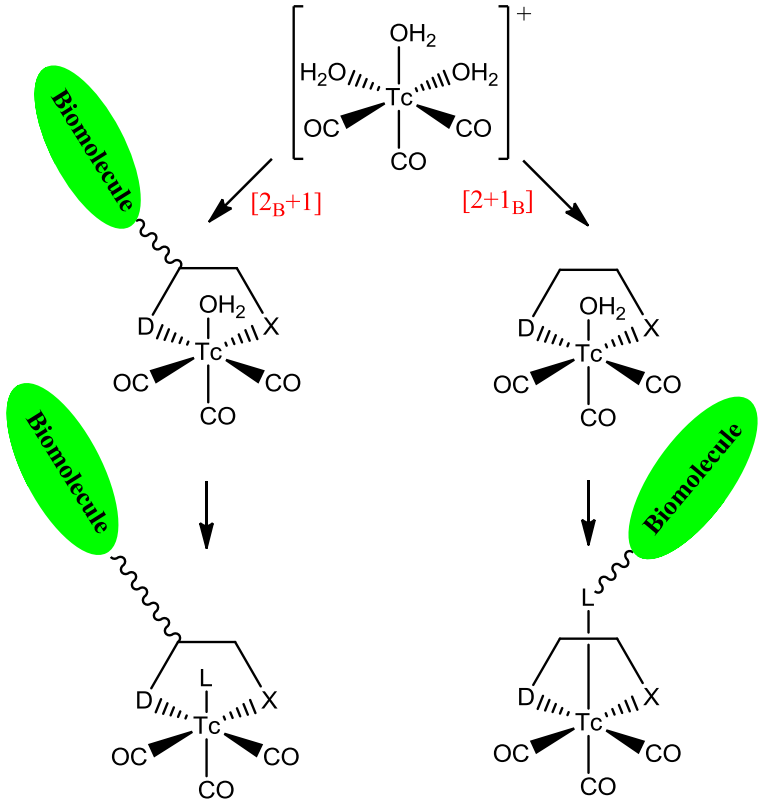

Figure 11 Schematic representation of the mixed [2+1] ligand concept for *fac*-[^{99m}Tc(CO)$_3$(H$_2$O)]$^+$, L = monodentate ligand, D-X = bidentate ligand with various donor atoms.[37]

Alberto and coworkers have reported the Cp-based technetium tricarbonyl complexes [(Cp-R)^{99m}Tc(CO)$_3$] (Cp =cyclopentadienyl, R=target-specific moiety) as diagnostic agents for carbonic anhydrases inhibitors (**Figure 12**).[38] Carbonic anhydrases are biological Zn enzymes that aid with the interconvention of water and carbon dioxide to form carbonic acid. Carbonic anhydrases are known to be present in most malignant tumors and thus are critical targets for cancer diagnosis. In addition, Cp-ligands are highly versatile and can be used in place of phenyl rings without affecting the bioactivity, as well as possibly mimicking ferrocene type moieties.[39,40]

[38] Can, D., Spingler, B., Schmutz, P., Mendes, F., Raposinho, P., Fernandes, C., Carta, F., Innocenti, A., Santos, I., Supuran, C. T., Alberto, R., *Angew Chem* **2012**, *51*, 3354 –3357.

[39] Sulieman, S., Can, D., Mertens, J., N'Dongo, H. W. P., Liu, Y., Schmutz, P., Bauwens, M., Spingler, B., Alberto, R., *Organometallics* **2012**, *31*, 6880-6886.

[40] Masi, S.; Top, S.; Boubekeur, L.; Jaouen, G.; Mundwiler, S.; Spingler, B.; Alberto, R., *Eur. J. Inorg. Chem.* **2004**, *10*, 2013-2017.

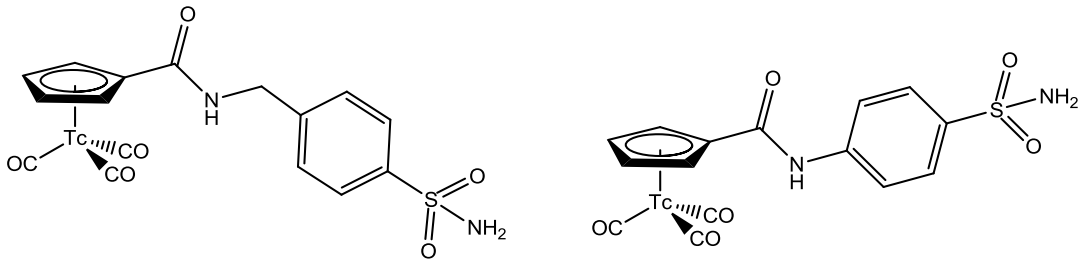

Figure 12 Cyclopentadienyl-based technetium complexes for carbonic anhydrase inhibitors.[39]

Alberto et al. have also reported the synthesis of bifuntional Cp-complexes of the type $[^{99m}Tc(CO)_3(\eta^5\text{-}C_5H_4COOR)]$ in water.[41] The bifunctionality of the Cp- ligands used provides an opportunity for one to attach multiple targeting agents simultaneously (**Figure 13**). This illustrates the versatile nature of cyclopentadienyl-based technetium complexes in general. Furthermore, the water medium conditions in which the reactions were conducted and the physiologically favored pH provides an added advantage of using this type of complexes.

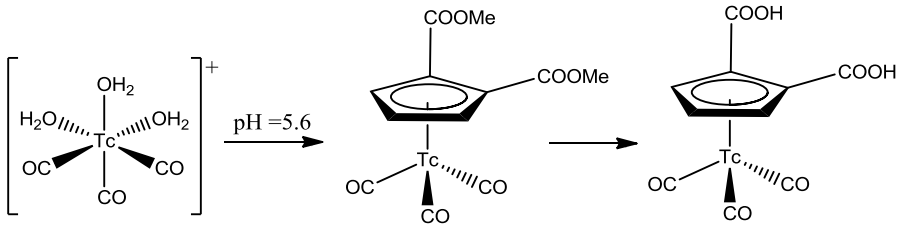

Figure 13 General synthetic approach for the bifunctional cyclopentadienyl-based technetium complexes.[41]

2.3.6.4 Single Amino Acid Chelate (SAAC) approach

To further exploit the properties of the *fac*-$[M(CO)_3]^+$ core, Valliant and coworkers[42] designed a chelating group that can aid in both fluorescence microscopy and radioimaging depending on whether a ^{99m}Tc or a Re metal centre is employed (**Figure 14**). The *fac*-$[Re(CO)_3]^+$ complexes are known to be fluorescent depending on the type of aromatic donor ligand used, while *fac*-$[^{99m}Tc(CO)_3]^+$ complexes have been widely explored as radio-tracers. While fluorescence

[41] Ursillo, S., Can, D., N'Dongo, H. W. P., Schmutz, P., Spingler, B., Alberto, R., *Organometallics.* **2014**, *33*, 6945-6952.

[42] Stephenson, K. A., Banerjee, S. R., Besanger, T., Sogbein, O. O., Levadala, M.K., McFarlane, N., Lemon, J.A., Boreham, D. R., Maresca, K. P., Brennan, J. D., Babich, J. W., Zubieta, J., Valliant, J. F., *J. Am. Chem. Soc.* **2004**, *126*, 8598-8599.

microscopy allows accurate *in vitro* interpretation of biological processes at the subcellular level, radioimaging aids in detection of this processes deep within the body. Using this approach, one can create complexes that are therapeutic and diagnostic just by using congeners as exemplified by Tc and Re in the following example.[25,35,42 43,44]

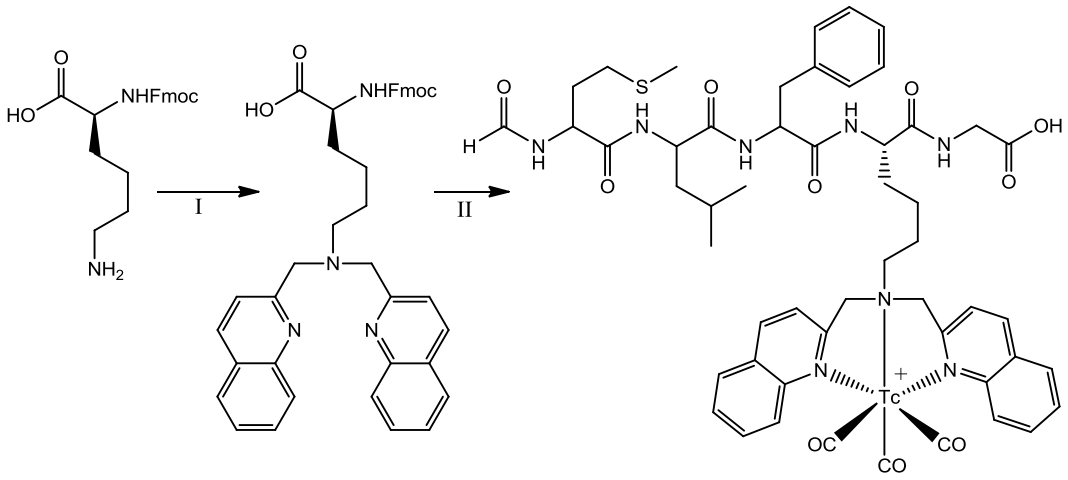

Figure 14 Schematic representation of the multi modality SAAC approach. I = $NaBH(OAc)_3$/quinoline-aldehyde and II = $[^{99m}Tc(CO)_3(H_2O)_3]^+$/fMLF(SAACQ)G.[42]

2.3.7 Rhenium, the Technetium-99m surrogate

In inorganic and organometallic chemistry, rhenium forms many compounds that are stoichiometrically analogous to those of technetium (i.e. $[TcO_4]^-$ and $[ReO_4]^-$). Due to the aforementioned statement and the fact that rhenium-based experimental synthesis can be conducted on a non radioactive isotope, rhenium complexes were to a large extend only used as non-radioactive surrogates for the development of radioactive technetium complexes. However, recent interest in theranostic drug development has evolved in ^{186}Re and ^{188}Re radionuclides being employed in a similar chemical manner as to that of ^{99m}Tc with a view of using their effective β-emitted particles as therapeutic functions.[45]

[43] Maresca, K. P., Hillier, S. M., Lu, G., Marquis, J.C., Zimmerman, C. N., Eckelman, W. C., Joyal, J. L., Babich, J. W., *Inorganica Chim. Acta.* **2012**, *389*, 168–175.

[44] Goffin, K. E., Joniau, S., Tenke, P., Slawin, K., Klein, E. A., Stambler, N., Strack, T., Babich, J., Armor, T., Vivien Wong, V., *J. Nucl. Med.* **2017**, *58*, 1408-1413.

[45] Engelbrecht, H. P., Cutler, C. S., Jurisson, S. S., den Drijver, L., Roodt, A., *Synth. React. Inorg. Met. –Org. Chem.* **2005**, *35*, 83-99.

In much of its chemistry, rhenium resembles technetium and for this reason the three radiopharmaceutical development stages of technetium discussed on page 5 to 16 also in many aspects represent the rhenium development. Similarities in the physical properties of Re and Tc makes it very difficult for biological systems that depends on properties such as shape, size and charge to differentiate between their analogous complexes. However, there exist a number of differences between Re and Tc. For one, they have different redox properties; Re complexes at higher oxidation are more difficult to reduce than their Tc counterparts and this may lead to different *in vivo* handling even for extremely analogous complexes. Secondly, ligand substitution is slower in Re than in Tc-based complexes because of the large ligand field splitting in rhenium complexes which may affect the electrochemical and kinetic properties of Re complexes *in vivo*.

2.4 Rhenium

2.4.1 A brief history of Rhenium

Rhenium, element 75, was discovered via its X-ray spectrum by Tacke, Noddack and Berg in 1925.[46] It is located in the third row of transition metals and in the same group (7) as technetium and manganese. This element occurs in nature with some copper ores and molybdenite (MoS_2) minerals, and naturally as two stable isotopes [^{185}Re (37.4%) and ^{187}Re (62.6%)] which are usually isolated as perrhenate ions $[ReO_4]^-$, similar in chemistry to the pertechnetate ions $[TcO_4]^-$.[47] It has one of the highest melting points (3180 ^oC) and the perrhenate ions can easily be precipitated as $KReO_4$. Rhenium-186 and -188 isotopes have been found to be medicinally important because of their physiologically effective β^--irradiation on cancer tissues. Similar to technetium, when rhenium is coordinated to ligands of different types, it can form a wide range of oxidation states ranging from -1 to 7 resulting in different coordination geometries.[48]

[46] Kemmitt, R. D. W., Peacock, R. D., Bailar, J. C., Emeléus, H. J., Nyholm, R., *The Chemistry of Manganese, Technetium and Rhenium*. Pergamon Press: Oxford., **1973**.

[47] McCleverty, J. A., Meyer, T. J., *Comprehensive Coordination Chemistry II: From Biology to Nanotechnology*. 2 Ed., Elsevier Science: Oxford., **2003**.

[48] Scerri, E., *Nat. Chem.* **2010**, *2*, 598.

2.4.2 Rhenium isotopes in nuclear medicine

The rhenium element has two β^- emitting radioactive isotopes that are very important in nuclear medicine, namely ^{186}Re ($t_{1/2}$ = 89.2 hours, E_{max} = 1.1 MeV) and ^{188}Re ($t_{1/2}$= 17.0 hours, E_{max} = 2.1 MeV). Both of them also have (weak) gamma photon emissions, providing thus an *in vivo* trace to evaluate uptakes. ^{186}Re can be obtained from neutron radiation of ^{185}Re, while ^{188}Re can be obtained from a ^{188}W generator system. Although both radionuclides can be used in nuclear medicine, ^{188}Re is found to be the most preferred radionuclide because of its shorter half-life and the higher penetrating depth of its emitted particles.

2.4.3 ^{188}Re-pharmaceuticals

Rhenium-188 (^{188}Re) is distinguished by its excellent physical characteristics such as its short half-life and its beta and gamma radiations in radiopharmaceutical therapy. One more advantage is the ready availability of the ^{188}W/^{188}Re generator which enables direct preparations in hospitals. [49] However, competition (**Table 2**) from other radionuclides that offers simplistic chemistry such as lutetium-177, yttrium-90 and iodine-131 causes the current utilization of ^{188}Re in clinical practices to be quite low. Nevertheless, ^{188}Re-based therapeutics (both target-specific and nontarget-specific) have demonstrated positive pharmacokinetics and dosimetric results in some preclinical and clinical evaluations.[2,49,50,51]

Table 2 Physical properties of current radionuclides radiopharmaceutical therapy.[2,49,51]

Radioniclide	$t_{1/2}$ (h)	E_γ (MeV) [Ab(%)]	Mean (E_β) (MeV)	Max(E_β) (MeV)	Mean (β) ST(mm)	Max (β) ST(mm)
^{188}Re	17	0.155 [15]	0.764	2.12	3.1	10.4
^{186}Re	89.2	0.137[9]	0.329	1.07	-	5.0
^{177}Lu	161	0.208 [6.1]	0.133	0.497	0.23	1.8
^{90}Y	64.1	-	0.935	2.28	4.0	11.3
^{131}I	192	0.364 [82]	0.182	0.610	0.39	2.3

E = energy, Ab = abundance, ST = particle range in soft tissue

Examples of ^{188}Re in radiopharmaceuticals are varied and include the following radiotherapeutics listed below:

[49] Ferro-Flores, G., Arteaga de Murphy, C., *Adv. Drug Deliv. Rev.* **2008**, *60*, 1389-401.

[50] Rattat, D., Schubiger, P. A., Berke, H. G., Schmalle, H., Alberto, R., *Cancer Biother. Radiopharm.* **2001**, *16*, 339-343.

[51] Schubiger, P. A., Alberto, R., Smith, A., *Bioconjugate Chem.* **1996**, *7*, 165-179.

1. ^{188}Re-liposome therapy – designed for Liver cancer.[52]
2. ^{188}Re-lipiodolo therapy – designed for hepatocellular cancer.[49]
3. ^{188}Re-hydrogel therapy – designed for breast tumor.[53]
4. ^{188}Re-fibrin glue therapy – designed for glioblastomas.[54]
5. ^{188}Re-hydroxyapatite – designed for bone therapy.[49]

2.4.3.1 ^{188}Re-Hydroxyethylidine diphosphonate (^{188}Re-HEDP)

One of the first ^{186}Re complexes to be used in radiopharmaceutical therapy was ^{186}Re-hydroxyethylidine diphosphonate (^{186}Re-HEDP) in 1979 by Galy and coworkers.[55] This complex was found to be very useful in the palliative treatment of metastatic bone pain. Furthermore, research has indicated that ^{186}Re-HEDP distribution is localized in metastatic foci within the bone in a similar manner to that of ^{99m}Tc bone-seeking agents.[56] For reasons already mentioned, extensive studies on ^{188}Re-HEDP have now been conducted since this discovery.[49,57,58,59,60]

A study by Kotzerke and Liepe on the comparison of ^{188}Re-HEDP, ^{186}Re-HEDP, ^{153}Sm-EDTMP and ^{89}Sr in the treatment of painful skeletal metastases revealed superiority of ^{188}Re-HEDP over all the other radiopharmaceuticals.[57] Further studies on ^{188}Re-HEDP as a radiopharmaceutical for osteoblastic bone metastases in rat models were conducted. They obtained results that were underestimated by 26% by the MIRDOSE software that calculates the internal radiation dose

[52] Ballot, S., Noiret, N., Hindré, F., Denizot, B., Garin, E., Rajerison, H., Benoit, J. -P., *Eur. J. Nucl. Med.* **2006**, *33*, 602–607.

[53] Azhdarinia, A., Yang, D. J., Yu, D. F., Mendez, R., Oh, C., Kohanim, S., *Pharm. Res.* **2005**, *22*, 776-783.

[54] Hafeli, U. O., Pauer, G. J., Unnithan, J., Prayson, R. A., *Eur. J. Pharm. Biopharm.* **2007**, *65*, 282-288.

[55] Mathieu, L., Chevalier, P., Galy, G., *Int. J. Appl. Radiat. Isot.* **1979**, *30*, 725-730.

[56] Lin., W.-Y., Hsieh, J. -F., Lin, C. -P., Hsieh, B. -T., Ting, G., Wang, S. -J., Knapp(Jr), F.F., *Nucl. Med. Biol.* **1999**, *26*, 455-459.

[57] Liepe, K., Kotzerke, J., *Nucl. Med. Commun.* **2007**, *28*, 623-630.

[58] Liepea, K., Geidel, H. H., Bergmannd, R., Haaseb, M., Rungea, R., Kotzerkea, J., *Nucl. Med. Commun.* **2009**, *30*, 693-699.

[59] van Aswegen, A., Roodt, A., Marais, J., Botha, J. M., Naude, H., Lotter, M. G., Goedhals, L., Doman, M. J., Otto. A. C., *Nucl. Med. Comms.* **1997**, *18*, 582-588.

[60] Kemp, G., van Aswegen, A., Roodt, A., Marais, J., Jansen, S. E., Goedhals, L., Otto, A.C., Louw, W., *International Atomic Energy Agency*, TecDoc-1029, Vienna, **1998**, 627-633.

estimates for radionuclides.[58] Franke et al. also investigated the effects of ^{188}Re-hydroxyethylidine diphosphonate (^{188}Re-HEDP).[61] Their research focused on gathering the dosimetric data of ^{188}Re-HEDP in thirteen prostate cancer patients with skeletal metastases. This study showed that ^{188}Re-HEDP was an effective radiopharmaceutical agent for the palliative treatment of metastatic bone pain even at low doses. Furthermore, over 60% of the ^{188}Re-HEDP was excreted in a majority of patients after two days.

2.4.3.2 ^{188}Rhenium labeled alendronate (^{188}Re-ABP)

Padilla et al. investigated the labeling of biphosphate alendronate (ABP) with SnF_2 reduced ^{188}Re and further compared the results to other bone metastases palliative agents and the analogue ^{99m}Tc-ABP imaging agent.[62] Their preliminary results showed significant rat bone uptake, lack of uptake in non-targeted organs and rapid urine elimination, proving that ^{188}Re-ABP could be a good therapeutic agent. More recent work by Shafiei and coworkers on biphosphate ligands similar to alendronate labeled with ^{188}Re such as ^{188}Re-PMA (a complex of ^{188}Re with pamidronate) has been reported as a potential new candidate for bone palliation therapy.[63]

2.4.3.3 ^{188}Rhenium tricarbonyl complexes

Rhenium tricarbonyl compounds represent an important class of group 7 transition metal complexes and have recently been the subject of intensive study. Apart from all the reasons already mentioned, the *fac*-Re tricarbonyl synthon possess a number of intrinsic property advantages for the construction of novel model radiopharmaceuticals. For one, some *fac*-$[Re(CO)_3]^+$ complexes have been reported to be excellent luminescent probes depending on the type of ligands used.[64] With this added advantage, *in vivo* biodistribution and pharmacokinetics of Re-based radiopharmaceuticals can even be followed by conventional and time resolved emission microscopy.[64,65,66]

[61] Liepe, K., Hliscs, R., Kropp, J., Runge, R., Knapp, Jr, F. F. R.,Franke, W. -G., *J. Nucl. Med.* **2003**, *44*, 953-960.

[62] de Murphy, C. A., Ferro-Flores, G., Pedraz-Lopez, M., Melendez-Alafort, L., Croft, B. Y., Ramirez, F. M., Padilla, J., *Appl. Radiat. Isot.* **2001**, *54*, 435-442.

[63] Erfani, M., Rahmani, N., Doroudi, A., Shafiei, M., *Nucl. Med. Biol.* **2017**, *49*, 1-7.

[64] Pitchumony, T. S., Banevicius, L., Janzen, N., Zubieta, J., Valliant, J. F., *Inorg. Chem.* **2013**, *52*, 13521-13528.

[65] Lam, S. -T., Zhu, N., Au, V. K. -M., Yam, V. W. -W., *Polyhedron.* **2015**, *86*, 10-16.

For example, Hoffman and coworkers investigated a ^{188}Re tricarbonyl complex[67] containing a $(serine)_3$ spacer, with a bidentate chelator and a trioxymethyl phosphine as a monodendate ligand (**Figure 16**). Upon evaluation of this complex with ^{188}Re and ^{99m}Tc, it was found that these complexes were highly hydrophilic and had a significantly improved biodistribution profile. Further evaluations showed that upon labeling, the peptide retained its biological activity and displayed substantial stability both *in vivo* and *in vitro*.[68]

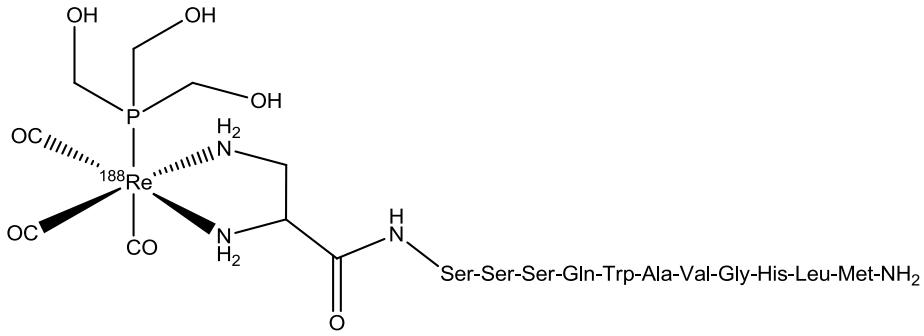

Figure 15 The structure of a ^{188}Re tricarbonyl core labeled with a peptide. [67, 68]

Recently, Paparidis *et al*. investigated the effect two separate Re tricarbonyl complexes, each covalently linked to a triphenylphosphonium cation, on cell growth of U-87 MG glioblastoma cells (**Figure 17**). [69] From their results they observed that both Re tricarbonyl complexes caused no noticeable cytotoxicity. These results would be very advantageous if one was to study the radiotoxicity of the same complexes using ^{188}Re. Paparidis *et al*. further observed that the free ligand from complex **A** (**Figure 17**) was able to significantly inhibit cell growth and caused 80% damage to the U-87 MG cells.

[66] Yazdani, A., Janzen, N., Banevicius, L., Czorny, S., Valliant, J. F., *Inorg. Chem.* **2015**, *54*, 1728-1736.

[67] Smith, C. J., Sieckman, G.L., Owen, N.K., Hayes, D.L., Mazuru, D.G., Volkert, W.A., Hoffman, T.J., *Anticancer Res.* **2003**, *23*, 63-70.

[68] Garcia-Garayoa, E., Schibli, R., Schubiger, P. A., *Nucl. Sci. Tech.* **2007**, *18*, 88-100.

[69] Paparidis, G., Akrivou , M., Tsachouridou , V., Shegani , A., Vizirianakis , I. S., Pirmettis , I., Papadopoulos , M. S., Papagiannopoulou, D., *Nucl. Med. Biol.* **2018**, *57*, 34-41.

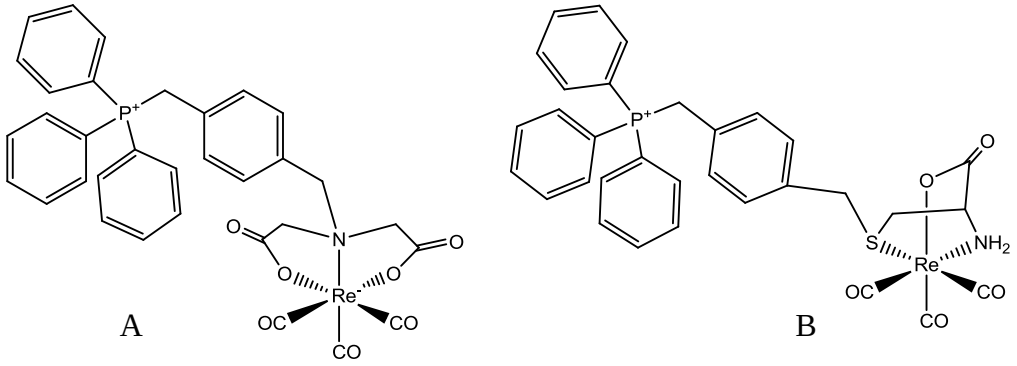

Figure 16 Re-tricarbonyl complexes linked to the triphenylphosphonium cation.[69]

Santos and coworkers[70] reported a synthesis method for the development of a novel ^{188}Re tricarbonyl complex for bone pain palliation (**Figure 18**). Pharmacokinetics and *in vivo* studies were performed on mice and high bone uptake, bone to blood radioactivity and fast blood clearance were observed.

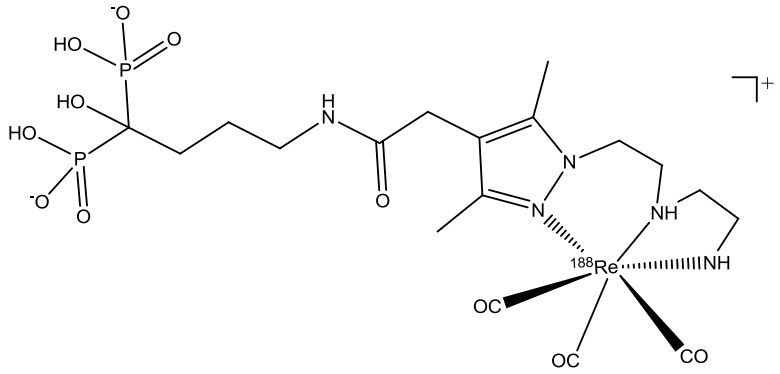

Figure 17 The structure of a ^{188}Re tricarbonyl contain a pedant bisphosphonate ligand.[70]

A recent interesting research focus area of group 7 transition metals tricarbonyl complexes is the development of [CpM(CO)$_3$] core entities (M = Re or Tc; Cp = cyclopentadienyl and analogs).[71] The versatile nature of Cp ligands, the ability to act as a small tridentate ligand (see example in **Figure 19**) and the low molecular weight may lead to interesting results as size and lipophilicity are two very important properties needed for a successful radiopharmaceutical, more especially those that need to cross the blood-brain-barrier.[72]

[70] Fernandes, C., Monteiro S., Belchior, A., Marques, F., Gano, L., Correia, J.D.G., Santos, I., *Nucl. Med. Biol.* **2016**, *43*, 150-157.

[71] Bernard, J., Ortner, K., Spingler, B., Pietzsch, H.-J., Alberto, R., *Inorg. Chem.*. **2003**, *42*, 1014-1022.

[72] Top, S., El Hafa, H., Vessikres, A., Quivy, J., Vaissermann, J., Hughes, D.W., McGlinchey, M.J., Mornon, J.-P., Thoreau, E., Jaouen, C., *J. Am. Chem. Soc.* **1995**, *117*, 8372-8380.

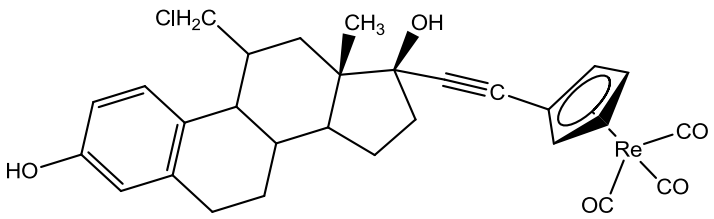

Figure 18 Linkage of an estradiol steroid to a cyclopentadienly bearing rhenium tricarbonyl core.[71,72]

It is clear that the ^{188}Re radionuclide can be used in a wide spectrum of radiopharmaceutical therapeutic applications even though in most cases the bioconjugate chemistry involved is more complex than that of other therapeutic radionuclides such as ^{177}Lu, ^{131}I and ^{90}Y. In addition, non-radioactive rhenium complexes can also serve as a prototype for radioactive technetium-99m and the unstable manganese tricarbonyl complexes.[73] Moreover, dosimetric, pharmacokinetic and clinical studies of ^{188}Re compounds have been the subject of intensive study lately.[74]

2.5 Ligand substitution reactions on *fac*-($M(CO)_3$) core

Rapid transition from one stable complex to another via ligand exchange is important in radiopharmaceutical application. The use of metal complexes such as those containing the *fac*-$[M(CO)_3]^+$ (M = Re and Tc) core with three labile coordination sites provide several advantages when investigation reaction mechanisms. For instance, the backbonding stabilized carbonyl ligands increase the lability of the other *trans* ligand via the so called "trans-effect" allowing them to be easily substituted with a wide variety of other ligands including pertinent biomolecules.[34] Due to the carbonyl ligand stability, ligand exchange kinetic reactions can be easily investigated on tricarbonyl cores. This is critical to quantify when working with fast decaying radioisotopes such as ^{99m}Tc and ^{188}Re, therefore complex formation and ligand exchange should be accomplished as fast as possible.[75] The tricarbonyl core offers diverse coordination chemistry more especially when chelating ligands that mimic some biological binding fashion is used. Studies have shown that various *fac*-$[M(CO)_3]^+$ core fragments can bind in multiple fashions to various proteins and may open new ways of developing

[73] Mokolokolo, P. P., Frei, A., Tsosane, M.S., Kama D.V., Schutte-Smith, M., Brink, A., Visser, H.G., Meola, G., Alberto, R., Roodt, A., *Inorganica Chim. Acta*. **2018**, *471*, 249-256.

[74] Leonidova A., Gasser, G., *ACS Chem. Biol.* **2014**, *9*, 2180−2193.

[75] Donnelly, P. S., *Dalton Trans.* **2011**, *40*, 999-1010.

radiopharmaceuticals in accordance to the [2+1] approach.[76,77,78,79] Hence, understanding substitution kinetics in such complexes becomes very important and will be examined in detail.

2.5.1 Substitution of the coordinated H_2O in *fac*-$[Re(CO)_3(H_2O)_3]^+$

The first ^{17}O NMR kinetic data obtained for the study of water exchange on *fac*-$[Re(CO)_3(H_2O)_3]^+$ was reported by Salignac and coworkers in 2003.[80] In their approach, a variety of ligands with diverse nucleophilicities such as acetonitrile (CH_3CN), trifluoroacetate (TFA), Thiourea (TU), $Hbipy^+$ (bipy = 2,2'-bipyridyl), bromide (Br^-), dimethylsulfide (DMS) and $Hphen^+$ (phen = 1,10-phenanthroline) were used to study the kinetic effect of *fac*-$[Re(CO)_3(H_2O)_3]^+$ on entering mono- and bidentate ligands. A relatively low rate constant of $k_{ex}^{298} = (6.3 \pm 0.1) \times 10^{-3}$ s^{-1} for the water exchange rate on *fac*-$[Re(CO)_3(H_2O)_3]^+$ and $k_{OH}^{298} = 27 \pm 1$ s^{-1} for the water exchange rate on *fac*-$[Re(CO)_3(OH)(H_2O)_2]$ was found. Further investigations revealed that a significant contribution from the basic form only appeared when $[H^+] < 3 \times 10^{-3}$ M and at concentrations higher than this limiting $[H^+]$, kinetic studies can solely be conducted on the triaqua cation. In addition, variable temperature studies let to activation parameters ($\Delta H^{\ddagger}_{ex} = 90 \pm 3$ kJ.mol^{-1} and $\Delta S^{\ddagger}_{ex} = +14 \pm 10$ J .K^{-1}.mol^{-1}) that were indicative of a dissociative type activation mechanism. This was further proved by following the reactions on ^1H, ^{13}C and ^{19}F NMR with appropriate ligands mentioned above. Calculations for the interchange rate constant were found to be in the same range as k_{ex} and this further indicated dissociative type activation.

In 2004 Grunndler *et al*. reported on substitution reactions on a *fac*-$[Re(CO)_3(H_2O)_3]^+$ using a High-Pressure NMR using donor ligands such as THT (tetrahydrothiophene), Pyz (pyrazine) and DMS.[81] They obtained results that were in agreement with those reported by Salignac and

[76] Brink, A., Helliwell, J.R., *IUCrJ.* **2017**, *4*, 283-290.

[77] Zobi, F., Spingler, B., Alberto, R., *ChemBioChem.* **2005**, *6*, 1397 - 1405.

[78] Binkley, S. L., Leeper, T.C., Rowlett, R.S., Herrick, R.S., Ziegler, C.J., *Metallomics.* **2011,** *3*, 909-916.

[79] Zobi, F., Spingler, B., Fox, T., Alberto, R., *Inorg. Chem.* **2003**, *42*, 2818-2820.

[80] Salignac, B., Grundler, P.V., Cayemittes, S., Frey, U., Scopelliti, R., Merbach, R.E., Hedinger, R., Hegetschweiler, K., Alberto, R., Prinz, U., Raabe, G., Kolle, U., Hall, S., *Inorg. Chem.* **2003**, *42*, 3516-3526.

[81] Grundler, P. V., Salignac, B., Cayemittes, S., Alberto, R., Merbach, A.E., *Inorg. Chem.* **2004**, *43*, 865-873.

coworkers. A summary of the kinetic data obtained by both Grundler and Salignac is given in **Table 3** below.

Table 3 Rate and equilibrium constants for the formation of f*ac*-$[Re(CO)_3(H_2O)_3]^+$ complex with various ligands at I = 1 M and T = 298 K

L	TFA[a]	Br^- [a]	CH_3CN[a]	DMS[a]	TU[a]	Pyz[b]	THT[b]	DMS[b]
$10^3\ k_{f,1}$ ($M^{-1}S^{-1}$)	0.81(1)	1.6(3)	0.76(4)	1.51(23)	2.49(9)	1.06(5)	1.28(7)	1.15(6)
$10^5\ k_{r,1}$ (S^{-1})	99(2)	230(100)	16(2)	3.9(1.7)	1.6(2)	0.45(4)	3.05(9)	14.2(8)
$10^3\ k_{f,2}$ ($M^{-1}S^{-1}$)				0.53(1)	4.7(1.7)			0.76(2)
$10^5\ k_{r,2}$ (S^{-1})				0.98(2)				1.62(5)
$10^3\ k_{f,3}$ ($M^{-1}S^{-1}$)				0.1(1)	5.7(1.2)			0.106(4)
$10^3\ k_{f,3}$ (S^{-1})				0.02(1)				0.20(2)
k_1 (M^{-1})	0.82(2)	0.7(3)	4.8(5)	38(18)	160(8)	273(15)	41(1)	8.3(1)

[a] - Ref. *79* and [b] - Ref. *80*, $k_{f,i}$ and $k_{r,i}$ represents formation rate and reverse reaction rate respectively were i=1(mono-), i=2(bi-) and i=3(tridentate) complexes.

The reaction of *fac*-$[Re(CO)_3(H_2O)_3]^+$ with DMS and CH_3CN let to the identifiable stepwise formation of the mono-, bi- and tri-substituted complexes.[80] Three signals representing each species were successfully characterized by ^1H NMR. The three equilibrium and formation rate constants for both DMS and CH_3CN substitution reactions on *fac*-$[Re(CO)_3(H_2O)_3]^+$ can be summarized as illustrated on the chemical **Equations** below:

$$[M(CO)_3(H_2O)_3]^+ + L \underset{k_{-1}}{\overset{k_1, K_1}{\rightleftharpoons}} [M(CO)_3(L)(H_2O)_2]^+ + H_2O$$

$$[M(CO)_3(L)(H_2O)_2]^+ + L \underset{k_{-2}}{\overset{k_2, K_2}{\rightleftharpoons}} [M(CO)_3(L)_2(H_2O)]^+ + H_2O$$

$$[M(CO)_3(L)_2(H_2O)_3]^+ + L \underset{k_{-3}}{\overset{k_3, K_3}{\rightleftharpoons}} [M(CO)_3(L)_3]^+ + H_2O$$

As mentioned earlier, interchange rate constants ($k_{i,1}$) can aid in determining whether a reaction mechanism is dissociatively or associatively activated. Upon calculating $k_{i,1,}$ Grundler and Salignac noted that $k_{i,1}$ increases slightly from harder donor (TFA, O-donor) ligands to softer

donor (TU, S-donor) ligands.[81] **Table 4** shows the calculated interchange $k_{i,1}$ constant found by Grundler and Salignac on their respective ligands.[81]

Table 4 Interchange rate constants $k_{i,1}$ for substitution of water on *fac*-$[Re(CO)_3(H_2O)_3]^+$ at 298K and I =1 M.[80,81]

Ligands	$10^3 k_{f,1}^{298}/M^{-1}s^{-1}$	$10^3 k_{i,1}{}^a/s^{-1}$
H_2O^b	6.3	6.3
TFA	0.81	2.9
Br^-	1.6	5.8
CH_3CN	0.76	12.7
Pyz	1.06	17.7
THT	1.28	21.3
DMS	1.52	22
TU	2.49	41.5
$Hbipy^+$	0.42	1.5
$Hphen^+$	0.35	1.3

[a] $k_{i,1}$= ($k_{f,1}$ f)/($K_{os}n_c$) with 1/f) probability factor = 1/12, n_c = coordination number = 3, for charged ligands K_{OS} = 1.1 M^{-1} , and for neutral ligands K_{OS} = 0.24 M^{-1}. [b] k_{ex} = rate constant for the exchange of a particular water molecule. *K*os represents the equilibrium constant for the formation of the outer sphere complex.

Studies of water exchange on *fac*-$[M(CO)_3(H_2O)_3]^x$ (M= group 6 and group 7 elements, ^{x} = 0, 1+ or 2+) have also been reported in literature as they too form tricarbonyl complexes similar to the Re-based triaqua complexes. For group 7 (M = Mn^I, Tc^I, Re^I), the exchange rate reported, varied significantly with Mn-based reaction rates being the fastest, followed by Tc and then Re. Selected kinetic data for the water exchange rate (k_{ex}) on triaqua complexes of group 6, 7 and 8 is shown in **Table 5** below.[80,82]

Table 5 kinetic data for water exchange reactions on selected $[M(CO)_3]$ group 6, 7 and 8 based triaqua complexes.

Complexes	k_{ex} (at 298K) (S^{-1})	$\Delta H^{\ddagger}$ ($kJ.mol^{-1}$)	$\Delta S^{\ddagger}$ ($J.K^{-1}.mol^{-1}$)	Mechanism	pK_a
$[Cr(CO)_3(H_2O)_3]$ [a]	11×10^4	50	+20	-	< 8
$[W(CO)_3(H_2O)_3]$ [a]	31	58	-22	-	< 4.5
$[Mn(CO)_3(H_2O)_3]^+$ [a]	23	72.5	+24.4	I_d	9-10
$[Tc(CO)_3(H_2O)_3]^+$ [a]	0.49	78.3	+11.7	I_d	-
$[Re(CO)_3(H_2O)_3]^+$ [b]	6.3×10^{-4}	90.3	+14.5	I_d	7.5
$[Re(CO)_3(OH)(H_2O)_3]$ [b]	27	-	-	-	-
$[Ru(CO)_3(H_2O)_3]^{2+}$ [b]	10^{-4}-10^{-3}	-	-	-	-0.14
$[Ru(CO)_3(OH)(H_2O)_3]^+$ [b]	5.3×10^{-10}	-	-	-	-

[a] - Ref *81*, [b] - Ref *79*

[82] Grundler, P. V., Helm, L., Alberto, R., Merbach, A.E., *Inorg. Chem.* **2006**, *45*, 10378-10390.

Selected kinetic data for the substitution of water as ligand from *fac*-$[M(CO)_3(H_2O)_3]^+$ (M= Mn, Tc or Re) by either a DMS or CH_3CN are listed in **Table 6**.[82] Both the *fac*-tricarbonyl triaqua Mn^I and Tc^I complexes exhibited the same behavior as that of Re^I based complexes; indicating all three of these complexes displayed a high affinity for softer S-binding DMS than for the harder N-binding CH_3CN. Activation volume ($\Delta V^{\ddagger}$) values for some reactions were calculated and are listed in **Table 6**. These value may aid in determining the mechanism profile as it is known that a negative $\Delta V_1^{\ddagger}$ is indicative of an associatively activated mechanism and a positive one is indicative of a dissociative mode.

Table 6 Thermodynamic parameters and kinetic data for substitution of water on fac-$[M(CO)_3(H_2O)_3]^+$ (M = Mn, Tc or Re) at 298 K.

	k_1 (M^{-1})	k_1 $\times 10^{-3}$ M^{-1} s^{-1}	k'_1 $\times 10^{-3}$ s^{-1}	$\Delta H_1^{\ddagger}$ kJ mol-1	$\Delta S_1^{\ddagger}$ J K^{-1} mol^{-1}	$\Delta V_1^{\ddagger}$ cm^3 mol^{-1}
			***fac*-$[Mn(CO)_3(H_2O)_3]^+$**			
CH_3CN	4.5(2)	1750(400)	29000	83.9	+41.3	+4.2
DMS	25.2(5)	5340(2000)	89000	71.2	+8.1	+11.3
H_2O	-	-	23000(4000)	72.5	+24.4	+7.1
			***fac*-$[Tc(CO)_3(H_2O)_3]^+$**			
CH_3CN	2.9(1)	39.9(1)	665	77.8	-10	-
DMS	14.9(1)	60.8(8)	1010	70.6	-31.7	-
H_2O	-	-	490(50)	78.3	+11.7	+3.8
			***fac*-$[Re(CO)_3(H_2O)_3]^+$**			
CH_3CN	4.8(5)	0.76(4)	13	98.6	+26.6	-
DMS	8.3(1)	1.18(6)	20	-	+14.5	-12
H_2O	-	-	5.4(2)	90.3	-	-
Pyz	237(15)	1.06(5)	17.7	-	-	+5.4

Schutte and coworkers investigated the steric and electronic effects of various bidentate ligands on the water/methanol substitution on *fac*-$[Re(L,L'\text{-Bid})(CO)_3(H_2O)]^n$ (L,L′-Bid = N,N′, N,O, O,O′ bidentate ligands) under pseudo first-order conditions.[83] They obtained kinetic results that suggested that certain O,O′ bidentate ligands activate the Re metal centre more than the N,O-Bid and the N,N′-Bid ligands. Utilizing this interesting information, Schutte *et al*. investigated further the effect of water/methanol exchange on a water-soluble *fac*-$[Re(CO)_3(L,L'\text{-Bid})(X)]$ (L,L′-

[83] Schutte, M., Kemp, G., Visser, H. G., Roodt, A., *Inorg. Chem*. **2011**, *50*, 12486-12498.

BidH = tropolone, X = H_2O, methanol) using thiocyanate ions as entering ligand.[84] From the results obtained it became evident that the aqua substitution of *fac*-[$Re(CO)_3$(Trop)(H_2O)] was about 10 times faster than the substitution reaction of methanol from *fac*-[$Re(CO)_3$(Trop)(MeOH)]. This study highlighted the importance of systematically designed ligands and the power of detailed kinetic evaluations on elucidating reaction mechanisms.

Brink *et al*. investigated the kinetic activity effects on the Re(I) tricarbonyl complexes,[85] using a series of *fac*-[Re(N,O′-Bid)$(CO)_3$(L)] (N,O′-BidH = various Schiff-base ligands, L = neutral monodentate ligand). Their study was focused on the electronic effects of different Schiff-base on the activation of the Re(I) metal centre. From their results, they observed that N,O salicylidene Schiff-base ligands activated rhenium complexes significantly, yielding rapid substitution reactions with rates that were very close to the ones reported for O,O′-bid flavanoid type of ligands.[85,86]

In summary, interesting work has been extensively conducted concerning the kinetic activity effects on the Re(I), Tc(I) and Mn(I) tricarbonyl complexes. Furthermore, systematic ligands alterations seems to be playing a larger role in tuning the selectivity and reactivity of most of these complexes,[83,84,85,86] and it is thus imperative to further explore various ligand modification techniques and evaluate their effect on model radiopharmaceuticals in detail to improve the knowledge base to aid in the design of more effective drugs.

2.6 Phosphine Ligands

As stated in Chapter 1, the use and modification of phosphine based ligand systems in radiopharmaceuticals was identified as an important research focus, and this section will therefore be concluded by highlighting parameters within phosphine chemistry which are considered of importance to this PhD study.

Phosphine ligands are one of the most widely used class of ligands in organometallic chemistry because of their versatile nature.[87] These ligands act as ‘soft’ σ-donating ligands and can be

[84] Schutte, M., Roodt, A., Visser, H. G., *Inorg. Chem.* **2012**, *51*, 11996-2006.

[85] Brink, A., Visser, H. G., Roodt, A., *Inorg. Chem.* **2013**, *52*, 8950-8961.

[86] Brink, A., Visser, H. G., Roodt, A., *Inorg. Chem.* **2014**, *53*, 12480-12488.

[87] Appleby, T., Woollins, J.D., *Coord. Chem. Rev.* **2002**, *235*, 121-140.

systematically tuned to act as either mono-, bi- or tridentate ligands. They coordinate easily to various metal centers though their lone electron pairs on the phosphorus atom. Examples of different phosphines that possess various coordination modes are shown in **Figure 20**.

Ligand properties play a key role on the overall properties of an organometallic complex. Thus, one of the disadvantages of phosphine ligands is that the majority of phosphine ligands are highly air sensitive. However, one can overcome this by working on specialized equipment such as glove boxes and Schlenk lines. The second disadvantage is that most of these ligands are not water soluble, and this makes it fundamentally unfit for human drug development.

Significant research has thus focused on overcoming these two obstacles in phosphine chemistry and numerous Re/Tc phosphorus-based radiopharmaceuticals have been designed, as already been described in section **2.4.3**.

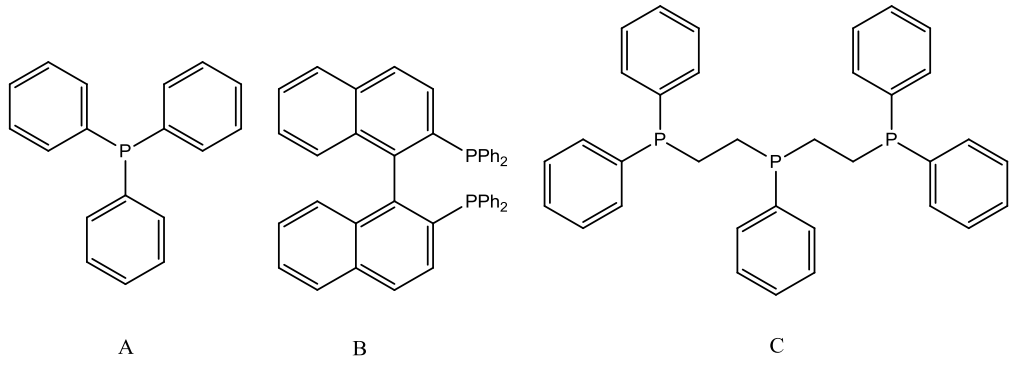

Figure 19 Tertiary phosphine ligands with different coordination modes. A = triphenylphosphine (monodentate), B = BINAP (bidentate), C = Triphos (tridentate).[88,89]

A wide variety of applications for organometallic complexes containing phosphine ligands has been reported in literature, with the majority of applications of these complexes in catalysis, luminescence, and anticancer studies.[87, 90 , 91] Organometallic complexes containing diphosphinoamine ligands $[(R_2)_2PN(R_1)P(R_2)_2]$ have been investigated extensively but

[88] Zanotti-Gerosa, A., Hems, W., Groarke, M., Hancock, F., *Platin. Met. Rev.* **2005**, *49*, 158-165.

[89] Phanopoulos, A., Miller, P.W., Long, N. J., *Coord. Chem. Rev.* **2015**, *299*, 39-60.

[90] Sainz-Gonzaloa, F. J., Elosuab, C., Fernández-Sáncheza, J. F., Popovicic, C., Fernándezc, I., F. L. Ortizc, F. L., Arreguib, F. J., Matiasb, I. R., Fernández-Gutiérreza, A., *Sens Actuators B Chem.* **2012**, *173*, 254- 261.

[91] Vergara, E., Casini, A., Sorrentino, F., Zava, O., Cerrada, E., Rigobello, M. P., Bindoli, A., Laguna, M., Dyson, P. J., *ChemMedChem.* **2010**, *5*, 96 - 102.

predominantly in the field of homogeneous catalysis in the past few years.[92,87] This sudden interest arose from the fact that a diphosphinoamine ligand offers a wide scope of versatility since they can be sterically (see **Figure 21**) and electronically altered on both the nitrogen and the phosphorus atom as was described earlier.[93]

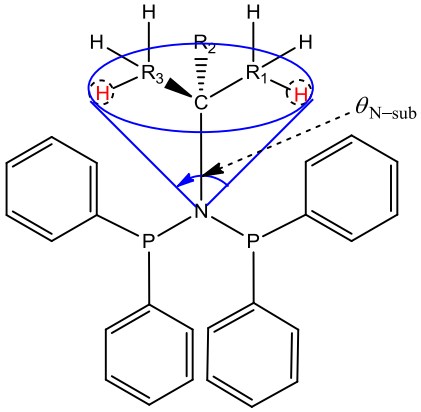

Figure 20 An example of a diphosphinoamine with a direct P-N-P back bone, the Effective Tolman-Based N-substituent ($\theta_{N\text{-}sub}$) is a steric parameter introduced to calculate the steric bulk on the nitrogen atom.[93]

2.6.1 Phosphine ligands in radiopharmaceuticals

When a [2+1] approach is to be used to synthesize radioactive tricarbonyl complexes from *fac*-$[M(CO)_3(H_2O)_3]^+$ (M = ^{99m}Tc or $^{186/188}$Re), monodentate phosphine ligands such as triphenylphosphine (PPh_3), 1,3,5-triaza-7-phosphaadamantane (PTA) and PTA/PPh_3 derivatives are generally used as neutral monodentate ligands to replace the 3rd labile remaining aqua species (**Figure 22**).[5,94,95] The PPh_3 ligand forms stable bonds with various metals and has a steric bulk that sometimes blocks extra coordination to metal centers.[96] The PTA ligand and its derivatives have an added advantage in that they are water-soluble which is a critical feature in radiopharmaceuticals.

[92] Gan, W., Fellay, C., Dyson, P. J., Laurenczy, G., *J. Coord. Chem.* **2010**, *63*, 2685-2694.

[93] Cloete, N., Visser, H. G., Engelbrecht, I., Overett, M. J., Gabrielli, W. F., Roodt, A., *Inorg. Chem.* **2013**, *52*, 2268-70.

[94] Triantis, C., Tsotakos, T., Tsoukalas, C., Sagnou, M., Raptopoulou, C., Terzis, A., Psycharis, V., Pelecanou, M., Pirmettis, I., Papadopoulos, M., *Inorg. Chem.* **2013**, *52*, 12995-3003.

[95] Papagiannopoulou, D., Triantis, C., Vassileiadis, V.; Raptopoulou, C. P., Psycharis, V., Terzis, A.; Pirmettis, I., Papadopoulos, M. S., *Polyhedron.* **2014**, *68*, 46-52.

[96] Edwards, D. S., Liu, S., *Phosphorus Sulfur Silicon Relat Elem.* **1999**, *144*, 493-496.

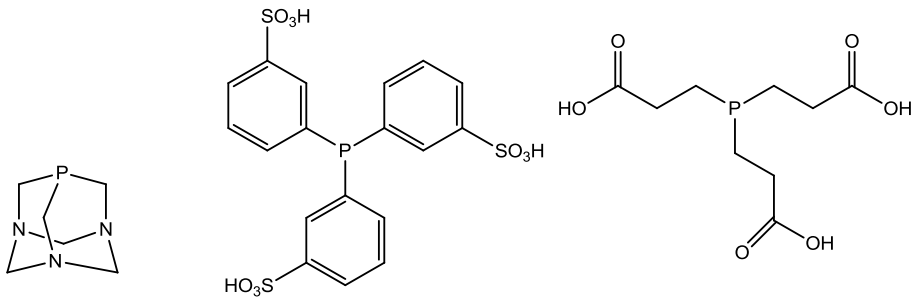

Figure 21 Examples of monodentate water-soluble tertiary phosphine ligands.[5,94,95,96]

Diphosphinoamines have also been used in radiopharmaceutical studies as bidendate ligands (**Figure 23**). Tisato et al. reported the use of diphosphinoamine ligands illustrated on Figure 23 on the synthesis of ^{99m}Tc-Nitrido synthons ($[TcN(PNP)]^{2+}$).[97] Their results indicated that coordinating diphosphinoamine ligand illustrated in **Figure 23** together with the bioactive 2-methoxyphenylpiperazine (2-MPP) pharmacophore to a Tc-Nitrido cores did not destroy the preferential affinity for $5HT_{1A}$ receptors that 2-MPP has. This interesting observation can be very useful for peripheral applications as maintaining the physiochemical property of the biomolecule is very critical in radio-labeling. Porchia et al. investigated further the use of diphosphinoamine ligands on the synthesis of radiopharmaceuticals sythons of the form *fac*- or *mer* – $[M(NPh)(PNP)]^{3+}$ (NPh = phenylamido), resulted in results that were similar to those observed by Tisato et al. for the Tc-Nitrido cores.[98]

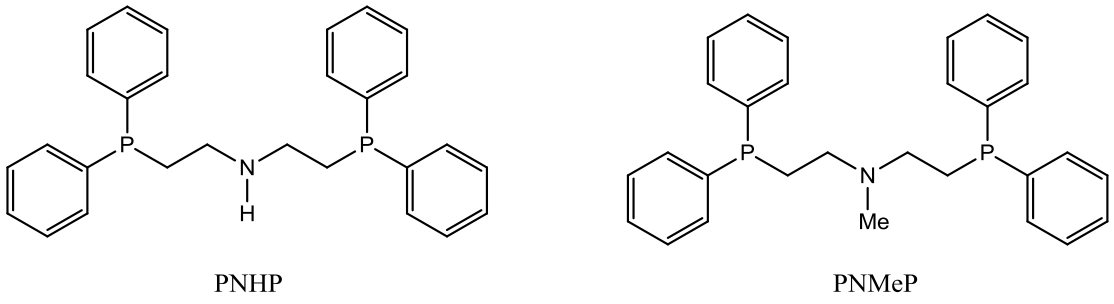

Figure 22 Diphosphinoamine ligands used by Bolzati and coworkers.[97]

[97] Bolzati, C., Malago, A. M. E., Uccelli, L., Boschi, A., Jones, A.G., Refosco, F., Duatti, A., Tisato, F., *Bioconjugate Chem.* **2003**, *14*, 1231-1242.

[98] Porchia, M., Tisato, F., Refosco, F., Bolzati, C., Cavazza-Ceccato, M., Giuliano Bandoli, G., Dolmella, A., *Inorg. Chem.* **2005**, *44*, 4766-4776.

Thieme et al. reported the successful use of a diphosphinoamine ligand similar to those utilized by Tisato et al. on the preparation of [^{188}Re(N)(PNP)] synthons and evaluated their biodistributions and imaging studies on rats.[99] They obtained promising results on their *in vivo* studies regarding the distribution of the complex and its clearance from the body. One more interesting observation was that uptake of the complexes in a sensitive organ such as the brain was not detected. These results further support the possibility of using PNP ligands for development of model radiopharmaceutical synthons.

Alberto et al. utilized water soluble bidentate phosphine ligands such as bis(bis(hydroxymethyl)phosphino)ethane and bis(bis(hydroxymethyl) phosphino)benzene as potential ligands for the development of ^{99m}Tc radiopharmaceuticals.[100] These complexes displayed both *in vivo* and *in vitro* stability upon evaluation suggesting that they can be used as chelating agents for the development of Tc and Re radiopharmaceuticals.

The use of polystyrene bound quaternary phosphines as activators of [$^{99m}TcO_4$]$^-$ has also been reported by Alberto and coworkers.[17] Through this method, they obtained [$^{99m}TcO_4$]$^-$ of high purity and could easily add a tridentade ligand such as 1,4,7-triazacyclononane to replace the phosphine group. Such methods can be used for direct synthesis of Tc/Re radiopharmaceutical building blocks.

Schiller et al. synthesized ^{188}Re complexes containing tetradentate NS_3 and monotendate P moieties.[101] Through using the Tolman cone angle and ^{31}P NMR, they observed that the *in vitro* stability of their complexes was dependent on the steric and the electronic properties of the coordinated phosphorus ligand. This stability was prominent only when the cone angles ranged between 140 and 145°. Furthermore, they observed that the hydrophilicity of the complex was increased by inserting carboxylic functions on the periphery at the monodentate phosphine ligand.

[99] Thieme, S., Agostini, S., Bergmann, R., Pietzsch, J., Pietzsch, H. J., Carta, D., Salvarese, N., Refosco, F., Bolzati, C., *Nucl. Med. Biol.* **2011**, *38*, 399-415.

[100] Schibli, R., Katti, K. V., Higginbotham, C., Volkert W. A., Alberto, R., *Nucl. Med. Biol.* **1999**, *26*, 711-716.

[101] Schiller, E., Seifert, S., Tisato, F., Refosco, F., Kraus, W., Spies, H., Pietzsch, H. -J., *Bioconjugate Chem.* **2005,** *16*, 634-643.

2.7 Conclusion

The versatility of phosphine ligand systems such as those P-N-P backbone holds great promise as radiopharmaceutical ligands more specifically when attached to favorable metal cores such as the *fac*-$[M(CO)_3]^+$ (M = Re, Tc) core. Furthermore, introduction of biologically active amine moieties on the backbone of the diphosphinoamine ligands will not only aid in tuning the bio-distribution of the radiopharmaceutical but may also ensure that the solubility of the entire complex is increased.

Moreover, the chemical analogy between Re and Tc presents the researcher with the possibility of developing Tc tricarbonyl agents as the matched pair of the analogous Re agents, making it possible to develop a radiopharmaceutical model that can attack from both the theranostic and diagnostic approach.

The overarching focus of this study as described in the following Chapters is therefore primarily on utilizing the versatile nature of the diphosphinoamine ligands and the kinetic stability of the *fac*-$[M(CO)_3]^+$ (M = Re, Tc) to develop a range of *fac*-$[M(CO)_3(PNP)]^+$ (M = Re, Tc; PNP = diphosphinoamine) complexes, which will then be fundamentally evaluated, taking cognisance of the literature as highlighted in this Chapter. The procedures and characterization methods used in developing these ligands and their respective tricarbonyl complexes is then the starting point which will be presented in detail in the following chapter.

3 Synthesis and characterization of diphosphinoamine (PNP) ligands together with Re(I), Tc(I) tricarbonyl complexes

What to expect!

The synthesis and characterization by IR, ^{1}H and ^{31}P spectroscopy of various diphosphinoamine (PNP) ligands, rhenium [Re^{I}-PNP] and technetium [$^{99/99m}Tc^{I}$-PNP] tricarbonyl complexes are described in detail in this chapter.

3.1 Introduction

The fundamental part of this project is to synthesize *fac*-$[M(L,L'\text{-Bid})(CO_3)Br]^{+}$ (M = Re^{I} or ^{99}Tc(I), L,L'-Bid = neutral bidentate coordinating PNP ligands, PNP = diphosphinoamine) complexes and evaluate both the free ligands and the metal complexes' chemical and biological activities. To achieve this, the $(NEt_4)_2[MX_3(CO)_3]$ (M = Re and ^{99}Tc, X = Br or Cl)[1] synthons were utilized as starting materials for all the metal complexes and various bidentate diphosphinoamine ligands (PNP) that were systematically tuned, both sterically and electronically, as substituents of two of the three halides atoms on the metal starting material.

The main interest focuses on the application of these complexes in diagnosis and radiotherapy aiming potentially primarily at cancer treatment. As mentioned in Chapter 2, only a small number of diphosphinoamine ligands containing technetium and rhenium compounds have been investigated as model radiopharmaceuticals. In most cases monodentate phosphine ligands are used and they are regularly deployed as ancillary ligands. [2,3,4,5,6]

[1] Alberto, R., Schibli, R., Schubiger P. A., Abram, U., Kaden A. T., *Polyhedron.* **1996**, *15*, 1079 - 1089.

[2] Bolzati, C., Mahmood, A., Malago, E., Uccelli, L., Boschi, A., Jones, A. G., Refosco, F., Duatti, A., Tisato, F., *Bioconjugate Chem.* **2003**, *14*, 1231-1242.

To increase the knowledge base of diphosphinoamine ligands as potential chelators in Tc^{I} and Re^{I} radiopharmaceutical models, a class of diphosphinoamine ligands illustrated in **Figure 3.1** were synthesized during the course of this study using the method described in **Scheme 3.1**. These ligands were specifically tuned to have systematic variations of steric and electronic properties on either the nitrogen or phosphorus atoms. All the ligands were then coordinated to a Re^{I} tricarbonyl moiety but due to the solubility issue in relevant solvents for Tc chemistry, only two ligands (**7** and **8**) were coordinated to a $^{99}Tc^{I}$ tricarbonyl complex.

To overcome this solubility challenge, a promising ligand **4** was synthesized. Although not yet executed, it is intended to increase the solubility of this ligand by either de-protecting the amine or connecting a water-soluble group such as a carboxylic acid, polyethylene glycol (PEG) or a sucrose moiety.

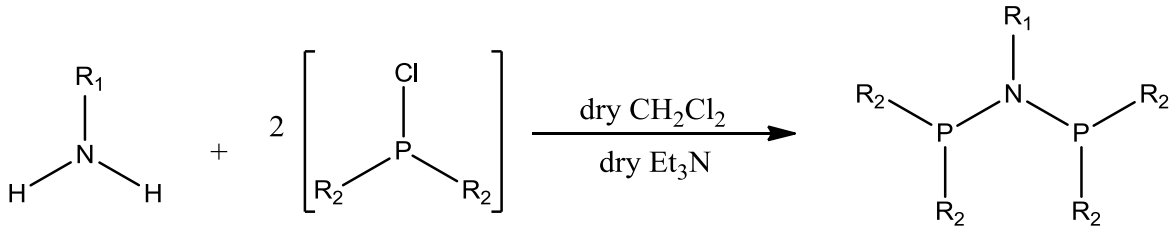

Scheme 3.1: General method for the synthesis of diphosphinoamine (PNP) ligands from a tertiary chlorophosphine reactants and a primary amine.[7,8]

[3] Porchia, M., Tisato, F., Refosco, F., Bolzati, C., Cavazza-Ceccato, M., Giuliano Bandoli, G., Dolmella, A., *Inorg. Chem.* **2005**, *44*, 4766-4776.

[4] Triantis, C., Tsotakos, T., Tsoukalas, C., Sagnou, M., Raptopoulou, C., Terzis, A., Psycharis, V., Pelecanou, M., Pirmettis, I., Papadopoulos, M., *Inorg. Chem.* **2013**, *52*, 12995-13003.

[5] Papagiannopoulou, D., Triantis, C., Vassileiadis, V., Raptopoulou, C. P., Psycharis, V., Terzis, A., Pirmettis, I., Papadopoulos, M. S., *Polyhedron.* **2014**, *68*, 46-52.

[6] Edwards, D. S., Liu, S., *Phosphorus, Sulfur, and Silicon and the Related Elements*. **1999**, *144*, 493-496.

[7] Balakrishna, M. S., Prakasha, T.K., Krishnamurthy, S. S., *J. Organomet. Chem*. **1990**, *390*, 203-216.

[8] Kuhlmann, S., Blann, K., Bollmann, A., Dixon, J.T., Killian, E., Maumela, M.C., Maumela, H., Morgan, D.H., Pretorius, M., Taccardi, N., Wasserscheid, P., *J. Catal*. **2007**, *245*, 279-284.

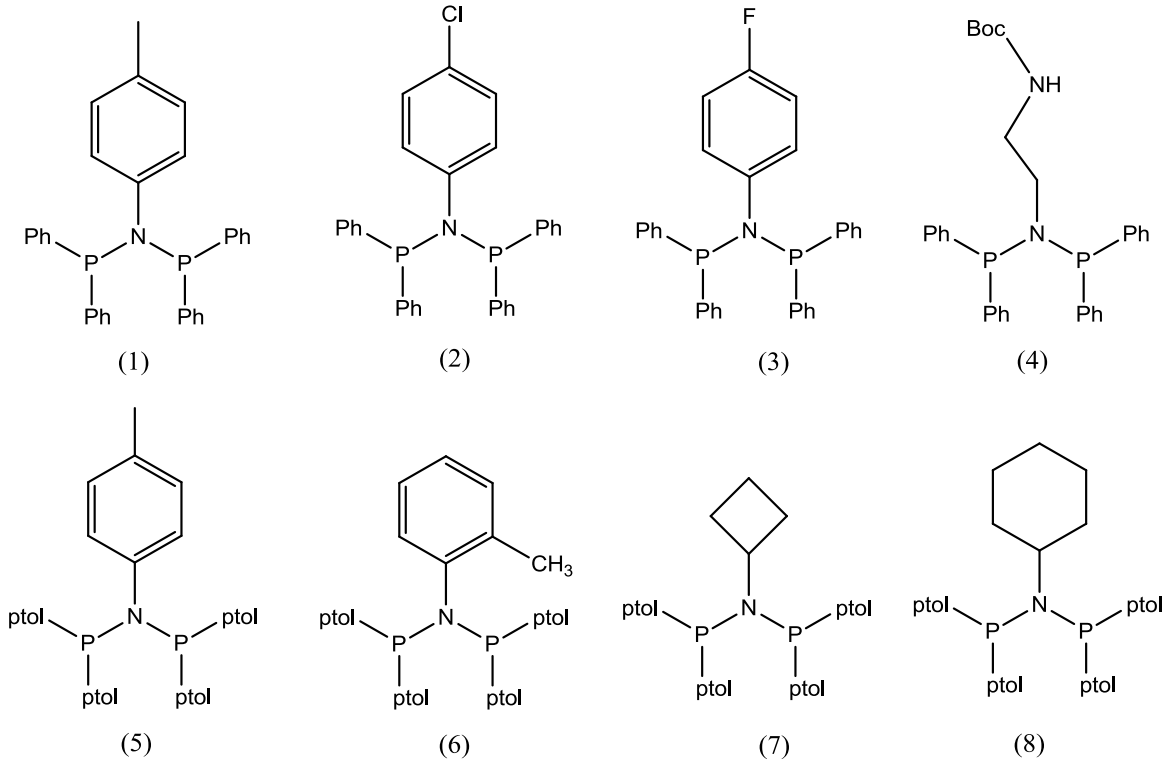

Figure 3.1: Diphosphinoamine (PNP) ligands with different electronic and steric properties on the N/P atom synthesized in this study: **1** *p*Tol-PhPNP, **2** *p*ClPh-PhPNP, **3** *p*FPh-PhPNP, 4 NBoc-PhPNP **5** *5-p*-tolyl-PNP, **6** 4-*p*-tolyl-*o*-tol, **7** Cbutyl-4-*p*-tolyl and **8** Chzyl-4-*p*-tolyl (Ph = phenyl, ptol = *para*-tolyl).

Table 3.1: Abbreviations and definition of all ligands shown in **Figure 3.1**.

No:	Abbreviations	Definition
1	*p*Tol-PhPNP	*N*,*N*-Bis(diphenylphosphino)-*p*-toluidine
2	*p*ClPh-PhPNP	*N*,*N*-Bis(diphenylphosphino)-4-chloroaniline
3	*p*FPh-PhPNP	*N*,*N*-Bis(diphenylphosphino)-4-fluoroaniline
4	NBoc-PhPNP	*N*,*N*-Bis(diphenylphosphino)- *N*-Boc-ethylenediamine
5	5-*p*-tolyl-PNP	*N*,*N*-Bis(di-*p*-tolylphosphino)-*p*-toluidine
6	4-*p*-tolyl-*o*-tol	*N*,*N*-Bis(di-*p*-tolylphosphino)-*o*-toluidine
7	Cbutyl-4-*p*-tolyl	*N*,*N*-Bis(di-*p*-tolylphosphino)cyclobutylamine
8	Chzyl-4-*p*-tolyl	*N*,*N*-Bis(di-*p*-tolylphosphino)cyclohexylamine

3.2 Materials and Methods

3.2.1 Reagents and Solvents

All chemicals (with the exception of dry solvents) used, were of analytical reagent grade, purchased from Sigma-Aldrich and were used without further purification. Dry solvents were purified and dried using methods prescribed in literature.[9] All reactions that required anhydrous conditions were performed under standard Schlenk-line conditions.

$[Re(CO)_5Br]$ was purchased from Strem Chemicals and was used as a precursor to synthesize $(NEt_4)_2[Re(CO)_3(Br)_3]$ as described in literature.[10]

CAUTION! ^{99}Tc is a weak β-emitter (E_{max} = 0.292 MeV; *half-life time* = 2.12×10^5 years). Even though radiation of small amounts of material can be completely shielded by the glass walls in a standard laboratory vessels, to avoid any contamination all ^{99}Tc experiments must be carried out in appropriately equipped laboratories.

3.2.2 Nuclear Magnetic Resonance Spectroscopy

The ^1H and ^{31}P NMR spectra were analyzed on 300 MHz Bruker FOURIER and 400 MHz AVANCE III nuclear magnetic resonance spectrometers operating at a temperature of 25 °C. For Tc-99 complexes, Bruker AV2 400 and 500 MHz NMR were used. All NMR spectra were collected using an appropriate deuterated solvent. Chemical shifts (δ), are reported in parts per million (ppm) using tetramethylsilane (TMS) as internal standard for ^1H NMR and 85 % H_3PO_4 (0 ppm) as external standard in a tightly closed capillary for ^{31}P NMR. ^{99}Tc NMR spectra were recorded relative to the signal of $[^{99}TcO_4]^-$. It should be noted that the ^{99}Tc nucleus (I = 9/2) has notable quadrupole moment, which may lead to line broadening.

3.2.3 Infrared Spectroscopy

Infrared spectra of the technetium complexes were analyzed as KBr pellets and recorded on a Bruker Tensor 27 Standard System spectrometer with a laser range of 4000 – 370 cm^{-1} coupled

[9] Perrin, D. D., Armarego.W. L. F., *Purification of Laboratory Chemicals*, 5th Ed, Great Britain: Butterworth-Heinemann Publishers, **2003**.

[10] Alberto, R., Egli, A., Abram, U., Hegetschweiler, K., Gramlich V., Schubiger, P.A., *J. Chem. Soc., Dalton Trans.* **1984**, 2815-2820.

to a personal computer. For rhenium complexes, infrared spectra were recorded on a Tensor 27 Fourier transform spectrometer (ATR) using a He-Ne laser with a laser at 632.6 nm and range of 3000 – 600 cm^{-1}.

3.3 Ligand Synthesis

All ligand synthesises were conducted under strict Schlenk conditions to minimize possible oxidation.

3.3.1 *N,N*-Bis(diphenylphosphino)-*p*-tolueneamine (1)

4-Aminotoluene (0.5423 g, 5.063 mmol) was dissolved in a dried dichloromethane (15.0 ml) and then the reaction mixture was vigorously stirred while placed in an ice bath. Triethylamine (2.2 ml, 15.78 mmol) was added to the mixture while stirring, followed by a slow addition of chlorodiphenylphosphine (2.0 ml, 10.81 mmol). The ice bath was removed after 30 min and the reaction was further stirred at room temperature for an additional 12 hours. The reaction solution was then loaded onto a column packed with neutral activated alumina (~35 g) and eluted with dichloromethane (30 mL). The solvent of the eluent was removed under reduced pressure and the white solid product was washed with cold methanol (2.150 g, 89 %).

^{1}H NMR (400.13 MHz, CD_2Cl_2) δ_H 2.23 (3H, s, 1 CH_3), 6.51 (2 H, d, *J* = 8.0 Hz, 2 CH), 6.77 (2 H, d, J = 8.1 Hz, 2 CH), 7.30 (20 H, m, 20 CH).
^{31}P NMR (161.97 MHz, CD_2Cl_2) δ_P 68.60 (s).

3.3.2 *N,N*-Bis(diphenylphosphino)-4-chloroanilineamine (2)

The synthetic procedure of this ligand was analogous to that described in **Section 3.3.1** except that 4-chloroaniline (0.640 g, 5.016 mmol) and chlorodiphenylphosphine (2.0 ml, 10.81 mmol) were used. A white solid product (2.090 g, 84 %) was obtained.

^{1}H NMR (400.13 MHz, CD_2Cl_2) δ_H 6.58 (2 H, d, *J* = 8.7 Hz, 2 CH), 6.90 (2 H, d, *J* = 8.7 Hz, 2 CH), 7.31 (20 H, m, 20 CH).
^{31}P NMR (161.97 MHz, CD_2Cl_2) δ_P 69.84 (s).

3.3.3 *N,N*-Bis(diphenylphosphino)-4-fluoroanilineamine (3)

The synthetic procedure of this ligand was analogous to that described in **Section 3.3.1** except that 4-fluoroaniline (480 μl, 5.10 mmol) and chlorodiphenylphosphine (2.0 ml, 10.81 mmol) were used. A white solid product (2.210 g, 90 %) was obtained. Single colourless crystals suitable for X-ray crystallography were obtained upon recrystallization from a mixture of dichloromethane and methanol (3:1; v/v).

^{1}H NMR (400.13 MHz, CD_2Cl_2) δ_H 6.59 (4 H, m, 4 CH), 7.34 (20 H, m, 20 CH).
^{31}P NMR (161.97 MHz, CD_2Cl_2) δ_P 70.61 (s).

3.3.4 *N,N*-Bis(diphenylphosphino)- *N*-Boc-ethylenediamine (4)

The synthetic procedure of this ligand was analogous to that described in **Section 3.3.1** except that N-Boc-ethylenediamine (807 μl, 5.10 mmol) and chlorodiphenylphosphine (2.0 ml, 10.81 mmol) were used. A white solid product (2.1787 g, 81 %) was obtained.

^{1}H NMR (300.18 MHz, CD_2Cl_2) δ_H 1.33 (9 H, m, 3 CH_3), 2.73 (2 H, d, J = 6.3 Hz, 2 CH), 3.37 (2H, m, 2 CH), 4.07 (1H, s, 1 NH), 7.37 (20 H, m, 20 CH)
^{31}P NMR (161.97 MHz, CD_2Cl_2) δ_P 63.78 (s).

3.3.5 *N,N*-Bis(di-*p*-tolylphosphino)-*p*-toluidine (5)

The synthetic procedure of this ligand was analogous to that described in **Section 3.3.1** except that 4-aminotoluene (0.2157 g, 2.013 mmol) and chloro-di(*p*-tolyl)phosphine (2.0 ml, 8.847 mmol) were used. A white solid product (0.805 g, 75 %) was obtained.

^{1}H NMR (300.18 MHz CD_2Cl_2) δ_H 2.15 (3 H, s, CH_3), 2.33 (12 H, s, 4 CH_3), 6.52 (2 H, d, J = 8.4 Hz, 2 CH), 6.78 (2 H, d, J = 8.4 Hz, 2 CH), 7.15 (8 H, m, 8 CH), 7.21 (8 H, m, 8 CH).
^{31}P NMR (161.97 MHz, CD_2Cl_2) δ_P 67.54 (s).

3.3.6 *N,N*-Bis(di-*p*-tolylphosphino)-*o*-tolueneamine (6)

The synthetic procedure of this ligand was analogous to that described in **Section 3.3.1** except that 2-aminotoluene (213.7 μl, 2.010 mmol) chloro-di(*p*-tolyl)phosphine (2.0 ml, 8.847 mmol) were used. A white solid product (0.705 g, 66 %) was obtained.

^{1}H NMR (400.13 MHz CD_2Cl_2) δ_H 2.65 (3 H, s, CH_3), 2.35 (12 H, s, 4 CH_3), 6.61 (1 H, d, *J* = 8.0 Hz, 1 CH), 6.81 (1 H, m, 1 CH), 7.02 (10 H, m, 10 CH), 7.22 (4 H, s, 4 CH), 7.31 (4 H, m, 4 CH).
^{31}P NMR (161.97 MHz, CD_2Cl_2) δ_P 60.22 (s).

3.3.7 *N,N*-Bis(di-*p*-tolylphosphino)cyclobutylamine (7)

The synthetic procedure of this ligand was analogous to that described in **Section 3.3.1** except that cyclobutylamine (171.7 µl, 2.011 mmol) chloro-di(*p*-tolyl)phosphine (2.0 ml, 8.847 mmol) were used. A white solid product (0.6531 g, 66 %) was obtained. Single colourless crystals suitable for X-ray crystallography were obtained upon recrystallization from a mixture of dichloromethane and methanol (3:1; v/v).

^{1}H NMR (300.18 MHz CD_2Cl_2) δ_H 1.35 (2 H, m, CH), 1.69 (4 H, m, 4 CH), 2.35 (12 H, s, 4 CH_3), 2.52 (2 H, m, 2 CH), 4.01 (1 H, m, 1 CH), 7.23 (16 H, m, 16 CH).
^{31}P NMR (161.97 MHz, CD_2Cl_2) δ_P 48.11 (s).

3.3.8 *N,N*-Bis(di-*p*-tolylphosphino)cyclohexylamine (8)

The synthetic procedure of this ligand was analogous to that described in **Section 3.3.1** except that cyclohexylamine (230.0 µl, 2.011 mmol) chloro-di(*p*-tolyl)phosphine (2.0 ml, 8.847 mmol) were used. A white solid product (0.5654 g, 54 %) was obtained. Single colourless crystals suitable for X-ray crystallography were obtained upon recrystallization from a mixture of dichloromethane and methanol (3:1; v/v).

^{1}H NMR (300.18 MHz CD_2Cl_2) δ_H 1.05 (3 H, m, 3 CH), 1.51 (5 H, m, 5 CH), 1.85 (2 H, m, 2 CH), 2.35 (12 H, m, 4 CH_3), 3.22 (1 H, m, 1 CH), 7.22 (16 H, m, 16 CH).
^{31}P NMR (161.97 MHz, CD_2Cl_2) δ_P 49.68 (s).

3.4 Synthesis of diaminophosphine oxides

All of the diphosphinoamine (PNP) ligands synthesised in this chapter were intentionally oxidized using hydrogen peroxide (H_2O_2) as the oxidizing agent to study their behaviour upon exposure to oxidizing agents. However, only the synthesis for ligands that yielded crystalline products suitable for single crystal analyses are described here. These dioxo (see **Figure 3.2**)

species originates from ligand **3**, **5** and **8** illustrated in **Figure 3.1**. All dioxo ligands were characterized by ^{1}H NMR, ^{31}P NMR and single crystal XRD. The crystal structures will be further discussed in detail in **Chapter 5**.

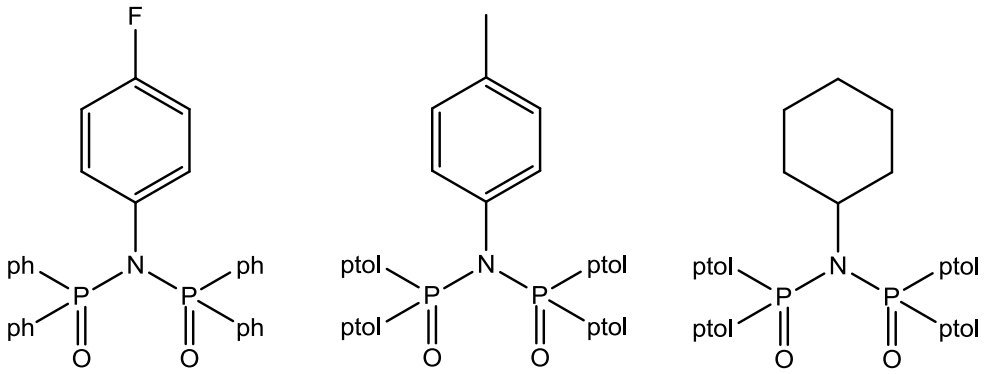

3a **5a** **8a**

Figure 3.2: Selected diphosphinoamine dioxide (PNPO) ligands with different electronic and steric properties on the N/P atom synthesized during this study

3.4.1 *N,N*-Bis(diphenylphosphineoxide)-4-fluoroanilineamine (3a)

N,N-Bis(diphenylphosphino)-4-fluoroaniline (0.10 g, 0.2086 mmol) was dissolved in dichloromethane (10 ml). Hydrogen peroxide (42.3 µl, 0.3760 mmol) was added slowly and the reaction mixture was left to stir for an hour after which the solvent was evaporated under atmospheric pressure. Recrystallization from dichloromethane/methanol (3:1, v/v) resulted in single colourless crystals suitable for X-ray crystallography (yield: 0.101 g, 95 %).

^{1}H NMR (300.18 MHz, CD_2Cl_2) δ_H 6.64 (2 H, m, 2 CH), 7.28 (14 H, m, 14 CH), 7.81 (8 H, m, 8 CH).

^{31}P NMR (161.97 MHz, CD_2Cl_2) δ_P 24.27 (s).

3.4.2 *N,N*-Bis(di-*p*-tolylphosphineoxide)-*p*-toluidine (5a)

The synthetic procedure of this ligand was analogous to that described in **Section 3.4.1** except that *N,N*-bis(di-*p*-tolylphosphino)-*p*-toluidine (0.10 g, 0.1881 mmol) was used. A white solid product was obtained and recrystallization from dichloromethane/methanol (3:1, v/v) resulted in single colourless crystals suitable for X-ray crystallography (yield: 0.0862 g, 81 %).

^{1}H NMR (400.13 MHz, CD_2Cl_2) δ_H 2.09 (3 H, d, *J* = 9.6 Hz, 1 CH_3), 2.26 (12 H, s, 4 CH_3), 6.77 (2 H, d, *J* = 8.2 Hz, 2 CH), 7.01 (8 H, m, 8 CH), 7.20 (2 H, d, *J* = 8.2 Hz, 2 CH), 7.63 (8 H, dd, *J* = 11.7, 8.1 Hz, 8 CH).

^{31}P NMR (161.97 MHz, CD_2Cl_2) δ_P 24.80 (s).

3.4.3 *N,N*-Bis(di-*p*-tolylphosphineoxide)cyclohexylamine (8)

The synthetic procedure of this ligand was analogous to that described in **Section 3.4.1** except that *N*,*N*-bis(di-*p*-tolylphosphino)cyclohexylamine (0.10 g, 0.1909 mmol) was used. A white solid product was obtained and recrystallization from dichloromethane/methanol (3:1, v/v) resulted in single colourless crystals suitable for X-ray crystallography (yield: 0.0822 g, 78 %).

^{1}H NMR (400.13 MHz, CD_2Cl_2) δ_H 0.82 (2 H, qd, *J* = 13.0, 3.1 Hz, 2 CH), 1.07 (1 H, tdd, *J* = 13.1, 9.8, 3.4 Hz, 1 CH), 1.41 (1 H, d, *J* = 13.0 Hz, 1 CH), 1.60 (4 H, d, *J* = 11.3 Hz, 4 CH), 2.36 (14 H, m, 4 CH_3 and 2 CH), 3.12 (1 H, m, 1 CH), 7.19 (8 H, m, 8 CH), 7.62 (8 Ch, m, 8 CH),

^{31}P NMR (161.97 MHz, CD_2Cl_2) δ_P 31.34 (s).

3.5 *fac*-$[Re^{I}(CO)_3]^+$ Complex Synthesis

The Re(I) and ^{99}Tc(I) tricarbonyl complexes were prepared as indicated schematically in **Scheme 3.2** below.

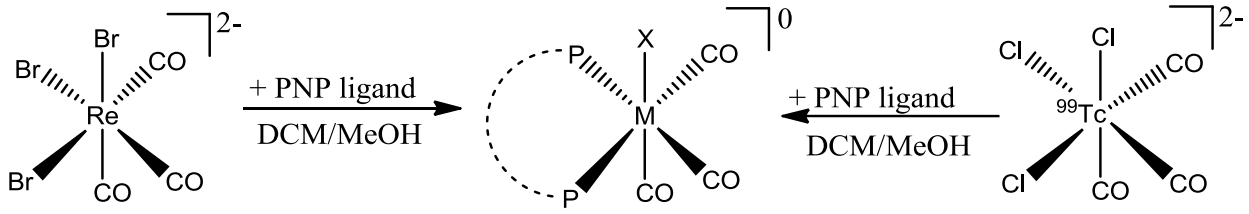

Scheme 3.2: Schematic representation of the synthesis of the *fac*-Re^{I}-PNP and *fac*-$^{99}Tc^{I}$-PNP tricarbonyl complexes from $(NEt_4)_2[Re(CO)_3Br_3]$ and $(NEt_4)_2[^{99}Tc(CO)_3Cl_3]$.

3.5.1 *fac*-$[NEt_4]_2[Re(CO)_3Br_3]$ (ReAA)

(NEt_4)Br (5.000 g, 0.02400 mol) was finely grounded into a powder in a mortar and pestle and dried in an oven at 50 ˚C for 2 hours. To the dried (NEt_4)Br on an oil bath (at 80˚C), 2,5,8-trioxanone diglyme (150 ml) was added under a nitrogen atmosphere and further heated for 1

hour. [$Re(CO)_5Br$] (5.000 g, 0.01230 mol) was then added to the mixture with vigorous stirring at 115˚C for 15 hours. The reaction mixture was cooled down to room temperature and the white precipitate was collected, washed with cold methanol and dichloromethane and then dried under vacuum. (Yield: 7.580 g, 87%). IR ν(CO, cm^{-1}): 1845.5, 1996.0.

3.5.2 *fac*-[Re(*p*Tol-PhPNP)$(CO)_3$Br]

ReAA (50.8 mg, 0.0660 mmol) was dissolved in 10 ml methanol and *N*,*N*-bis(diphenylphosphino)-*p*-toluidine (32.7 mg, 0.0687 mmol) was added to the solution. The mixture was stirred at 50 ˚C for 2 hours and then the solvent was evaporated. The resulting white solid was filtered and washed with methanol. (Yield: 31.1 mg, 57 %).

^{1}H NMR (400.13 MHz $CDCl_3$) δ_H 2.98 (3H, s, 1 CH_3), 6.55 (2H, d, J = 8.2 Hz, 2 CH), 6.77 (2 H, d, J = 8.3 Hz, 2 CH), 7.35 (16 H, m, 16 CH), 7.53 (4H, m, 4 CH).
^{31}P NMR (161.97 MHz, $CDCl_3$) δ_P 48.54 (s).
IR ν(CO, cm^{-1}): 1886, 1932, 2020.

3.5.3 *fac*-[Re(*p*Tol-PhPNP)$(CO)_3(O^iPr)$]

This complex was obtained by dissolving the *fac*-[Re(*p*Tol-PNP)$(CO)_3$Br] from **3.5.2** in dicloromethane and layering this solution with 2-Propanol. Slow evaporation of this solution resulted in white crystals suitable of X-ray analysis.

^{1}H NMR (300.18 MHz CD_2Cl_2) δ_H 1.33 (3 H, m, 1 CH_3), 2.19 (3 H, s, 1 CH_3), 3.29 (2 H, q, *J* = 7.3 Hz, 1 CH_2), 6.57 (2 H, d, *J* = 8.5 Hz, 2 CH), 6.84 (2 H, d, *J* = 8.4 Hz , 2 CH), 7.47 (20 H, m, 20 CH).
^{31}P NMR (161.97 MHz, $CDCl_3$) δ_P 58.39 (s).
IR ν(CO, cm^{-1}): 1902, 1960, 2031, 3056.

3.5.4 *fac*-[Re(*p*ClPh-PhPNP)$(CO)_3$Br]

The synthetic procedure was analogous to that described in **3.5.2** except that *N*,*N*-bis(diphenylphosphino)-4-chloroaniline (33.4 mg, 0.0673 mmol) was used. (Yield 31.5 mg, 56 %). Recrystallization from dichloromethane/methanol (3:1, v/v) resulted in single colourless crystals suitable for X-ray crystallography.

^{1}H NMR (400.13 MHz $CDCl_3$) δ_H 6.58 (2 H, d, *J*= 8.7 Hz, 2 CH), 6.94 (2H, d, *J* = 8.8 Hz), 7.40 (20 H, m, 20 CH).

^{31}P NMR (161.97 MHz, $CDCl_3$) δ_P 49.38 (s).

IR *v*(CO, cm^{-1}): 1898, 1950, 1963, 2027.

3.5.5 *fac*-[Re(*p*FPh-PhPNP)(CO)$_3$Br]

The synthetic procedure was analogous to that described in **3.5.2** except *N*,*N*-bis(diphenylphosphino)-4-fluorophenylamine (32.8 mg, 0.0651 mmol) was used. Yield (28.0 mg, 56 %). Recrystallization from dichloromethane/methanol (3:1, v/v) resulted in single colourless crystals suitable for X-ray crystallography.

^{1}H NMR (400.13 MHz $CDCl_3$) δ_H 6.66 (4 H, m, 4 CH), 7.39 (20 H, m, 20 CH).

^{31}P NMR (161.97 MHz, $CDCl_3$) δ_P 49.91 (s).

IR *v*(CO, cm^{-1}): 1900, 1950, 1963, 2027.

3.5.6 *fac*-[Re(NBoc-PhPNP)(CO)$_3$Br]

The synthetic procedure was analogous to that described in **3.5.2** except *N*,*N*-bis(diphenylphosphino)- N-Boc-ethylenediamine (34.4 mg, 0.0601 mmol) was used. Yield (28.0 mg, 51 %). Recrystallization from dichloromethane/methanol (3:1, v/v) resulted in single colourless crystals suitable for X-ray crystallography.

^{1}H NMR (400.13 MHz, CD_2Cl_2) δ_H 1.40 (9 H, s, 3 CH_3), 2.93 (2 H, m, 2 CH), 3.18 (2 H, m, 2 CH), 4.27 (1 H, s, 1 NH), 7.84 (20 H, m, 20 CH),

^{31}P NMR (161.97 MHz, CD_2Cl_2) δ_P 46.15 (s).

IR *v*(CO, cm^{-1}): 1700, 1895, 1947, 2028, 2932, 2980, 3059, 3384.

3.5.7 *fac*- [Re(5-*p*-tolyl-PNP)(CO)$_3$Br]

The synthetic procedure was analogous to that described in **3.5.2** except *N*,*N*-bis(di-*p*-tolylphosphino)-*p*-toluidine (35.10 mg, 0.066 mmol) was used (Yield: 33.6 mg, 58%).

^{1}H NMR (400.13 MHz, $CDCl_3$) δ_H 2.13 (3 H, s, 1 CH_3), 2.28 (6 H, s, 2 CH_3), 2.33 (6 H, s, 2 CH_3), 6.56 (2 H, m, 2 CH), 6.76 (2 H, d, J = 8.2 Hz, 2 CH), 7.07 (4 H, m, 4 CH), 7.13 (4 H, m, 4 CH), 7.27 (4 H, m, 4 CH), 7.38 (4 H, m, 4 CH).

^{31}P NMR (161.97 MHz, $CDCl_3$) δ_P 47.77 (s), 51.27 (s).

IR ν(CO, cm^{-1}): 1907, 1963, 2029.

3.5.8 *fac*-[Re(4-*p*-tolyl-*o*-tol-PNP)(CO)$_3$Br]

The synthetic procedure was analogous to that described in **3.5.2** except *N*,*N*-bis(di-*p*-tolylphosphino)-*o*-tolueneamine (31.40 mg, 0.0591 mmol) was used. Yield (30.2 mg, 60 %).

^{1}H NMR (400.13 MHz $CDCl_3$) δ_H 2.22 (15 H, m, 5 CH_3), 7.11 (20 H, m, 20 CH).

^{31}P NMR (161.97 MHz, $CDCl_3$) δ_P 44.3 (s).

IR ν(CO, cm^{-1}): 1905, 1943, 2027.

3.5.9 *fac*-[Re(Cbutyl-4-*p*-tolyl)(CO)$_3$Br]

The synthetic procedure was analogous to that described in **3.5.2** except *N*,*N*-bis(di-*p*-tolylphosphino)cyclobutylamine (32.2 mg, 0.0662 mmol) was used. Yield (32.9 mg, 56 %). Recrystallization from dichloromethane/methanol (3:1, v/v) resulted in single colourless crystals suitable for X-ray crystallography.

^{1}H NMR (400.13 MHz $CDCl_3$) δ_H 1.14 (2 H, m, 2 CH), 1.46 (2 H, s, 2 CH), 1.77 (2 H, m, 2 CH), 2.35 (12 H, s, 4 CH_3), 3.73 (1 H, m, 1 CH),7.21 (8 H, m, 8 CH), 7.51 (4 H, m, 4 CH), 7.61 (4 H, m, 4 CH).

^{31}P NMR (161.97 MHz, $CDCl_3$) δ_P 42.3 (s).

IR ν(CO, cm^{-1}): 1881, 1905, 1940, 2021.

3.5.10 *fac*-[Re(Chzyl-4-*p*-tolyl)(CO)$_3$Br]

The synthetic procedure was analogous to that described in **3.5.2** except *N*,*N*-bis(di-*p*-tolylphosphino)cyclohexylamine (34.0 mg, 0.0649 mmol) was used (Yield: 45.5 mg, 80 %). Recrystallization from dichloromethane/methanol (3:1, v/v) resulted in single colourless crystals suitable for X-ray crystallography.

^{1}H NMR (400.13 MHz, $CDCl_3$) δ_H 0.58 (1 H, m, 1 CH), 0.75 (2 H, m, 2 CH), 0.91 (2 H, m, 2 CH), 1.30 (5 H, d, m,5 CH), 2.37 (12 H, d, J= 8.5 Hz, 4 CH_3), 3.07 (1 H, m, 1 CH), 7.19 (8 H, m, 8 CH), 7.55 (4 H, m, 4 CH), 7.70 (4 H, m, 4 CH)

^{31}P NMR (161.97 MHz, $CDCl_3$) δ_P 43.2 (s).

IR ν(CO, cm^{-1}): 1890, 1944, 2008.

3.6 *fac*-[^{99}Tc^{I}(CO)$_3$]$^+$ Complex Synthesis

$[NEt_4]_2[^{99}TcCl_3(CO)_3]$ was synthesized in an appropriately equipped radio-laboratory using a procedure reported by Alberto and coworkers.[11]

3.6.1 *fac*-[^{99}Tc(5-*p*-tolyl-PNP)(CO)$_3$Cl]

^{99}TcAA (17.4 mg, 0.0320 mmol) was dissolved in methanol (6.00 ml). *N*,*N*-bis(di-*p*-tolylphosphino)-*p*-toluidine (18.3 mg, 0.034 mmol) was dissolved in dichloromethane (4 ml) and added to the first solution. The reaction mixture was stirred at 50 ˚C for 24 hours and then the solvent was evaporated. The resulting orange solid was then dissolved in dichloromethane and layered with 2-propanol and left to recrystallize.

^{99}Tc NMR (90.1 MHz, $CDCl_3$) δ_{Tc} -957.63 (sharp peak), -1045.82 (sharp peak), -1525.50 (broad peak), -1601.08 (broad peak).

^{31}P NMR (162 MHz, $CDCl_3$) δ_P 20.32 (s), 23.03 (s), 25.66 (s), 35.55 (s).

Upon further investigation utilizing single crystal XRD it was observed that the P-N bond was cleaved. This motivated our investigation as to possible oxidation mechanisms which will influence the stability of the PNP ligand system as presented in paragraph 3.4.

[11] Alberto, R., Schibli, R., Schubiger, P. A., Abram, U., Kaden, A. T., *Polyhedron.* **1996,** *15*, 1079 - 1089.

3.6.2 *fac*-[^{99}Tc(Cbutyl-4-*p*-tolyl)(CO)$_3$Cl]

^{99}TcAA (27.8 mg, 0.051 mmol) was dissolved in DCM (4.00 ml). *N*,*N*-Bis(di-*p*-tolylphosphino)cyclobutylamine (25.0 mg, 0.054 mmol) was dissolved in DCM (4 ml) and added to the first solution. The reaction mixture was stirred at 55 ˚C overnight whereafter the solvents were evaporated under reduced pressure. The resulting solid was washed with H_2O and dried under vacuum. (Yield: 35.0 mg, 96 %).

^{99}Tc NMR (90.1 MHz, $CDCl_3$) δ_{Tc} -1472.98 (broad peak).

^{31}P NMR (162 MHz, $CDCl_3$) δ_P 69.86 (broad peak).

IR ν(CO, cm^{-1}): 1918,1961, 2035.

3.6.3 *fac*-[^{99}Tc(Chzyl-4-*p*-tolyl)(CO)$_3$Cl]

^{99}TcAA (29.6 mg, 0.054 mmol) was dissolved in dichloromethane (4.0 ml). *N*,*N*-Bis(di-*p*-tolylphosphino)cyclohexylamine (24.9 mg, 0.048 mmol) was dissolved in DCM (4 ml) and added to the first solution. The reaction mixture was stirred at 55 ˚C overnight whereafter the solvents were evaporated under reduced pressure. The resulting solid was washed with H_2O and dried under vacuum. (Yield: 33.0 mg, 90 %). Crystals suitable for X-ray diffraction were obtained by recrystalization in dichloromethane.

^{1}H NMR (400 MHz $CDCl_3$) δ_H 1.06 (3 H, m, 3 CH), 1.53 (5 H, m, 5 CH), 1.89 (2 H, dd, *J* = 22.7, 11.2 Hz, 2 CH), 2.38 (12 H, d, s, 4 CH_3), 3.24 (1 H, m, 1 CH), 7.18 (16 H, m, 16 CH).

^{99}Tc NMR (90.1 MHz $CDCl_3$) δ_{Tc} -1452.49 (broad peak).

^{31}P NMR (162 MHz, $CDCl_3$) δ_P 68.69 (broad peak).

IR ν(CO, cm^{-1}): 1918, 1964, 2038

3.7 Discussion

Ligand synthesis: All PNP ligands namely *p*Tol-PhPNP (**1**), *p*ClPh-PhPNP (**2**), *p*FPh-PhPNP (**3**), NBoc-PhPNP (**4**), 5-*p*-tolyl-PNP (**5**), 4-*p*-tolyl-*o*-tol (**6**), Cbutyl-4-*p*-tolyl (**7**) and Chzyl-4-*p*-tolyl (**8**) were synthesized successfully using pre-selected amines and chlorophosphine precursors. The synthetic methods used were similar to those previously reported in literature.[7,8,12,13] The synthesis of the PNP ligands allowed for specific manipulations and resulted in systematic adjustments to both steric and electronic properties. Overall high yields were obtained and the ligands were stable after the removal of impurities by washing with specific solvents described in each synthesis procedure.

Ligands **1**, **2** and **3** are similar in that they each contain two phenyl substituents on the P atoms and differ only by the substituent on the *para* position of the phenyl ring attached to the N atom. These variations were systematically chosen to induce different electronic effects on the N atom. The last four ligands (**5**, **6**, **7** and **8**) contain a tetra-*p*-tolyl PNP backbone and vary only by the substituent on the N atom. The *p*-tolyl groups on the P atom were chosen to induce different steric effects on the P atom, while the *p*-toly, *o*-tolyl, cyclobutyl and cyclohexyl goups on the N atom were selected for systematic variations of the steric bulk on the N atom. To study the spatial arrangements of these ligands, X-ray crystallographic analysis were conducted for ligands **3**, **7** and **8** and will be discussed in detail in **Chapter 4**.

The ultimate purpose was always to coordinate the PNP ligands to the $[M(CO)_3]^+$ (M = Re or ^{99}Tc). Upon coordination of the 5-*p*-tolyl-PNP (**5**)[14] to $[M(CO)_3]^+$ (M = Re or ^{99}Tc), the PNP ligand was found to be cleaved (**Figure 3.3**). This was very clear from the two ^{31}P resonance peaks at 47.77 and 51.27 ppm observed for the Re complex and 20.23, 23.03, 25.66, 35.55 ^{31}P resonance peaks observed for the Tc complex. We therefore decided to study the stability, oxidative nature and the spatial arrangements of these PNP ligands by intentionally oxidizing the free ligands (**1** to **8**) using hydrogen peroxide. This process was followed by ^{31}P NMR (**Table**

[12] Cloete, N., Visser, H. G., Roodt, A., Gabrielli, W. F., *Acta Cryst.* **2009,** E*65*, o3081.

[13] Engelbrecht, I., Visser, H. G., Roodt, A., *Acta Cryst.* **2011,** E*67*, o2041-o2042.

[14] See **Chapter 5** of this PhD thesis for detailed crystallographic information.

3.2) and in cases where suitable single crystals were obtained, X-ray crystallographic analysis was done and will be discussed in detail in **Chapter 5**.

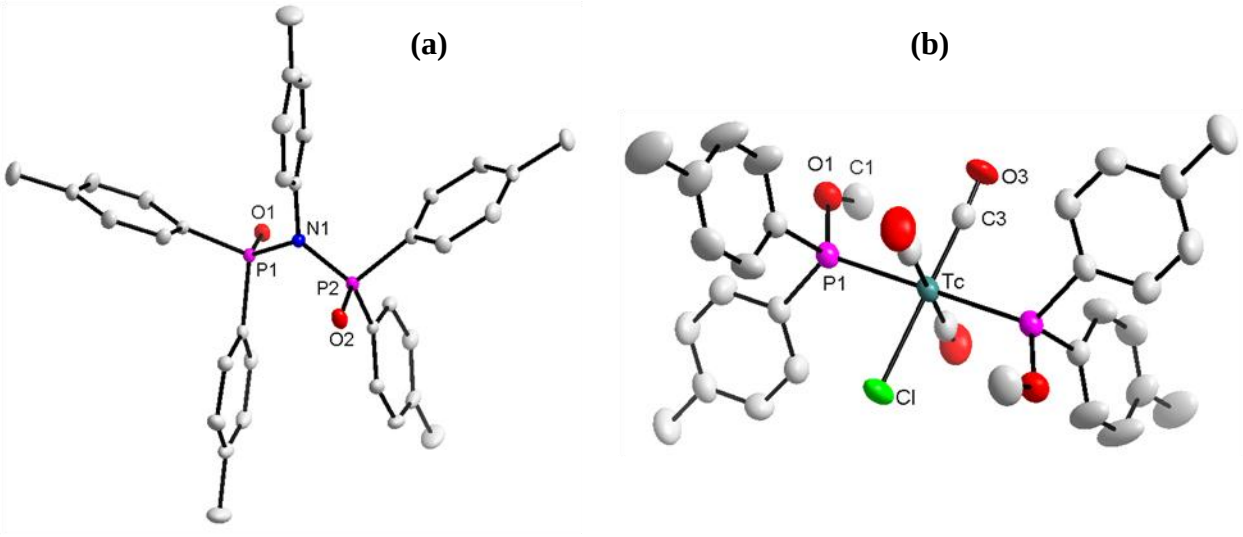

Figure 3.3 Crystal structures of oxidized (**a**) 5-*p*-tolyl-PNP[14] ligand and a methanol cleaved (**b**) 5-*p*-tolyl-PNP ^{99}Tc complex.[(a) crystal system = Triclinic, space group = $P\bar{1}$, Z= 2, Rint = 0.0461 and 99.5% completeness; **(b)** crystal system = zmonoclinic, space group = $P2_1/c$, Z= 4, Rint = 0.0343 and 99.9% completeness].

Owing to their internal symmetry, the ^{31}P NMR (**Table 3.2**) data of both the free and the oxidized PNP ligands were fairly easily interpretable as they gave singlet ^{31}P resonance peaks. The free PNP ligands gave singlets with chemical shifts varying roughly between 48 and 70 ppm. Upon oxidation, the peak range shifted to between 31 and 20 ppm indicating a significant electronic change between the free and the oxidized ligands. No second order P–P coupling was observed for both the free and the oxidized ligands. These results confirm the high purity of the bulk material obtained from these ligand syntheses which is critical when evaluating biological studies.

To increase the versatility and solubility of these ligands, a new system of PNP ligands containing functional groups such as carboxylic acids and amines is on the development stage. Ligand **4** in **Figure 3.1** was obtained from using a protected amine and forms part of this new system. This ligand (**4**) also contains the tetraphenyl PNP backbone similar to ligand **1**, **2** and **3**, but differ significantly by the N-Boc-ethylenediamine moiety on the N atom. Of all the ligands synthesized, Ligand **4** dissolves easily in multiple solvents unlike the remaining PNP ligands and has become a subject in further investigation. Another ligand containing a water soluble group

(aminobutyric acid) on the N atom similar to ligand 4 is also been investigated but so far the pure product could not be isolated.

Rhenium and Technetium complex synthesis: All of the ligands described in **Figure 3.1** were coordinated according to **Scheme 3.2** to a rhenium moiety using $(Et_4N)_2[Re(CO)_3Br_3]$ (ReAA) as the metal precursor. The majority of these complexes gave reasonably good yields and yielded crystalline products suitable for X-ray analysis. Because of this, Re(I) tricarbonyl complexes proved to be excellent models for solid state analysis.

The ^{99}Tc(I) tricarbonyl complexes behaved in a similar fashion to those of the rhenium core however due to most of the ligands' insolubility in water, it was not possible to conduct reactions using the more radiopharmaceutical appropriate ^{99m}Tc. However, to confirm proof-of-concept for the Tc-PNP complexes, three experiments were evaluated using ^{99}TcAA and from the characterization by IR, ^{31}P and ^{99}Tc NMR it was clear that the ^{99}Tc(I) tricarbonyl complexes were behaving in a similar manner as the Re(I) tricarbonyl complexes with similar ligands. The crystal structures of similar ^{99}Tc- and Re-PNP ligands are evaluated in **Chapter 7**. A comparison of the ^{31}P NMP peaks of free and metal coordinated ligands is illustrated in **Table 3.2** below.

Table 3.2: ^{31}P NMR data of the free PNP and PNPO ligands versus the Re/Tc coordinated ligands.

	Ligands	^{31}P NMR	^{31}P NMR (Oxidized)	^{31}P NMR (Re-PNP)	^{31}P NMR (Tc-PNP)
1	*N*,*N*-Bis(diphenylphosphino)-*p*-toluidine	68.60	24.14[b]	48.54	-
2	*N*,*N*-Bis(diphenylphosphino)-4-chloroaniline	69.84	24.55[b]	49.38	
3	*N*,*N*-Bis(diphenylphosphino)-4-fluoroaniline	70.61	24.27	49.91	-
4	*N*,*N*-Bis(diphenylphosphino)-*N*-Boc-ethylenediamine	63.78	31.69[b]	46.15	-
5	*N*,*N*-Bis(di-*p*-tolylphosphino)-*p*-toluidine	67.54	24.80	47.77 & 51.27 [a]	20.23, 23.03, 25.66 & 35.55 [a]
6	*N*,*N*-Bis(di-*p*-tolylphosphino)-*o*-toluidine	60.22	25.34[b]	44.30	-
7	*N*,*N*-Bis(di-*p*-tolylphosphino)cyclobutylamine	48.11	30.31[b]	42.30	69.86 (broad peak)
8	*N*,*N*-Bis(di-*p*-tolylphosphino)cyclohexylamine	49.68	31.34	43.20	68.69 (broad peak)

[a] indicative of a cleaved P-N bond of the PNP ligand. [b] indicates values obtained from ^{31}P NMR experiments were by a 1:2 mole ration of PNP:H_2O_2 was utilized. Typical ^{31}P NMR experimental conditions involved 10 mg of PNP mixed with 4 ul of H_2O_2 in 600 ul of a deuterated dichloromethane solvent, using a 5 mm NMR tube.

3.8 Conclusion

The synthetic procedure and characterization of 8 PNP ligands namely *p*Tol-PhPNP (**1**), *p*ClPh-PhPNP (**2**), *p*FPh-PhPNP (**3**), NBoc-PhPNP (**4**), 5-*p*-tolyl-PNP (**5**), 4-*p*-tolyl-*o*-tol (**6**), Cbutyl-4-*p*-tolyl (**7**) and Chzyl-4-*p*-tolyl (**8**) is described in details in this chapter. Moreover, interests in stability and oxidation of these PNP ligands lead to the synthesis of oxidized PNP ligand systems. This interest was induced by amongst other, the cleaving of the P-N bond observed in one of the Re and the Tc complexes.

To evaluate the application of these PNP ligands to radiopharmaceutical drug development, eight Re-PNP and three ^{99}Tc-PNP tricarbonyl complexes were synthesized. However, solubility challenges hampered the formation of ^{99m}Tc-PNP complexes. This solubility issue is currently being addressed by new synthetic methods were by more water soluble groups such as carboxylic acids and amines will be attached on the periphery of the PNP ligands, as illustrated by ligand **4**. The ultimate goal is to manipulate the solubility of the PNP ligand to create physiologically acceptable $^{186/188}$Re and ^{99m}Tc complexes which can be characterized or administered in appropriate solvents such as water, ethanol or dimethyl sulfoxide.

4 Single crystal X-ray diffraction study of diphosphinoamine ligands

What to expect!

A detailed crystallographic evaluation of three non-coordinated diphosphinoamine (PNP) ligands will be presented in this chapter.

4.1 Introduction

A detailed literature review revealed that success in many organometallic oriented researches can be attributed significantly to systematic ligand design. The major application of stepwise ligand design is in catalysis and radiopharmaceuticals. For example, since the Wilkinson catalyst was reported, intense research on manipulating the steric and electronic nature of phosphine ligands for catalytic purposes has increased.[1] On the other hand, after the report of aqueous tricarbonyl (*fac*-$[M(CO)_3(H_2O)_3]^+$) complexes by Alberto and coworkers,[2] a great amount of work has gone into systematically designing mono-, bi- and tridentate ligands that can substitute the three labile water molecule and increase the activity and the selectivity of the respective complex.

Without any doubt, phosphine ligands are a widely utilized ligand system in organometallic chemistry.[1] Literature searches revealed a wide range of mono-, bi- and tridentate tertiary phosphine ligands utilized across various disciplines in natural sciences.[3] In this study, various diphosphinoamine (PNP) ligands were systematically synthesized to obtain different steric and electronic properties on the N or P atom (see **Chapter 3**). As illustrated in **Figure 4.1**, three ligand crystal structures namely *N*,*N*-bis(diphenylphosphino)-4-fluoroaniline, *N*,*N*-bis(di-*p*-tolylphosphino)cyclobutylamine and *N*,*N*-bis(di-*p*-tolylphosphino)cyclohexylamine will be

[1] Appleby, T., Woollins, J. D., *Coord. Chem. Rev.* **2002,** *235*, 121-140.

[2] Alberto, R., Schibli R., Waibel R., Abram U., Schubiger P. A., *Coord. Chem. Rev.* **1999,** *190*, 901-919.

[3] Groom, C. R., Bruno, I. J., Lightfoot, M. P., Ward, S. C., *Acta Cryst.* **2016,** *B72*, 171-179

discussed in this chapter. The general crystallographic data and refinement parameters of these compounds are summarized in **Table 4.1**.

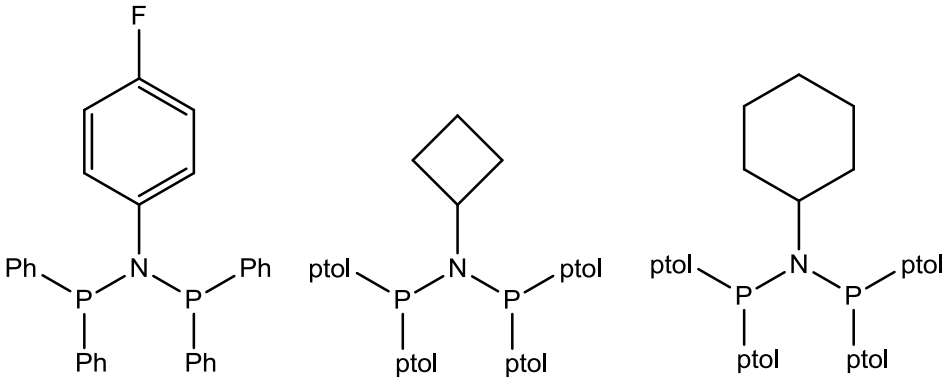

3 (*p*FPh-PhPNP) **7** (Cbutyl-4-*p*-tolyl) **8** (Chzyl-4-*p*-tolyl)

Figure 4.1 Examples of diphosphinoamine (PNP) ligands with different electronic and steric properties on the N/P atom synthesized in this study: (**3**) *N*,*N*-Bis(diphenylphosphino)-4-fluoroaniline **(***p*FPh-PhPNP), (**7**) *N*,*N*-Bis(di-*p*-tolylphosphino)cyclobutylamine **(**Cbutyl-4-*p*-tolyl) and (**8**) *N*,*N*-Bis(di-*p*-tolylphosphino)cyclohexylamine **(**Chzyl-4-*p*-tolyl). Molecular numbering is reminiscent of that found in **Chapter 3**. (Ph = phenyl, *p*-tolyl = *para*-tolyl, cbutyl = cyclobutyl, chzyl = cyclohezyl).

The main focus will be to investigate the steric and electronic effects induced by the R-group (*p*FPhenyl, cyclobutyl and cyclohexzyl) on the N atom as illustrated in **Figure 4.1**.

Various possible conformations of non-coordinated solid state disphosphinoamine ligands have been reported in literature.[4] The conformation of the type C_{2V}′ experiences the highest steric interactions between the groups on the phosphorus atom and thus it is the least favored one. Conformations C_{2V} and C_S were thus predicted for these types of compounds synthesized in this study. The three conformations are illustrated in **Figure 4.2.** It has been suggested that the higher the steric bulk on the R group the more likely is it that the C_S conformation will be observed.

[4] Keat, R., Manojlovic-Muir, L., Muir, K. W., Rycroft, D. S., *J. Chem. Soc. Dalton Trans*, **1981**, 2192-2198.

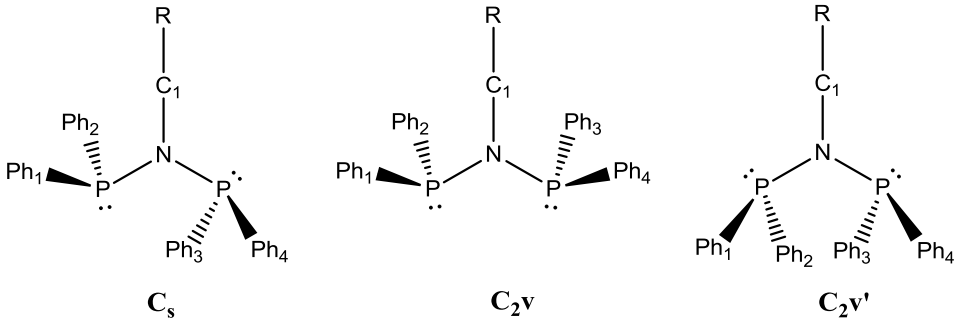

Figure 4.2 Various possible diphosphinoamine conformations. (Ph = phenyl group, R = alkyl group).

Conformations adopted by the three ligands presented in **Figure 4.1** will be discussed in the following paragraphs.

To define the steric bulk induced by these ligand, a steric parameter defined as the *Effective Tolman-based N-substituent steric effect* ($\theta_{N\text{-}sub}$) (**Figure 4.3**) which mimics the original Tolman cone angle reported in literature[5] will be used to calculate the steric bulk represented by the R group coordinated to the N atom (see **Figure 4.2**) of the presented ligands (see **Figure 4.1**). The value of $\theta_{N\text{-}sub}$ is calculated using **Equation 4.1** described below.

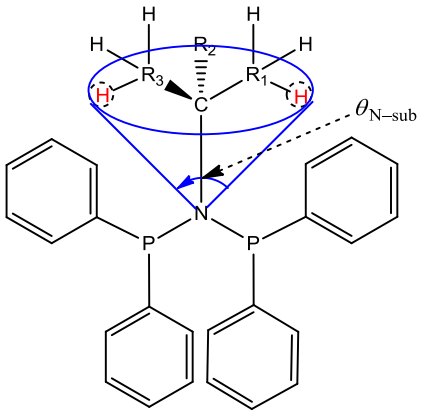

Figure 4.3 The *Effective Tolman-Based N-substituent* ($\theta_{N\text{-}sub}$), a steric parameter used to calculate the steric bulk on the nitrogen atom of diphosphinoamine ligands.

$$\theta = \frac{2}{3}\sum_{i=1}^{3}\frac{\theta_i}{2} \qquad \ldots\ldots \textbf{Equation 4.1}$$

To elucidate the conformation adopted by these ligands (**3**, **7** and **8**) and the steric bulk ($\theta_{N\text{-}sub}$) presented by the R group (*p*FPhenyl, cyclobutyl and cyclohexyl) attached to the N atom,

[5] Cloete, N., Visser, H. G., Engelbrecht, I., Overett, M. J., Gabrielli, W. F., Roodt, A., *Inorg Chem.* **2013,** *52,* 2268-2270.

diffraction data were collected for each ligand and the crystal structures were solved using programs described in the following paragraph.

4.2 Experimental

Diffraction data for (**3**) *p*FPh-PhPNP, (**7**) Cbutyl-4-*p*-tolyl and (**8**) Chzyl-4-*p*-tolyl were collected at 100 K on a Bruker X8 Apex II 4K diffractometer using monochromated Mo Kα radiation with a wavelength of λ = 0.71073 Å. All the cell parameters were refined using the XPREP4 and SAINT-Plus[6] program while SADABS[7] and multiscan techniques were used for the absorption corrections. The structures were solved by either the direct methods or by the use of SIR97[8] and refined on F^2 using anisotropic displacement parameters for all non-hydrogen atoms. SHELXL-97 [9, 10] and WinGX [11] were used for structure solutions and refinements respectively. The molecular graphics were drawn using the DIAMOND program.[12] All aromatic, methylene and methyl hydrogen atoms were placed in geometrically idealized positions (C-H = 0.95 Å to 0.98 Å) and constrained to ride on their parent atoms with $U_{iso}(H) = 1.2U_{eq}(C)$ and $U_{iso}(H) = 1.5U_{eq}(C)$ respectively.

For all three PNP ligands, a summary of the general crystal data and refinement parameters is given in **Table 4.1**. A complete list of the bond distances, bond angles, atomic coordinates, hydrogen coordinates, torsion angles and anisotropic displacement parameters for these ligands are found in the supplementary data (**Appendix A**). However, in the paragraphs that follow, selected bond distances and angles are also listed and discussed. Hydrogen atoms and numbering for certain carbon atoms were omitted for clarity on some molecular structures. For aromatic rings, the first and the second digit represents the ring number and the specific C- atom in the ring respectively.

[6] *SAINT-Plus*, version 6.02 (including XPREP); Bruker AXA, Inc.: Madison, WI, USA, **1999**.

[7] *SADABS*, version 2004/1; Bruker AXS, Inc.: Madison, WI, USA, **2004**.

[8] Altomare, A., Burla, M.C., Camalli, M., Cascarano, G.L., Giacovazzo, C., Guagliardi, A., Moliterni, A.G.G., Polidori, G., Spagna,R., *J. Appl. Cryst*., **1999**, *32*, 837-838.

[9] Sheldrick, G. M., SHELXL97; University of Göttingen: Göttingen, Germany, **1997**.

[10] Sheldrick, G. M., *Acta Crystallogr*. **2008**, *A64*, 112-122.

[11] Farrugia, L. J., *J. Appl. Crystallogr*. **1999**, *32*, 837-838.

[12] Brandenburg, K., Putz, H., DIAMOND, release 3.1b; Crystal Impact GbR: Bonn, Germany, **2005**.

Table 4.1 General X-ray crystal data and refinement parameters of (**3**) *p*FPh-PhPNP, (**7**) Cbutyl-4-*p*-tolyl and (**8**) Chzyl-4-*p*-tolyl.

Crystallographic data	***p*FPh-PhPNP (3)**	**Cbutyl-4-*p*-tolyl (7)**	**Chzyl-4-*p*-tolyl (8)**
Empirical formula	$C_{30}H_{24}F_1N_1P_2$	$C_{32}H_{35}N_1P_2$	$C_{34}H_{39}N_1P_2$
Formula weight (g mol^{-1})	479.44	495.55	523.60
Temperature (K)	100(2)	100(2)	100(2)
Crystal system	Monoclinic	Triclinic	Triclinic
Space group	$P2_1/n$	$P\bar{1}$	$P\bar{1}$
Unit cell dimensions			
a (Å)	10.157(2)	11.471(2)	10.145(2)
b (Å)	14.003(2)	12.020(2)	12.466(3)
c (Å)	17.266(3)	12.232(2)	13.495(4)
α (°)	90	64.263(4)	75.985(2)
β (°)	99.790(3)	82.100(5)	69.761(2)
γ (°)	90	68.273(5)	67.446(2)
Volume (Å^3)	2420(16)	1710.7(4)	1467(11)
Z	4	2	2
Density (g cm^{-3})	1.532	1.167	1.185
Crystal colour	Colourless	Colourless	Colourless
Crystal morphology	Cuboid	Cuboid	Cuboid
Crystal size (mm^3)	0.493 x 0.352 x 0.244	0.450 x 0.360 x 0.280	0.399 x 0.164 x 0.154
μ (mm^{-1})	0.207	0.174	0.171
F(000)	1000	528	560
θ range (°)	1.883 - 27.999	1.912 - 28.000	1.621 - 27.999
	$-13 \le h \le 13$	$-15 \le h \le 15$	$-9 \le h \le 13$
Index ranges	$-18 \le k \le 18$	$-15 \le k \le 15$	$-15 \le k \le 16$
	$-17 \le l \le 22$	$-12 \le l \le 16$	$-17 \le l \le 17$
Reflections collected	43293	25431	27786
Unique reflections	5830	6745	7071
Reflections with I > 2σ(I)	5004	5375	4649
R_{int}	0.0600	0.0544	0.0775
Completeness to theta (°, %)	25.2, 99.5	25.2, 99.2	25.2, 99.8
Data / restraints / parameters	5830 / 0 / 307	6747 / 0 / 320	7071 / 0 / 339
Goodness-of-fit on F2	1.068	1.041	1.144
R [I > 2σ(I)]	R_1 = 0.0345	R_1 = 0.0429	R_1 = 0.0871
	wR_2 = 0.0911	wR_2 = 0.1132	wR_2 = 0.2118
R (all data)	R_1 = 0.0423	R_1 = 0.0577	R_1 = 0.136
	wR_2 = 0.0985	wR_2 = 0.1251	wR_2 = 0.2797
ρmax, ρmin (e.Å^{-3})	0.329, -0.306	0.392, -0.330	1.708, -1.312

(**3**) *p*FPh-PhPNP = *N*,*N*-Bis(diphenylphosphino)-4-fluoroaniline

(**7**) Cbtyl-4-*p*-tolyl = *N*,*N*-Bis(di-*p*-tolylphosphino)cyclobutylamine

(**8**) Chzyl-4-*p*-tolyl = *N*,*N*-Bis(di-*p*-tolylphosphino)cyclohexylamine

4.3 *N,N*-Bis(diphenylphosphino)-4-fluoroaniline (3)

The title ligand, *p*FPh-PhPNP (**3**) was synthesized as described in **Paragraph 3.3.3**. This ligand crystallizes in the monoclinic crystal system in the $P2_1/n$ space group with four formula units in the unit cell (Z = 4). The asymmetric unit contains one independent molecule. The molecular structure of the title ligand (*p*FPh-PhPNP), including the atomic numbering scheme is illustrated in **Figure 4.4**.

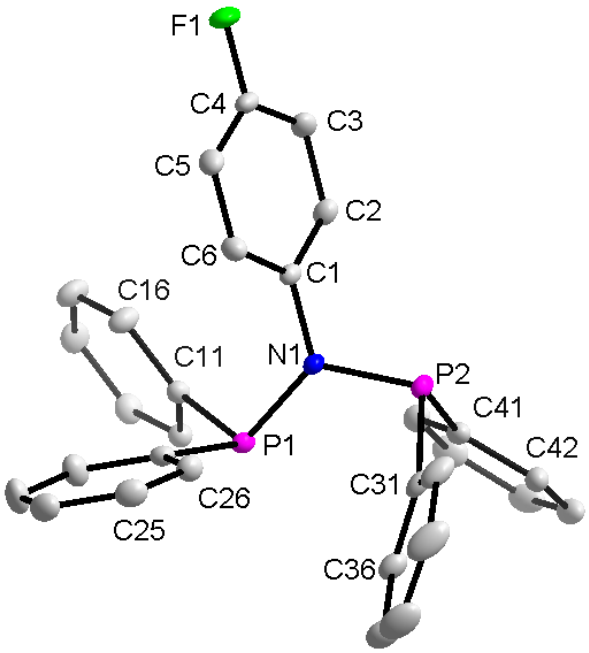

Figure 4.4 Molecular representation of *p*FPh-PhPNP (**3**) ligand. All displacement ellipsoid are drawn at 50% probability level.

Table 4.2 Selected bond lengths and bond angles for the crystal structure of *p*FPh-PhPNP (**3**) (Å and °)

Atoms	Bond length (Å)	Atoms	Bond angle (°)
N1 – C1	1.4401(16)	P1 – N1 – P2	121.20(7)
N1 – P1	1.7283(13)	C1 – N1 – P1	123.82(9)
N1 – P2	1.7300(12)	C1 – N1 – P2	114.74(9)
P1 – C11	1.8340(15)	N1 – P1 – C11	106.39(6)
P1 – C21	1.8338(15)	N1 – P1 – C21	105.46(7)
P2 – C31	1.8344(15)	N1 – P2 – C31	102.88(6)
P2 – C41	1.8278(15)	N1 – P2 – C41	104.17(6)
		C11 – P1 – C21	101.46(6)
		C31 – P2 – C41	100.78(7)

Selected bond distances and angles are summarized in **Table 4.2**. The values reported in this table were found to be in the same range as the values of similar structures such as *N*,*N*-bis(diphenyl-phosphino)ethyl-amine, *N*,*N*-bis(diphenyl-phosphino)-1,2-dimethyl-propyl-amine and *N*,*N*-bis(diphenyl-phosphanyl)cyclo-propyl-amine reported in literature.[13,14,15,16,17] The *Effective Tolman-based N-substituent steric effect* ($\theta_{N\text{-}sub}$) of the *p*FPh-PhPNP ligands was calculated using **Equation 4.1** and **Figure 4.3** and found to be 50.4 °. To accommodate the steric bulk on the N atom, the fluorinated aniline ring is orientated at an angle of 66.62 ° from the plane created by atoms P1/C1/P2 (**Figure 4.5**). Furthermore, angles around the P atom range between 100.78(7) ° and 106.39(6) °, indicating a slight distortion from the ideal 109.5 ° angle of a tetrahedral geometry. Finally a C_s conformation as seen in **Figure 4.2** and **Figure 4.4** is adopted by the *p*FPh-PhPNP ligand in the solid state.

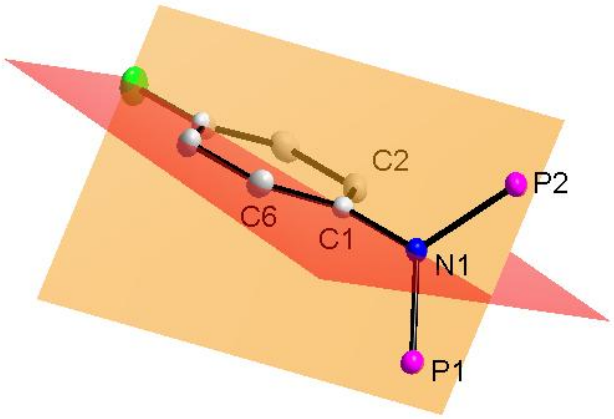

Figure 4.5 Structural view of plane constructed through C1-C6 (red) and C1/P1/P2/N1 (orange) on the *p*FPh-PhPNP (**3**) ligand.

No classic hydrogen interactions were observed for this ligand in the unit cell. However, the crystal structure of *p*FPh-PhPNP is seen to be stabilized by an abundant number of C-H···Cg (π-ring) interaction as illustrated in **Table 4.3**, **Figure 4.6** and **Figure 4.7**.

[13] Cloete, N., Visser, H. G., Roodt, A., Gabrielli, W. F., *Acta Cryst*, **2009,** E*65*, o3081.

[14] Cloete, N., Visser, H. G., Roodt, A., Dixon, J. T., Blann, K., *Acta Cryst*, **2008,** E*64*, o480

[15] Engelbrecht, I., Visser, H. G., Roodt, A., *Acta Cryst.* **2010,** E*66*, o2881.

[16] Engelbrecht, I., Visser, H. G., Roodt, A., *Acta Cryst.* **2010,** E*66*, o3322-o3323.

[17] Fei, Z., Scopeleti, R., Dyson, P. J., *Dalton Trans*. **2003**, 2772-2779.

Figure 4.8 illustrates the packing manner of the molecules in the unit cell when viewed along the *a*-axis.

Table 4.3 C-H···Cg(π-ring) interactions for *p*FPh-PhPNP ligand (**3**).

X-H(I)···Cg(J)	Symmetry	H···Cg (Å)	X-H··· Cg (°)	X··· Cg (Å)
C26-H13···Cg(4)	#1	2.90	139	3.649(2)
C25-H15···Cg(1)	#2	2.86	141	3.630(2)
C5-H20···Cg(5)	#3	2.67	143	3.461(2)
C15-H29···Cg(4)	#4	2.78	133	3.485(2)
C23-H32···Cg(2)	#5	2.93	141	3.698(2)
C35-H33···Cg(3)	#6	2.89	150	3.725(2)

Symmetry transformation used to generate equivalent to atoms: **#1** x, y, z; **#2** -½-x,- ½+y, ½-z; **#3** -½+x, ½-y,- ½+z; **#4** ½+x, ½-y,- ½+z; **#5** ½-x,- ½+y, ½-z; **#6** -x,-y,1-z; Cg1 = centroid atoms of C1,C2,C3,C4,C5,C6; Cg2 = centroid atom of C11,C12,C13,C14,C15,C16; Cg3 = centroid atom of C21,C22,C23,C24,C25,C26; Cg4 = centroid atom of C31,C32,C33,C34,C35,C36; Cg5 = centroid atom of C41,C42,C43,C44,C45,C46.

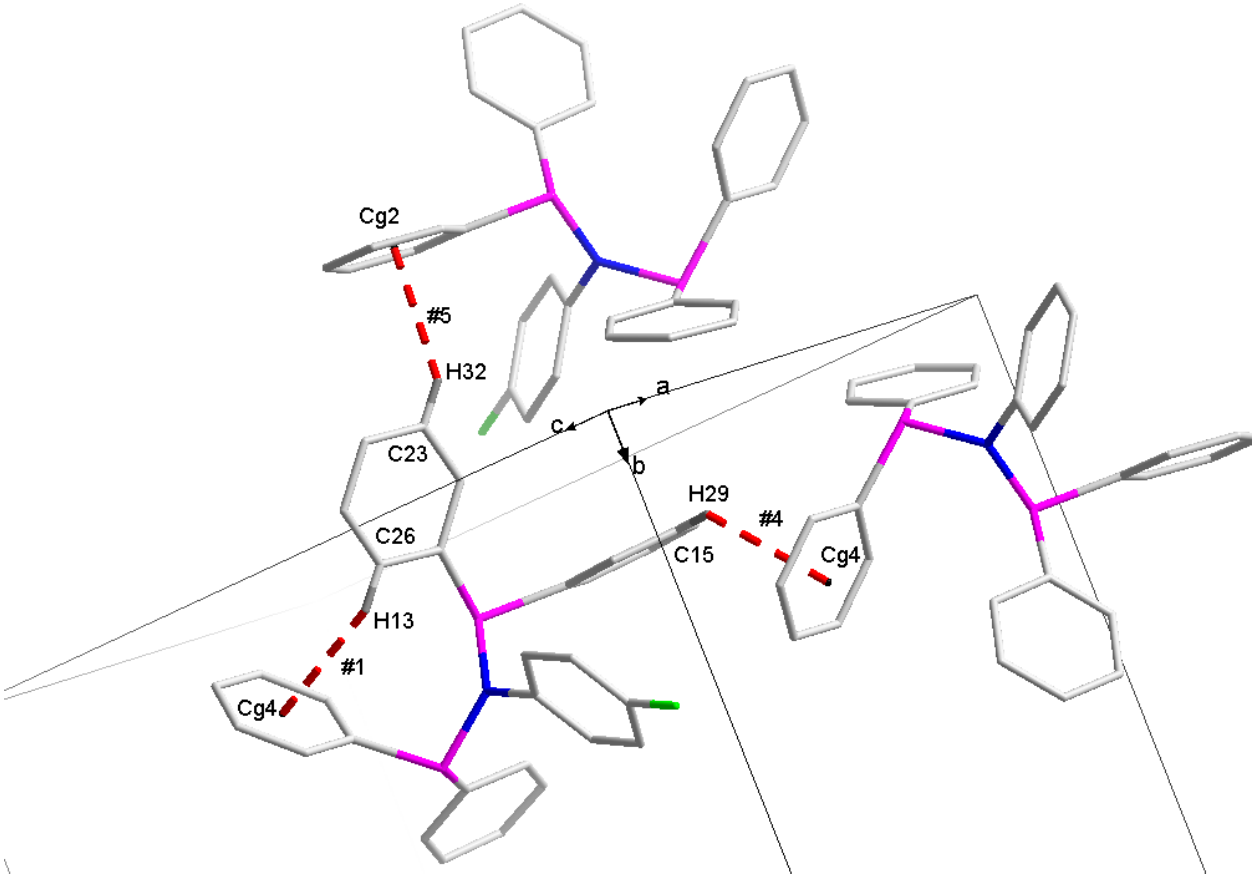

Figure 4.6 Graphic representation of some of the C-H···Cg (red dashed bonds) interactions observed for ligand *p*FPh-PhPNP (**3**).

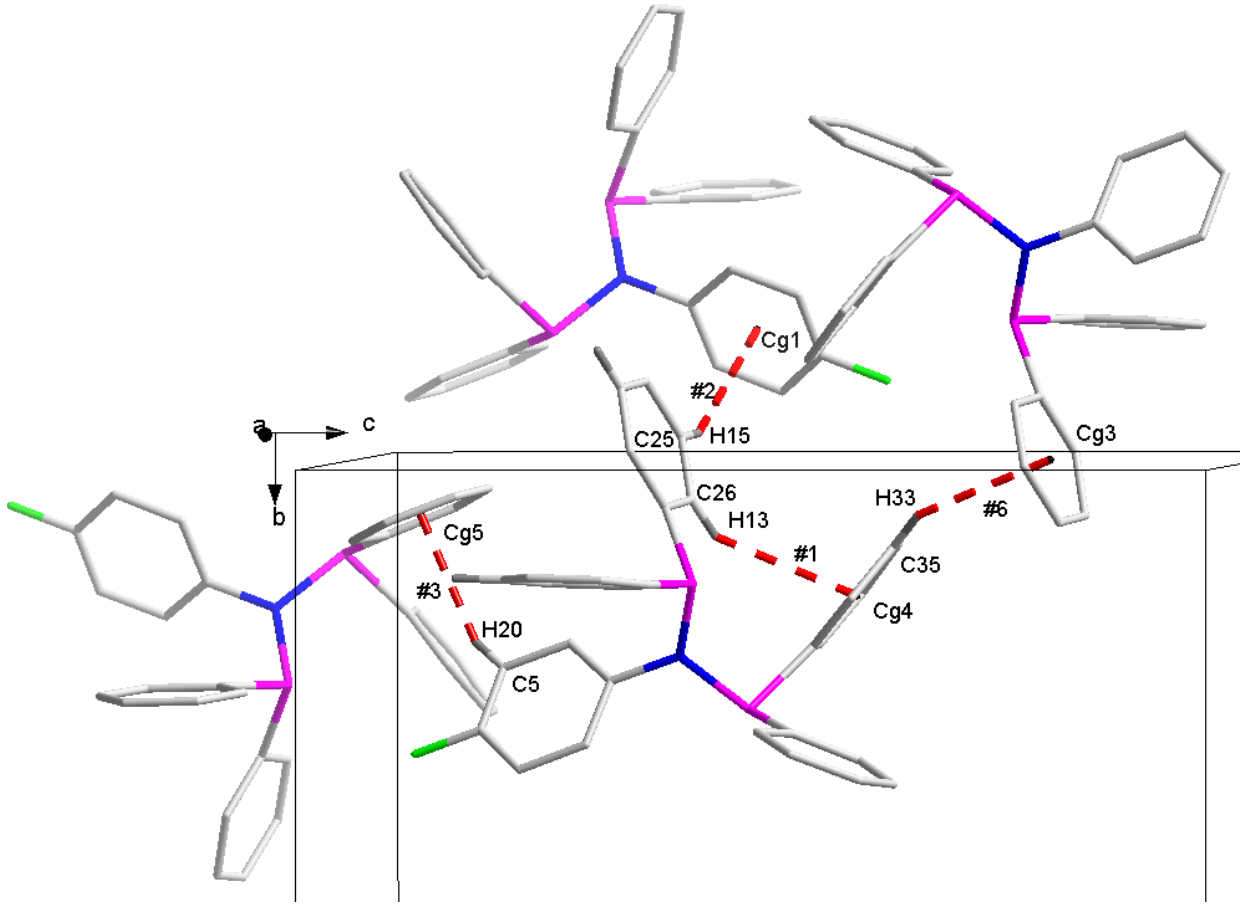

Figure 4.7 Graphic representation of some of the C-H···Cg (red dashed bonds) interactions observed for ligand *p*FPh-PhPNP (**3**).

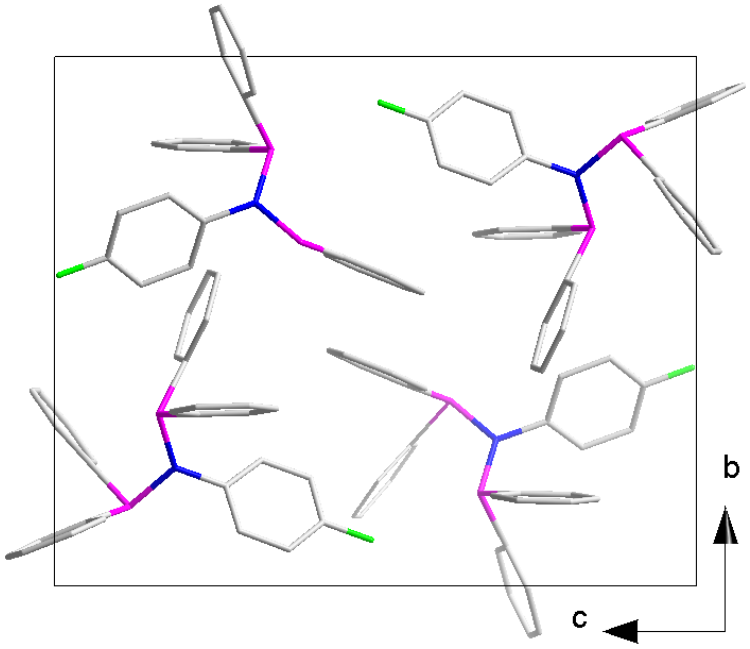

Figure 4.8 Crystal packing of *p*FPh-PhPNP (**3**) ligand in the unit cell, viewed along the *a*-axis.

4.4 *N,N*-Bis(di-*p*-tolylphosphino)cyclobutylamine (7)

The title ligand, Cbtyl-4-*p*-tolyl (**7**) was synthesized as described in **Paragraph 3.3.7**. This ligand crystallizes in the triclinic crystal system in the $P\bar{1}$ space group with two formula units in the unit cell (Z = 2). The asymmetric unit contains one independent molecule. The molecular structure of the title ligand Cbtyl-4-*p*-tolyl (**7**) including the atomic numbering scheme is illustrated in **Figure 4.9**.

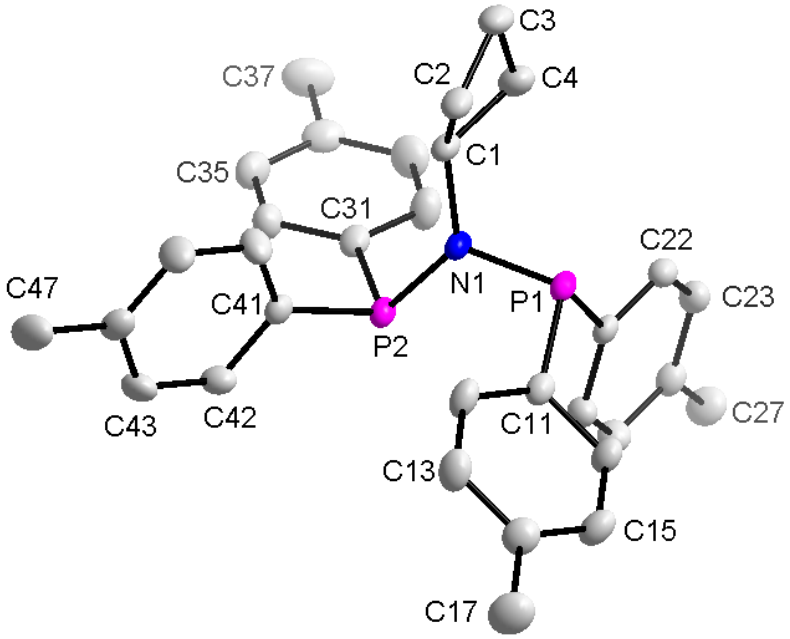

Figure 4.9 Molecular representation of Cbtyl-4-*p*-tolyl (**7**) ligand. All displacement ellipsoid are drawn at 50% probability level.

Table 4.4 Selected bond lengths and bond angles for the crystal structure of Cbtyl-4-*p*-tolyl (**7**) (Å and °)

Atoms	**Bond length (Å)**	**Atoms**	**Bond angle (°)**
N1 – C1	1.481(2)	P1 – N1 – P2	119.92(8)
N1 – P1	1.7184(14)	C1 – N1 – P1	115.86(10)
N1 – P2	1.7133(14)	C1 – N1 – P2	122.70(10)
P1 – C11	1.8207(18)	N1 – P1 – C11	103.58(7)
P1 – C21	1.8353(16)	N1 – P1 – C21	104.08(7)
P2 – C31	1.8363(17)	N1 – P2 – C31	101.36(7)
P2 – C41	1.8286(17)	N1 – P2 – C41	106.15(7)
		C11 – P1 – C21	102.69(7)
		C31 – P2 – C41	102.10(7)

Selected bond distances and angles are summarized in **Table 4.4**. The values reported in this table were also found to be in the same range as the values of similar structures reported in literature.[13,14,15,16] The *Effective Tolman-based N-substituent steric effect* ($\theta_{N\text{-}sub}$) of the Cbtyl-4-*p*-tolyl ligands was calculated using **Equation 4.1** and **Figure 4.3** and found to be 73.4 °. To accommodate the steric bulk on the N atom, the N atom adopts an almost planer geometry to the plane created by atoms C1P1/P2/N1 (**Figure 4.10**). Furthermore, angles around the P atom range between 101.36(7) ° and 106.15(7) °, indicating a slight distortion from the ideal 109.5 ° angle for a tetrahedral geometry. A C_s conformation as seen in **Figure 4.2** and **Figure 4.9** is adopted by the Cbtyl-4-*p*-tolyl ligand in its solid state. To relieve some of the torsional strain the cyclobutane group on the N atom adopts a puckered conformation instead of a planar one. Finally, the angles 119.92(8)°, 115.86(10)° and 122.70(10)° around the N atom indicate that the N atom adopts a trigonal hybridized (sp^2) geometry.

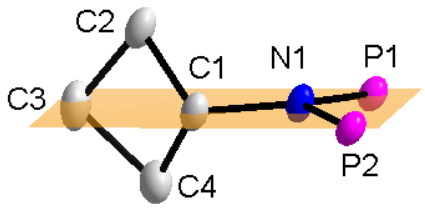

Figure 4.10 Structural view of plane constructed through atom C1/P1/P2/N1 (orange) on the Cbtyl-4-*p*-tolyl (**7**) ligand.

No classic hydrogen interactions were observed for this ligand in the unit cell. However, the crystal structure of Cbtyl-4-*p*-tolyl is also stabilized by an abundant number of C-H···Cg (π-ring) interactions as illustrated in **Table 4.5**, and **Figure 4.11**.

Figure 4.12 indicates the packing manner the molecules pack in the unit cell when viewed along the *c*-axis.

Table 4.5 C-H···Cg(π-ring) interactions for Cbtyl-4-*p*-tolyl (**7**) ligand.

X-H(I)···Cg(J)	Symmetry	H···Cg (Å)	X-H···Cg (°)	X···Cg (Å)
C45-H19···Cg(4)	#1	2.96	149	3.808(2)
C43-H27···Cg(2)	#2	2.86	144	3.671(2)
C37-H34A···Cg(2)	#3	2.81	128	3.498(3)

Symmetry transformation used to generate equivalent to atoms: **#1** -x, -x, 2-z; **#2** 1-x, -y, 2-z; **#3** x, -1+y, z; Cg(2) = centroid atom of C11,C12,C13,C14,C15,C16; Cg(4) = centroid atom of C31,C32,C33,C34,C35,C36.

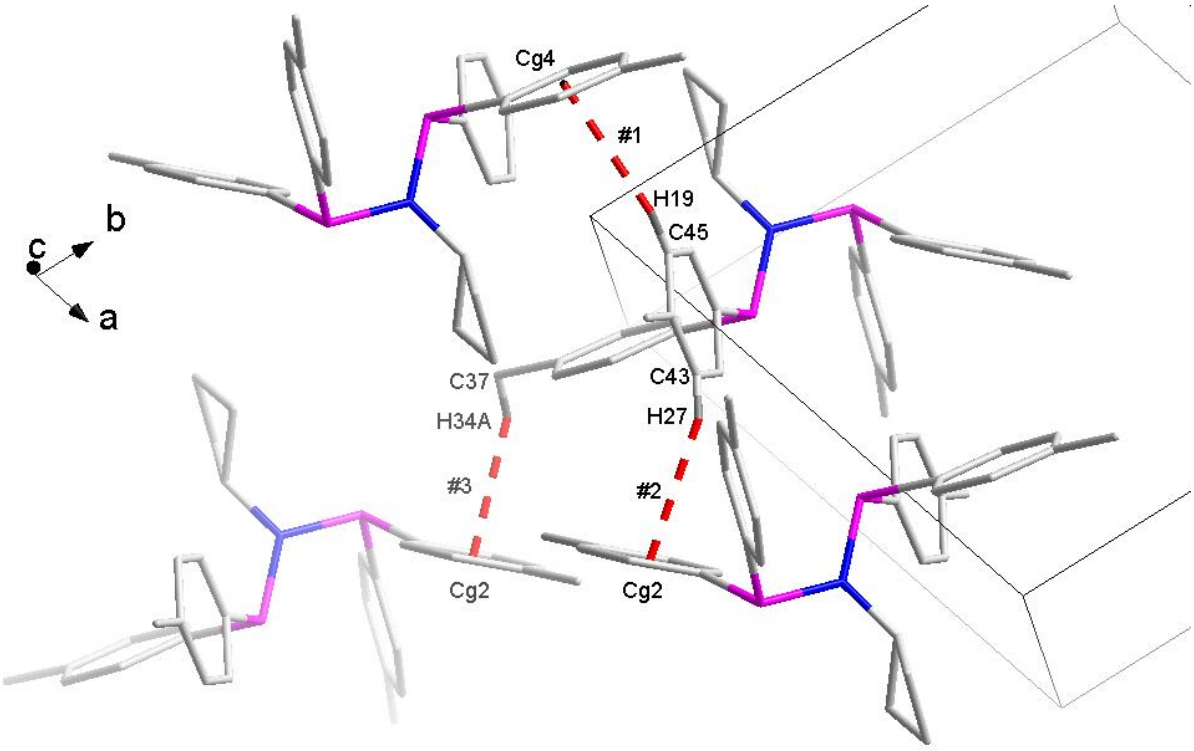

Figure 4.11 Graphical representation of the C-H···Cg (red dashed bonds) interactions observed for ligand Cbtyl-4-*p*-tolyl (**7**).

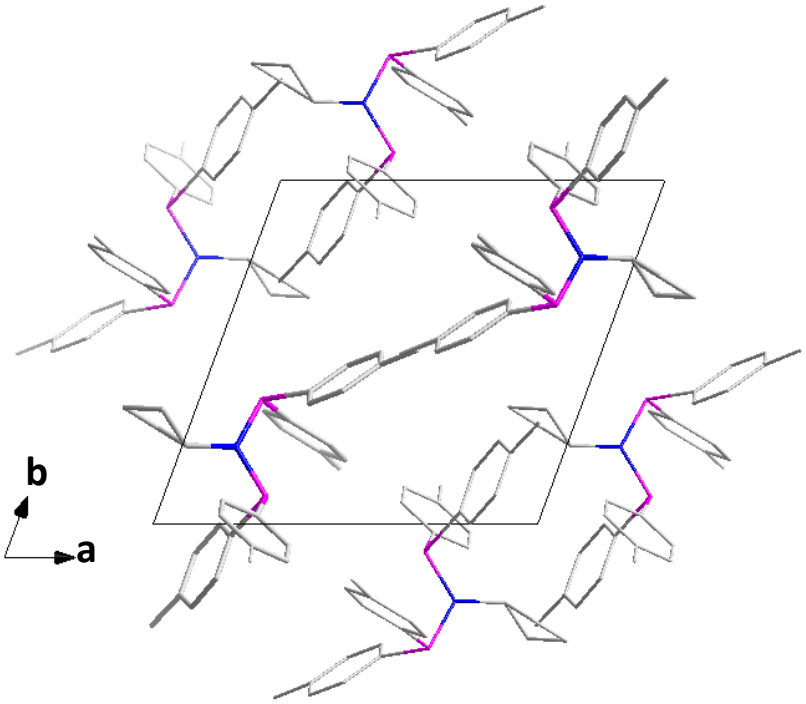

Figure 4.12 Crystal packing of Cbtyl-4-*p*-tolyl (**7**) ligand in the unit cell, viewed along the *c*-axis.

4.5 *N,N*-Bis(di-*p*-tolylphosphino)cyclohexylamine

The title ligand, Chzyl-4-*p*-tolyl (**8**) was synthesized as described in **Paragraph 3.3.8**. This ligand crystallizes in the triclinic crystal system in the $P\bar{1}$ space group with two formula units in the unit cell (Z = 2). The asymmetric unit contains one independent molecule. The molecular structure of the title ligand Chzyl-4-*p*-tolyl (**8**) including the atomic numbering scheme is illustrated in **Figure 4.13**.

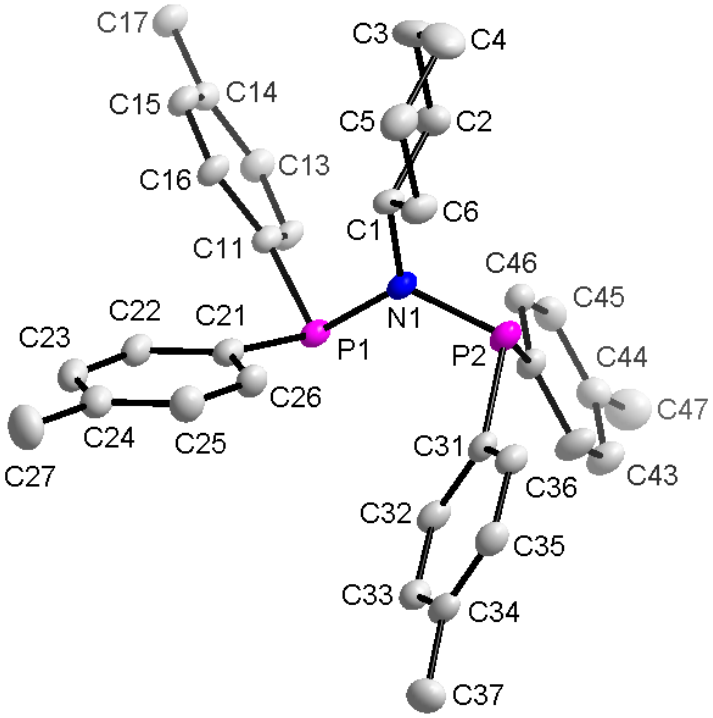

Figure 4.13 Molecular representation of Chzyl-4-*p*-tolyl (**8**) ligand. All displacement ellipsoid are drawn at 50% probability level.

Table 4.6 Selected bond lengths and bond angles for the crystal structure of Chzyl-4-*p*-tolyl (**8**) (Å and °)

Atoms	**Bond length (Å)**	**Atoms**	**Bond angle (°)**
N1 – C1	1.478(4)	P1 – N1 – P2	120.58(16)
N1 – P1	1.726(3)	C1 – N1 – P1	121.6(2)
N1 – P2	1.713(3)	C1 – N1 – P2	117.7(2)
P1 – C11	1.833(3)	N1 – P1 – C11	104.18(14)
P1 – C21	1.829(3)	N1 – P1 – C21	103.02(15)
P2 – C31	1.835(4)	N1 – P2 – C31	104.08(15)
P2 – C41	1.824(4)	N1 – P2 – C41	104.32(14)
		C11 – P1 – C21	101.47(15)
		C31 – P2 – C41	103.44(16)

Selected bond distances and angles are summarized in **Table 4.6**. The values reported in this table were also found to be in the same range as the values of similar structures reported in literature.[13,14,15,16] The *Effective Tolman-based N-substituent steric effect* ($\theta_{N\text{-}sub}$) of the Chzyl-4-*p*-tolyl ligands was calculated using **Equation 4.1** and **Figure 4.3** and found to be 85.6 °. To accommodate the steric bulk on the N atom, the N atom adopts an almost planer geometry to the plane created by atoms C1/P1/P2/N1 (**Figure 4.14**). The cychlohexyl group attached to the N atom adopts a less sterically demanding chair conformation to accommodate the steric bulk on the N atom. In addition, the angles around the N atom are indicative of a sp^2 hybridized N atom. Furthermore, angles around the P atom range between 101.47(15) ° and 104.32(14) °, indicating a slight contraction from the ideal 109.5 ° angle for a tetrahedral geometry. Finally a C_s conformation as seen in **Figure 4.2** and **Figure 4.4** is adopted by the Chzyl-4-*p*-tolyl ligand in its solid state.

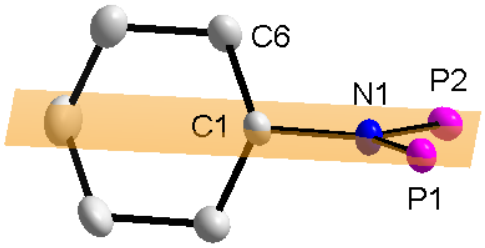

Figure 4.14 Structural view of plane constructed through C1/P1/P2 (orange) on the Chzyl-4-*p*-tolyl (**8**) ligand.

No classic hydrogen interactions were observed for this ligand in the unit cell. However, the crystal structure of Chzyl-4-*p*-tolyl (**8**), similar to the two previous structures described above is stabilized by C-H···Cg (π-ring) interactions as illustrated in **Table 4.7** and **Figure 4.15**.

Figure 4.16 illustrates the packing manner of the molecules in the unit cell when viewed along the *b*-axis.

Table 4.7 C-H···Cg(π-ring) interactions for Chzyl-4-*p*-tolyl (**8**) ligand.

X-H(I)···Cg(J)	Symmetry	H···Cg (Å)	X-H···Cg (°)	X···Cg (Å)
C17-H23B···Cg(4)	#1	3.05	123	3.668(1)
C33-H34···Cg(5)	#2	2.80	146	3.615(5)

Symmetry transformation used to generate equivalent to atoms: **#1** 2-x, 1-y,-z; **#2** 1-x, 2-y, -z; Cg(4) = centroid atom of C31,C32,C33,C34,C35,C36; Cg5 = centroid atom of C41,C42,C43,C44,C45,C46.

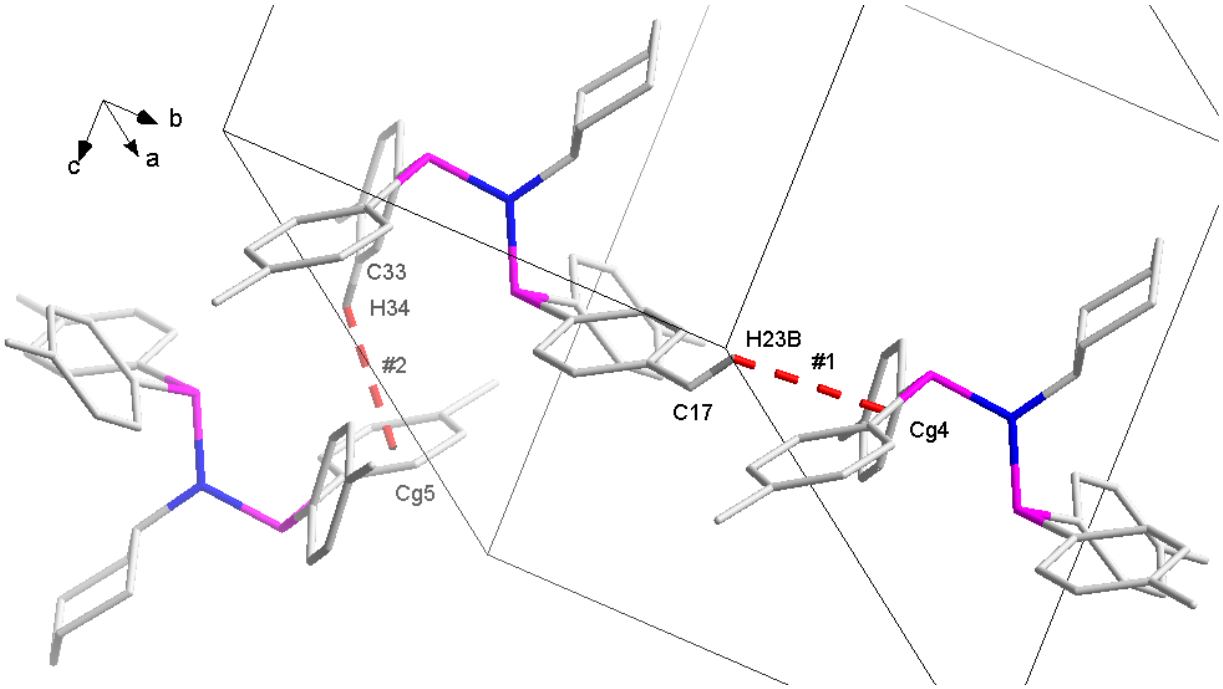

Figure 4.15 Graphical representation of the C-H···Cg (red dashed bonds) interactions observed for ligand Chzyl-4-*p*-tolyl (**8**).

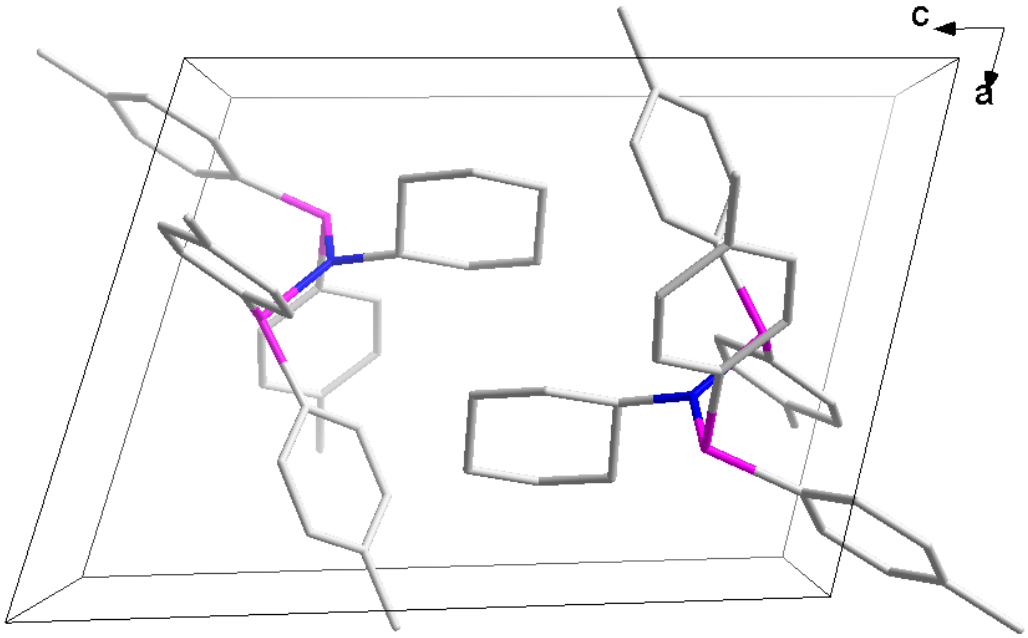

Figure 4.16 Crystal packing of Chzyl-4-*p*-tolyl (**8**) ligand in the unit cell, viewed along the *b*-axis**.**

4.6 Discussion

Although the chemical structure of *p*FPh-PhPNP (**3**) is very similar to that of the reported of *N*,*N*-Bis(diphenylphosphino)aniline (Ph-PNP),[17] evaluation of their crystal structures showed a significant geometrical difference as illustrated in **Figure 4.17** and **Figure 4.18**. This observation indicates the significant difference that a small change in ligand engineering can have on the overall steric properties of a ligand. **Table 4.8** summarizes the different bond distances and angles observed between the two crystal structures which differ primarily by the F-atom on the C4 atom.

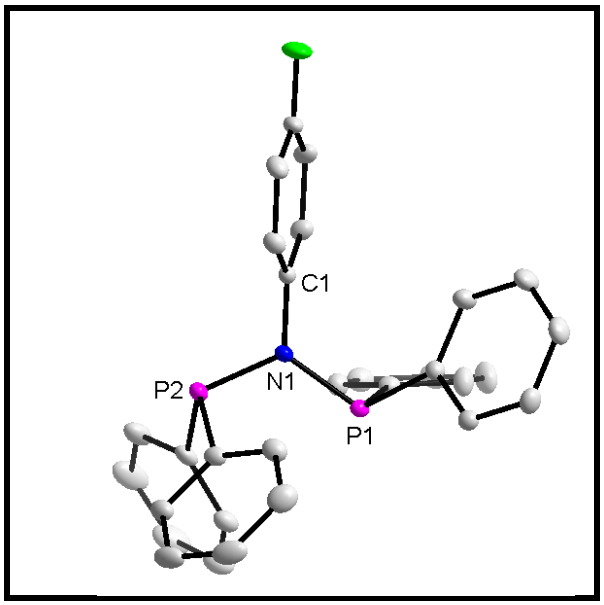

Figure 4.18 Graphical representation of *p*FPh-PhPNP (**3**). All displacement ellipsoid are drawn at 50% probability

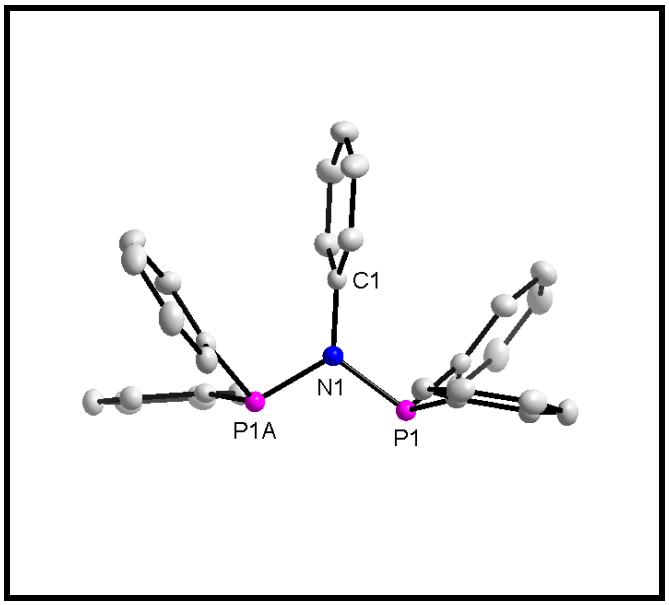

Figure 4.17 Graphical representation of Ph-PNP[17]. All displacement ellipsoid are drawn at 50% probability. P1A is generated through symmetry –x, y, ½-z.

Table 4.8 Selected information indicating the difference between *p*FPh-PhPNP (**3**) and Ph-PNP[17]

Ligand	C1-N1 (Å)	N-P_{ave} (Å)	P – N – P (°)	Conformation	Space group
F-Ph-PNP (**3**)	1.440(2)	1.7292(13)	121.20(7)	C_s	$P2_1/n$
Ph-PNP[17]	1.455(4)	1.7315(15)	113.37(14)	C_{2V}	$C2/c$

[17] see ref 17

From the above information, it appears that the electronic effect that the F atom added to the ligand contributed to the conformation change from C_2v to Cs and the P-N-P bond angle from 113.37(14) to 121.20(7) degrees from ligand Ph-PNP[17] to *p*FPh-PhPNP (**3**). The *Effective*

Tolman-based N-substituent steric effect ($\theta_{N\text{-}sub}$) calculated from the crystallographic data for the *p*FPh-PhPNP (**3**) and Ph-PNP are 50.4° and 50.2°, respectively. Hence this change in packing conformation is seemingly induced by electronic effects and not by steric effects. This illustrates that not only the steric bulk on the N atom in PNP ligands is able to affect the geometry, but also the electronic properties can have a significant influence.

The remaining two crystal structures of Cbtyl-4-*p*-tolyl (**7**) and Chzyl-4-*p*-tolyl (**8**) discussed in this chapter are similar to the crystal structures of *N*,*N*-Bis(diphenylphosphanyl)cyclobutanamine (Cbtyl-PNP) [18] and *N*,*N*-bis(diphenylphosphanyl)cyclohexylamine (Chzyl-PNP) [19] reported in literature except for the *p*-tolyl group on the P atoms. No significant difference on the steric bulk ($\theta_{N\text{-}sub}$), bond lengths, bond angles and the conformations were observed. This indicates that the addition of a methyl group on the *para*- position of the phenyl rings attached to the P atom did not add any significant effect except for the change in crystal systems and space groups. Moreover, the cyclohexyl substituent on the N atom is oriented in the chair conformation rather than the corresponding sterically demanding boat conformation, while the cyclobutyl group on **7** also adopts a less sterically demanding puckered conformation.

Table 4.9 Selected information indicating the difference between various diphosphinoamine ligands.

Ligand	C1-N1 (Å)	N-P_{ave} (Å)	P – N – P (°)	Conformation	Space group
Cbtyl-4-*p*-tolyl (**7**)	1.481(2)	1.7159(14)	119.92(8)	C_s	$P\bar{1}$
Cbtyl-PNP[18]	1.478(2)	1.7165(16)	123.53(8)	C_s	$P2_1$
Chzyl-4-*p*-tolyl (**8**)	1.478(4)	1.7195(3)	120.58(16)	C_s	$P\bar{1}$
Chzyl-PNP[19]	1.4971(17)	1.7204(12)	119.68(7)	C_s	$P2_1/n$

[18] see ref 18, [19] see ref 19.

[18] Engelbrecht, I., Visser, H. G., Roodt, A., *Acta Crysta.* **2011,** E*67*, o2041-o2042.

[19] Naicker, D., Pansuriya, P. B., Friedrich, H. B., *Z. Kristallogr.* **2016,** *231*, 653-656.

4.7 Conclusion

In this chapter three diphosphinoamine (PNP) ligands namely *p*FPh-PhPNP (**3**), Cbutyl-4-*p*-tolyl (**7**) and Chzyl-4-*p*-tolyl (**8**) were presented. The majority of the bond distances and angles were very comparable and all three structures adopted a Cs conformation. The packing modes of all three PNP ligands included a number of intermolecular interactions but no classic hydrogen interactions were observed.

One of the major aims of this chapter was to deduce crystallographically the steric bulk presented as ($\theta_{N\text{-}sub}$) for each ligand. From these ($\theta_{N\text{-}sub}$) values, a correlation between the steric bulk on the N atom of a PNP ligand and the solid state conformation adopted by each ligand was investigated. This correlation proved that both the steric and the electronic effects can individually have a major impact on the solid state conformation adopted by each ligand.

In the following chapter, oxidation of the non-coordinated PNP ligands by an oxidizing agent such as hydrogen peroxide was performed to further investigate the stability and the solid state structural correlation between the free and oxidized PNP ligands.

5 Single crystal X-ray diffraction study of diphosphinoamineoxides

What to expect!

A detailed crystallographic evaluation of three non-coordinated diphosphinoamineoxide (PNPO) ligands will be presented in this chapter.

5.1 Introduction

The chemistry of *O*-monodentate and *O,O*-bidentate phosphine oxide ligands with the P-N-P backbone has enjoyed a wide variety of applications particularly in the field of f-block elements (lanthanides and actinides) photoluminescence and liquid-liquid extraction studies.[1,2,3,4] The flexible electronic and steric properties of these ligands in conjunction with the highly oxophilic nature of f-block elements enable the synthesis of a wide range of complexes with different coordination schemes. These ligands can be systematically altered on both the nitrogen and the phosphorus atoms.

Although not well developed, phosphorylated ligands containing the P=O group have also been used in group 7 transition metals (manganese, technetium and rhenium) coordination chemistry studies.[5,6,7,8] This is perhaps not surprising given the widespread use of phosphorylyted molecules in transition metal chemistry.

[1] Redmond, M. P., Cornet, S.M., Woodall, S.D., Whittaker, D., Collison, D., Helliwell, M., Natrajan, L.S., *Dalton Trans.* **2011,** *40*, 3914-3926.

[2] Aladzheva, I. M., Bykhovskaya, O.V., Nelyubina, Y.V., Klemenkova, Z.S., Petrovskii, P.V., Odinets, I.L *Inorganica Chim. Acta.* **2011,** *373* 130-136.

[3] Aparna, K., Krishnamurthy, S., Nethaji, M., *Z. Anorg. Allg. Chem.* **1995,** *621*, 1913-1921.

[4] Bokolo, K., Courtois, A., Delpuech, J.J., Elkaim, E., Protas, J., Rinaldi, D., Rodehiiser, L., Rubinill, P., *J. Am. Chem. Soc.* **1984,** *106*, 6333-6338.

[5] Depree, G. J., Childerhouse, N.D., Nicholson, B.K., *J. Organomet. Chem.* **1997,** *553*, 143-151.

In this chapter, three diphosphinoamineoxide (PNPO) ligands, namely *N*,*N*-bis(diphenylphosphineoxide)-4-fluoroaniline, *N*,*N*-bis(di-*p*-tolylphosphineoxide)-*p*-toluidine and *N*,*N*-bis(di-*p*-tolylphosphineoxide)cyclohexylamine which were crystallized (see Figure 5.1) and characterized by X-ray structure analysis to gain information regarding the stability of these ligands towards oxidation and their solid state spatial requirements, will be discussed. The general crystallographic data and refinement parameters of these crystals are summarized in **Table 5.1**.

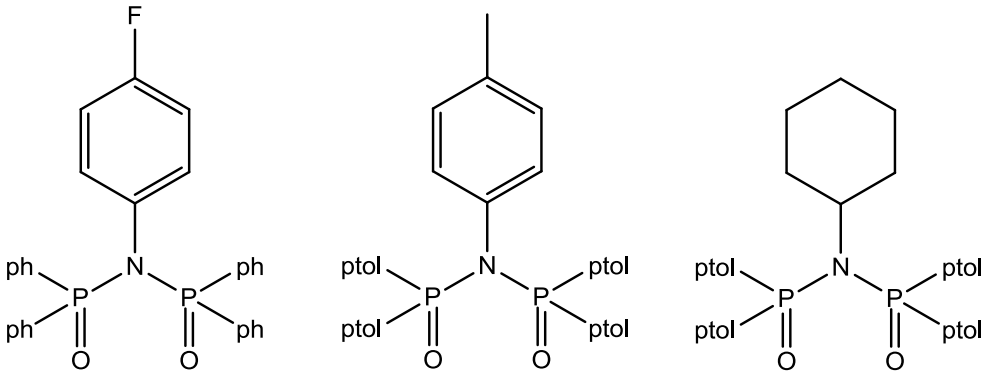

3a (*p*FPh-PhPNPO) **5a** (5-*p*-tolyl-PNPO) **8a** (Chzyl-4-*p*-tolyl-PNPO)

Figure 5.1 Diphosphinoamine oxide (PNPO) ligands with different electronic and steric properties on the N/P atom crystallized in this study: **3a** *N*,*N*-Bis(diphenylphosphineoxide)-4-fluoroaniline (*p*FPh-PhPNPO), **5a** *N*,*N*-Bis(di-*p*-tolylphosphineoxide)-*p*-toluidine (5-*p*-tolyl-PNPO) and **8a** *N*,*N*-Bis(di-*p*-tolylphosphineoxide)cyclohexylamine (Chzyl-4-*p*-tolyl-PNPO). Molecular numbering is reminiscent of that found in Chapter 3, except the "a" symbol which implies the oxidized PNP ligand.

5.2 Experimental

Diffraction data for (**3a**) *p*FPh-PhPNPO, (**5a**) 5-*p*-tolyl-PNPO and (**8a**) Chzyl-4-*p*-tolyl-PNPO were collected at 100 K on a Bruker X8 Apex II 4K diffractometer using monochromated Mo Kα radiation with a wavelength of λ = 0.71073 Å. All the cell parameters were refined using the XPREP4 and SAINT-Plus[9] program while SADABS[10] and multiscan techniques were used for

[6] Freiberg, E., Davis, W.M., Nicholson, T., Davison, A., Jones, A.G., *Inorg. Chem.* **2002,** *41*, 5667-5674.

[7] Abram, U., Alberto, R., Dilworth, J.R., Zheng, Y., Ortner, K., *Polyhedron.* **1999,** *18*, 2995-3003.

[8] Bhattacharyya, S., Chakraborty, I., Dirghangi, B.K., Chakravorty, A., *Inorg. Chem.* **2001,** *40*, 286-293.

[9] *SAINT-Plus*, version 6.02 (including XPREP); Bruker AXA, Inc.: Madison, WI, USA, **1999**.

[10] *SADABS*, version 2004/1; Bruker AXS, Inc.: Madison, WI, USA, **2004**.

the absorption corrections. The structures were solved by either the direct methods or by the use of SIR97[11] and refined on F^2 using anisotropic displacement parameters for all non-hydrogen atoms. SHELXL-97 [12,13] and WinGX [14] were used for structure solutions and refinements respectively. The molecular graphics were drawn using the DIAMOND program. [15] All aromatic, methylene and methyl hydrogen atoms were placed in geometrically idealized positions (C-H = 0.95 Å to 0.98 Å) and constrained to ride on their parent atoms with U_{iso}(H) = 1.2U_{eq}(C) and U_{iso}(H) = 1.5U_{eq}(C) respectively.

For all three PNPO ligands, a summary of the general crystal data and refinement parameters is given in **Table 5.1**. All the bond distances, bond angles, atomic coordinates, hydrogen coordinates, torsion angles and anisotropic displacement parameters for these ligands are found in the supplementary data (**Appendix A**). Short extracts of the most important bond parameters are however given under each paragraph. Hydrogen atoms and numbering for certain carbon atoms were omitted for clarity on selected molecular structures. For aromatic rings, the first and the second digit represents the ring number and the specific C-atom in the ring respectively.

[11] Altomare, A., Burla, M. C., Camalli, M., Cascarano, G. L., Giacovazzo, C., Guagliardi, A., Moliterni, A. G. G., Polidori, G., Spagna, R., *J. Appl. Cryst*., **1999**, *32*, 837-838.

[12] Sheldrick, G. M., SHELXL97; University of Göttingen: Göttingen, Germany, **1997**.

[13] Sheldrick, G. M., *Acta Crystallogr*. **2008**, *A64*, 112-122.

[14] Farrugia, L. J., *J. Appl. Crystallogr*. **1999**, *32*, 837-838.

[15] Brandenburg, K., Putz, H., DIAMOND, release 3.1b; Crystal Impact GbR: Bonn, Germany, **2005**.

Table 5.1 Crystallographic data of (**3a**) *p*FPh-PhPNPO, (**5a**) 5-*p*-tolyl-PNPO and (**8a**) Chzyl-4-*p*-tolyl-PNPO.

Crystallographic data	***p*FPh-PhPNPO (3a)**	**5-*p*-tolyl-PNPO (5a)**	**Chzyl-4-*p*-tolyl-PNPO (8a)**
Empirical formula	$C_{30}H_{24}F_1N_1O_2P_2$	$C_{35}H_{35}N_1O_2P_2$	$C_{35}H_{43}N_1O_4P_2Cl_2$
Formula weight (g mol^{-1})	511.44	563.58	674.54
Temperature (K)	100(2)	100(2)	100(2)
Crystal system	Monoclinic	Triclinic	Orthorhombic
Space group	*C*2/*c*	$P\bar{1}$	*Pbca*
Unit cell dimensions			
a (Å)	11.841(1)	11.879(1)	12.661(3)
b (Å)	19.664(1)	12.494(2)	20.375(4)
c (Å)	11.966(1)	12.882(5)	26.473(5)
α (°)	90	108.073(3)	90
β (°)	118.603(2)	116.492(4)	90
γ (°)	90	101.740(4)	90
Volume (Å^3)	2446(16)	1489.6(10)	6829(2)
Z	4	2	8
Density (g cm^{-3})	1.389	1.256	1.312
Crystal colour	Colourless	Colourless	Colourless
Crystal morphology	Needles	Cuboid	Cuboid
Crystal size (mm^3)	0.767 x 0.133 x 0.126	0.450 x 0.360 x 0.280	0.399 x 0.164 x 0.154
μ (mm^{-1})	0.215	0.178	0.323
F(000)	1064	596	2848.0
θ range (°)	2.243 - 27.995	1.943 - 27.999	0.77 - 28.42
	$-15 \leq h \leq 15$	$-12 \leq h \leq 15$	$-16 \leq h \leq 16$
Index ranges	$-25 \leq k \leq 25$	$-16 \leq k \leq 16$	$-27 \leq k \leq 27$
	$-12 \leq l \leq 15$	$-17 \leq l \leq 17$	$-35 \leq l \leq 26$
Reflections collected	21820	26185	133618
Unique reflections	2951	7154	8250
Reflections with I > 2σ(I)	2674	6467	6595
R_{int}	0.0409	0.0461	0.0809
Completeness to theta (°, %)	25.2, 99.6	25.2, 99.5	26.0, 100.0
Data / restraints / parameters	2951 / 0 / 165	7154 / 0 / 366	8250 / 0 / 389
Goodness-of-fit on F2	1.084	1.119	1.210
R [I > 2σ(I)]	$R_1 = 0.0312$	$R_1 = 0.0525$	$R_1 = 0.0726$
	$wR_2 = 0.0813$	$wR_2 = 0.1395$	$wR_2 = 0.1907$
R (all data)	$R_1 = 0.0354$	$R_1 = 0.0576$	$R_1 = 0.0873$
	$wR_2 = 0.0865$	$wR_2 = 0.1466$	$wR_2 = 0.2047$
ρmax, ρmin (e.Å^{-3})	0.404, -0.335	1.080, -0.440	1.40, -0.91

(**3a**) *p*FPh-PhPNPO = *N*,*N*-Bis(diphenylphosphino oxide)-4-fluoroaniline

(**5a**) 5-*p*-tolyl-PNPO = *N*,*N*-Bis(di-*p*-tolylphosphino oxide)-*p*-toluidine

(**8a**) Chzyl-4-*p*-tolyl-PNPO = *N*,*N*-Bis(di-*p*-tolylphosphino oxide)cyclohexylamine

5.3 *N,N*-Bis(diphenylphosphineoxide)-4-fluoroaniline (3a)

The title ligand, *p*FPh-PhPNPO (**3a**) was synthesized as described in **Paragraph 3.4.1**. This ligand crystallizes in the monoclinic crystal system in the *C*2/*c* space group with four formula units in the unit cell (Z = 4). The asymmetric unit contains half of the titled ligand molecule while the other half is generated through the (1-x, y, ½+z) symmetry. The molecular structure of the free *p*FPh-PhPNPO (**3a**) ligand, including the atomic numbering scheme is illustrated on **Figure 5.2**.

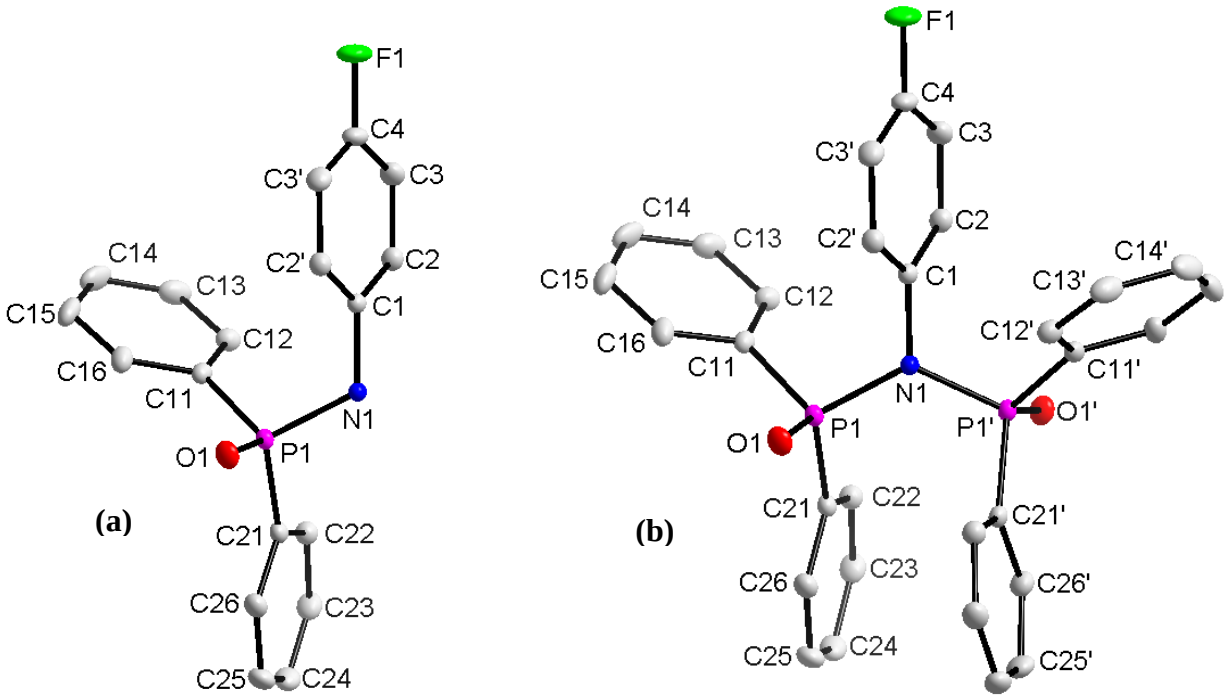

Figure 5.2 (**a**) Molecular representation of *p*FPh-PhPNPO (**3a**) ligand in the asymmetric unit. All displacement ellipsoid are drawn at 50% probability level. (**b**) X′ equivalent atoms are generated through symmetry 1-x, y, ½+z.

Table 5.2 Selected bond lengths and bond angles for the crystal structure of *p*FPh-PhPNPO (**3a**) (Å and °)

Atoms	Bond length (Å)	Atoms	Bond angle (°)
N1 – C1	1.450(2)	P1 – N1 – P1’	126.86(9)
N1 – P1	1.7011(8)	C1 – N1 – P1	116.57(4)
N1 – P1’	1.7011(8)	C1 – N1 – P1’	116.57(4)
P1 – C11	1.8022(14)	N1 – P1 – C11	104.22(6)
P1 – C21	1.7990(13)	N1 – P1 – C21	106.12(6)
P2 – C11’	1.8022(14)	O1 – P1 – N1	115.83(5)
P2 – C21’	1.7990(13)	O1 – P1 – C21	111.63(6)
P1 – O1	1.4803(11)	O1 – P1 – C11	111.45(6)
P1’ – O1’	1.4803(11)	C11 – P1 – C21	106.94(6)

Selected bond distances and angles are summarized in **Table 5.2**. The values reported in this table were found to be comparable to those encountered in similar structures such as (S)-*N*,*N*-bis(diphenylphosphinoyl)alanine methyl ester and *N*,*N*-bis(diphenylphosphoryl)-2-(pyridine-2-yl)ethylamine reported in literature.[16,17] To accommodate the resulting steric bulk on the ligand, the P=O groups are orientated in a *anti* conformation as illustrated in **Figure 5.3** viewed from a plane created through atom P1/N1/P1′ and adopts an almost planar geometry to the line created through P1 and P1'. Furthermore, the angle created by the P1-N-P1′ bonds is 126.86(9) ° and is indicative of a highly distorted trigonal hybridization (sp^2) geometry adopted by the N atom, which typically are 120 ° for standard sp^2 geometry.

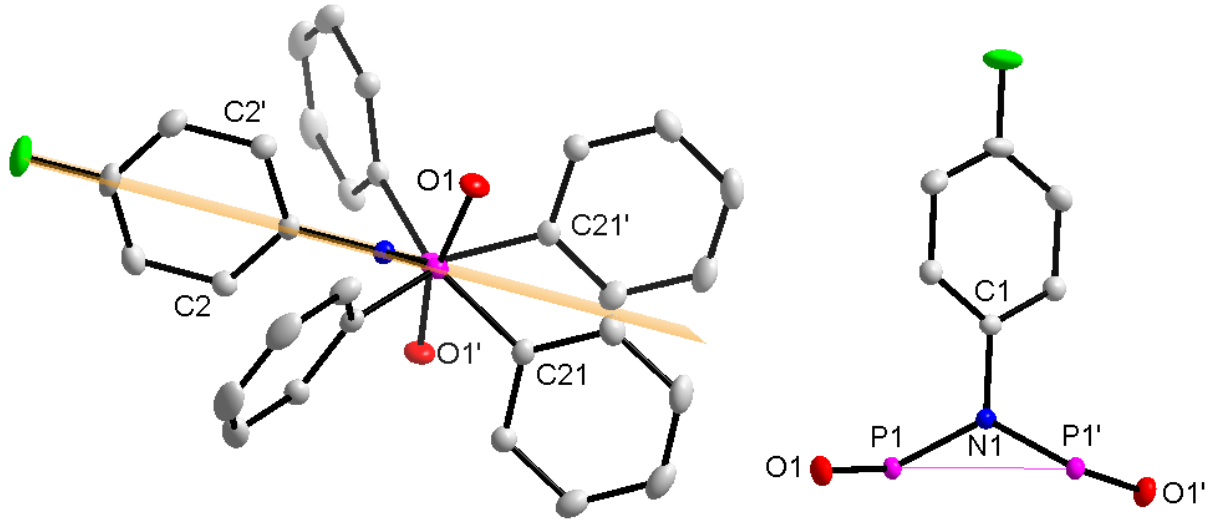

Figure 5.3 Structural view of plane constructed through P1/N1/P1′ and a line through P1 and P1′ on the *p*FPh-PhPNPO (**3a**) ligand.

To stabilize the solid state, two classic hydrogen bond interactions and a single π - π stacking were observed for this ligand in the unit cell as illustrated in **Table 5.3**, **Figure 5.4** and **Figure 5.5**. **Figure 5.6** further illustrates the packing mode of the molecules in the unit cell as viewed along the *c*-axis.

Table 5.3 Classical hydrogen bonds observed on the *p*FPh-PhPNPO (**3a**) ligand.

D-H···A	Symmetry	D-H (Å)	H···A (Å)	D···A (Å)	D-H···A (°)
C12-H10···O1	#1	0.93	2.40	3.309(2)	164
C2-H12···O1	#1	0.93	2.53	3.371(2)	150

Symmetry transformation used to generate equivalent to atoms: **#1** x, -y,-½ + z.

[16] Song, K., Gao, H., Liu, F., Pan, J., Guo, L., Zai, S., Wu, Q., *Eur. J. Inorg. Chem.* **2009**, *20*, 3016-3024.

[17] Slawin, A. M. Z., Woollins, J. D., Zhanga, Q., *J. Chem. Soc., Dalton Trans.* **2001**, *0*, 621-632.

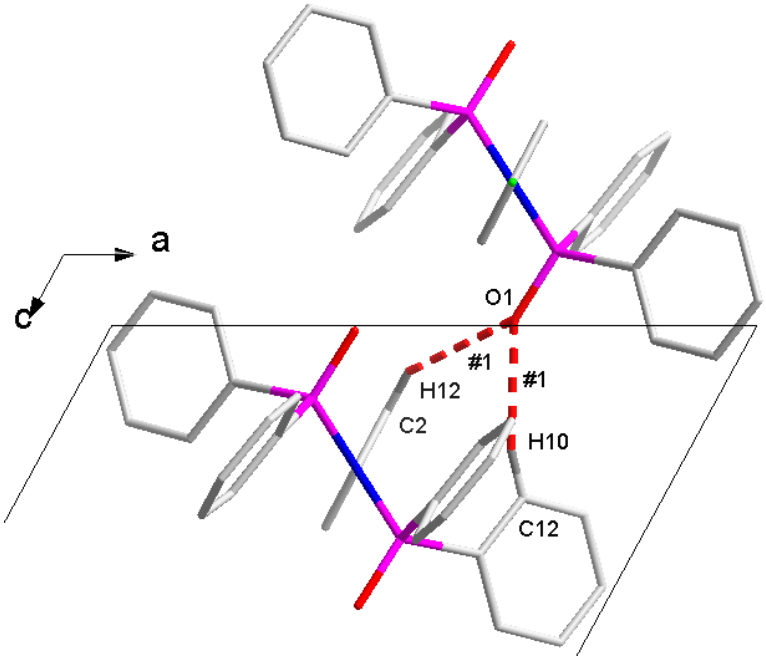

Figure 5.4 Graphical representation of classic hydrogen bonds observed on the *p*FPh-PhPNPO (**3a**) ligand.

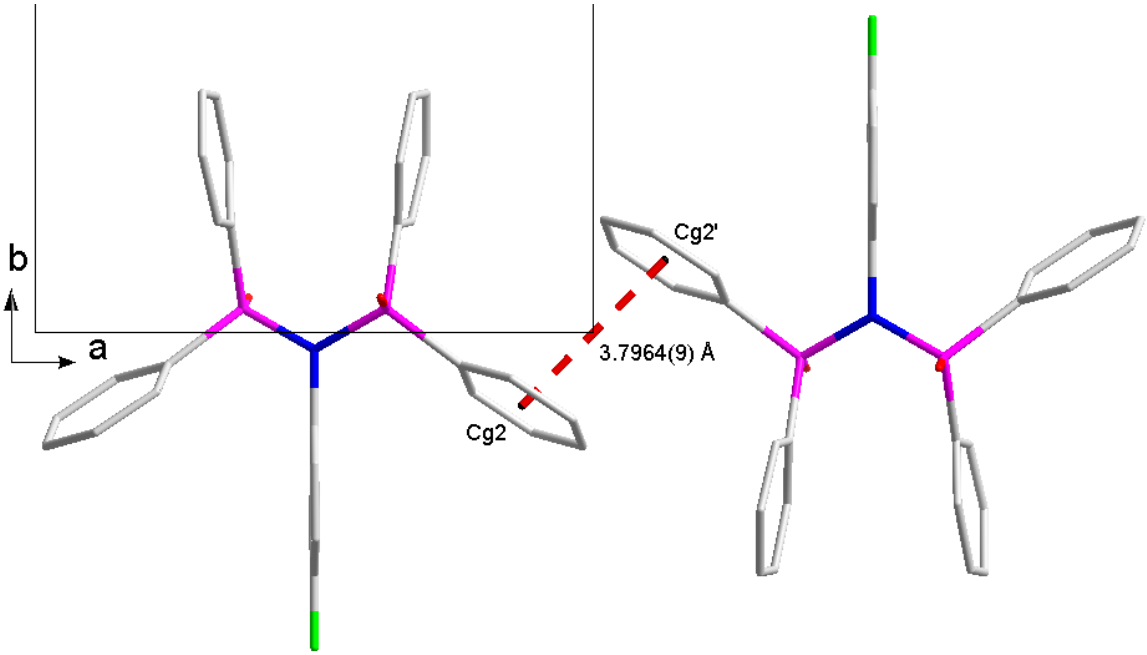

Figure 5.5 Graphic representation π - π stacking observed on the free *p*FPh-PhPNPO (**3a**) ligand. Cg2 is a centroid atom of C11,C12,C13,C14,C15,C16. Projected through the 2-x, -y, 1-z symmetry operator.

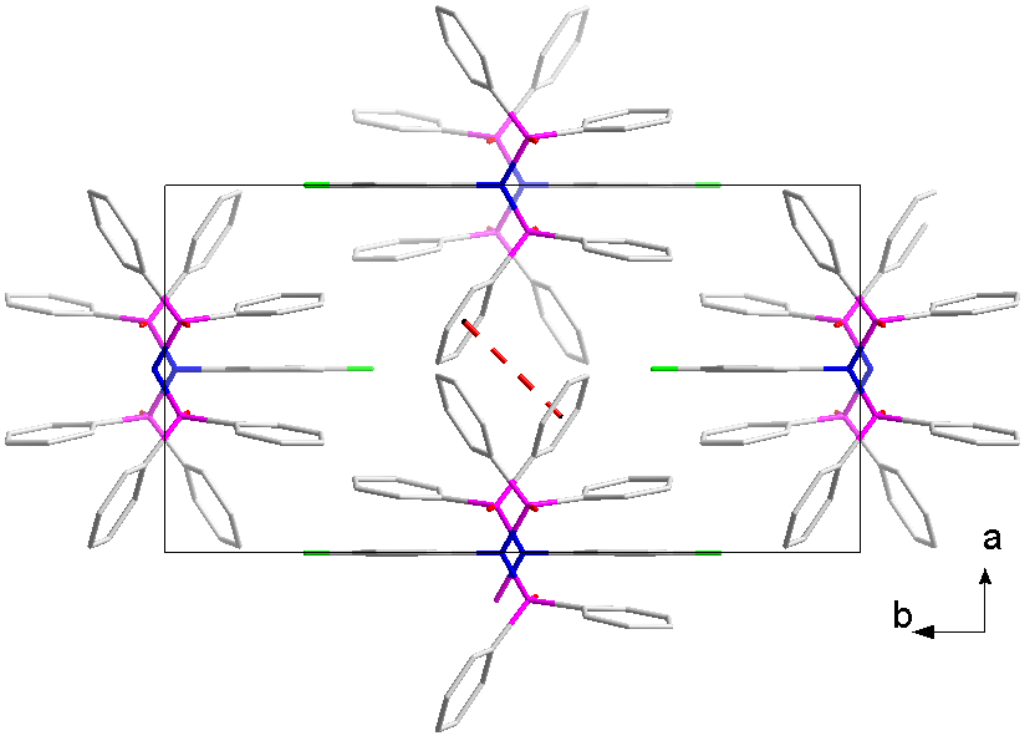

Figure 5.6 Crystal packing of *p*FPh-PhPNPO (**3a**) ligand in the unit cell, viewed along the *c*-axis. H-atoms were omitted for clarity.

5.4 *N,N*-Bis(di-*p*-tolylphosphineoxide)-*p*-toluidine

The title ligand, 5-*p*-tolyl-PNPO (**5a**) was synthesized as described in **Paragraph 3.4.2**. This ligand crystallizes in the triclinic crystal system in the $P\bar{1}$ space group with two formula units in the unit cell (Z = 2). The asymmetric unit contains one independent molecule. The molecular structure of the free 5-*p*-tolyl-PNPO (**5a**) ligand, including the atomic numbering scheme is illustrated in **Figure 5.7**.

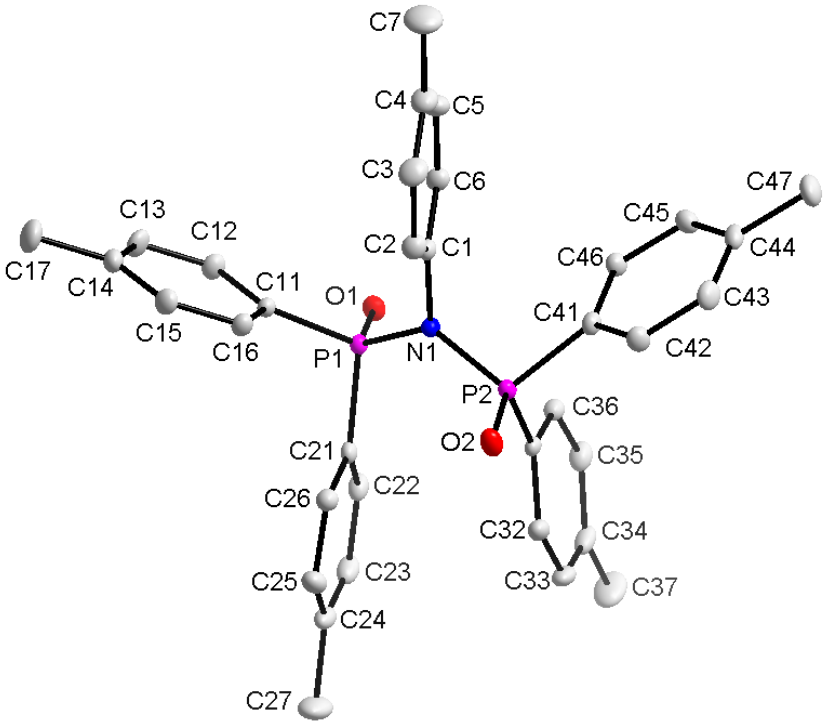

Figure 5.7 Molecular representation of 5-*p*-tolyl-PNPO (**5a**) ligand. All displacement ellipsoid are drawn at 50% probability level.

Table 5.4 Selected bond lengths and bond angles for the crystal structure of 5-*p*-tolyl-PNPO (**5a**) (Å and °)

Atoms	**Bond length (Å)**	**Atoms**	**Bond angle (°)**
N1 – C1	1.456(2)	P1 – N1 – P2	127.01(10)
N1 – P1	1.6984(17)	C1 – N1 – P1	116.32(12)
N1 – P2	1.6997(17)	C1 – N1 – P2	116.65(12)
P1 – C11	1.805(2)	N1 – P1 – C11	105.35(9)
P1 – C21	1.799(2)	N1 – P1 – C21	105.86(8)
P2 – C31	1.809(2)	N1 – P2 – C31	106.42(9)
P2 – C41	1.804(2)	N1 – P2 – C41	104.80(9)
P1 – O1	1.4745(15)	C11 – P1 – C21	106.47(9)
P2 – O2	1.4733(16)	C31 – P2 – C41	105.92(9)

Selected bond distances and angles are summarized in **Table 5.4**. The values reported in this table were also found to be comparable to those encountered in similar structures in literature.[16,17] As stated previously, to accommodate the resulting steric bulk on the ligand, the P=O groups are orientated in a *anti* conformation as illustrated in **Figure 5.8**, viewed from a plane created through atom P1/N1/P2 and adopts an almost planar geometry to the line created through P1 and P2. Furthermore, the angle created by the P1-N-P2 bonds is 127.01(10) ° and is indicative of a highly distorted trigonal hybridization (sp^2) geometry adopted by the N atom.

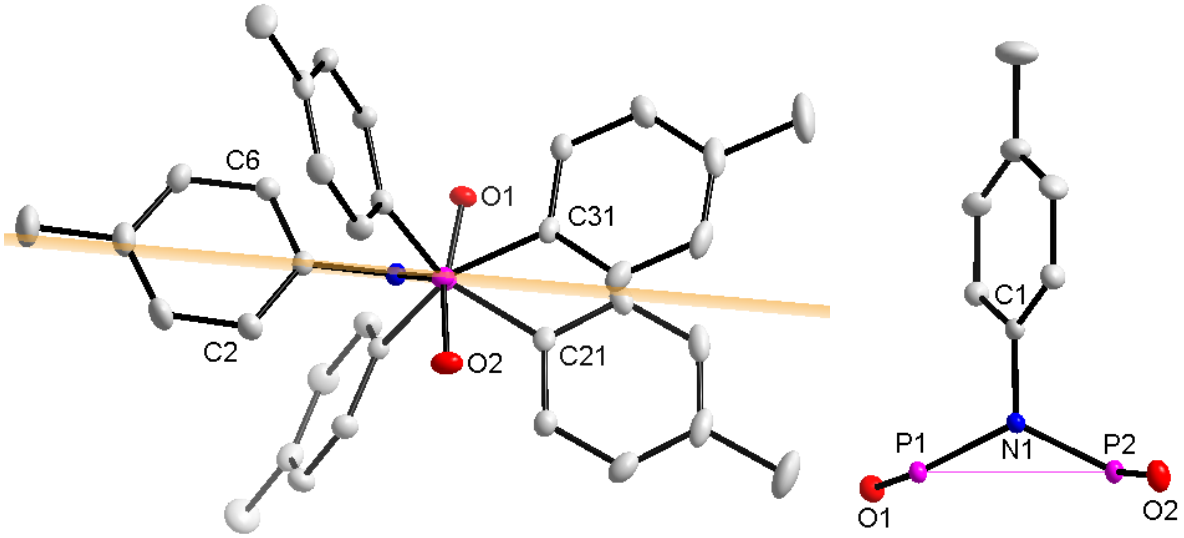

Figure 5.8 Structural view of plane constructed through atoms P1/N1/P2 and a line through P1 and P2 on the 5-*p*-tolyl-PNPO (**5a**) ligand.

A number of classic hydrogen bond interactions were observed in the unit cell of this crystal structure as illustrated in **Table 5.5** and **Figure 5.9**. Moreover, this crystal structure is further stabilized by a single π - π stacking and a single C-H···Cg (π ring) interaction as illustrated in **Table 5.6**, **Figure 5.10** and **Figure 5.11**.

Table 5.5 Classic hydrogen bonds observed on the 5-*p*-tolyl-PNPO (**5a**) ligand.

D-H···A	Symmetry	D-H (Å)	H···A (Å)	D···A (Å)	D-H···A (°)
C36-H7···O1	#1	0.93	2.54	3.452(3)	170
C6-H9···O1	#1	0.93	2.49	3.344(3)	153
C2-H15···O2	#2	0.93	2.55	3.414(3)	155
C46-H16···O1	#1	0.93	2.38	3.298(3)	168
C16-H22···O2	#2	0.93	2.33	3.239(3)	164

Symmetry transformation used to generate equivalent to atoms: **#1** 1-x, 1-y, -z **#2** -x, 1-y, -z

Table 5.6 C-H···Cg(π-ring) interactions for 5-*p*-tolyl-PNPO (**5a**) ligand.

X-H(I)···Cg(J)	Symmetry	H···Cg (Å)	X-H···Cg (°)	X···Cg (Å)
C47-H31B···Cg4	#1	2.82	131	3.524(3)

Symmetry transformation used to generate equivalent to atoms: **#1** 1-x, 1-y, 1-z; Cg(4) = centroid atom of C31,C32,C33,C34,C35,C36.

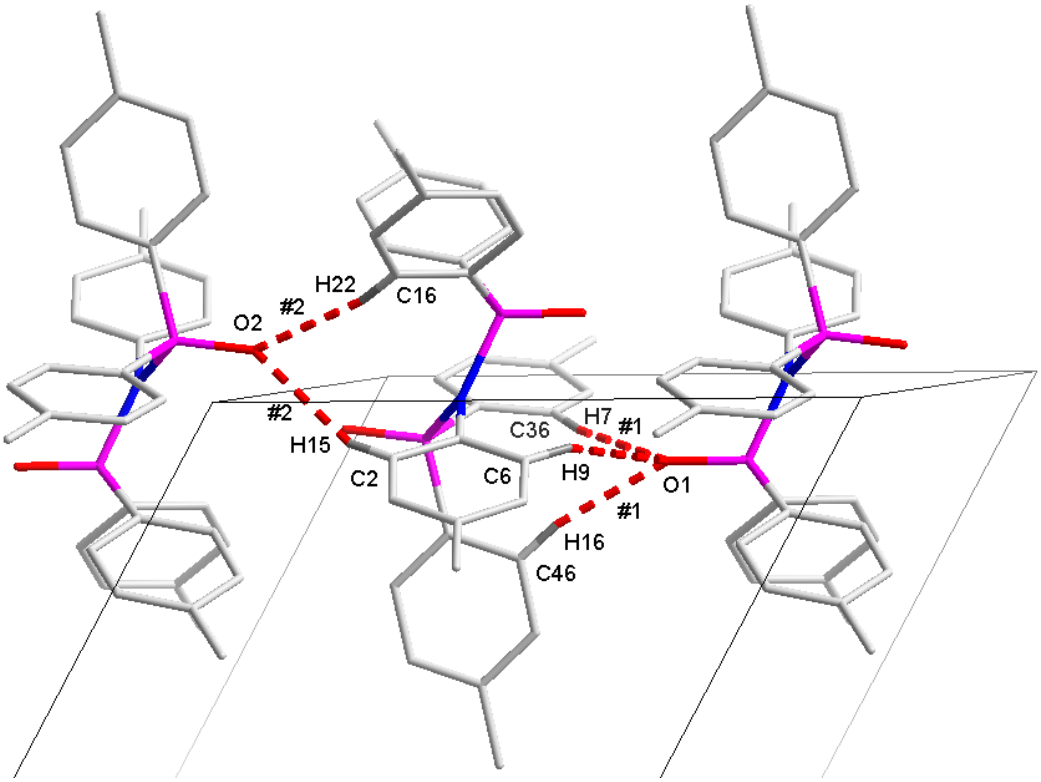

Figure 5.9 Graphic representation of classic hydrogen bonds observed for the 5-*p*-tolyl-PNPO (**5a**) ligand. A typical C-H···O2 bifurcation and a trifurcation for C-H···O1 is observed.

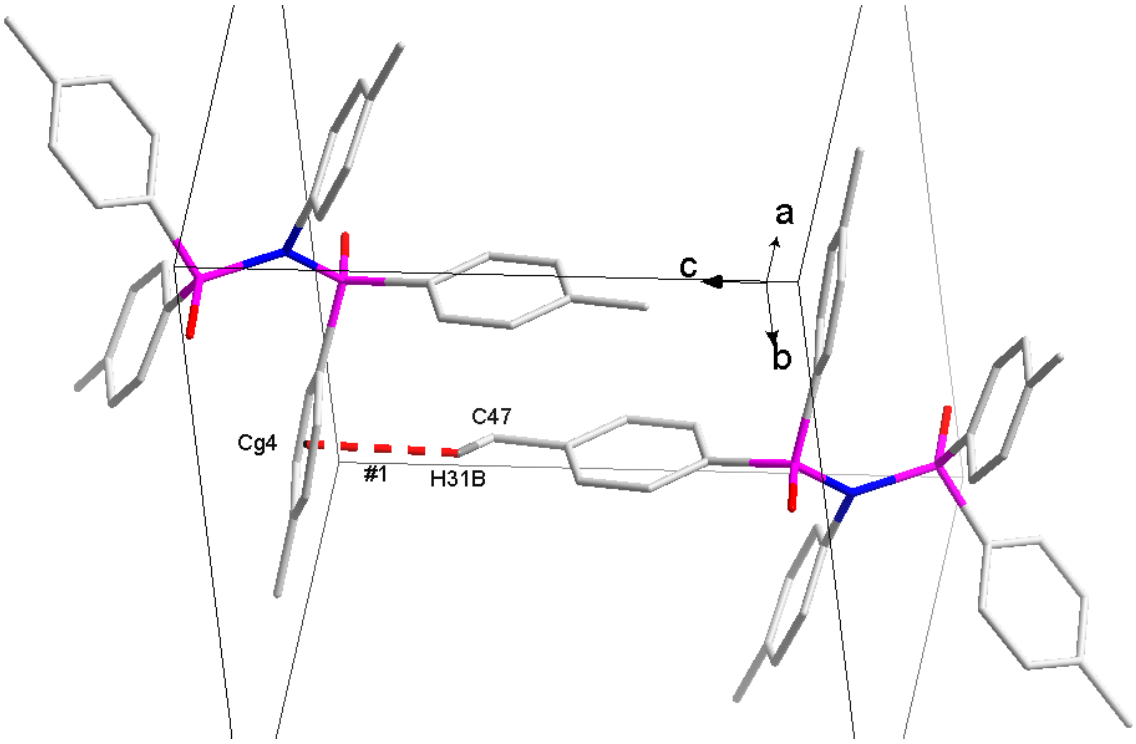

Figure 5.10 Graphic-representation of the C-H···Cg interactions observed on a free 5-*p*-tolyl-PNPO (**5a**) ligand.

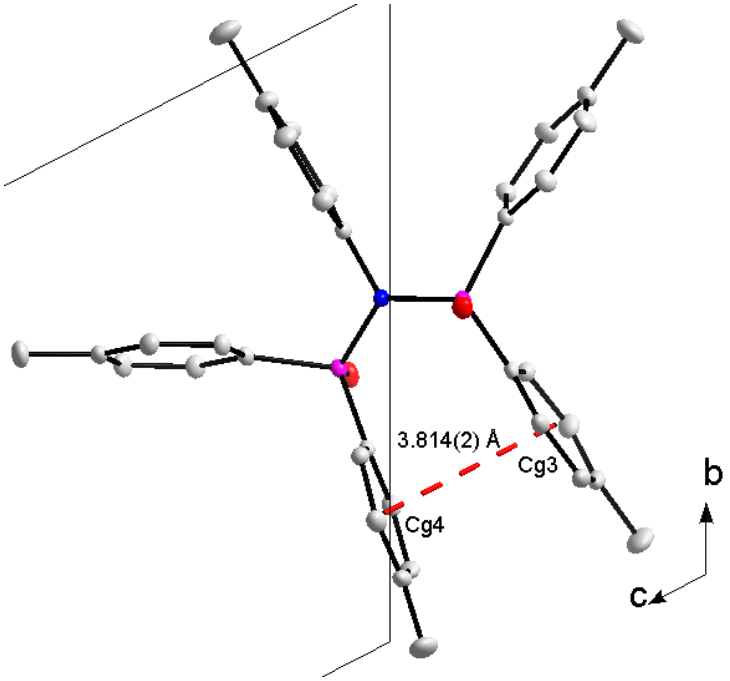

Figure 5.11 Graphic-representation of an intra π - π stacking observed on the 5-*p*-tolyl-PNPO (**5a**) ligand. Cg3 and Cg4 are centroid atoms of C21,C22,C23,C24,C25,C26 and C31,C32,C33,C34,C35,C36 respectively.

The molecule 5-*p*-tolyl-PNPO (**5a**) packs in a head to tail fashion along the *c*-axis as illustrated in **Figure 5.12A**. A sinusoidal packing fashion observed is illustrated in **Figure 5.12B**.

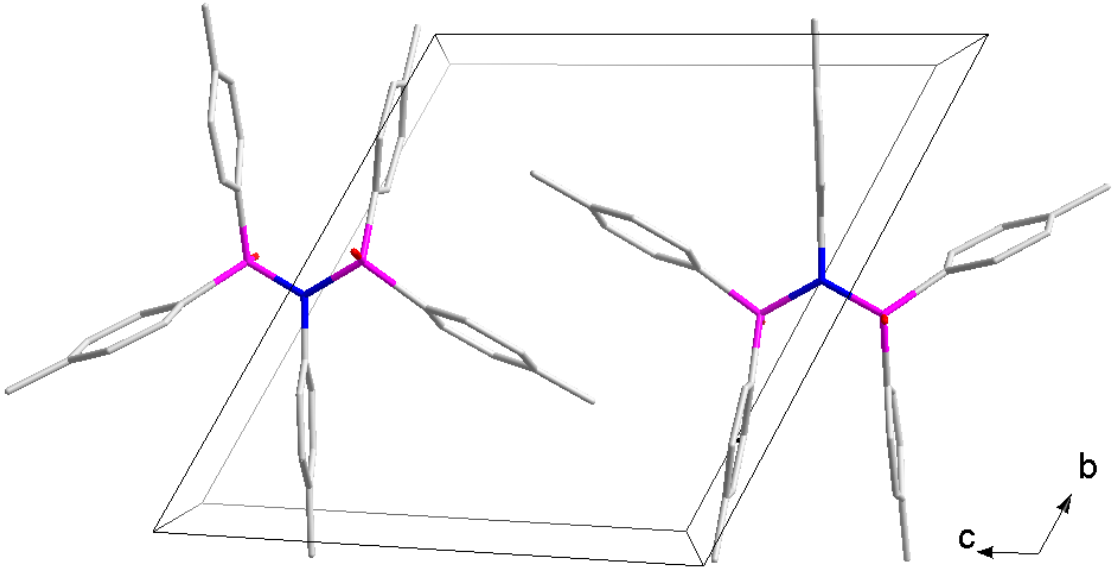

Figure 5.12A Crystal packing of 5-*p*-tolyl-PNPO (**5a**) ligand in the unit cell, viewed along the *a*-axis.

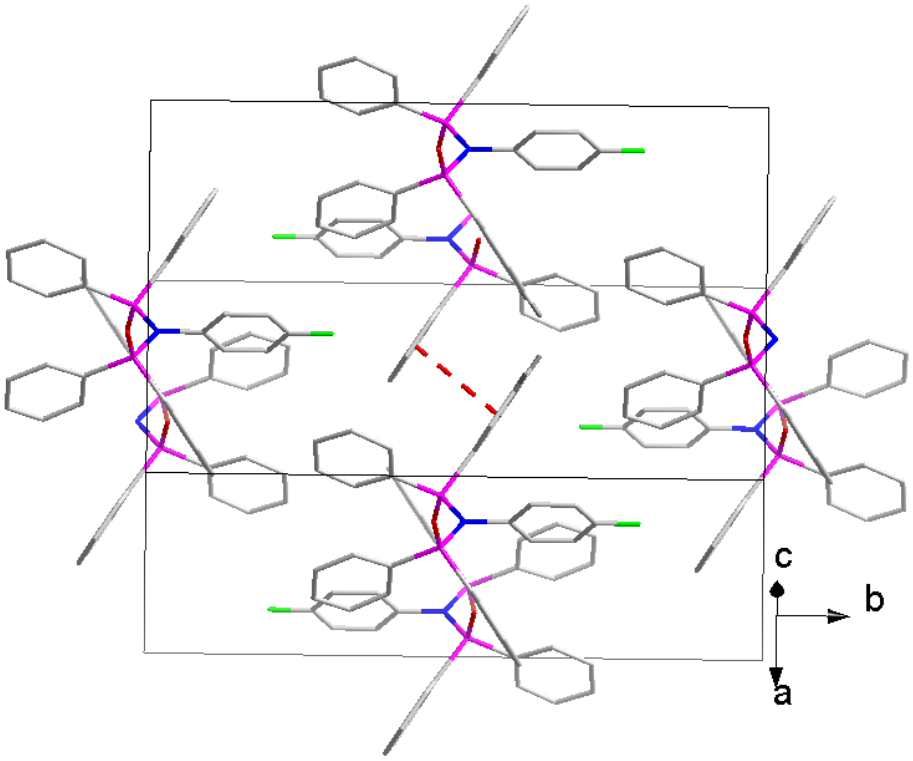

Figure 5.12B A sinusoidal packing fashion observed on the crystal packing of the 5-*p*-tolyl-PNPO **(5a)**.

5.5 *N,N*-Bis(di-*p*-tolylphosphineoxide)cyclohexylamine

The title ligand Chzyl-4-*p*-tolyl-PNPO (**8a**) was synthesized as described in **Paragraph 3.3.8**. This ligand crystallizes in the orthorhombic crystal system in the *Pbca* space group with eight formula units in the unit cell (Z = 8). The asymmetric unit contains one independent molecule and a dichloromethane solvent moiety. The molecular structure of the free Chzyl-4-*p*-tolyl-PNPO (**8a**) ligand, including the atomic numbering scheme is illustrated in **Figure 5.13**.

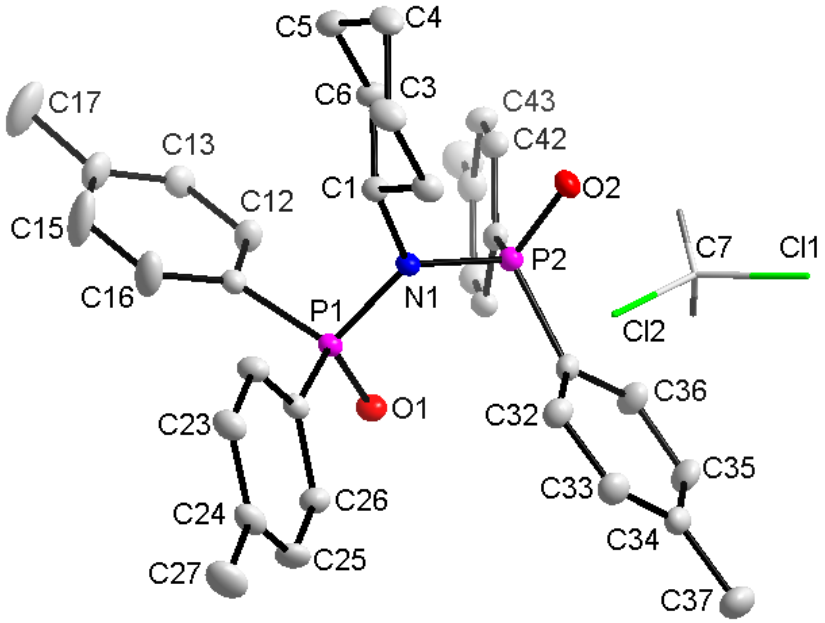

Figure 5.13 Molecular representation of Chzyl-4-*p*-tolyl-PNPO (**8**) ligand. All displacement ellipsoid are drawn at 50% probability level. Dichloromethane moiety presented in stick format for clarity.

Table 5.7 Selected bond lengths and bond angles for the crystal structure of Chzyl-4-*p*-tolyl (**8**) (Å and °)

Atoms	**Bond length (Å)**	**Atoms**	**Bond angle (°)**
N1 – C1	1.507(2)	P1 – N1 – P2	121.16(10)
N1 – P1	1.6892(17)	C1 – N1 – P1	116.47(13)
N1 – P2	1.6814(18)	C1 – N1 – P2	121.64(13)
P1 – C11	1.803(2)	N1 – P1 – C11	104.93(9)
P1 – C21	1.803(2)	N1 – P1 – C21	108.97(9)
P2 – C31	1.797(2)	N1 – P2 – C31	108.11(10)
P2 – C41	1.802(2)	N1 – P2 – C41	109.71(9)
P1 – O1	1.481(2)	C11 – P1 – C21	109.13(10)
P2 – O2	1.497(2)	C31 – P2 – C41	110.18(10)

Selected bond distances and angles are summarized in **Table 5.7**. The values reported in **Table 5.7** were found to be comparable to those encountered in similar structures in literature.[16,17] To accommodate the resulting steric bulk on the ligand, the P=O groups are again, as mentioned above, orientated in a *anti* conformation as illustrated in **Figure 5.14** viewed from a plane created through atom P1/N1/P2, and adopts a chair-like conformation to the line created through P1 and P2. Furthermore, the angle created by the P1-N-P2 bonds is 121.16(10) ° and is indicative of a highly trigonal hybridization (sp^2) geometry adopted by the N atom whose classic value typically is 120 °.

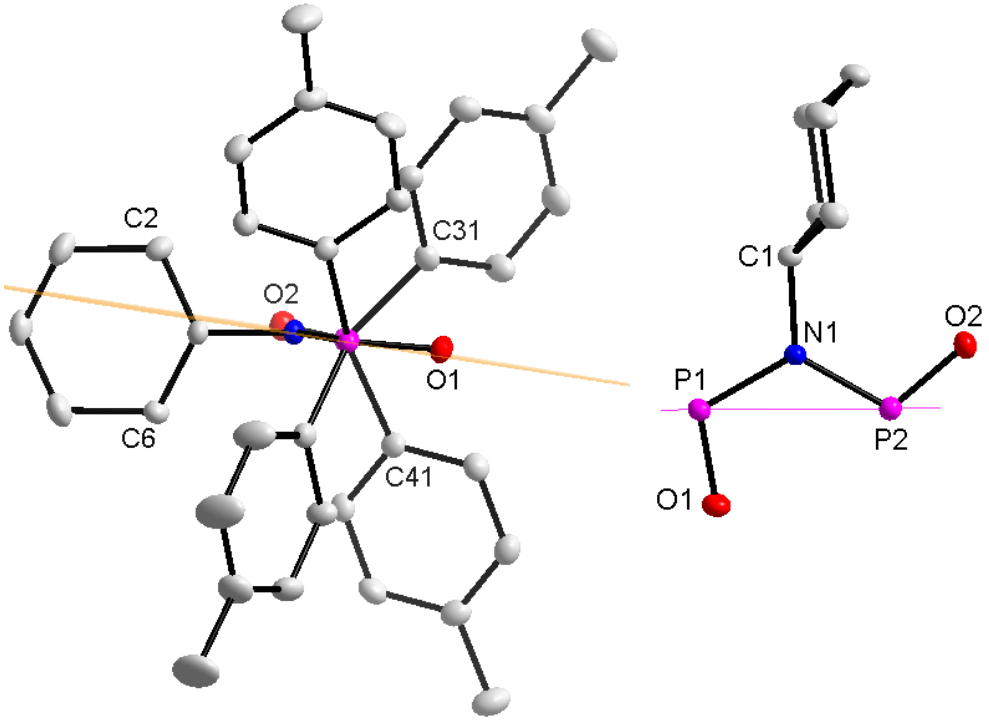

Figure 5.14 Structural view of plane constructed through P1/N1/P2 and a line through P1 and P2 on the Chzyl-4-*p*-tolyl-PNPO (**8a**) ligand.

The solid state is stabilized by two classic hydrogen bonds and four C-H···Cg (π ring) interactions in the unit cell as illustrated in **Table 5.8**, **Table 5.9** and **Figure 5.15** to **Figure 5.17**.

Table 5.8 Classic hydrogen bonds observed on the Chzyl-4-*p*-tolyl-PNPO (**8a**) ligand.

D-H···A	Symmetry	D-H (Å)	H···A (Å)	D···A (Å)	D-H···A (°)
C25-H25···O1	#1	0.93	2.48	3.352(4)	156
C47-H47B···O1	#2	0.96	2.56	3.484(5)	162

Symmetry transformation used to generate equivalent to atoms: **#1** -½+x, y, ½-z; **#2** ½+x, y, ½-z.

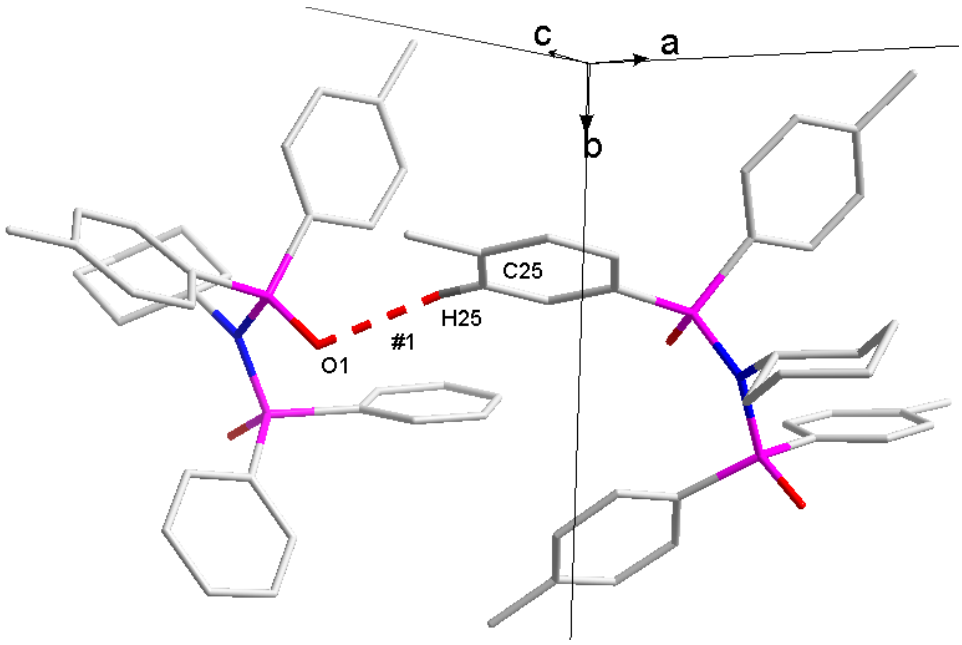

Figure 5.15 Graphic representation of one of the classic hydrogen bond observed for Chzyl-4-*p*-tolyl-PNPO (**8a**) ligand.

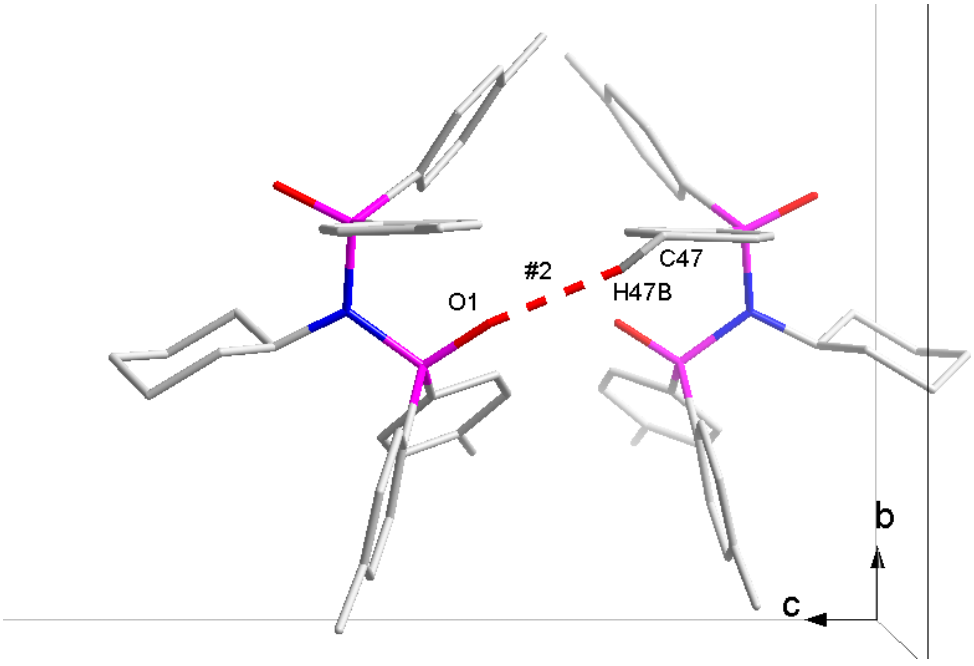

Figure 5.16 Graphic representation of one of the classic hydrogen bond observed for Chzyl-4-p-tolyl-PNPO (8a) ligand.

Table 5.9 C-H···Cg(π-ring) interactions for Chzyl-4-*p*-tolyl-PNPO (**8a**) ligand.

X-H(I)···Cg(J)	Symmetry	H···Cg (Å)	X-H···Cg (°)	X···Cg (Å)
C12-H12···Cg(5)	#1	2.90	166	3.806(4)
C17-H17C···Cg(5)	#2	2.72	137	3.492(4)
C45-H37C···Cg(4)	#3	2.97	144	3.759(4)
C37-H37C···Cg(3)	#4	2.95	158	3.856(4)

Symmetry transformation used to generate equivalent to atoms: **#1** x, y, z; **#2** 1½-x, ½+y, z; **#3** ½-x, ½+y, z; **#4** ½+x, y, ½-z; Cg(3) = centroid atom of C21,C22,C23,C24,C25,C26; Cg(4) = centroid atom of C31,C32,C33,C34,C35,C36; Cg5 = centroid atom of C41,C42,C43,C44,C45,C46.

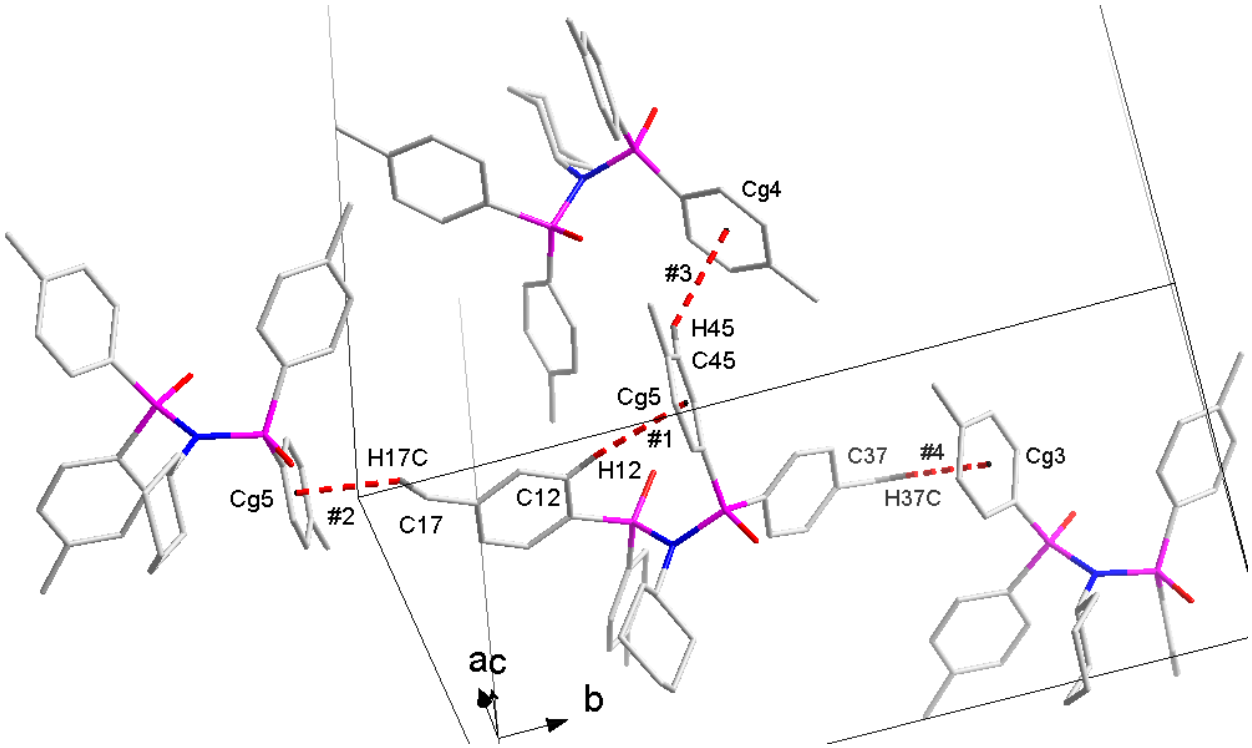

Figure 5.17 Graphic representation of the C-H···Cg interactions observed on a free Chzyl-4-*p*-tolyl-PNPO (**8a**) ligand.

Figure 5.18 illustrates the packing manner of the Chzyl-4-*p*-tolyl-PNPO (**8a**) molecules in the unit cell viewed along the *a*-axis.

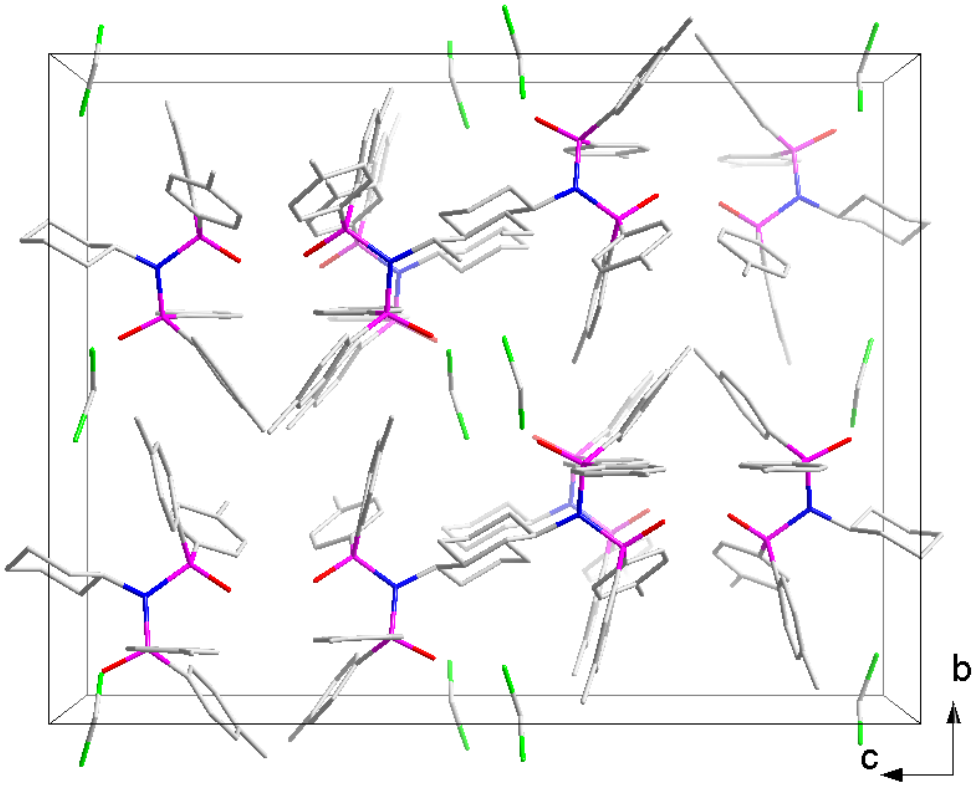

Figure 5.18 Crystal packing of Chzyl-4-*p*-tolyl-PNPO (**8a**) ligand in the unit cell, viewed along the a-axis. H-atoms were omitted for clarity.

5.6 Discussion

The most striking differences between the oxidized and the non-oxidized PNP ligands is the complete change of "C_s" conformation of the *p*FPh-PhPNP (**3**) and its oxidized *p*FPh-PhPNPO (**3a**) form, as well as the retainment of the "C_s" conformation of Chzyl-4-*p*-tolyl (**8**) and its oxidized Chzyl-4-*p*-tolyl-PNPO (**8a**) form illustrated in **Figure 5.19** and **Figure 5.20** respectively.

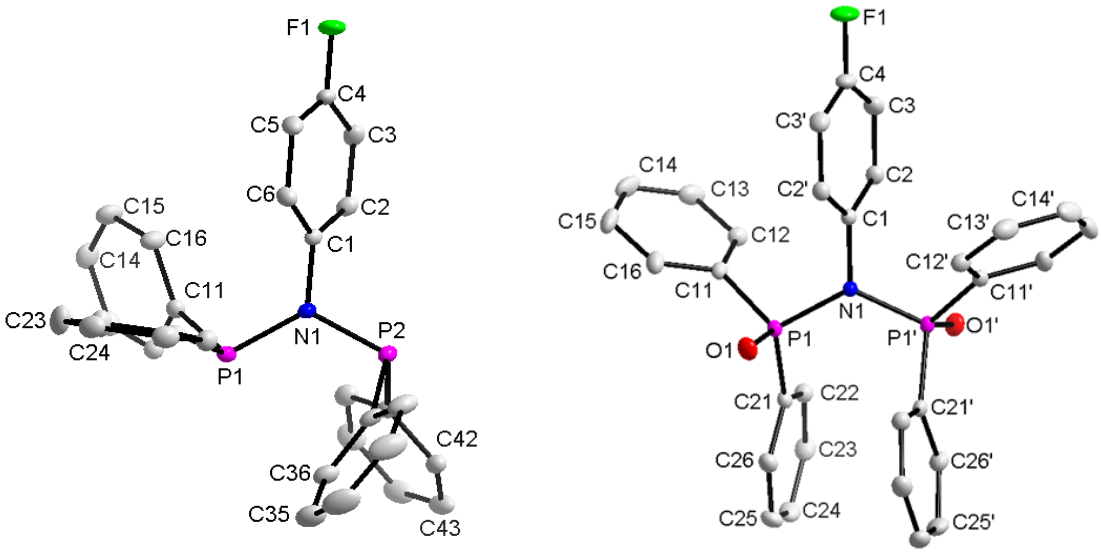

Figure 5.19 Illustration of the complete change of the Cs conformation between the non-oxidized and the oxidized *p*FPh-PhPNPO ligand.

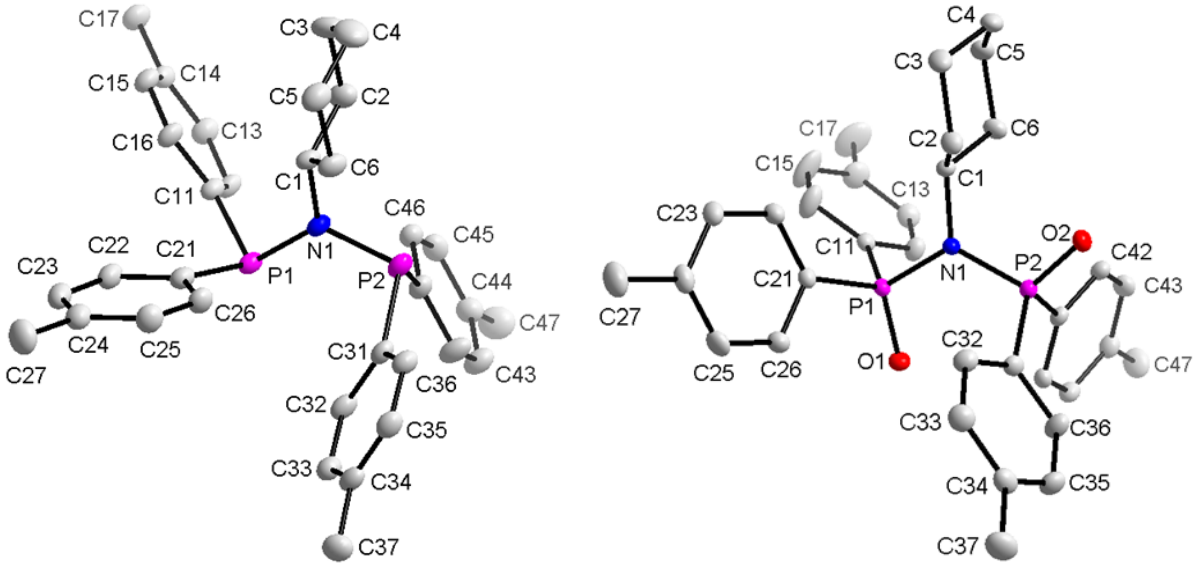

Figure 5.20 Illustrating the retainment of the C_s conformation between the un-oxidized and the oxidized Chzyl-4-*p*-tolyl PNPO ligand.

The C1-N bonds of the oxidized ligands are relatively longer than the non-oxidized ones, whereas the N-P bonds are significantly shorter for the oxidized ligands when compared to the non-oxidized (see **Table 5.10**). This is expected considering the change in P(III) to P(V) for the phosphorus atoms. The *Effective Tolman-based N-substituent steric effect* ($\theta_{N\text{-}sub}$) of the *p*FPh-PhPNP (**3**) and its oxidized form is exactly the same, whereas the ($\theta_{N\text{-}sub}$) between the Chzyl-4-*p*-tolyl (**8**) and its oxidized form differ by only 0.3 ° (Table 5.10).

Table 5.10 Comparison of the selected bond distances, angles and $\theta_{N\text{-}sub}$ for the oxidized and non-oxidized PNP ligands.

ligand	C1-N (Å)	N-P1 (Å)	N-P2 (Å)	P-N-P (°)	$\theta_{N\text{-}sub}$ (°)
F-Ph-PNP (**3**)[a]	1.440(2)	1.7283(13)	1.7300(12)	121.20(7)	50.4
*p*FPh-PhPNPO (**3a**)	1.450(2)	1.7011(8)	1.7011(8)	126.86(9)	50.4
Chzyl-4-*p*-tolyl (**8**)[a]	1.478(4)	1.726(3)	1.713(3)	120.58(16)	85.6
Chzyl-4-*p*-tolyl-PNPO (**8a**)	1.507(2)	1.689(2)	1.681(2)	121.16(10)	85.3

[a] see Chapter 4 of this PhD study.

Further investigations on the oxidized and the non-oxidized Chzyl-4-*p*-tolyl PNP ligands revealed that the angles around the N atom are relatively constant for both molecules, whereas the bond angles around the N atom for the oxidized and the non-oxidized *p*FPh-PhPNP are significantly different as illustrated in **Table 5.10**. The angles around the P atom are significantly larger on the oxidized ligand as illustrated on **Table 5.11**. Again, this is to be expected considering the change in P-atom oxidation state, as well as the fact that the P-atoms are now more tetrahedral with the introduction of the 4th group (=O) in each case.

Table 5.11 Selected bond angles illustrating the difference between oxidized and un-oxidized PNP ligands.

Ligand	N1-P1-C1 (°)	N1-P1-C21 (°)	N1-P2-C31 (°)	N1-P2-C41 (°)	C11-P1-C21 (°)
F-Ph-PNP (**3**)[a]	106.3(6)	105.46(7)	102.88(6)	104.17(6)	101.46(6)
*p*FPh-PhPNPO (**3a**)	104.22(6)	106.12(6)	104.22(6)	106.12(6)	106.94(6)
Chzyl-4-*p*-tolyl (**8**)[a]	104.18(14)	103.02(15)	104.08(15)	104.32(14)	101.47(15)
Chzyl-4-*p*-tolyl-PNPO (**8a**)	104.93(9)	108.97(9)	108.11(10)	109.71(9)	109.13(10)

[a] see Chapter 4 of this PhD study.

Similar observations in terms of structural geometry were observed for 5-*p*-tolyl-PNPO (**5a**) as in the *p*FPh-PhPNPO (**3a**) as illustrated in **Figure 5.21**. At the point of printing this chapter, the

non-oxidized structure of the 5-*p*-tolyl-PNP (**5**) ligand was not yet obtained**. Figure 5.21** also illustrates the overlay of oxidized and non-oxidized 5-*p*-tolyl-PNPO (**5a**) and *p*FPh-PhPNPO (**3a**), whereby the phenyl rings on the P atoms were allowed to freely rotate around the P atom. These overlays are meant to illustrate the difference between the P-N-P cores of oxidized and non-oxidized PNP ligands. From the overlay of ligand **8**[18] and **8a** it is clear that the P-N-P core is kept intact, while a slight difference can be observed from the overlay of ligand **3**[18] and **3a**.

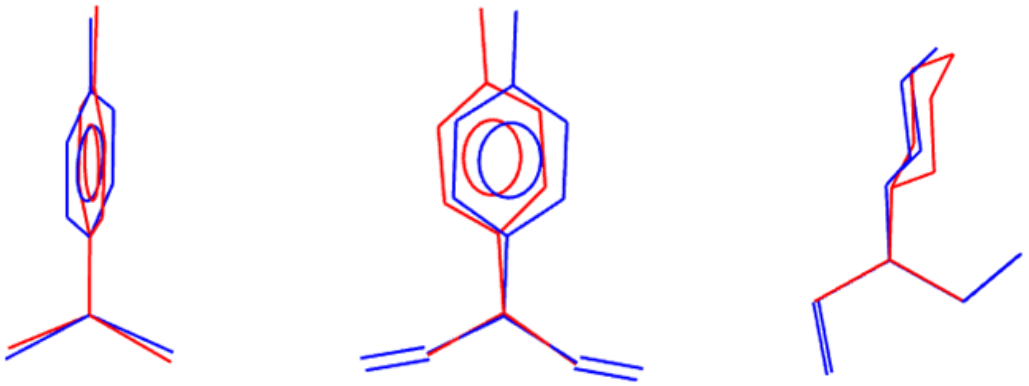

3a + 5a
RMS: 0.0306

3 + 3a
RMS: 0.0433

8 + 8a
RMS: 0.0225

Figure 5.21 Graphic illustration of the overlay of oxidized and non-oxidized ligands of **3**[18] and **8**[18] together with an overlay of 5-*p*-tolyl-PNPO (**5a**) and *p*FPh-PhPNPO (**3a**).

5.7 Conclusion

Crystallographic analysis of three diphosphinoamine oxides namely *p*FPh-PhPNPO (**3a**), 5-*p*-tolyl-PNPO (**5a**) and Chzyl-4-*p*-tolyl-PNPO (**8a**) were presented in this chapter. As indicated, this part of the PhD thesis forms part of the overarching PNP ligand stability investigations. The structures of **3a** and **5a** were comparable with relation to bond lengths and angles, while the structures of **8**[18] and **8a** were similar with respect to adopted conformation, bond angles and bond lengths.

Knowledge of the solid and solution state of these ligands (both oxidized and non-oxidized) is particularly important to better understand not only their exceptional stability towards bond cleavage through oxidation, but also to comprehend the various probable coordination

[18] See **Chapter 4** of this PhD study.

possibilities which these ligands may possess. It was possible to preliminarily infer the ligands' arrangement from NMR spectroscopy studies, but now these assumptions have been corroborated by the crystal structures obtained through X-ray diffraction studies.

To better understand the coordination abilities of these ligands, pure non-oxidized ligands synthesized in **Chapter 3** were coordinated to the *fac*-$[Re(CO)_3]^+$ metal precursor. The results obtained from this consecutive study are next presented in **Chapter 6**.

6 Single crystal X-ray diffraction study of *fac*-[Re(CO$_3$)(PNP)X] complexes

What to expect!

A detailed crystallographic evaluation of four diphosphinoamine (PNP) ligands coordinated to the fac-Re(I) tricarbonyl synthon will be presented in this chapter.

6.1 Introduction

Facial tricarbonyl complexes of group 7 transition metals (Mn, Tc and Re) have been extensively investigated for more than two decades.[1,2] Moreover, a particular focus has been directed towards the aqueous tricarbonyl species as they contain labile H_2O moieties and kinetically stable tricarbonyl ligands in the low-spin d^6 tricarbonyl core.[3] These studies have significantly influenced the design of model radiopharmaceutical agents, particularly were the ^{99m}Tc transition metal is concerned.

The influence of various ligand systems on the kinetic stability and biological activity of these tricarbonyl complexes is also a fertile area of research (see **Chapter 2**). Knowledge gained from these investigations have assisted in optimizing the conditions required for labeling, particularly where radioactive elements such as Re-188/186 and Tc-99/99m were concerned. The search of mono-, bi- and tridentate ligands and the functionalization of this respective ligands to stimulate required properties for targeting organs, is therefore an ongoing process.

[1] Alberto, R., Egli, A., Abram, U., Hegetschweiler, K., Gramlich, V., Schubiger, P. A., *J. Chem. Soc., Dalton Trans.* **1994**, 2815-2820.

[2] Alberto, R., Schibli, R., Egli, A., Schubiger, A. P., *J. Am. Chem. Soc.* **1998,** *120*, 7987-7988.

[3] Alberto, R., Schibli, R., Waibel, R., Abram, U., Schubiger, P. A., *Coord. Chem. Rev.* **1999,** *190-192*, 901-919.

There is therefore a clear need for a continued systematic ligand design strategy as opposed to the random "hit and miss" approach practiced in many drug development research. Although the former presents a more complex approach, research in various fields such as catalysis have shown what success systematic ligand design can offer.[4,5]

One of the major aims of this project was to crystallographycally determine the coordination chemistry of various diphosphinoamine (PNP) ligands using various crystallizing techniques and single crystal X-ray diffraction. To attain this, four different *fac*-[Re(CO_3)(PNP)X] complexes namely *fac*-[Re(*p*Tol-PhPNP)$(CO)_3(O^iPr)$] (**1c**), *fac*-[Re(*p*ClPh-PhPNP)$(CO)_3$Br] (**2c**), *fac*-[Re(*p*FPh-PhPNP)$(CO)_3$Br] (**3c**) and *fac*-[Re(Cbutyl-4-p-tolyl)$(CO)_3$Br] (**7c**) were crystallized and investigated with single crystal X-ray diffraction (**Figure 6.1**). These Re-PNP complexes will be described in this chapter where a primary focus will be on selected inter and intramolecular bond parameters, molecular interactions and crystal packing modes.

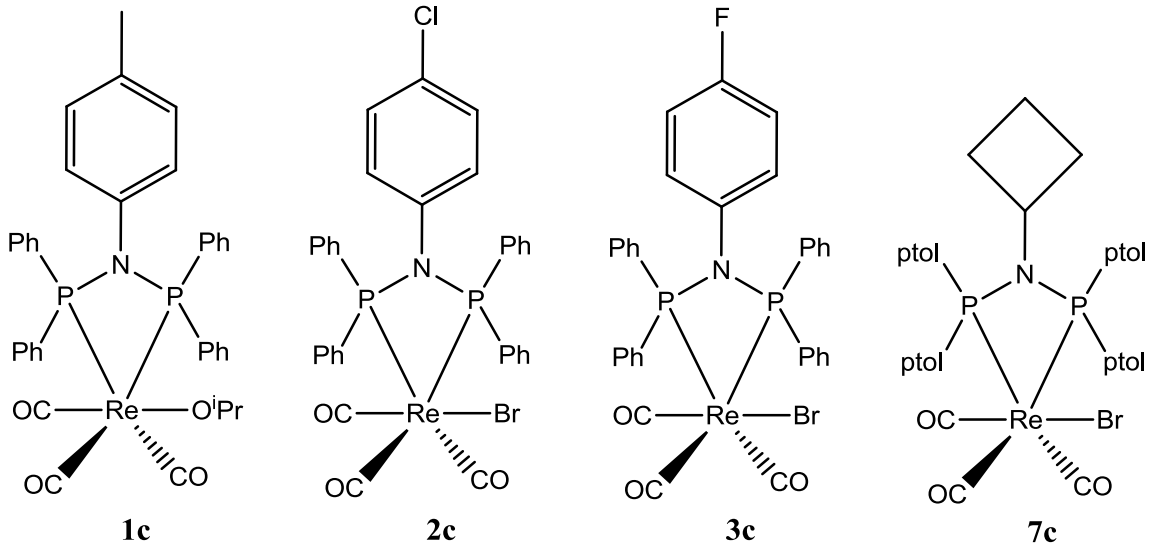

Figure 6.1 Re-PNP tricarbonyl complexes with various electronic and steric properties on the PNP ligand crystallized and described in this study: **1c** *fac*-[Re(*p*Tol-PhPNP)$(CO)_3(O^iPr)$], **2c** *fac*-[Re(*p*ClPh-PhPNP)$(CO)_3$Br], **3c** *fac*-[Re(*p*FPh-PhPNP)$(CO)_3$Br] and **7c** *fac*-[Re(Cbutyl-4-p-tolyl)$(CO)_3$Br]. Molecular numbering is reminiscent of that found in **Chapter 3,** except that the "c" symbol indicates the corresponding **Re**-PNP complex.

[4] Cloete, N., Visser, H. G., Engelbrecht, I., Overett, M. J., Gabrielli, W. F., Roodt, A., *Inorg Chem.*. **2013,** *52*, 2268-2270.

[5] Bollmann, A., Blann, K., Dixon, J. T., Hess, F. M., Killian, E., Maumela, H., McGuinness, D. S., Morgan, D. H., Neveling, A., Otto, S., Overett, M., Slawin, A. M. Z., Wasserscheid, P., Kuhlmann, S., *J. Am. Chem. Soc.*, **2004**, *126*, 14712-14713.

6.2 Experimental

Diffraction data for (**1c**) *fac*-[Re(*p*Tol-PhPNP)(CO)$_3$(O^{i}Pr)], (**2c**) *fac*-[Re(*p*ClPh-PhPNP)(CO)$_3$Br], (**3c**) *fac*-[Re(*p*FPh-PhPNP)(CO)$_3$Br] and (**7c**) *fac*-[Re(Cbutyl-4-*p*-tolyl)(CO)$_3$Br] were collected at 100 K on a Bruker X8 Apex II 4K diffractometer using monochromated Mo Kα radiation with a wavelength of λ = 0.71073 Å. All the cell parameters were refined using the XPREP4 and SAINT-Plus[6] program while SADABS[7] and multiscan techniques were used for the absorption corrections. The structures were solved by either the direct methods or by the use of SIR97[8] and refined on F^2 using anisotropic displacement parameters for all non-hydrogen atoms. SHELXL-97 [9,10] and WinGX[11] were used for structure solutions and refinements respectively. The molecular graphics were drawn using the DIAMOND program.[12] Structural overlays were drawn utilizing the Mercury program.[13] All aromatic, methylene and methyl hydrogen atoms were placed in geometrically idealized positions (C-H = 0.95 Å to 0.98 Å) and constrained to ride on their parent atoms with U_{iso}(H) = 1.2U_{eq}(C) and U_{iso}(H) = 1.5U_{eq}(C) respectively.

For all four complexes, a summary of the general crystal data and refinement parameters is given in **Table 6.1**, with selected bond parameters reported and discussed under each relevant sub-paragraph. Complete lists of bond distances, bond angles, atomic coordinates, hydrogen coordinates, torsion angles and anisotropic displacement parameters for these complexes are found in the supplementary data (**Appendix A**). Hydrogen atoms and numbering for certain carbon atoms were omitted for clarity on some molecular structures. For aromatic rings, the first and the second digit represents the ring number and the specific C-atom in the ring respectively.

---

[6] *SAINT-Plus*, version 6.02 (including XPREP); Bruker AXA, Inc.: Madison, WI, USA, **1999**.

[7] *SADABS*, version 2004/1; Bruker AXS, Inc.: Madison, WI, USA, **2004**.

[8] Altomare, A., Burla, M. C., Camalli, M., Cascarano, G. L., Giacovazzo, C., Guagliardi, A., Moliterni, A. G. G., Polidori, G., Spagna,R., *J. Appl. Cryst*., **1999**, *32*, 837-838.

[9] Sheldrick, G. M., SHELXL97; University of Göttingen: Göttingen, Germany, **1997**.

[10] Sheldrick, G. M., *Acta Crystallogr*. **2008**, *A64*, 112-122.

[11] Farrugia, L. J., *J. Appl. Crystallogr*. **1999**, *32*, 837-838.

[12] Brandenburg, K., Putz, H., DIAMOND, release 3.1b; Crystal Impact GbR: Bonn, Germany, **2005**.

[13] Macrae, C. F., Bruno, I. J., Chisholm, J. A., Edgington, P. R., McCabe, P., Pidcock, E., Rodriguez-Monge, L., Taylor, R., van de Streek, J., Wood, P. A., *J. Appl. Cryst*., **2008**, 41, 466-470.

Table 6.1 General X-ray crystal data and refinement parameters of (**1c**) *fac*-[Re(*p*Tol-PhPNP)$(CO)_3(O^iPr)$], (**2c**) *fac*-[Re(*p*ClPh-PhPNP)$(CO)_3$Br], (**3c**) *fac*-[Re(*p*FPh-PhPNP)$(CO)_3$Br] and (**7c**) *fac*-[Re(Cbutyl-4-*p*-tolyl)$(CO)_3$Br].

Crystallographic data	[Re(*p*Tol-PNP)$(CO)_3(O^iPr)$] (**1a**)	[Re(*p*ClPh-PNP)$(CO)_3$Br] (**2c**)	[Re(*p*FPh-PNP)$(CO)_3$Br] (**3c**)	[Re(Cbutyl-4-*p*-tolyl)$(CO)_3$Br] (**7c**)
Empirical formula	$C_{37}H_{32}NO_4P_2Re$	$C_{33}H_{24}BrClNO_3P_2$ Re	$C_{33}H_{24}BrFNO_3P_2Re$	$C_{35}H_{35}BrNO_3P_2Re$
Formula weight (g mol^{-1})	802.77	846.03	829.58	846.49
Temperature (K)	100(2)	100(2)	100(2)	100(2)
Crystal system	Monoclinic	Monoclinic	Monoclinic	Monoclinic
Space group	$P2_1/c$	$P2_1/c$	$P2_1/c$	Pn
Unit cell dimensions				
a (Å)	10.460(2)	11.290(1)	10.541(2)	9.6064(13)
b (Å)	18.582(3)	14.623(2)	15.625(3)	17.193(2)
c (Å)	18.295(4)	19.017(2)	18.685(3)	20.222(3)
α (°)	90	90	90	90
β (°)	114.802(17)	90.834(4)	90.929(5)	96.442(4)
γ (°)	90	90	90	90
Volume ($Å^3$)	3228.0(12)	3139.3(2)	3077.1(19)	3318.7(8)
Z	4	4	4	4
Density (g cm^{-3})	1.652	1.790	1.791	1.694
Crystal colour	Colourless	Colourless	Colourless	Colourless
Crystal morphology	Cuboid	Cuboid	Cuboid	Cuboid
Crystal size (mm^3)	0.46 x 0.37 x 0.20	0.24 x 0.20 x 0.20	0.44 x 0.29 x 0.18	0.60 x 043 x 0.19
μ (mm^{-1})	3.905	5.366	5.393	4.997
F(000)	1592	1640	1608	1666
θ range (°)	1.645 - 27.998	2.985 - 27.999	1.699 - 27.998	1.184 - 28.422
	$-11 \le h \le 13$	$-14 \le h \le 14$	$-13 \le h \le 13$	$-12 \le h \le 11$
Index ranges	$-24 \le k \le 24$	$-19 \le k \le 19$	$-20 \le k \le 20$	$-22 \le k \le 22$
	$-24 \le l \le 17$	$-17 \le l \le 25$	$-15 \le l \le 24$	$-19 \le l \le 27$
Reflections collected	60132	57533	56318	58883
Unique reflections	7782	7568	7415	13260
R_{int}	0.0543	0.0669	0.0534	0.0399
Completeness to theta (°, %)	25.2, 99.9	25.2, 99.9	25.2, 99.9	26.0 , 99.7
Data / restraints / parameters	7782/ 4 / 408	7568 / 5 / 406	7415 / 1 / 379	13260 / 11 / 398
Goodness-of-fit on F^2	1.049	1.051	1.084	1.056
R [$I > 2\sigma(I)$]	$R_1 = 0.0270$	$R_1 = 0.0253$	$R_1 = 0.0261$	$R_1 = 0.0269$
	$wR_2 = 0.0715$	$wR_2 = 0.0510$	$wR_2 = 0.0601$	$wR_2 = 0.0640$
R (all data)	$R_1 = 0.0292$	$R_1 = 0.0317$	$R_1 = 0.0290$	$R_1 = 0.0287$
	$wR_2 = 0.0727$	$wR_2 = 0.0529$	$wR_2 = 0.0615$	$wR_2 = 0.0656$
ρ_{max}, ρ_{min} (e.$Å^{-3}$)	2.50, -1.49	0.72, -0.753	1.77, -1.16	2.106, -1.587

*p*Tol-PhPNP - *N*,*N*-Bis(diphenylphosphino)-*p*-toluidine
*p*ClPh-PhPNP - *N*,*N*-Bis(diphenylphosphino)-4-chloroaniline
*p*FPh-PhPNP - *N*,*N*-Bis(diphenylphosphino)-4-fluoroaniline
Cbutyl-4-*p*-tolyl - *N*,*N*-Bis(di-*p*-tolylphosphino)cyclobutylamine

6.3 *N,N*-[Re(*p*Tol-PhPNP)(CO)$_3$(O^{i}Pr)] (1c)

The title complex, *fac*-[Re(*p*Tol-PhPNP)(CO)$_3$(O^{i}Pr)] (**1c**) was synthesized as described in **Paragraph 3.5.3**. This complex crystallizes in the monoclinic crystal system in the $P2_1/c$ space group with four formula units in the unit cell (Z = 4). The asymmetric unit contains one independent molecule. The molecular structure of the title complex, including the atomic numbering scheme is illustrated in **Figure 6.2**.

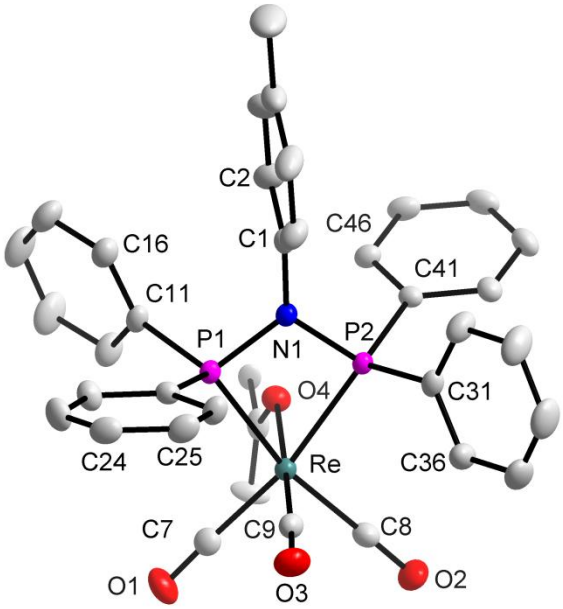

Figure 6.2 Molecular representation of *fac*-[Re(*p*Tol-PhPNP)(CO)$_3$(O^{i}Pr)] (**1c**) complex. All displacement ellipsoids are drawn at 50% probability level.

Table 6.2 Selected bond lengths and bond angles for the crystal structure of *fac*-[Re(*p*Tol-PhPNP)(CO)$_3$(O^{i}Pr)] (**1c**) (Å and °)

Atoms	Bond length (Å)	Atoms	Bond angle (°)
Re – P1	2.4412(10)	P1 – Re – P2	66.96(3)
Re – P2	2.4571(10)	P2 – N1 – P1	104.34(14)
Re – O4	2.157(3)	N1 – P1 – Re	94.54(9)
Re – C7	1.964(4)	N1 – P2 – Re	94.14(9)
Re – C8	1.967(4)	O4 – Re – C9	175.96(12)
Re – C9	1.917(3)	C7 – Re – C8	90.68(14)
C7 – O1	1.139(4)	C9 – Re – C8	88.58(14)
C8 – O2	1.133(4)	C9 – Re – C7	87.53(14)
C9 – O3	1.136(4)		
N1 – P1	1.714(2)		
N1 – P2	1.707(3)		
N1 – C1	1.450(4)		

Selected bond distances and angles are summarized in **Table 6.2**. The three carbonyl ligands are facially orientated to the Re(I) metal centre with two sites coordinated to the neutral bidentate *p*Tol-PhPNP (**1**)[14] PNP ligand, while the final 6th position is occupied by a negatively charged 2-propenol moiety. The octahedral geometry around the Re(I) is distorted as indicated primarily by the small P-Re-P bite angle of only 66.96(3)° and to a lesser extent by the O4-Re-C9 angle of 175.96(12)°. The bond distance values reported in **Table 6.2** for Re-P and Re-C were found to be comparable to those encountered on similar structures such as [*N*,*N*-bis(diphenylphosphino)propylamine-k^2*P,P'*]bromidotricarbonyl-rhenium(I) and [bis(diphenyl-phosphino)amine-*P,P'*]bromotricarbonylrhenium(I) reported in literature.[15, 16] The *Effective Tolman-based N-substituent steric effect* ($\theta_{N\text{-}sub}$) of the *p*Tol-PhPNP **(1)** ligand was calculated using **Equation 4.1** and **Figure 4.3** from **Chapter 2** and found to be 57.2 °. The Re-O4 bond distance of 2.157(3) Å is also found to be in the same range as the values of other Re(I) tricarbonyl complexes containing Re^{I}-O bonds reported in literature.[17,18] Furthermore, the P(1)-N(1)-P(1) angle of 104.34(14)° is indicative of a slightly distorted tetrahedral geometry around the N atom.

No classic hydrogen interactions were observed in this complex in the unit cell. However, the crystal structure of *fac*-[Re(*p*Tol-PhPNP)$(CO)_3(O^iPr)$] **(1c)** is stabilized by three C-H···Cg (π-ring) interactions and two C-O···Cg (π-ring) as illustrated in **Table 6.3**, **Table 6.4**, **Figure 6.3** and **Figure 6.4**.

Table 6.3 C-H···Cg(π-ring) interactions observed on *fac*-[Re(*p*Tol-PhPNP)$(CO)_3(O^iPr)$] (**1c**) complex.

X-H(I) ···Cg(J)	Symmetry	H···Cg (Å)	X-H···Cg (°)	X···Cg (Å)
C26 -H26···Cg(1)	#1	2.91	103	3.248(4)
C46-H46···Cg(1)	#1	2.98	103	3.316(4)
C24-H24···Cg(6)	#2	2.63	148	3.457(4)

Symmetry transformation used to generate equivalent to atoms: **#1** x, y, z; **#2** 2-x, ½+y,½-z; Cg1 = centroid atoms of Re1,P1,N1,P2; Cg6 = centroid atom of C41,C42,C43,C44,C45,C46;

[14] See **Chapter 3** of this PhD thesis.

[15] Schutte, M., Visser, H. G., Brink, A., *Acta Cryst.* **2009**, E*65*, m1575-1576.

[16] Graziani, R., Casellato, U., *Acta Cryst.* **1996**, C*52*, 850-852.

[17] Schutte, M., Kemp, G., Visser, H. G., Roodt, A., *Inorg. Chem.* **2011,** *50*, 12486-12498.

[18] Mokolokolo, P. P., Frei, A., Tsosane, M.S., Kama D. V., Schutte-Smith, M., Brink, A., Visser, H. G., Meola, G., Alberto, R., Roodt, A., *Inorganica Chim. Acta*. **2018,** *471*, 249-256.

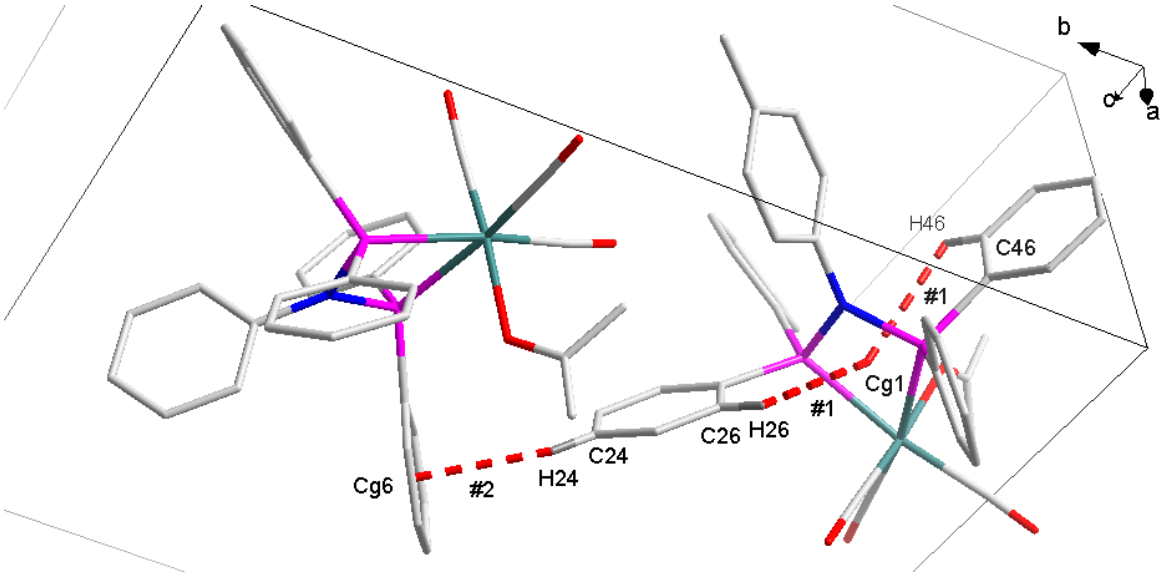

Figure 6.3 Graphic representation of some of the C-H···Cg (red dashed bonds) interactions observed for ligand *fac*-[Re(*p*Tol-PhPNP)(CO)$_3$(O^{i}Pr)] (**1c**).

Table 6.4 C-O···Cg(π-ring) interactions observed on *fac*-[Re(*p*Tol-PhPNP)(CO)$_3$(O^{i}Pr)] (**1c**) complex.

C-O(I)···Cg(J)	Symmetry	O···Cg (Å)	C-O···Cg (°)	C···Cg (Å)
C8-O2···Cg(2)	#1	3.569(4)	120.0(3)	4.251(4)
C8-O2···Cg(4)	#1	3.267(4)	101.4(3)	3.664(4)

Symmetry transformation used to generate equivalent to atoms: **#1** 2-x, -½+y,½-z; Cg2 = centroid atoms of C1,C2,C3,C4,C5,C6; Cg4 = centroid atom of C21,C22,C23,C24,C25,C26.

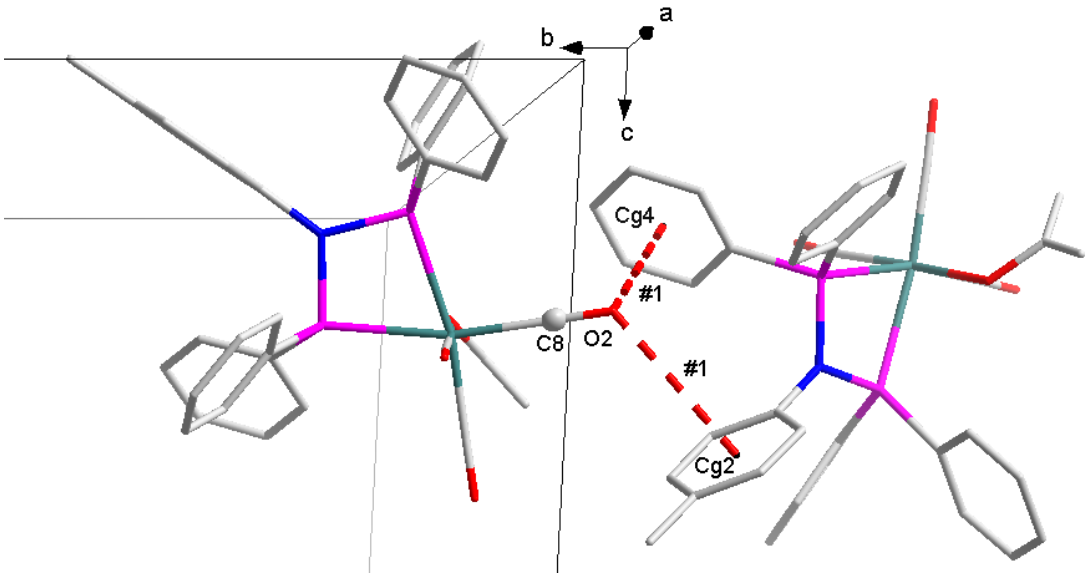

Figure 6.4 Graphic representation of some of the C-O···Cg (red dashed bonds) interactions observed for ligand *fac*-[Re(*p*Tol-PhPNP)(CO)$_3$(O^{i}Pr)] (**1c**).

Figure 6.5 shows how the molecules pack in a heat to tail square packing fashion in the unit cell when viewed along the *a*-axis.

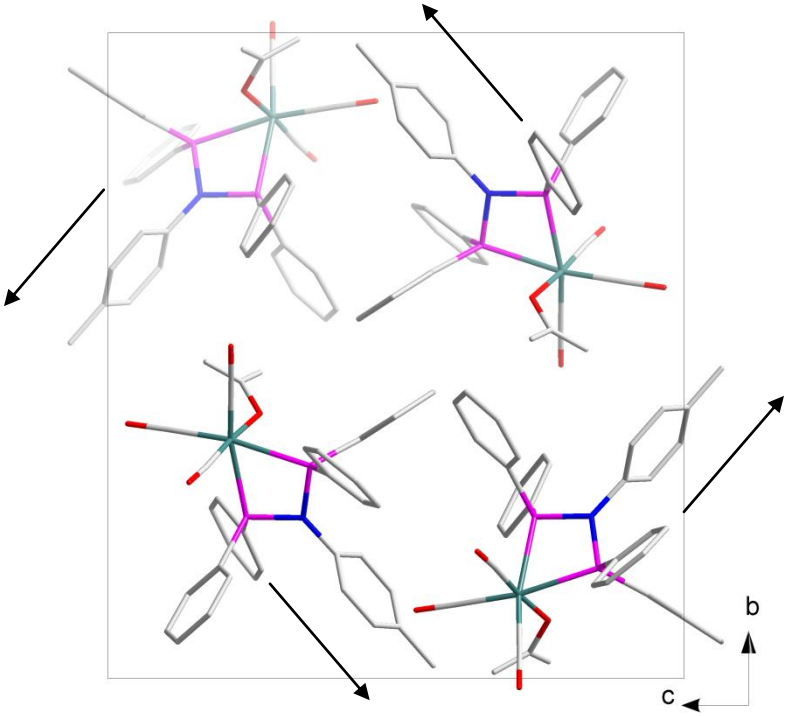

Figure 6.5 Crystal packing of *fac*-[Re(*p*Tol-PhPNP)$(CO)_3$(O^iPr)] (**1c**) complex in the unit cell, viewed along the *a*-axis

6.4 *fac*-[Re(*p*ClPh-PhPNP)(CO)$_3$Br] (2c)

The title complex, *fac*-[Re(*p*ClPh-PhPNP)(CO)$_3$(Br)] (**2c**) was synthesized as described in **Paragraph 3.5.4**. This complex crystallizes in the monoclinic crystal system in the $P2_1/c$ space group with four formula units in the unit cell (Z = 4). The asymmetric unit contains one independent molecule. The molecular structure of the title complex, including the atomic numbering scheme is illustrated in **Figure 6.6**.

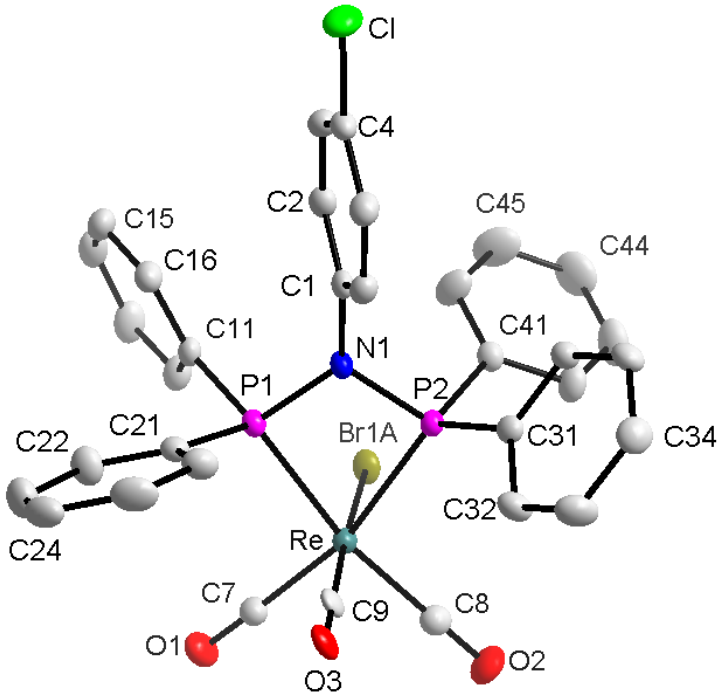

Figure 6.6 Molecular representation of *fac*-[Re(*p*ClPh-PhPNP)(CO)$_3$(Br)] (**2c**) complex. All displacement ellipsoids are drawn at 50% probability level.

Table 6.5 Selected bond lengths and bond angles from the *fac*-[Re(*p*ClPh-PhPNP)(CO)$_3$(Br)](**2c**) complex (Å and °)

Atoms	Bond length (Å)	Atoms	Bond angle (°)
Re – P1	2.4425(9)	P1 – Re – P2	67.38(3)
Re – P2	2.4431(10)	P2 – N1 – P1	104.34(12)
Re – Br1A	2.6296(11)	N1 – P1 – Re	94.00(8)
Re – C7	1.964(3)	N1 – P2 – Re	93.89(9)
Re – C8	1.963(3)	Br1A – Re – C9	177.7(4)
Re – C9	1.899(2)	C7 – Re – C8	92.78(13)
C7 – O1	1.135(4)	C9 – Re – C8	91.3(2)
C8 – O2	1.139(4)	C9 – Re – C7	90.7(2)
C9 – O3	1.108(2)	C1 – N1 – P1	129.34(19)
N1 – P1	1.714(3)	C1 – N1 – P2	126.29(19)
N1 – P2	1.717(2)		

The crystal structure of *fac*-[Re(*p*ClPh-PhPNP)$(CO)_3$(Br)] (**2c**) has three carbonyl ligands that are facially orientated to the Re(I) metal centre with two sites coordinated to the neutral bidentate *p*ClPh-PhPNP[14]PNP ligand, while the final 6th position is occupied by a negatively charged bromido moiety. This crystal structure showed a 70/30 % statistical disorder on the bromido ligand on the apical Br-Re-C9-O3 axes, requiring Shelx compatible restraints to be introduced. This disorder seems to be enhanced by the small P-M-P bite angle of 67.38(3)° which in principle allows the three carbonyl ligand and the bromido in the 6 position to orient themselves with more freedom around the metal center. Selected bond angles are summarized in **Table 6.5**.

The bond distance values reported in **Table 6.5** were found to be in the same range as the values of similar structures reported in literature.[15,16,17,18] The *Effective Tolman-based N-substituent steric effect* ($\theta_{N\text{-}sub}$) of the *p*ClPh-PhPNP **(2)** ligand was calculated using **Equation 4.1** and **Figure 4.3** from **Chapter 2** and found to be 50.3 °.

The octahedral geometry around the Re(I) is also distorted as indicated by a small P-Re-P bite angle of 66.96(3)° and Br1-Re-C9 angle of 177.7(4)°. Furthermore, angles around the N atom are 104.34(12)°, 126.29(19° and 129.34(19)°, indicating a significant distortion from the ideal 109.5 ° and 120 ° angles expected for a tetrahedral and a trigonal geometries, respectively.

Three classic hydrogen bond interactions were observed for this complex in the unit cell (**Table 6.6** and **Figure 6.7**). In addition, the crystal structure of *fac*-[Re(*p*ClPh-PhPNP)$(CO)_3$(Br)] (**2c**) is stabilized by three C-Y···Cg (π-ring) (Y = O or Cl) interactions as illustrated in **Table 6.7**, **Figure 6.8** and **Figure 6.9**.

Table 6.6 Classic hydrogen bonds observed on *fac*-[Re(*p*ClPh-PhPNP)$(CO)_3$(Br)] (**2c**) complex.

D-H···A	Symmetry	D-H (Å)	H···A (Å)	D···A (Å)	D-H···A (°)
C12-H12···Br1A	#1	0.93	2.76	3.456(4)	132
C15-H15···Br1A	#2	0.93	2.85	3.723(4)	157
C34-H34···Br1A	#3	0.93	2.93	3.727(4)	145

Symmetry transformation used to generate equivalent to atoms: #1 x, y, z; **#2** x, ½-y, ½+z; **#2** 1-x, y, z.

Table 6.7 C-Y···Cg(π-ring) interactions observed on *fac*-[Re(*p*ClPh-PhPNP)(CO)$_3$(Br)] (**2c**) complex.

X-Y(I)···Cg(J)	Symmetry	Y···Cg (Å)	X-Y···Cg (°)	X···Cg (Å)
C4-Cl1···Cg(4)	#1	3.379(2)	137.02(11)	4.800(4)
C7-O1···Cg(2)	#2	3.469(3)	105.7(2)	3.931(4)
C9-O3···Cg(1)	#3	3.794(16)	135.7(11)	4.652(6)

Symmetry transformation used to generate equivalent to atoms: **#1** x, ½-y, ½+z; **#2** 1-x, ½+y, ½-z; **#3** -x, ½+y, ½-z; Cg(1) = centroid atom of C1,C2,C3,C4,C5,C6; Cg(2) = centroid atom of C11,C12,C13,C14,C15,C16; Cg(4) = centroid atom of C31,C32,C33,C34,C35,C36.

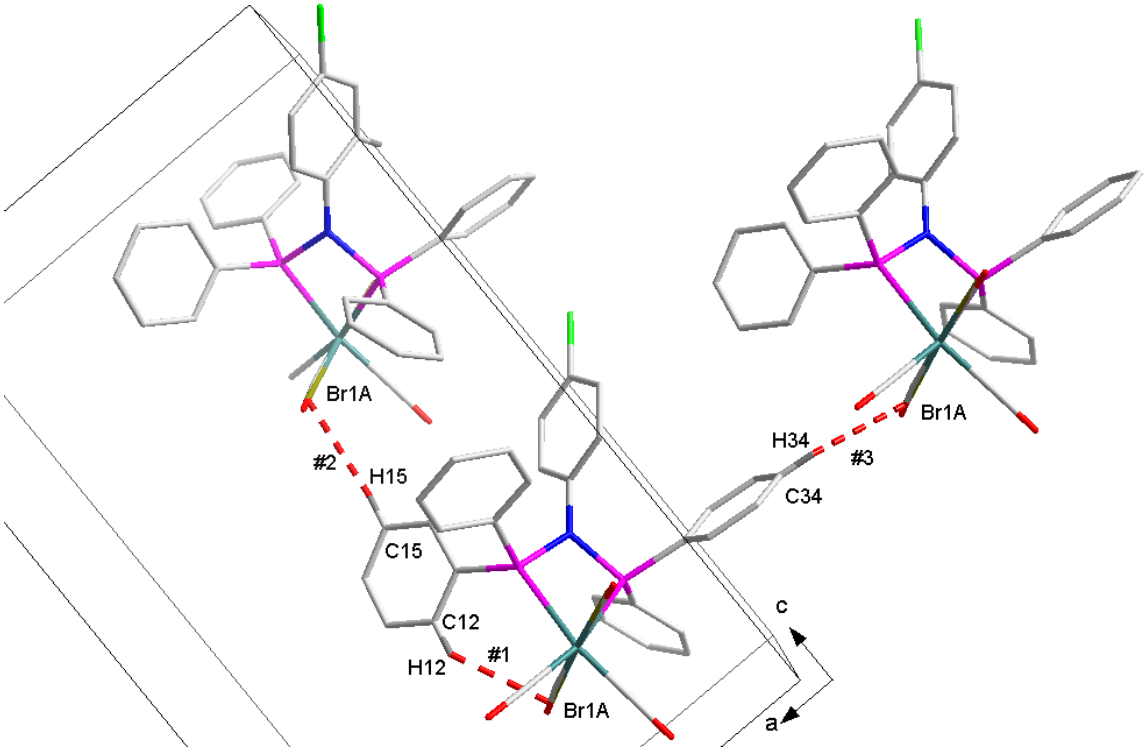

Figure 6.7 Graphic representation of the classical hydrogen bonds observed for the *fac*-[Re(*p*ClPh-PhPNP)(CO)$_3$(Br)] (**2c**) complex

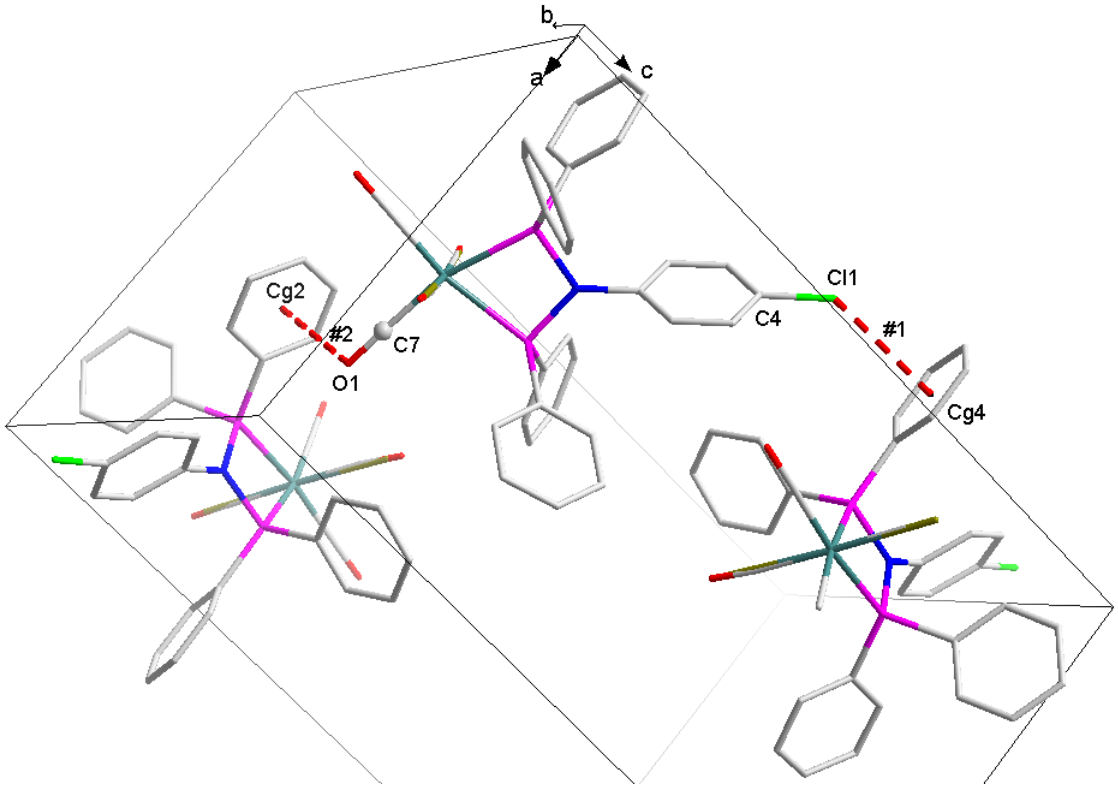

Figure 6.8 Graphic representation of selected C-Y···Cg(π-ring) observed on *fac*-[Re(*p*ClPh-PhPNP)$(CO)_3$(Br)] (**2c**) complex.

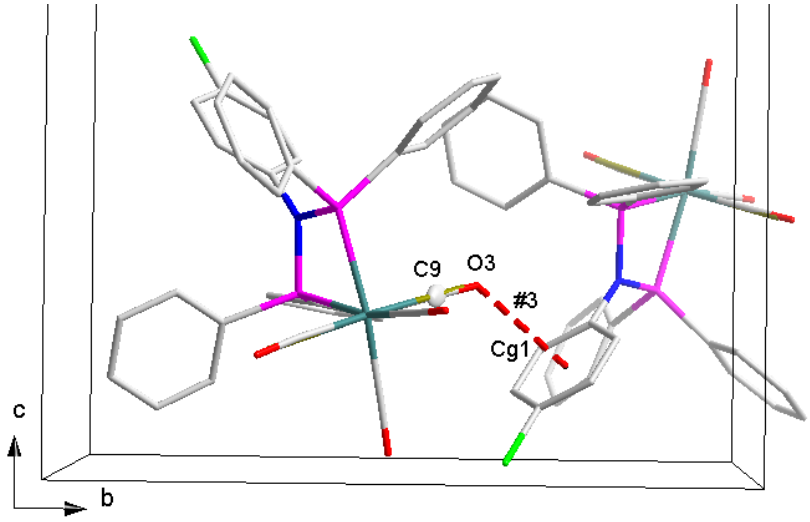

Figure 6.9 Graphic representation of selected C-Y···Cg(π-ring) observed on *fac*-[Re(*p*ClPh-PhPNP)$(CO)_3$(Br)] (**2c**) complex.

The molecular packing observed in **Figure 6.10** owes it to the number of hydrogen bonds and C-Y···Cg(π-ring) interactions observed on this molecule. It is clear that these interactions tightly tie the crystal lattice together.

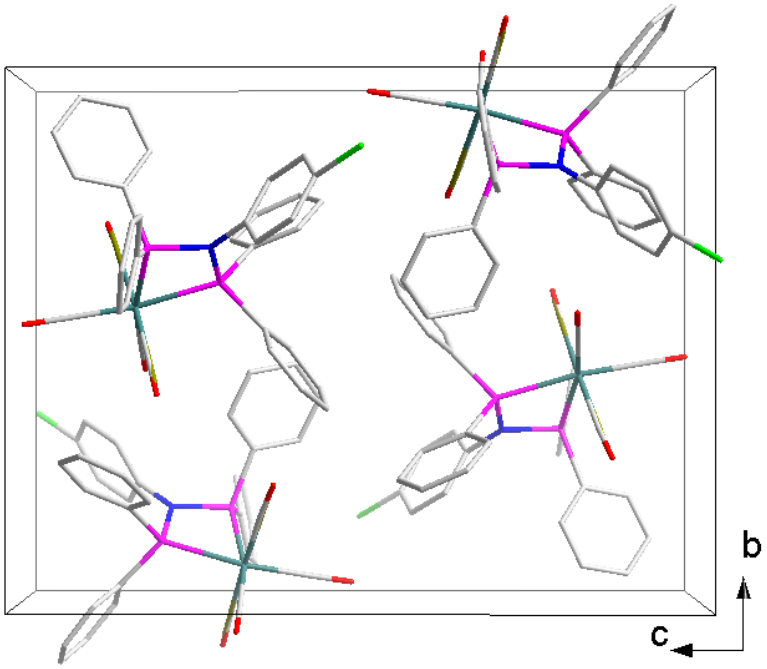

Figure 6.10 Crystal packing observed on the *fac*-[Re(*p*ClPh-PhPNP)(CO)$_3$(Br)] (**2c**) complex in the unit cell, viewed along the a-axis.

6.5 *fac*-[Re(*p*FPh-PhPNP)(CO)$_3$Br] (3c)

The title complex, *fac*-[Re(*p*FPh-PhPNP)(CO)$_3$(Br)] (**3c**) was synthesized as described in **Paragraph 3.5.5**. This complex crystallizes in the monoclinic crystal system in the $P2_1/c$ space group with four formula units in the unit cell (Z = 4). The asymmetric unit contains one independent molecule. The molecular structure of the title complex, including the atomic numbering scheme is illustrated in **Figure 6.11**.

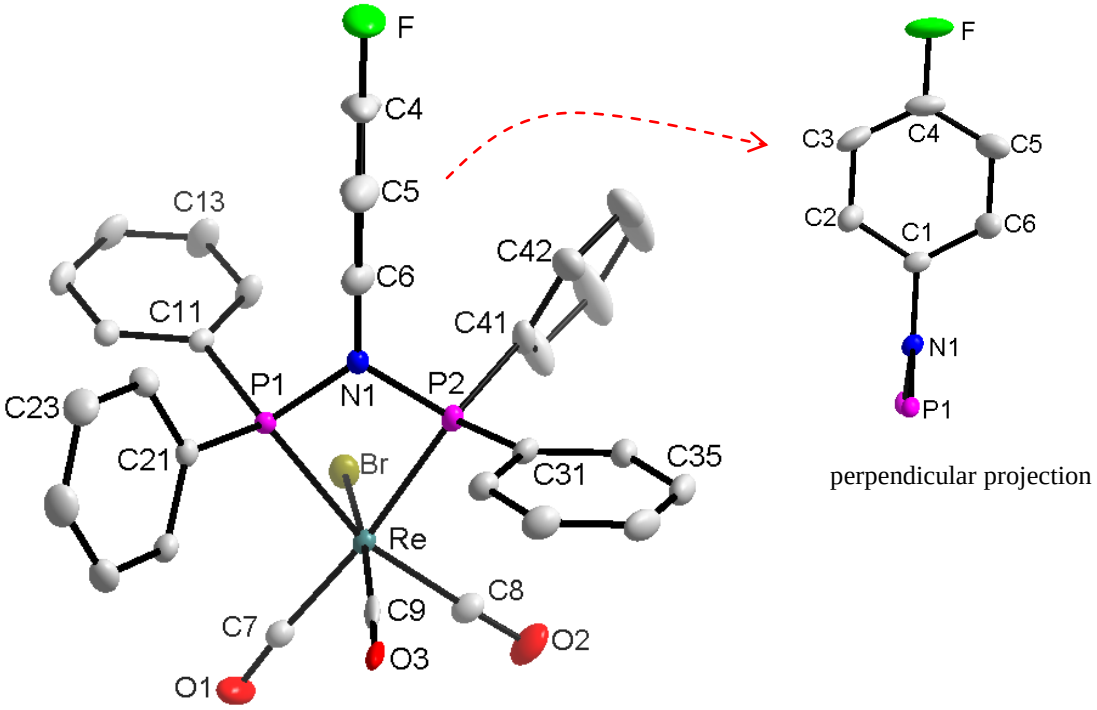

Figure 6.11 Molecular representation of *fac*-[Re(*p*FPh-PhPNP)(CO)$_3$(Br)] (**3c**) complex. All displacement ellipsoids are drawn at 50% probability level.

Table 6.8 Selected bond lengths and bond angles from the *fac*-[Re(*p*FPh-PhPNP)(CO)$_3$(Br)] (**3c**) complex (Å and °)

Atoms	Bond length (Å)	Atoms	Bond angle (°)
Re – P1	2.4754(10)	P1 – Re – P2	66.78(3)
Re – P2	2.4383(10)	P2 – N1 – P1	104.67(14)
Re – Br1	2.6350(10)	N1 – P1 – Re	93.37(9)
Re – C7	1.968(3)	N1 – P2 – Re	94.82(9)
Re – C8	1.949(3)	Br – Re – C9	171.70(9)
Re – C9	1.9179(19)	C7 – Re – C8	91.59(14)
C7 – O1	1.141(4)	C9 – Re – C8	89.34(13)
C8 – O2	1.138(4)	C9 – Re – C7	87.66(13)
C9 – O3	1.049(3)	C1 – N1 – P1	128.6(2)
N1 – P1	1.711(2)	C1 – N1 – P2	126.69(19)
N1 – P2	1.706(3)		

The crystal structure of *fac*-[Re(*p*FPh-PhPNP)(CO)$_3$(Br)] (**3c**) has three carbonyl ligands that are facially orientated to the Re(I) metal centre with two sites coordinated to the neutral bidentate *p*FPh-PhPNP (**3**)[14] PNP ligand, while the final 6th position is occupied by a negatively charged bromido moiety. Unlike the previous crystal structure of the *fac*-[Re(*p*ClPh-PhPNP)(CO)$_3$(Br)] (**2c**), the crystal structure of *fac*-[Re(*p*FPh-PhPNP)(CO)$_3$(Br)] (**3c**) showed no statistical disorder on the apical Br-Re-C9-O3 axes. However, the small P-M-P bite angle of 66.78(3)° observed in this structure is comparable to the 67.38(3)° observed on the crystal structure of *fac*-[Re(*p*ClPh-PhPNP)(CO)$_3$(Br)] (**2c**). This bite angle would in principle to a certain degree also allow free orientation of the carbonyl ligand and the bromido in the 6 position around the metal center. Furthermore, the basic coordination mode between **2c** and **3c** as manifested by the Re-C and the Re-P bonds illustrated in **Table 6.5** and **Table 6.8** is also very similar.

The bond distance values reported in **Table 6.8** were also found to be in the same range as the values of similar structures reported in literature.[15,16,17,18] The *Effective Tolman-based N-substituent steric effect* ($\theta_{N\text{-}sub}$) of the *p*FPh-PhPNP **(3)** ligand was calculated using **Equation 4.1** and **Figure 4.3** from **Chapter 2** and found to be 85.1 °. The octahedral geometry around the Re(I) is also distorted as indicated by a small P-Re-P bite angle of 66.78(3)° and Br-Re-C9 angle of 171.70(9)°. Furthermore, angles around the N atom ranges between 104.67(12)° and 128.6(2)°, indicating a significant distortion from the ideal 109.5 ° angle for a tetrahedral geometry. One may therefore conclude that the N atom adopts a trigonal (sp^2) hybridization geometry to accommodate the steric bulk on the nitrogen.

There is an abundant number of inter- and intramolecular interactions within this structure. Firstly, three classic hydrogen bond interactions were observed in the unit cell (**Table 6.9** and **Figure 6.12**). In addition, the crystal structure of *fac*-[Re(*p*FPh-PhPNP)(CO)$_3$(Br)] (**3c**) is stabilized by three C-H···Cg (π-ring) interactions as illustrated in **Table 6.10** and **Figure 6.13**. Lastly this structure is stabilized by four C-O···Cg (π-ring) interactions illustrated in **Table 6.11**, **Figure 6.14** and **Figure 6.15**.

Table 6.9 Classical hydrogen bonds observed on *fac*-[Re(*p*FPh-PhPNP)(CO)$_3$(Br)] (**3c**) complex.

D-H···A	Symmetry	D-H (Å)	H···A (Å)	D···A (Å)	D-H···A (°)
C46-H46···Br1	#1	0.93	2.83	3.456(4)	145
C2-H2···O2	#2	0.93	2.51	3.723(4)	143
C22-H22···O3	#3	0.93	2.56	3.727(4)	134

Symmetry transformation used to generate equivalent to atoms: #1 x, y, z **#2** 1-x, ½+y, ½-z; **#2** 2-x, ½+y, ½-z.

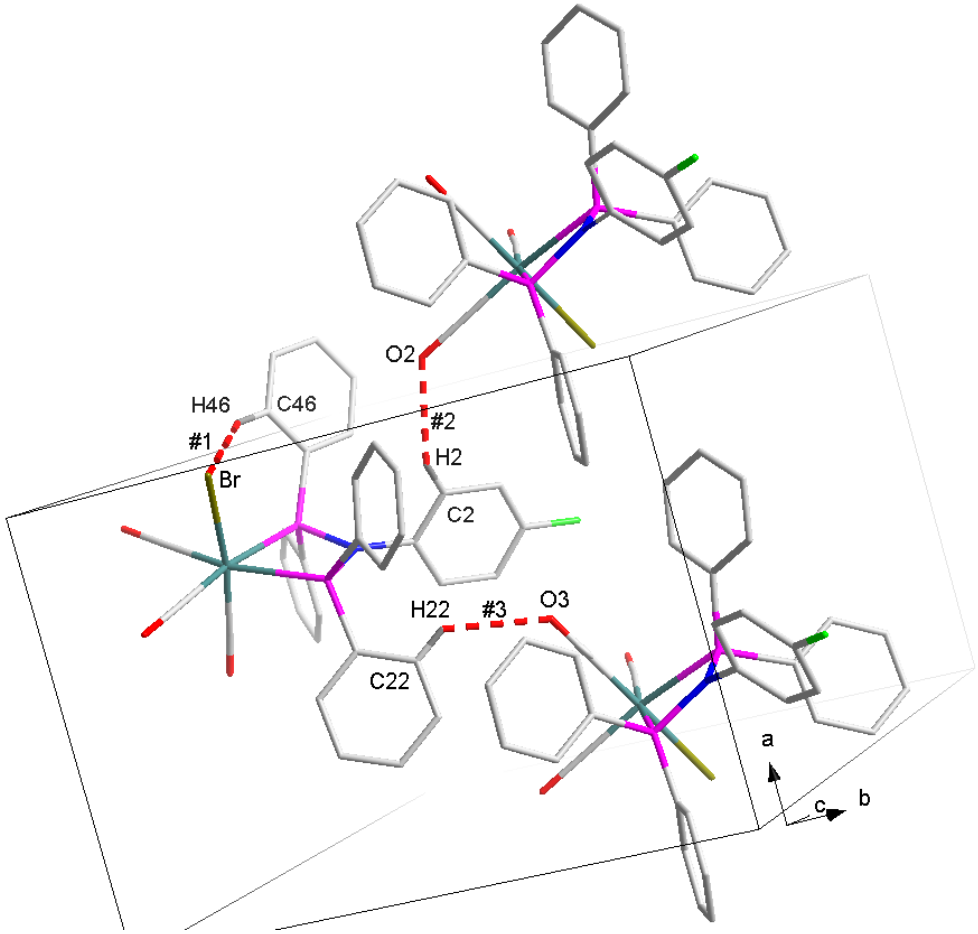

Figure 6.12 Graphic representation of the classical hydrogen bonds observed on *fac*-[Re(*p*FPh-PhPNP)(CO)$_3$(Br)] (**3c**) complex.

Table 6.10 C-H···Cg(π-ring) interactions for *fac*-[Re(*p*FPh-PhPNP)(CO)$_3$(Br)] (**3c**) complex.

X-H(I) ···Cg(J)	Symmetry	H···Cg (Å)	X-H···Cg (°)	X···Cg (Å)
C12-H12···Cg(1)	#1	2.93	104	3.280(4)
C32-H32···Cg(1)	#1	2.93	102	3.258(4)
C35-H35···Cg(3)	#2	2.93	158	3.805(4)

Symmetry transformation used to generate equivalent to atoms: **#1** x, y, z; **#2** x, ½-y, ½+z; Cg1 = centroid atom of Re,P1,N1,P2; Cg3 = centroid atom of C11,C12,C13,C14,C15,C16.

Table 6.11 C-O···Cg(π-ring) interactions for *fac*-[Re(*p*FPh-PhPNP)(CO)$_3$(Br)] (**3c**) complex.

X-O(I)···Cg(J)	Symmetry	H···Cg (Å)	X-H···Cg (°)	X···Cg (Å)
C7-O1···Cg(2)	#1	3.977(3)	154.2(2)	2.029(4)
C7-O1···Cg(5)	#1	3.134(3)	106.8(2)	3.632(4)
C8-O2···Cg(6)	#2	3.657(4)	140.3(2)	4.591(4)
C9-O3···Cg(2)	#3	3.392(3)	133.1(2)	4.180(3)

Symmetry transformation used to generate equivalent to atoms: **#1** x, ½-y,-½+z; **#2** 1-x, 2-y, -z; Cg2 = centroid atom of C1,C2,C3,C4,C5,C6; Cg5 = centroid atom of C31,C32,C33,C34,C35,C36; Cg6 = centroid atom of C41,C42,C43,C44,C45,C46.

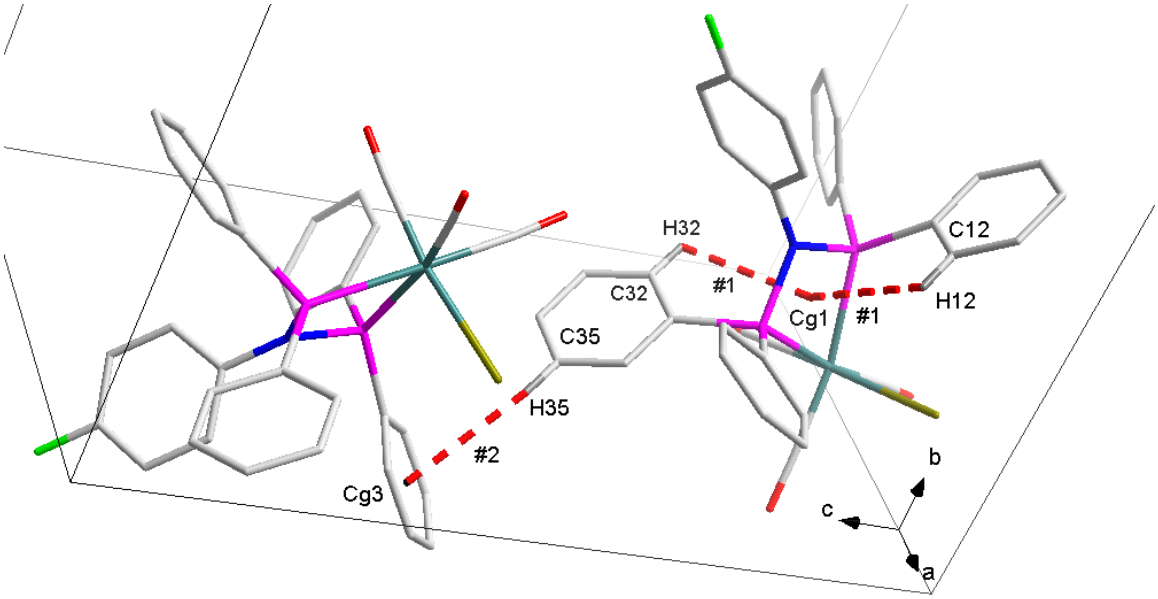

Figure 6.13 Graphic representation of the C-H···Cg (red dashed bonds) interactions observed on the *fac*-[Re(*p*FPh-PhPNP)(CO)$_3$(Br)] (**3c**) complex.

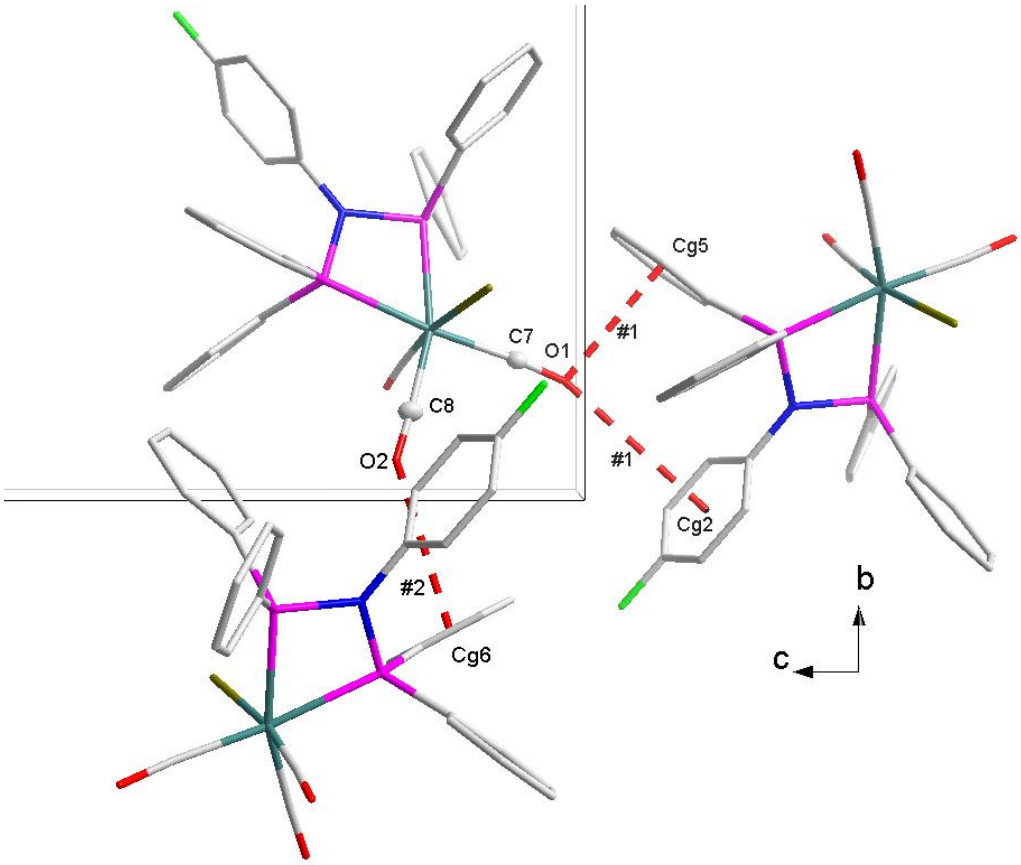

Figure 6.14 Graphic representation of the C-O···Cg (red dashed bonds) interactions observed on the *fac*-[Re(*p*FPh-PhPNP)$(CO)_3$(Br)] (**3c**) complex.

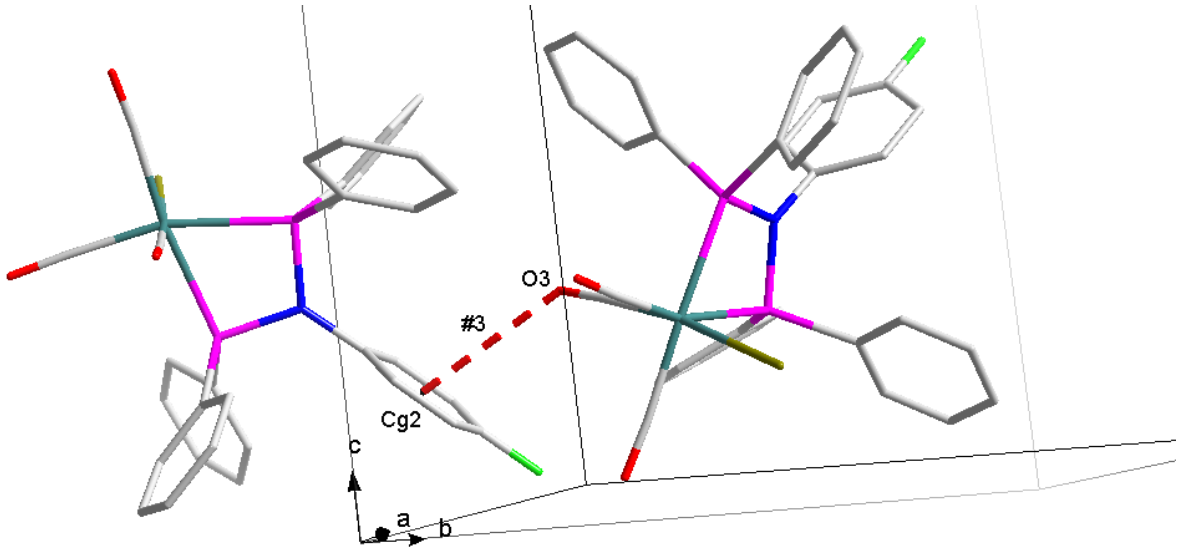

Figure 6.15 Graphic representation of the C-O···Cg (red dashed bonds) interactions observed on the *fac*-[Re(*p*FPh-PhPNP)$(CO)_3$(Br)] (**3c**) complex.

The molecular packing observed in **Figure 6.16** is also evident due to the number of hydrogen bonds, C-H···Cg and C-O···Cg(π-ring) interactions observed in this structure. It is again clear that these interactions tightly hold the crystal lattice together.

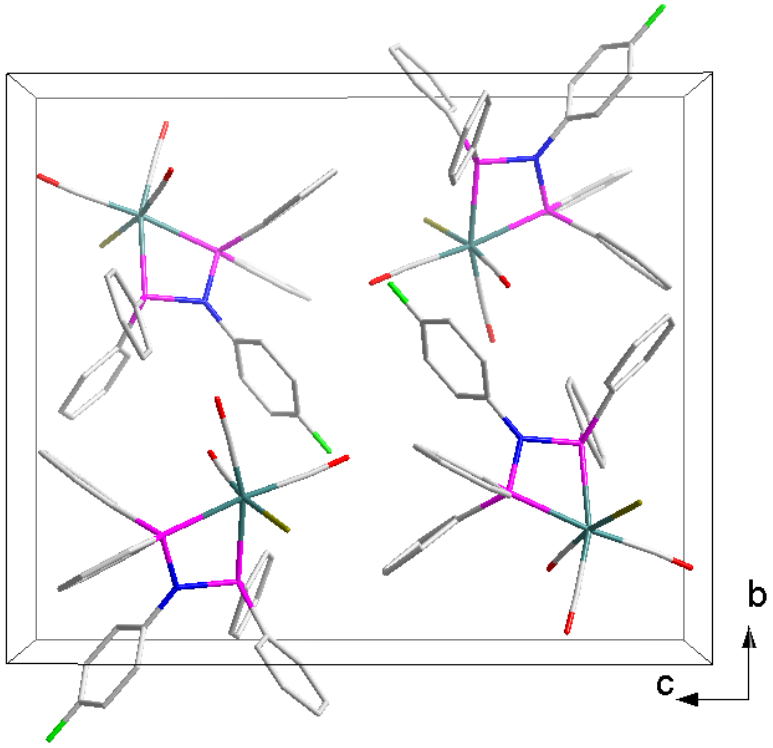

Figure 6.16 Crystal packing observed on the f*ac*-[Re(*p*FPh-PhPNP)(CO)$_3$(Br)] (**3c**) complex in the unit cell, as viewed along the *a*-axis.

6.6 *fac*-[Re(Cbutyl-4-*p*-tolyl)(CO)$_3$Br] (7c)

The title complex *fac*-[Re(Cbutyl-4-*p*-tolyl)(CO)$_3$Br] (**7c**) was synthesized as described in **Paragraph 3.5.9**. This complex crystallizes in the monoclinic crystal system in the *Pn* space group with four formula units in the unit cell (Z = 4). The asymmetric unit contains two independent molecules. The molecular structure of the title complex, including the atomic numbering scheme is illustrated in **Figure 6.17**.

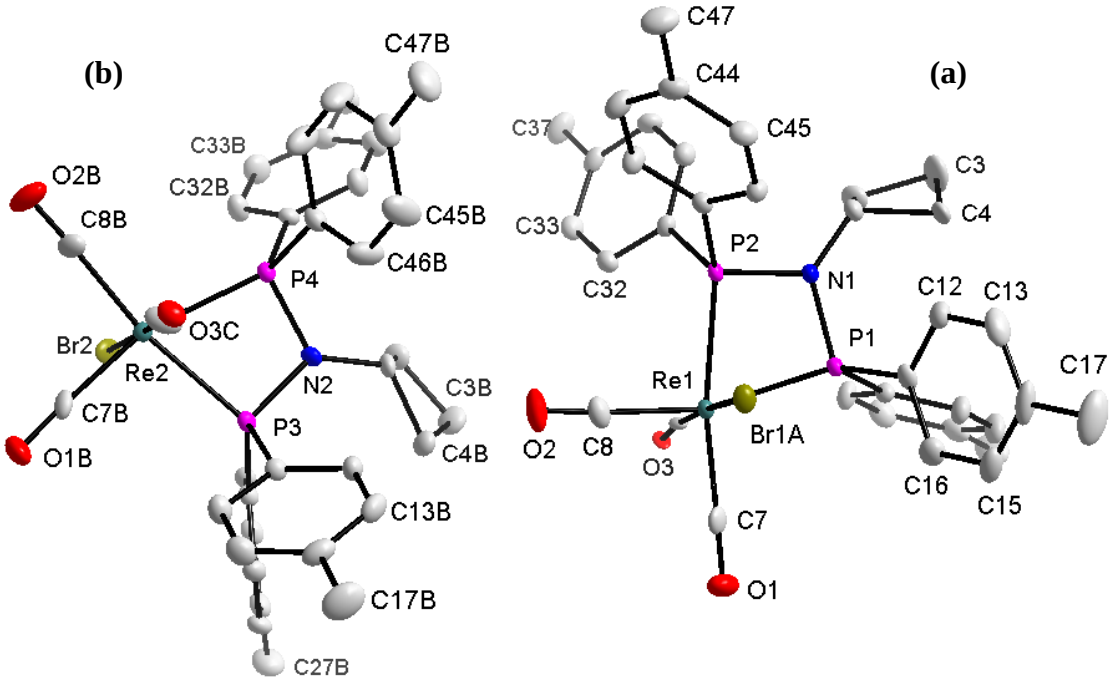

Figure 6.17 Molecular representation of *fac*-[Re(Cbutyl-4-*p*-tolyl)(CO)$_3$Br] (**7c**) complex. All displacement ellipsoids are drawn at 50% probability level.

Table 6.12 Selected bond lengths and bond angles for *fac*-[Re(Cbutyl-4-*p*-tolyl)(CO)$_3$Br] (**7c**) complex (Å and °).

Bond length (Å)		
Atoms	**Molecule A**	**Molecule B**
Re1 – P1	2.4617(15)	2.4322(16)
Re1 – P2	2.4459(16)	2.4732(15)
Re1 – Br1A	2.5729(10)	2.5783(13)
Re1 – C7	1.969(7)	1.935(7)
Re1 – C8	1.951(7)	1.963(7)
Re1 – C9	1.8604(3)	1.898(3)
C7 – O1	1.137(9)	1.155(8)
C8 – O2	1.147(7)	1.144(9)
C9 – O3	1.169(9)	1.191(4)
N1 – P1	1.710(5)	1.694(5)
N1 – P2	1.716(5)	1.712(6)
Bond angle (°)		
Atoms		
P1 – Re1 – P2	66.79(5)	66.43(5)
P2 – N1 – P1	104.1(3)	104.2(3)
N1 – P1 – Re	94.35(17)	95.33(19)
N1 – P2 – Re	94.77(18)	93.42(17)
Br1A – Re – C9	176.084(6)	176.079(6)
C7 – Re1 – C8	92.7(3)	92.8(3)
C9 – Re1 – C8	91.8(4)	89.8(5)
C9 – Re1 – C7	87.6(4)	88.6(6)
C1 – N1 – P1	129.8(4)	131.0(4)
C1 – N1 – P2	125.6(4)	124.7(4)

Additional analysis involved the refinement of **7c** into the *P*1 space group which contains no other symmetry operation besides the identity. In *P*1, four independent molecules in the asymmetric unit were obtained which is therefore consistent with the space group allocation of *Pn* and $P\bar{1}$. Attempts to solve the structure in the space group of $P\bar{1}$ were also not successful and this might be due to the different statistical disorders observed from the two independent molecules in the unit cell.

The crystal structure of *fac*-[Re(Cbutyl-4-*p*-tolyl)(CO)$_3$Br] (**7c**) has three carbonyl ligands that are facially orientated to the Re(I) metal centre, while the remaining positions are occupied by a bromido moiety and a neutral bidentate Cbutyl-4-*p*-tolyl (**7**)[14] PNP ligand. The two complex

molecules of *fac*-[Re(Cbutyl-4-*p*-tolyl)$(CO)_3$Br] (**7c**) illustrated in **Figure 6.17** show a 50/50 and 60/40 % statistical disorder on the apical Br-Re-C9-O3 axes for molecule A and B respectively, thus requiring Shelx compatible restraints to be introduced upon refinement. Due to the similarities with respect to bond distances and angles as illustrated in **Table 6.12**, the discussions that will follow will only be on one molecule.

The *Effective Tolman-based N-substituent steric effect* ($\theta_{N\text{-}sub}$) of the Cbutyl-4-*p*-tolyl **(7)** ligand was calculated using **Equation 4.1** and **Figure 4.3** from **Chapter 2** and found to be 73.4 °. Similar to previously discussed structures of *fac*-[Re(*p*ClPh-PhPNP)$(CO)_3$(Br)] (**2c**) and the *fac*-[Re(*p*FPh-PhPNP)$(CO)_3$(Br)] (**3c**), the structure of *fac*-[Re(Cbutyl-4-*p*-tolyl)$(CO)_3$Br] (**7c**) also contains a small P-Re-P bite angle of 66.79(3)°. This small bite angle may in principle allow less restricted orientations of the three carbonyl and the bromido ligands, thus in some instances resulting in structural disorders. Selected bond distances and angles are summarized in **Table 6.12**.

The bond distance values reported in **Table 6.12** were also found to be in the same range as the values of similar structures reported in literature.[15,16,17,18] The octahedral geometry around the Re(I) is distorted as indicated by the small P-Re-P bite angle of 66.79(3)° and the Br1A-Re1-C9 angle of 176.084(6)°. Furthermore, the angles around the N atom range between 104.1(3)° and 129.8(4)°, indicating that the N atom adopts a trigonal (sp^2) hybridization geometry to accommodate the steric bulk on the nitrogen.

There is again a number of inter- and intramolecular interactions within this structure. Firstly, seven classic hydrogen interactions were observed for this complex in the unit cell (**Table 6.14**, **Figure 6.18** and **Figure 6.19**). In addition, this crystal structure is further stabilized by three C-H···Cg (π-ring) interactions as illustrated in **Table 6.15** and **Figure 6.20**. Finally, four C-O···Cg (π-ring) interactions occur and are illustrated in **Table 6.16**, **Figure 6.21** and **Figure 6.22**.

Table 6.13 Classic hydrogen bonds observed on *fac*-[Re(Cbutyl-4-*p*-tolyl)(CO)$_3$Br] (**7c**) complex.

D-H···A	Symmetry	D-H (Å)	H···A (Å)	D···A (Å)	D-H···A (°)
C4B-H4BA···O2	#1	0.97	2.56	3.424(8)	148
C22B-H22B···O2B	#2	0.93	2.46	3.247(9)	142
C23-H23···Br2	#3	0.93	2.84	3.713(7)	157
C23-H23···O3B	#3	0.93	2.54	3.446(11)	165
C27-H27A···Br1A	#4	0.96	2.77	3.642(9)	152
C37-H37A···O3A	#5	0.96	2.51	3.452(11)	167
C42-H42···O1	#6	0.93	2.51	3.234(9)	135

Symmetry transformation used to generate equivalent to atoms: #1 x, y, z; **#2** -1+x, y, z; **#3** -1+x, -1+y, z; **#4** -½+x, -y, -½+z; **#5** ½+x, -y, -½+z; **#6** 1+x, y, z.

Table 6.14 C-H···Cg(π-ring) interactions for *fac*-[Re(Cbutyl-4-*p*-tolyl)(CO)$_3$Br] (**7c**) complex.

X-H(I) ···Cg(J)	Symmetry	H···Cg (Å)	X-H···Cg (°)	X···Cg (Å)
C4B-H4B···Cg(8)	#1	2.93	151	3.809(7)
C15-H15···Cg(5)	#2	2.95	130	3.626(8)
C35-H35···Cg(3)	#3	2.80	179	3.728(7)

Symmetry transformation used to generate equivalent to atoms: **#1** x, y, z; **#2** -1+x, y, z; **#3** 1+x, y, z; Cg3 = centroid atom of C21,C22,C23,C24,C25,C26; Cg5 = centroid atom of C41,C42,C43,C44,C45,C46; Cg8 = centroid atom of C21B,C22B,C23B,C24B,C25B,C26B.

Table 6.15 C-O···Cg(π-ring) interactions for *fac*-[Re(Cbutyl-4-*p*-tolyl)(CO)$_3$Br] (**7c**) complex.

X-O(I) ···Cg(J)	Symmetry	H···Cg (Å)	X-H···Cg (°)	X···Cg (Å)
C7-O1···Cg(4)	#1	3.478(6)	121.4(5)	4.184(8)
C7-O1···Cg(10)	#2	3.758(6)	113.0(5)	4.331(8)
C9A-O3A···Cg(2)	#3	3.848(12)	86.1(12)	3.96(2)
C8B-O2B···Cg(7)	#4	3.589(7)	123.2(5)	4.323(8)

Symmetry transformation used to generate equivalent to atoms: **#1** -1+x, y, z; **#2** -1-x, -1+y, z; **#3** x, y, z; **#4** 1+x, y, z; Cg2 = centroid atom of C11,C12,C13,C14,C15,C16; Cg4 = centroid atom of C31,C32,C33,C34,C35,C36; Cg7 = centroid atom of C11B,C12B,C13B,C14B,C15B,C16B; Cg10 = centroid atom of C41B,C42B,C43B,C44B,C45B,C46B.

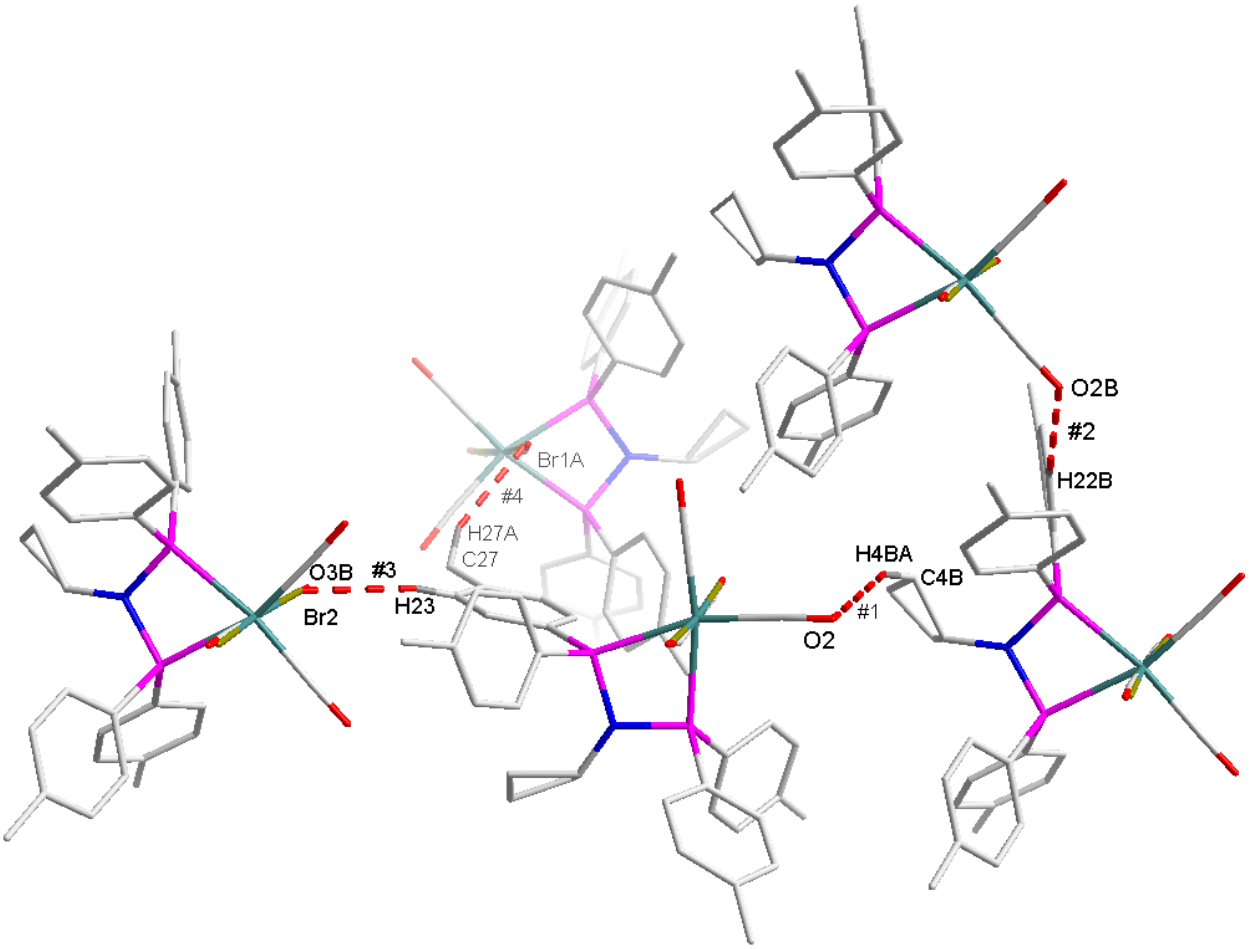

Figure 6.18 Graphic representation of selected classical hydrogen bonds observed on *fac*-[Re(Cbutyl-4-*p*-tolyl)$(CO)_3$Br] (**7c**) complex.

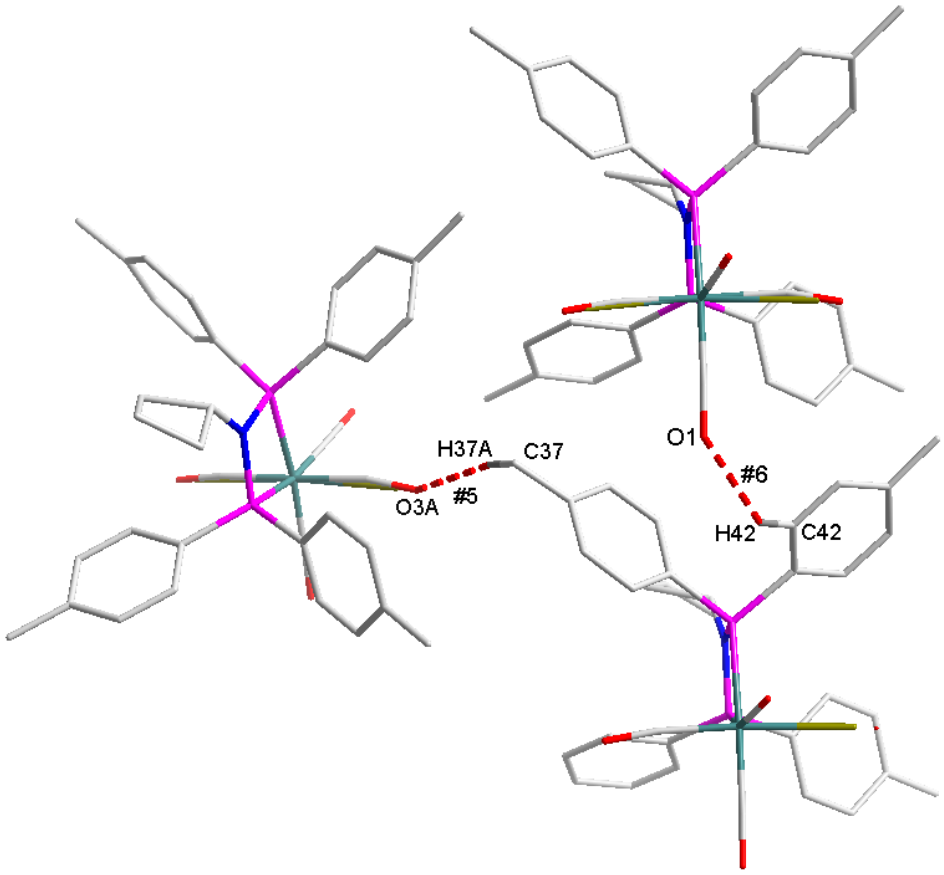

Figure 6.19 Graphic representation of selected classical hydrogen bonds observed on *fac*-[Re(Cbutyl-4-*p*-tolyl)(CO)$_3$Br] (**7c**).

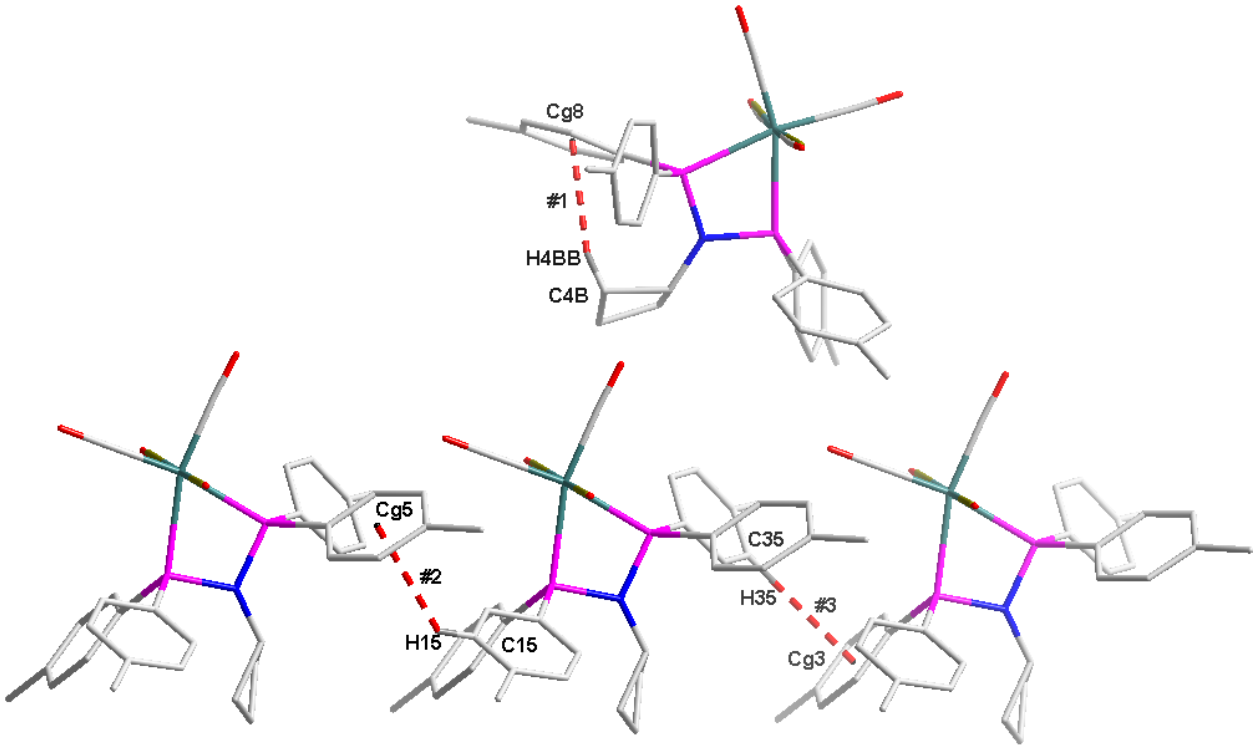

Figure 6.20 Graphic representation of the C-H···Cg (red dashed bonds) interactions observed on the *fac*-[Re(Cbutyl-4-*p*-tolyl)$(CO)_3$Br] (**7c**) complex.

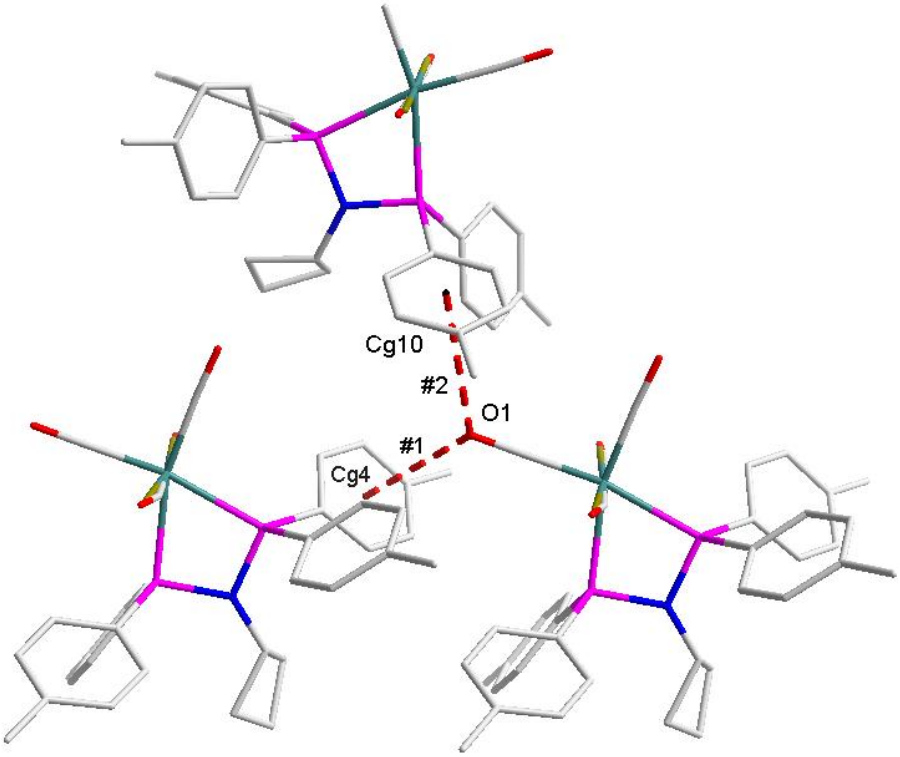

Figure 6.21 Graphical representation of the C-O···Cg (red dashed bonds) interactions observed on the *fac*-[Re(Cbutyl-4-*p*-tolyl)$(CO)_3$Br] (**7c**) complex.

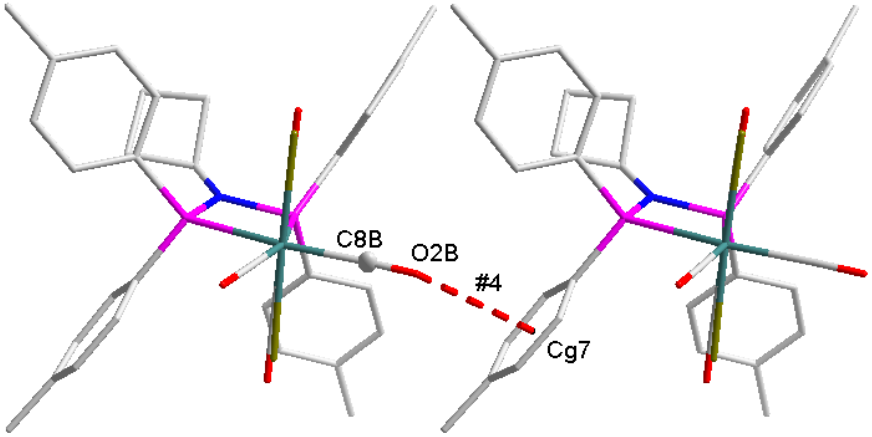

Figure 6.22 Graphic representation of the C-O···Cg (red dashed bonds) interactions observed on the *fac*-[Re(Cbutyl-4-*p*-tolyl)(CO)$_3$Br] (**7c**) complex.

The molecules pack in an alternating fashion as observed in the unit cell when viewed along the *a*-axis.

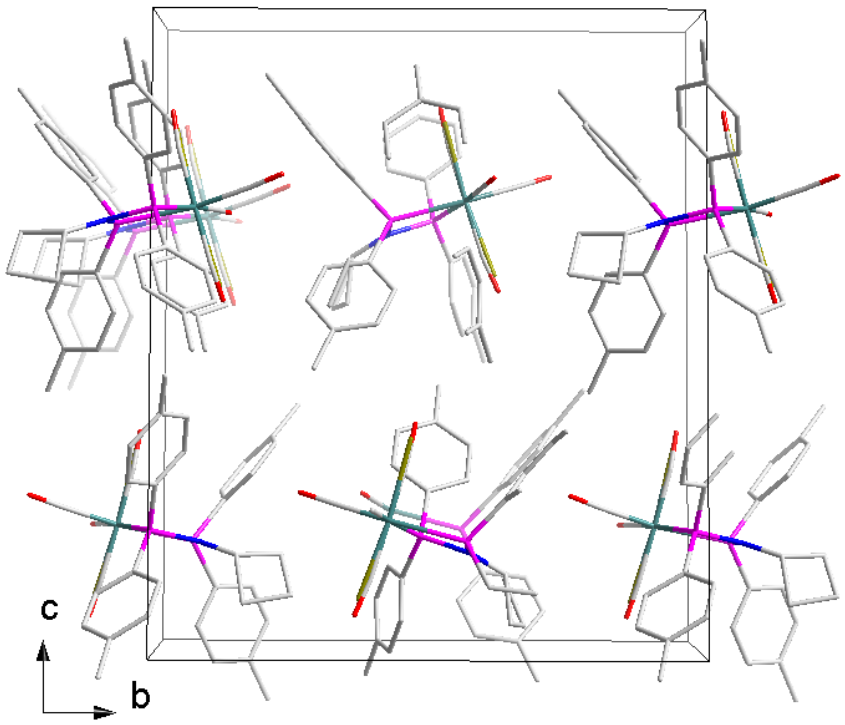

Figure 6.23 Crystal packing observed on the *fac*-[Re(Cbutyl-4-*p*-tolyl)(CO)$_3$Br] (**7c**) complex in the unit cell, viewed along the *a*-axis.

6.7 Discussion

This chapter describes the solid state structures of four Re-PNP complexes, namely *fac*-[Re(*p*Tol-PhPNP)$(CO)_3$(O^iPr)] (**1c**), *fac*-[Re(*p*ClPh-PhPNP)$(CO)_3$(Br)] (**2c**), *fac*-[Re(*p*FPh-PhPNP)$(CO)_3$(Br)] (**3c**) and *fac*-[Re(Cbutyl-4-*p*-tolyl)$(CO)_3$Br] (**7c**). The first three (**1c**, **2c** and **3c**) complexes display very similar molecular structures. They each contain two phenyl substituents on each of the P atoms of the PNP backbone and only vary by a single substituent (*para* tolyl, *para*-chloro and *para*-fluoro) on the N atom. Furthermore, **2c** and **3c** contains a bromide moiety in the sixth position while **1c** contains a 2-propenol substituent. Despite this, the basic coordination modes as manifested by the Re-C and the Re-P bonds illustrated in **Table 6.17** are remarkably similar. The values illustrated suggest that the central rigidity induced by the PNP ligand architecture at the metal centre on all three these complexes is maintained.

Table 6.16 Selected bond lengths of complex **1c**, **2c** and **3c** illustrating bond similarities between these complexes.

Atoms	Complex (1c)	Complex (2c)	Complex (2c)
		Bond length (Å)	
Re1 – P1	2.4412(10)	2.4425(9)	2.4754(10)
Re1 – P2	2.4571(10)	2.4431(10)	2.4383(10)
Re1 – C7	1.964(4)	1.964(3)	1.968(3)
Re1 – C8	1.967(4)	1.963(3)	1.949(3)
Re1 – C9	1.917(3)	1.899(2)	1.9179(19)

Complex **7c** is considerably different from the first three mentioned complexes in that it contains a cyclobutyl substituent on the N atom and two *para*-tolyl substituents on each of the P atoms of the PNP backbone. Complex **2c** and **7c** respectively showed (i) a statistical disorder of 70/30 % for the Br atom in **2c** on the apical Br-Re-C9-O3 axes, while (ii) 7c contained two independent molecules in the asymmetric unit each with its own disorder of 50% for one molecule and 60/40 % for the other molecule, also on the apical Br-Re-C9-O3 axes. Moreover, comparison of the bond distances and angles of **1c**, **2c**, **3c**, **7c** and other complexes reported in literature were all very similar.[15,16,17,18]

One may therefore conclude that there is a general coordination geometry rigidity that is maintained within the ligand architecture in these types of complexes, most probably due to the small P-Re-P bite angle observed within the molecular structures. This is further supported by

the results obtained from structural overlays of complex **1c**, **2c**, and **3c** as illustrated in **Figure 6.24** below. **Table 6.18** summarizes the different bond distances and angles observed between the four different structures.

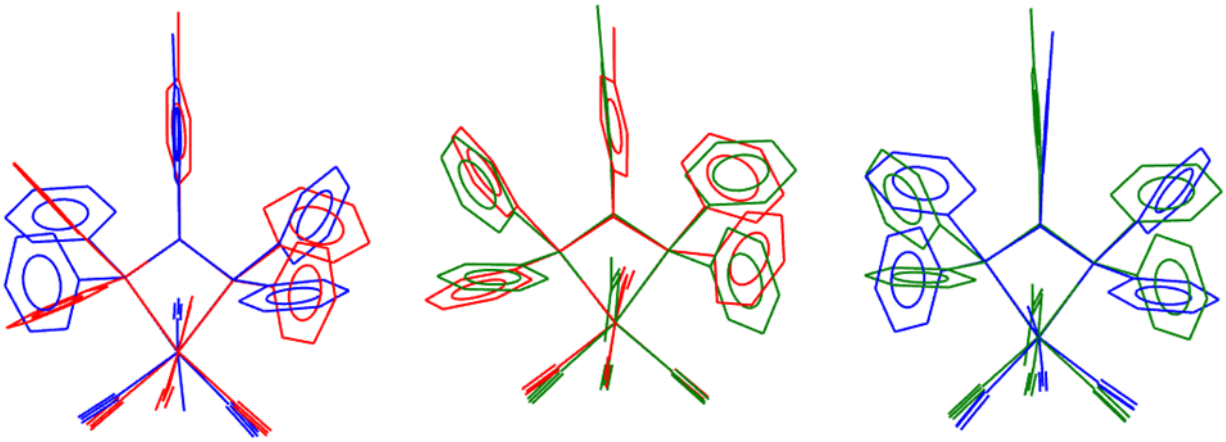

2c + **3c**
RMS: 0.0152

2c + **1c**
RMS: 0.00765

1c + **3c**
RMS: 0.0176

Figure 6.24 Graphical illustration of the overlay of **1c** (green), **2c** (red) and **3c** (blue). Hydrogen atoms are omitted for clarity.

Table 6.17 Selected information indicating the difference between complex **1c**, **2c**, **3c** and **7c**.

Complexes	C1-N1 (Å)	N-P$_{ave}$ (Å)	P – M – P (°)	P – N – P (°)	Space group
fac-[Re(*p*Tol-PhPNP)(CO)$_3$(O^{i}Pr)] (1c)	1.450(4)	1.7105	66.96(3)	104.34(14)	$P2_1/c$
fac-[Re(*p*ClPh-PhPNP)(CO)$_3$(Br)] (2c)	1.446(4)	1.7155	67.38(3)	104.34(12)	$P2_1/c$
fac-[Re(*p*FPh-PhPNP)(CO)$_3$(Br)] (3c)	1.444(4)	1.7085	66.78(3)	104.67(14)	$P2_1/c$
fac-[Re(Cbutyl-4-*p*-tolyl)(CO)$_3$Br] (7c)	1.470(8)	1.7130	66.79(5)	104.1(3)	*Pn*

Attempts were made to solve the crystal structure of **7c** in the space group of $P2_1/c$ for the purpose of comparison to structures of **1c**, **2c** and **3c**. The refinement of **7c** in this space group $P2_1/c$ was unsuccessful and could not be solved.

6.8 Conclusion

In this chapter four Re-PNP tricarbonyl complexes namely *fac*-[Re(*p*Tol-PhPNP)$(CO)_3$(O^iPr)] (**1c**), *fac*-[Re(*p*ClPh-PhPNP)$(CO)_3$(Br)] (**2c**), *fac*-[Re(*p*FPh-PhPNP)$(CO)_3$(Br)] (**3c**) and *fac*-[Re(Cbutyl-4-*p*-tolyl)$(CO)_3$Br] (**7c**) were presented. These complexes were all structurally comparable in relation to bond distances and angles. In all of these structures, a small P-Re-P bite angle of around 67 ° was observed. A clear PNP system stabilized Re tricarbonyl core was observed in this study.

Crystallographic evaluation of these complexes is particularly important for better understanding of the spatial arrangements and geometrical stability of Re-PNP tricarbonyl complexes. The only major obstacle that was encountered upon solving these crystal structures emerged from the statistical disorder observed on the apical Br-Re-C9-O3 axes for either Br atom alone or both the Br and the CO moiety.

The following chapter expands on the solid state behavior of Metal-PNP complexes, and the structural evaluation of two isostructural *fac*-$M(CO)_3^+$ (M= Re(I) and ^{99}Tc(I)) compounds, and one promising water soluble Re-PNP tricarbonyl complex will be discussed in detail. The main focus will be placed on structural rigidity maintained as one switches from a Re^I to a $^{99}Tc^I$ metal centre.

7 Single crystal X-ray diffraction study of *fac*-[M(CO$_3$)(PNP)X] {M = Re(I) and ^{99}Tc(I), PNP =Chzyl-4-*p*-tolyl and NBoc-PhPNP } complexes

What to expect!

A detailed crystallographic evaluation of N,N-bis(di-p-tolylphosphino)cyclohexylamine (PNP) ligand coordinated to a Re(I) and ^{99}Tc(I) tricarbonyl moiety and that of fac-[Re(CO$_3$)(NBoc-PhPNP)Br] will be presented in this chapter.

7.1 Introduction

^{99m}Tc is still considered to be one of the most important radionuclides in diagnostic nuclear medicine and represents roughly 85 % of clinically administered radiopharmaceuticals.[1,2] However, from the chemical point of view, the artificial nature of technetium makes it difficult for a chemist to conduct technetium experiments in a normal laboratory. Therefore, technetium experiments may only be conducted in rated chemical laboratories that specialize in the use of radioactive procedures.

To overcome the above-mentioned drawback, non-radioactive rhenium complexes with similar structures are regularly used as prototype agents for the radioactive technetium complexes in academia.[3] Thorough investigations are therefore very essential when conducting such

[1] King, R. B., *Encyclopedia of Inorganic Chemistry and Bioinorganic Chemistry*. 2 ed.; John Wiley & Sons Ltd.: **2011.**

[2] Engelbrecht, H. P., Cutler, C. S., Jurisson, S. S., Drijver, L. d., Roodt, A., *Synth. React. Inorg. Met. Org. Chem.* **2005,** *35*, 83-99.

[3] Engelbrecht, H. P.; Den Drijver, L.; Steyl, G.; Roodt, A., *Comptes Rendus Chimie*. **2005,** *8*, 1660-1669.

experiments to ensure that no significant chemical deviations are observed when switching from a rhenium to the radioactive technetium metal center.

While ^{99m}Tc complexes are used for diagnostic purposes, radioactive rhenium such as ^{186}Re and ^{188}Re can also be used as a therapeutic alternative.[2] This implies that the two (Re and Tc) can work hand in hand by providing different biological information to scientists when their homologous complexes are utilized. Thus in this study, rhenium complexes should not only be viewed as prototype agents but also as potential therapeutic agents.

Moreover, for a successful labeling, physiochemical properties of the resulting radioactive complex such as hydrophilicity, should adopt those of the labeled biomolecule. Consequently, the size of the metal complex should be kept as small as possible. In addition to these requirements, necessary conditions such as 98% final purity yield, one step preparation, extremely low biomolecule concentrations and sufficient radionuclide half-life (enough time for synthesis, injection and imaging) are also very important when designing a radiopharmaceutical drug to be used for routine clinical applications.[4]

Due to the above-mentioned requirements, it is therefore imperative that one designs ligands that are (i) highly stable, to ensure that no secondary or metabolized compounds are produced in a typical biological environment (ii) highly hydrophilic, to ensure that the initial physicochemical properties of the biomolecule remains reasonably unaffected (iii) easily coordinated to the respective metal center, particularly in "one step synthesis".

An integral part of this overarching study was to synthesize and crystallographically characterize Re(I) and ^{99}Tc(I) congeners using the *fac*-$M(CO)_3^+$ metal core. To achieve this several complexes were synthesized as described in **Chapter 3**. Thus, the two isostructural metal complexes, namely *fac*-[Re(Chzyl-4-*p*-tolyl)$(CO)_3$Br] (**8c**) and *fac*-[^{99}Tc(Chzyl-4-*p*-tolyl)$(CO)_3$Cl] (**8d**) will first be presented in this chapter. However, secondly and very important, the crystal structure of a *water soluble* promising complex of *fac*-[Re(NBoc-PhPNP)$(CO)_3$Br] (**4c**) will also be presented. The synthesis and characterization of these complexes have been

[4] Alberto, R., Schibli R., Waibel R., Abram U., Schubiger P. A., *Coord. Chem. Rev.* **1999,** *190*, 901-919.

extensively investigated and discussed in **Chapter 3**. Thus, our main focus in this chapter is the structural rigidity and similarities. **Figure 7.1** illustrates graphically the three molecules that will be discussed herein.

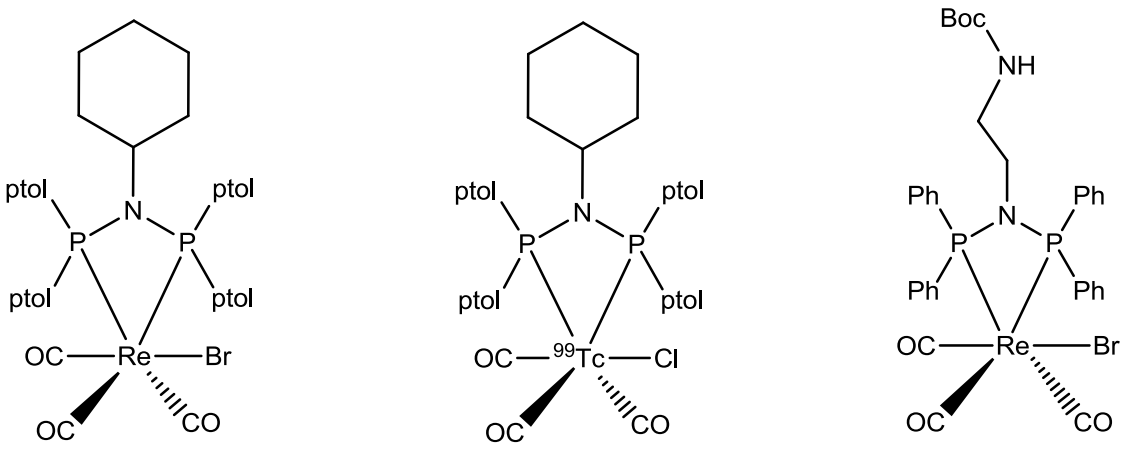

Figure 7.1 The tricarbonyl complexes of Re(I) and ^{99}Tc(I) crystallized in this study: **8c** *fac*-[Re(Chzyl-4-*p*-tolyl)$(CO)_3$Br], **8d** *fac*-[^{99}Tc(Chzyl-4-*p*-tolyl)$(CO)_3$Cl] and **4c** of *fac*-[Re(NBoc-PhPNP)$(CO)_3$Br]. Molecular numbering is reminiscent of that found in **Chapter 3,** except the "c" symbol which indicates a Re-PNP complex and the "d" a Tc-PNP complex.

7.2 Experimental

Diffraction data for *fac*-[Re(Chzyl-4-*p*-tolyl)$(CO)_3$Br] (**8c**) and *fac*-[Re(NBoc-PhPNP)$(CO)_3$Br] (**4c**) were collected at 100 K on a Bruker X8 Apex II 4K diffractometer using monochromated Mo Kα radiation with a wavelength of λ = 0.71073 Å, while the data for *fac*-[^{99}Tc(Chzyl-4-*p*-tolyl)$(CO)_3$Cl] (**8d**) was collected at 182 K using MoKα radiation (λ = 0.71073 Å) with a graphite monochromator on an Oxford Diffraction CCD Xcalibur system with a Ruby detector. All the cell parameters were refined using the XPREP4 and SAINT-Plus[5] program while SADABS[6] and multiscan techniques were used for the absorption corrections. The structures were solved by either direct methods or by the use of SIR97[7] and refined on F^2 using anisotropic

[5] *SAINT-Plus*, version 6.02 (including XPREP); Bruker AXA, Inc.: Madison, WI, USA, **1999**.

[6] *SADABS*, version 2004/1; Bruker AXS, Inc.: Madison, WI, USA, **2004**.

[7] Altomare, A., Burla, M. C., Camalli, M., Cascarano, G.L., Giacovazzo, C., Guagliardi, A., Moliterni, A. G. G., Polidori, G., Spagna, R., *J. Appl. Cryst*., **1999**, *32*, 837-838.

displacement parameters for all non-hydrogen atoms. SHELXL-97 [8,9] and WinGX[10] were used for structure solutions and refinements respectively. The molecular graphics were drawn using the DIAMOND program.[11] Structural overlays were drawn utilizing the Mercury program.[12] All aromatic, methylene and methyl hydrogen atoms were placed in geometrically idealized positions (C-H = 0.95 Å to 0.98 Å) and constrained to ride on their parent atoms with U_{iso}(H) = 1.2U_{eq}(C) and U_{iso}(H) = 1.5U_{eq}(C) respectively.

A summary of the general crystal data and refinement parameters is given in **Table 7.1** for all three the complexes and selected bond parameters for every structure are presented under each sub-paragraph. Complete list of bond distances, bond angles, atomic coordinates, hydrogen coordinates, torsion angles and anisotropic displacement parameters for the three complexes are found in the supplementary data (**Appendix A**). Hydrogen atoms and numbering for certain carbon atoms were omitted for clarity on some molecular structures. For aromatic rings, the first and the second digit represents the ring number and the specific C-atom in the ring respectively.

[8] Sheldrick, G. M., SHELXL97; University of Göttingen: Göttingen, Germany, **1997**.

[9] Sheldrick, G. M., *Acta Crystallogr*. **2008**, *A64*, 112-122.

[10] Farrugia, L. J., *J. Appl. Crystallogr*. **1999**, *32*, 837-838.

[11] Brandenburg, K., Putz, H., DIAMOND, release 3.1b; Crystal Impact GbR: Bonn, Germany, **2005**.

[12] Macrae, C. F., Bruno, I. J., Chisholm, J. A., Edgington, P. R., McCabe, P., Pidcock, E., Rodriguez-Monge, L., Taylor, R., van de Streek, J., Wood, P. A., *J. Appl. Cryst*., **2008**, 41, 466-470.

Table 7.1 General X-ray Crystal data and refinement parameters of **8c** *fac*-[Re(Chzyl-4-*p*-tolyl)$(CO)_3$Br], **8d** *fac*-[^{99}Tc(Chzyl-4-*p*-tolyl)$(CO)_3$Cl] and **4c** *fac*-[Re(NBoc-PhPNP)$(CO)_3$Br].

Crystallographic data	*fac*-[Re(Chzyl-4-*p*-tolyl)$(CO)_3$Br] (**8c**)	*fac*-[^{99}Tc(Chzyl-4-*p*-tolyl)$(CO)_3$Cl] (**8d**)	*fac*-[Re(Nboc-PhPNP)$(CO)_3$Br] (**4c**)
Empirical formula	$C_{37}H_{39}BrNO_3P_2Re$	$C_{37}H_{39}ClNO_3P_2Tc$	$C_{34}H_{34}BrN_2O_5P_2Re$
Formula weight (g mol^{-1})	873.74	741.99	878.68
Temperature (K)	100(2)	182.9(6)	100(2)
Crystal system	Triclinic	Triclinic	Monoclinic
Space group	*P*1	*P*1	$P2_1/c$
Unit cell dimensions			
a (Å)	9.7040(17)	9.6163(3)	11.402(2)
b (Å)	9.8836(17)	9.8939(4)	18.286(2)
c (Å)	10.5780(19)	10.6904(4)	17.070(2)
α (°)	92.787(6)	92.440(3)	90
β (°)	111.417(5)	111.690(3)	109.229(4)
γ (°)	104.512(6)	104.279(3)	90
Volume (Å^3)	903.2(3)	905.27(6)	3360(2)
Z	1	1	4
Density (g cm^{-3})	1.606	1.358	1.737
Crystal colour	Colourless	Yellow	Colourless
Crystal morphology	Cuboid	Cuboid	Cuboid
Crystal size (mm^3)	0.24 x 0.11 x 0.09	0.22 x 0.12 x 0.10	0.614 x 0.332 x 0.211
μ (mm^{-1})	4.593	0.594	4.944
F(000)	432	382	1728
θ range (°)	3.230 - 28.000	3.022 - 28.282	2.839 - 28.000
	$-12 \le h \le 8$	$-12 \le h \le 12$	$-15 \le h \le 15$
Index ranges	$-11 \le k \le 13$	$-13 \le k \le 13$	$-15 \le k \le 24$
	$-13 \le l \le 13$	$-14 \le l \le 14$	$-22 \le l \le 22$
Reflections collected	15530	15505	62025
Unique reflections	6933	8599	8077
R_{int}	0.0452	0.0389	0.0516
Completeness to theta (°, %)	25.2, 99.7	25.2, 99.8	25.2, 99.4
Data / restraints / parameters	6933 / 3 / 420	8599/ 4 / 411	8077 / 3 / 437
Goodness-of-fit on F^2	1.015	1.021	1.166
R [$I > 2\sigma(I)$]	R_1 = 0.0239	R_1 = 0.0436	R_1 = 0.0232
	wR_2 = 0.0515	wR_2 = 0.0851	wR_2 = 0.0526
R (all data)	R_1 = 0.0240	R_1 = 0.0502	R_1 = 0.0275
	wR_2 = 0.0515	wR_2 = 0.0890	wR_2 = 0.0544
ρ_{max}, ρ_{min} (e.Å^{-3})	1.68, -0.75	0.80, -0.50	0.768, -0.935

Chzyl-4-*p*-tolyl = *N*,*N*-bis(di-*p*-tolylphosphino)cyclohexylamine.
NBoc-PhPNP = *N*,*N*-bis(diphenylphosphino)-N-Boc-ethylenediamine

7.3 *fac*-Re(Chzyl-4-*p*-tolyl)(CO)$_3$Br] (8c)

The title complex, *fac*-[Re(Chzyl-4-*p*-tolyl)(CO)$_3$Br] (**8c**) was synthesized as described in **Paragraph 3.5.10**. This complex crystallizes in the triclinic crystal system in the *P*1 space group with one formula unit in the unit cell (Z = 1). The asymmetric unit (the complete unit cell) contains one independent molecule. The molecular structure of the title complex, including the atomic numbering scheme is illustrated in **Figure 7.2**.

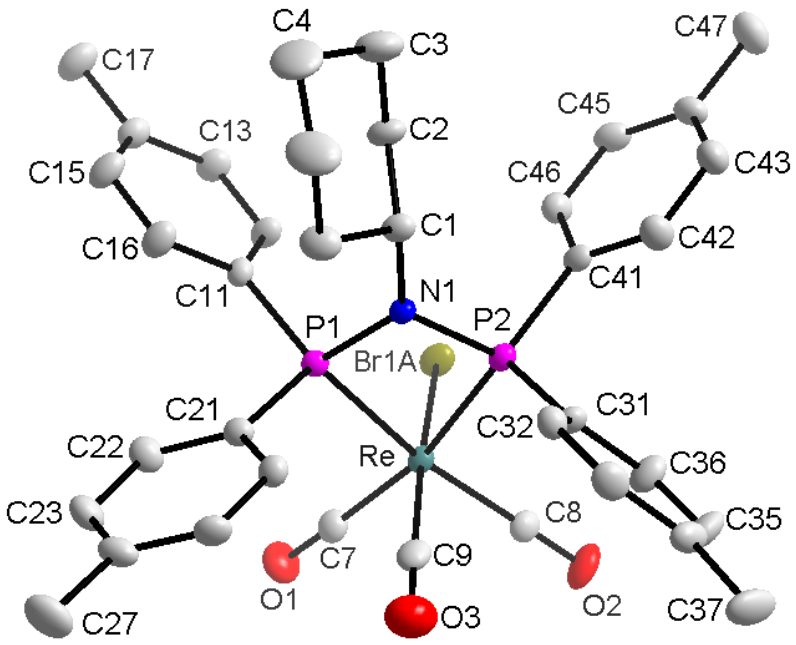

Figure 7.2 Molecular representation of *fac*-[Re(Chzyl-4-*p*-tolyl) (CO)$_3$Br] (**8c**) complex. All displacement ellipsoids are drawn at 50% probability level.

Table 7.2 Selected bond lengths and bond angles for the crystal structure of *fac*-[Re(Chzyl-4-*p*-tolyl) (CO)$_3$Br] (**8c**) (Å and °)

Atoms	Bond length (Å)	Atoms	Bond angle (°)
Re – P1	2.4586(16)	P1 – Re – P2	66.09(5)
Re – P2	2.4635(15)	P2 – N1 – P1	103.8(2)
Re – Br1A	2.6489(10)	N1 – P1 – Re	95.31(16)
Re – C7	1.956(6)	N1 – P2 – Re	94.73(15)
Re – C8	1.945(6)	Br1A – Re – C9	170.0(3)
Re – C9	1.947(9)	C7 – Re – C8	94.0(3)
C7 – O1	1.145(7)	C9 – Re – C8	89.7(3)
C8 – O2	1.150(7)	C9 – Re – C7	87.5(3)
C9 – O3	1.138(10)	C1 – N1 – P1	130.2(4)
N1 – P1	1.698(4)	C1 – N1 – P2	125.1(4)
N1 – P2	1.713(5)		

The crystal structure of *fac*-[Re(Chzyl-4-*p*-tolyl)$(CO)_3$Br] (**8c**) has three carbonyl ligands that are facially orientated to the Re(I) metal centre, while the remaining positions are occupied by a bromido moiety and a neutral bidentate Chzyl-4-*p*-tolyl (8)[13] PNP ligand. The crystal structure of *fac*-[Re(Chzyl-4-*p*-tolyl)$(CO)_3$Br] (**8c**) showed a 85/15 % statistical disorder on the apical Br-Re-C9-O3 axes, thus requiring relevant Shelx compatible restraints to be introduced on the refinement of the structure.

Selected bond distances and angles are summarized in **Table 7.2**. The three carbonyl ligands are facially orientated to the Re(I) metal centre. The octahedral geometry around the Re(I) is distorted as indicated by a small P-Re-P bite angle of 66.96(3)° and O4-Re-C9 angle of 170.0(3)°. The bond distance values reported in **Table 7.2** for Re-P, Re-Br and Re-C were found to be comparable to those encountered in similar structures such as [*N*,*N*-Bis(diphenylphosphino)propylamine-k^2*P,P'*]bromidotricarbonylrhenium(I) and [Bis(diphenylphosphino)amine-*P,P'*]bromidotricar-bonylrhenium(I) reported in literature.[14,15]. The *Effective Tolman-based N-substituent steric effect* ($\theta_{N\text{-}sub}$) of the Chzyl-4-*p*-tolyl **(8)** ligand was calculated using **Equation 4.1** and **Figure 4.3** from **Chapter 2** and found to be 85.1 °. Angles around the N atom range between 103.8(2)° and 130.2(4)°, indicating a significant distortion from the ideal 109.5 ° angle for a tetrahedral geometry. In fact, one can safely conclude that the N atom basically adopted a trigonal hybridization state.

To stabilize the solid state structure of *fac*-[Re(Chzyl-4-*p*-tolyl)$(CO)_3$Br] (**8c**), two intramolecular hydrogen interactions exist for this complex in the unit cell as illustrated in **Table 7.3** and **Figure 7.3**.

Table 7.3 Intramolecular hydrogen interactions observed in the *fac*-[Re(Chzyl-4-*p*-tolyl)$(CO)_3$Br] (**8c**) complex.

D-H···A	Symmetry	D-H (Å)	H···A (Å)	D···A (Å)	D-H···A (°)
C46-H12···Br1A	#1	0.93	2.82	3.597(6)	142
C12-H46···Br1A	#1	0.93	2.98	3.574(6)	160

Symmetry transformation used to generate equivalent to atoms: **#1** x, y, z.

[13] See **Chapter 3** of this PhD thesis.

[14] Schutte, M., Visser, H. G., Brink, A., *Acta Cryst.* **2009**, E*65*, m1575-1576.

[15] Graziani, R., Casellato, U., *Acta Crystal.* **1996**, C*52*, 850-852.

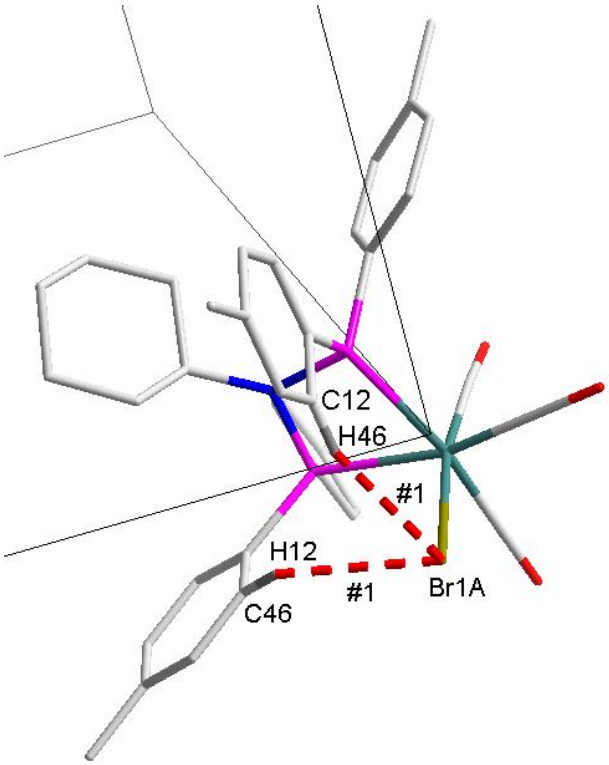

Figure 7.3 Graphic representation of the classical intra molecular hydrogen bonds observed on *fac*-[Re(Chzyl-4-*p*-tolyl)$(CO)_3$Br] (**8c**) complex.

Moreover, the crystal structure of *fac*-[Re(Chzyl-4-*p*-tolyl)$(CO)_3$Br] (**8c**) is further stabilized by three C-H···Cg (π-ring) interactions and one C-O···Cg (π-ring) as illustrated in **Table 7.4**, **Table 7.5** and **Figure 7.4**.

Table 7.4 C-H···Cg(π-ring) interactions observed on *fac*-[Re(Chzyl-4-*p*-tolyl)$(CO)_3$Br] (**8c**) complex.

X-H(I)···Cg(J)	Symmetry	H···Cg (Å)	X-H···Cg (°)	X···Cg (Å)
C2-H2B···Cg(3)	#1	2.93	162	3.864(8)
C35-H23···Cg(4)	#2	2.88	151	3.718(7)
C37-H27C···Cg(3)	#3	2.84	131	3.544(8)

Symmetry transformation used to generate equivalent to atoms: **#1** x, y, z; **#2** x, -1+y,z; #3 -1+x, -1+y, z; Cg3 = centroid atoms of C11,C12,C13,C14,C15,C16; Cg4 = centroid atom of C21,C22,C23,C24,C25,C26.

Table 7.5 C-O···Cg(π-ring) interactions observed in the *fac*-[Re(Chzyl-4-*p*-tolyl)$(CO)_3$Br] (**8c**) complex.

X-O(I)···Cg(J)	Symmetry	O···Cg (Å)	X-O···Cg (°)	X···Cg (Å)
C7-O1···Cg(6)	#4	3.733(6)	119.4(4)	4.412(7)

Symmetry transformation used to generate equivalent to atoms: **#4** x, y,-1+z Cg6 = centroid atoms of C41,C42,C43,C44,C45,C46.

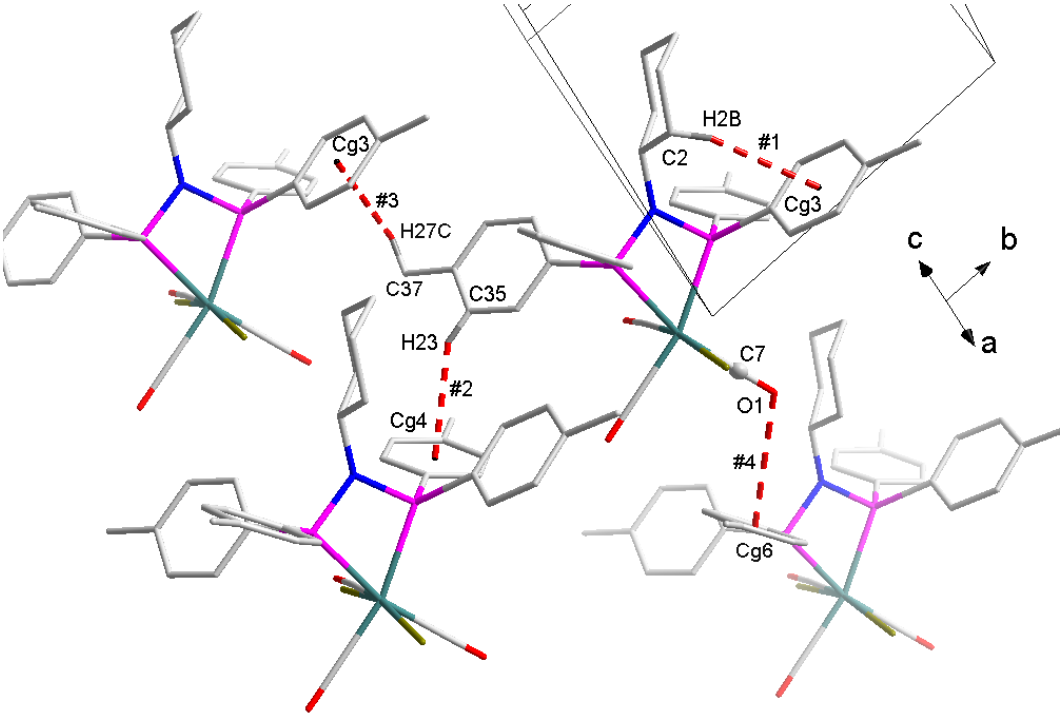

Figure 7.4 Graphic representation of the C-H···Cg and C-O···Cg interactions observed on *fac*-[Re(Chzyl-4-*p*-tolyl)(CO)$_3$Br] (**8c**) complex.

Figure 7.6 illustrates how a single molecule of complex **8c** packs in the unit cell along the *a*-axis.

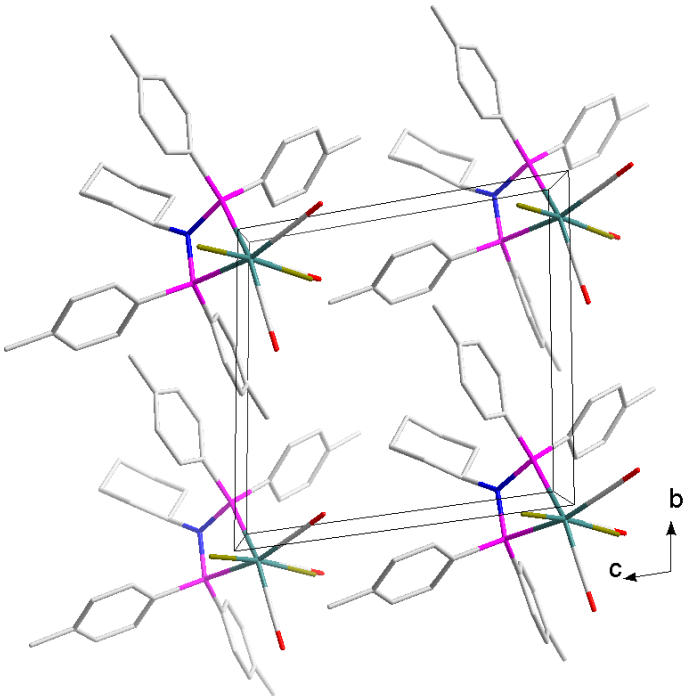

Figure 7.5 Crystal packing of the *fac*-[Re(Chzyl-4-*p*-tolyl)(CO)$_3$Br] (**8c**) complex in the unit cell, viewed along the *a*-axis

7.4 *fac*-[^{99}Tc(Chzyl-4-*p*-tolyl)(CO)$_3$Cl] (8d)

The title complex *fac*-[^{99}Tc(Chzyl-4-*p*-tolyl)(CO)$_3$Cl] (**8d**) was synthesized as described in **Paragraph 3.6.3**. This complex crystallizes in the triclinic crystal system in the *P*1 space group with one formula unit in the unit cell (Z = 1). The asymmetric unit (again the complete unit cell) contains one independent molecule. The molecular structure of the title complex, including the atomic numbering scheme is illustrated on **Figure 7.6**.

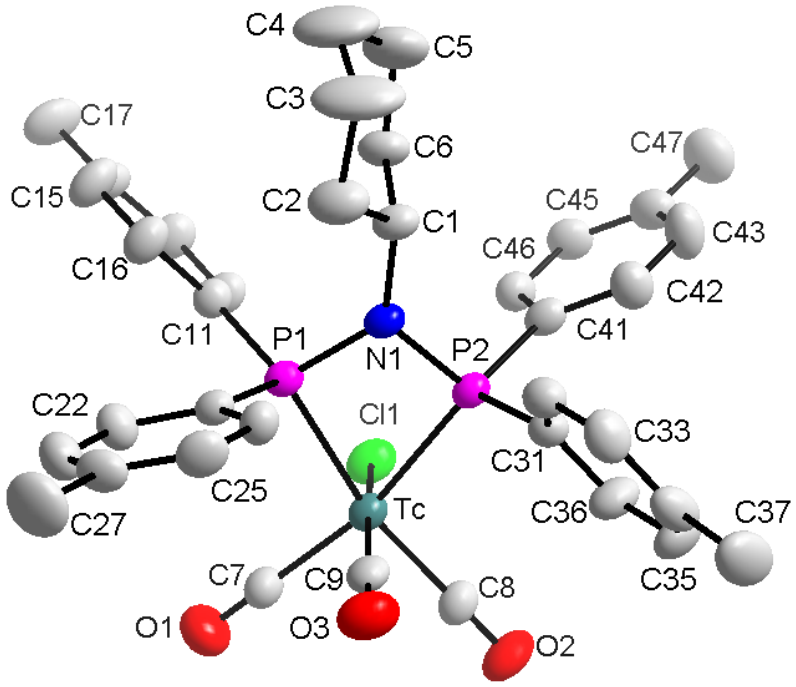

Figure 7.6 Molecular representation of *fac*-[^{99}Tc(Chzyl-4-*p*-tolyl)(CO)$_3$Cl] (**8d**) complex. All displacement ellipsoid are drawn at 50% probability level.

Table 7.6 Selected bond lengths and bond angles for the crystal structure of *fac*-[^{99}Tc(Chzyl-4-*p*-tolyl)(CO)$_3$Cl] (**8d**) (Å and °)

Atoms	Bond length (Å)	Atoms	Bond angle (°)
Tc – P1	2.4711(14)	P1 – Tc – P2	66.16(4)
Tc – P2	2.4523(14)	P2 – N1 – P1	104.0(2)
Tc – Cl1	2.5151(15)	N1 – P1 – Tc	94.24(15)
Tc – C7	1.958(6)	N1 – P2 – Tc	95.53(16)
Tc – C8	1.953(6)	Cl1 – Tc – C9	170.73(16)
Tc – C9	1.937(6)	C7 – Tc – C8	93.8(3)
C7 – O1	1.119(7)	C9 – Tc – C8	87.0(2)
C8 – O2	1.116(7)	C9 – Tc – C7	89.3(2)
C9 – O3	1.085(7)	C1 – N1 – P1	129.1(4)
N1 – P1	1.717(5)	C1 – N1 – P2	126.0(4)
N1 – P2	1.694(4)		

The crystal structure of *fac*-[^{99}Tc(Chzyl-4-*p*-tolyl)$(CO)_3$Br] (**8c**) has three carbonyl ligands that are facially orientated to the Re(I) metal centre, while the remaining positions are occupied by a chlorido moiety and a neutral bidentate Chzyl-4-*p*-tolyl (8)[13] PNP ligand. Unlike the previous crystal structure of **8c**, the solid state structure of *fac*-[^{99}Tc(Chzyl-4-*p*-tolyl)$(CO)_3$Cl] (**8d**) showed no statistical disorder on the apical Cl-Tc-C9-O3 axes. However, the small P-Tc-P bite angle of 66.16(4)° which is almost equal to the previous one. Moreover, in spite of this structure not showing the statistical disorder and having a chlorido ligand instead of a bromido ligand, it is still isostructural to the Re-Bromido analog, **8c**.

The bond distances reported in **Table 7.6** were also found to be in the same range as the values of similar structures reported in literature.[14,15] The *Effective Tolman-based N-substituent steric effect* ($\theta_{N\text{-}sub}$) of the Chzyl-4-*p*-tolyl **(8)** ligand was calculated using **Equation 4.1** and **Figure 4.3** from **Chapter 2** and found to be 84.6 ° compared to 85.1 for the corresponding Re complex, **8c**. The octahedral geometry around the Tc(I) is distorted as indicated by a small P-Tc-P bite angle of 66.16(4)° and Cl1-Tc-C9 angle of 170.73(16)°. Furthermore, angles around the N atom range between 104.0(2)° and 129.1(4)°, indicating a significant distortion from the ideal 109.5 ° angle for a tetrahedral geometry. One can also again conclude that the N atom adopts a distorted trigonal (sp^2) hybridization geometry to accommodate the steric bulk on the nitrogen.

In the solid state structure of *fac*-[^{99}Tc(Chzyl-4-*p*-tolyl)$(CO)_3$Cl] (**8d**), two intramolecular hydrogen interactions exists in the unit cell as illustrated in **Table 7.7** and **Figure 7.7**.

Table 7.7 Intramolecular hydrogen bond interactions observed for *fac*-[^{99}Tc(Chzyl-4-*p*-tolyl)$(CO)_3$Cl] (**8d**) complex.

D-H···A	Symmetry	D-H (Å)	H···A (Å)	D···A (Å)	D-H···A (°)
C12-H12···Cl1	#1	0.93	2.61	3.503(6)	162
C46-H46···Cl1	#1	0.93	2.71	3.474(6)	140

Symmetry transformation used to generate equivalent to atoms: **#1** x, y, z.

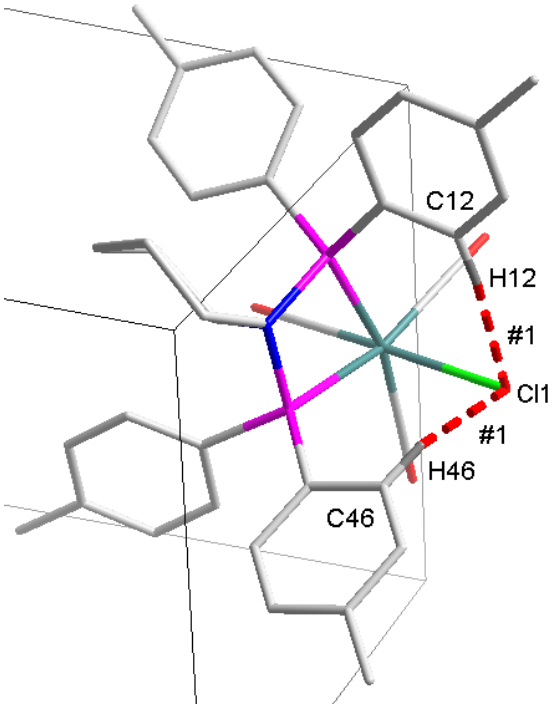

Figure 7.7 Graphic representation of the intramolecular hydrogen bonds observed on *fac*-[^{99}Tc(Chzyl-4-*p*-tolyl)(CO)$_3$Cl] (**8d**) complex.

The crystal structure of *fac*-[^{99}Tc(Chzyl-4-*p*-tolyl)(CO)$_3$Cl] (**8d**) is further stabilized by four C-H···Cg (π-ring) interactions and two C-O···Cg (π-ring) as illustrated in **Table 7.8**, **Table 7.9**, **Figure 7.8** and **Figure 7.7**.

Table 7.8 C-H···Cg(π-ring) interactions observed on *fac*-[^{99}Tc(Chzyl-4-*p*-tolyl)(CO)$_3$Cl] (**8d**) complex.

X-H(I)···Cg(J)	Symmetry	H···Cg (Å)	X-H···Cg (°)	X···Cg (Å)
C6-H6A···Cg(3)	#1	2.94	161	3.866(7)
C15-H15···Cg(6)	#2	2.97	143	3.756(7)
C35-H35···Cg(4)	#3	2.87	151	3.712(7)
C37-H37B···Cg(3)	#4	2.76	145	3.588(8)

Symmetry transformation used to generate equivalent to atoms: **#1** x, y, z; **#2** x, 1+y, z; **#3** x, -1+y, z; **#4** -1+x, -1+y, z; Cg3 = centroid atoms of C11,C12,C13,C14,C15,C16; Cg4 = centroid atom of C21,C22,C23,C24,C25,C26; Cg6 = centroid atom of C41,C42,C43,C44,C45,C46.

Table 7.9 C-O···Cg(π-ring) interactions observed on *fac*-[^{99}Tc(Chzyl-4-*p*-tolyl)(CO)$_3$Cl] (**8d**) complex.

X-O(I)···Cg(J)	Symmetry	O···Cg (Å)	X-O···Cg (°)	X···Cg (Å)
C9-O3···Cg(5)	#1	3.968(6)	82.0(4)	3.965(7)
C7-O1···Cg(6)	#2	3.867(6)	121.1(4)	4.547(7)

Symmetry transformation used to generate equivalent to atoms: **#1** x, y, z; **#2** x, y,-1+z; Cg5 = centroid atoms of C31,C32,C33,C34,C35,C36; Cg6 = centroid atoms of C41,C42,C43,C44,C45,C46.

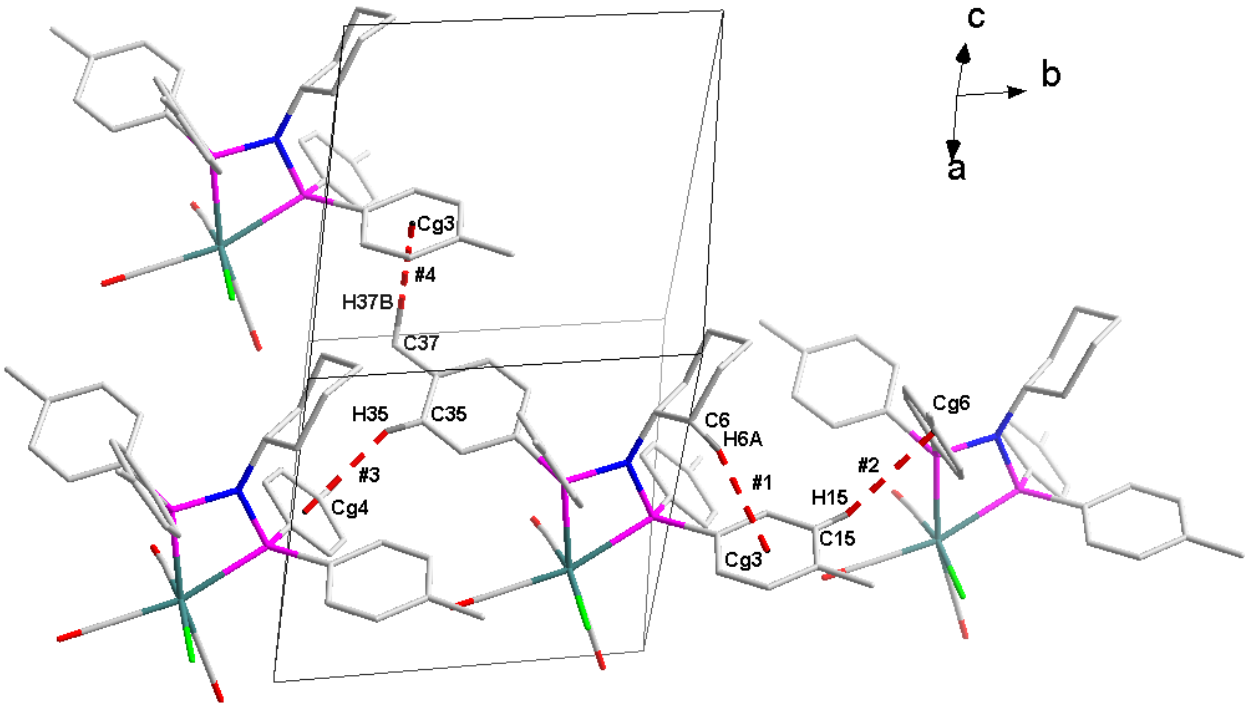

Figure 7.8 Graphic representation of the C-H···Cg interactions observed for the *fac*-[^{99}Tc(Chzyl-4-*p*-tolyl)(CO)$_3$Cl] (**8d**) complex.

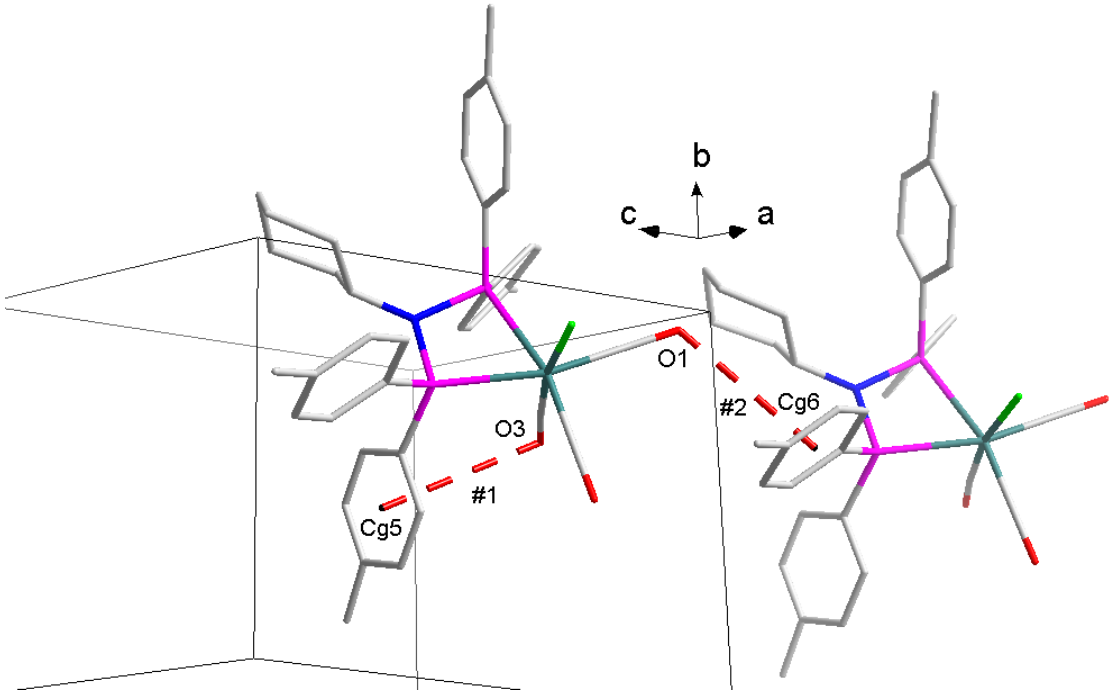

Figure 7.9 Graphic representation of the C-O···Cg interactions observed for the *fac*-[^{99}Tc(Chzyl-4-*p*-tolyl)(CO)$_3$Cl] (**8d**) complex

Figure 7.10 illustrates how a single molecule of complex **8c** packs in a unit cell along the *a*-axis. A head to tail packing fashion can be seen when the packing is viewed along the *c*-axis.

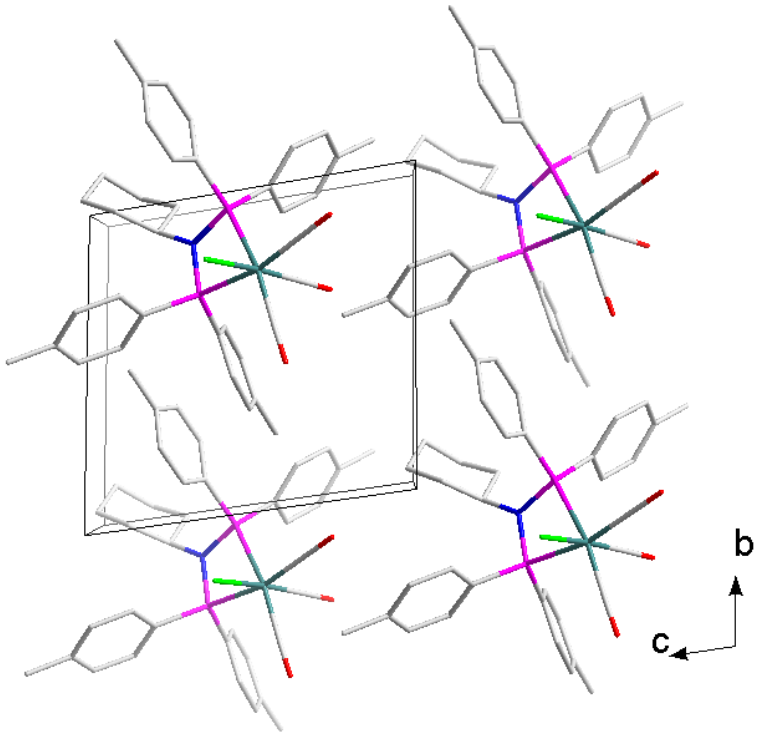

Figure 7.10 Crystal packing of *fac*-[^{99}Tc(Chzyl-4-*p*-tolyl)(CO)$_3$Cl] (**8d**) complex in the unit cell, viewed along the *a*-axis

7.5 *fac*-[Re(NBoc-PhPNP)(CO)$_3$Br] (4c)

The title complex, *fac*-[Re(NBoc-PhPNP)(CO)$_3$Br] (**4c**) was synthesized as described in **Paragraph 3.5.6**. Colourless cube-like crystals were obtained for this compound from a solution of dichloromethane/methanol (1:1). This complex crystallizes in the monoclinic crystal system in the $P2_1/c$ space group with four formula unit in the unit cell (Z = 4). The asymmetric unit contains one independent molecule. The molecular structure of the title complex, including the atomic numbering scheme is illustrated in **Figure 7.11**.

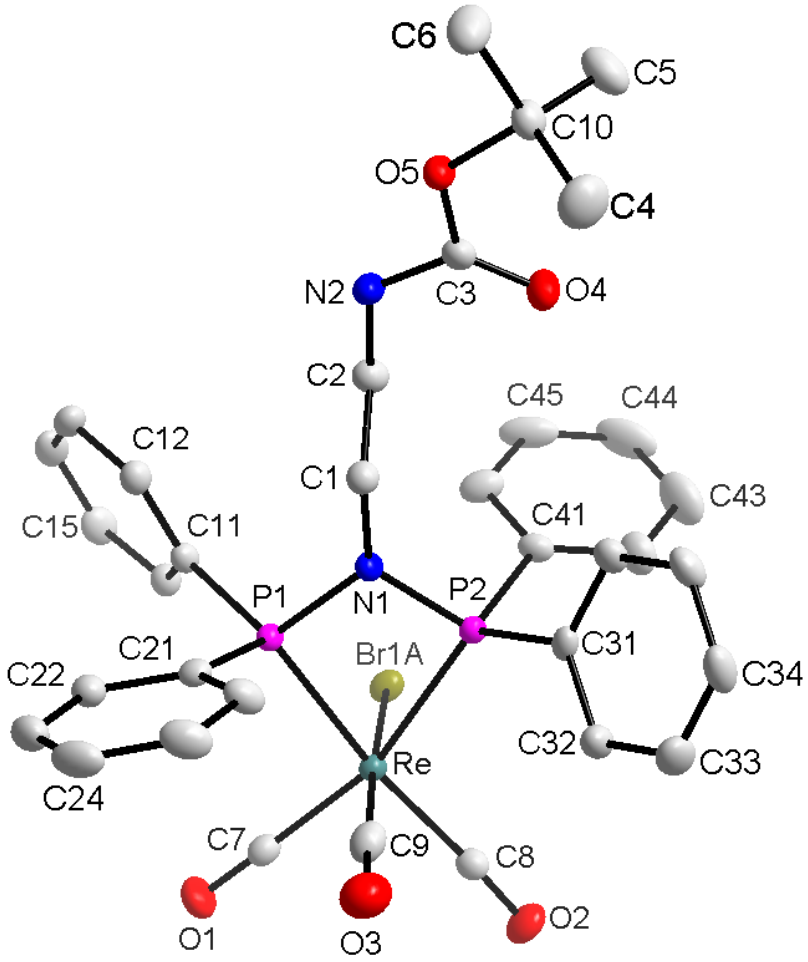

Figure 7.11 Molecular representation of *fac*-[Re(Nboc-PhPNP)(CO)$_3$Br] (**4c**) complex. All displacement ellipsoid are drawn at 50% probability level.

Table 7.10 Selected bond lengths and bond angles for the crystal structure of *fac*-[Re(NBoc-PhPNP)$(CO)_3$Br] (**4c**) (Å and °)

Atoms	Bond length (Å)	Atoms	Bond angle (°)
Re – P1	2.4314(10)	P1 – Re – P2	66.77(3)
Re – P2	2.4636(10)	P2 – N1 – P1	104.73(13)
Re – Br1A	2.6291(11)	N1 – P1 – Re	94.87(9)
Re – C7	1.948(3)	N1 – P2 – Re	93.46(8)
Re – C8	1.968(3)	B1A – Re – C9	174.71(17)
Re – C9	1.897(6)	C7 – Re – C8	92.96(12)
C7 – O1	1.144(4)	C9 – Re – C8	86.74(18)
C8 – O2	1.139(4)	C9 – Re – C7	87.08(19)
C9 – O3	1.153(2)	C1 – N1 – P1	125.19(19)
N1 – P1	1.696(2)	C1 – N1 – P2	129.26(19)
N1 – P2	1.706(2)		

The crystal structure of *fac*-[Re(NBoc-PhPNP)$(CO)_3$Br] (**4c**) shows three carbonyl ligands that are facially orientated to the Re(I) metal centre, while the remaining positions are occupied by a bromido moiety and a neutral bidentate NBoc-PhPNP (**4**)[13] PNP ligand. Similar to some previously described crystals, the crystal structure of *fac*-[Re(NBoc-PhPNP)$(CO)_3$Br] (**4c**) also showed a 70/30 % statistical disorder on the apical Br-Re-C9-O3 axes, thus requiring Shelx compatible restraints to be introduced on the refinement of the structure.

Selected bond distances and angles are summarized in **Table 7.10**, with the three carbonyl ligands facially coordinated to the Re(I) metal centre. The octahedral geometry around the Re(I) is distorted as indicated by a small P-Re-P bite angle of 66.77(3)° and O4-Re-C9 angle of 174.71(17)°. The bond distance values reported in **Table 7.10** for Re-P, Re-Br and Re-C were found to be comparable to those encountered on similar structures found in literature.[14,15] The *Effective Tolman-based N-substituent steric effect* ($\theta_{N\text{-}sub}$) of the NBoc-PhPNP **(4)** ligand was calculated using **Equation 4.1** and **Figure 4.3** from **Chapter 2** and found to be 72.0 °. Angles around the N atom range between 104.73(13)° and 129.26(19)°, indicating that the N atom adopted a highly distorted trigonal hybridization state.

Four hydrogen interactions were observed for this complex in the unit cell to stabilize the solid state structure of *fac*-[Re(NBoc-PhPNP)$(CO)_3$Br] (**4c**) as illustrated in **Table 7.11** and **Figure 7.12**. Moreover, this complex is further stabilized by a single C-H···Cg (π-ring) interactions and one Re-Br···Cg (π-ring) as illustrated in **Table 7.12** and **Figure 7.13**.

Table 7.11 Intra- and intermolecular hydrogen interactions observed on *fac*-[Re(NBoc-PhPNP)$(CO)_3$Br] (**4c**) complex.

D-H···A	Symmetry	D-H (Å)	H···A (Å)	D···A (Å)	D-H···A (°)
C4-H4C···O4	#1	0.96	2.41	3.006(5)	120
C5-H5A···O4	#1	0.96	2.39	2.991(4)	121
C16-H16···Br1A	#1	0.93	2.82	3.576(4)	139
C15-H15···O4	#2	0.93	2.56	3.299(4)	137

Symmetry transformation used to generate equivalent to atoms: **#1** x, y, z; **#2** 2-x, ½+y, ½-z.

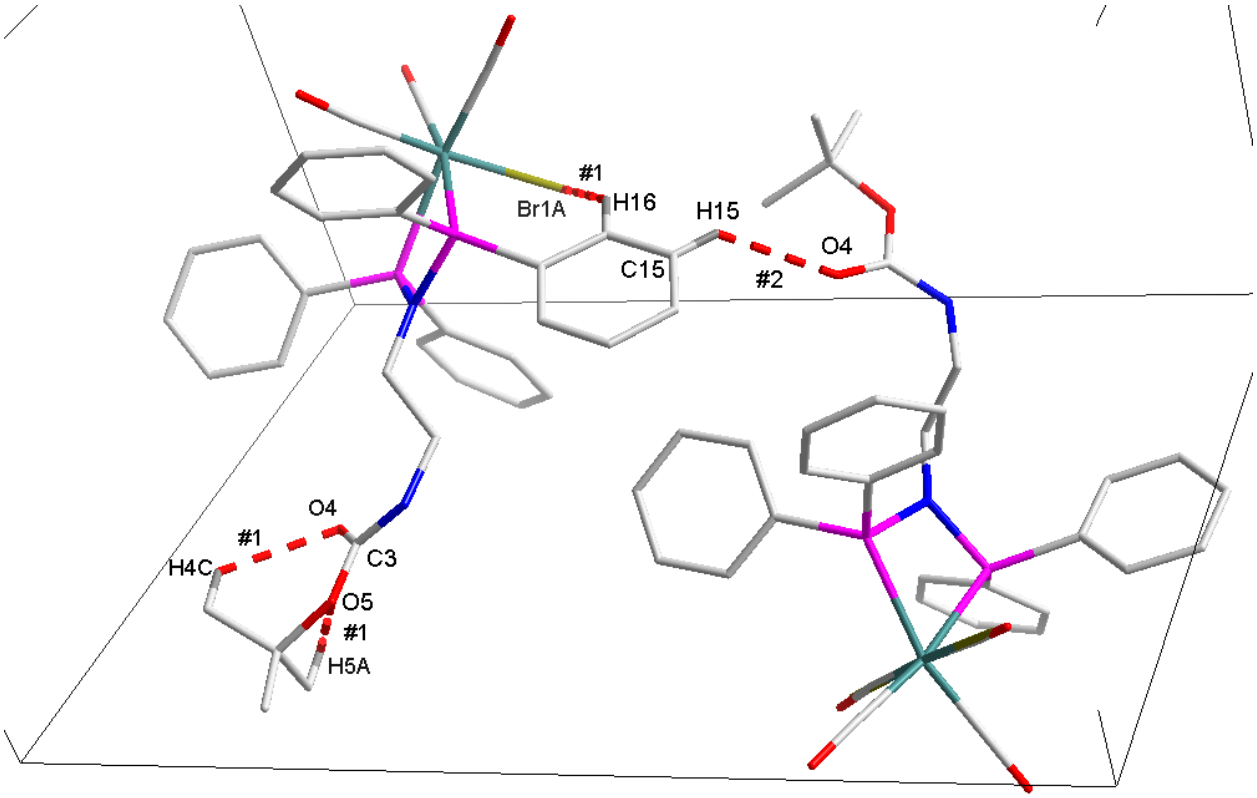

Figure 7.12 Graphic representation of the intra- and intermolecular hydrogen bonds observed for the *fac*-[Re(NBoc-PhPNP)$(CO)_3$Br] (**4c**) complex.

Table 7.12 X-Y···Cg(π-ring) (X = C or Re,Y = H or Br) interactions observed on *fac*-[Re(NBoc-PhPNP)$(CO)_3$Br] (**4c**) complex.

X-Y(I)···Cg(J)	Symmetry	Y···Cg (Å)	X-Y···Cg (°)	X···Cg (Å)
C35-H35···Cg(1)	#1	2.96	122	3.537(4)
Re1-Br1A···Cg(2)	#2	3.986(2)	96.11(3)	5.003(3)

Symmetry transformation used to generate equivalent to atoms: **#1** 2-x, -½+y, ½-z **#2** x, ½+y, -½+z; Cg1 = centroid atoms of C11,C12,C13,C14,C15,C16; Cg2 = centroid atom of C21,C22,C23,C24,C25,C26.

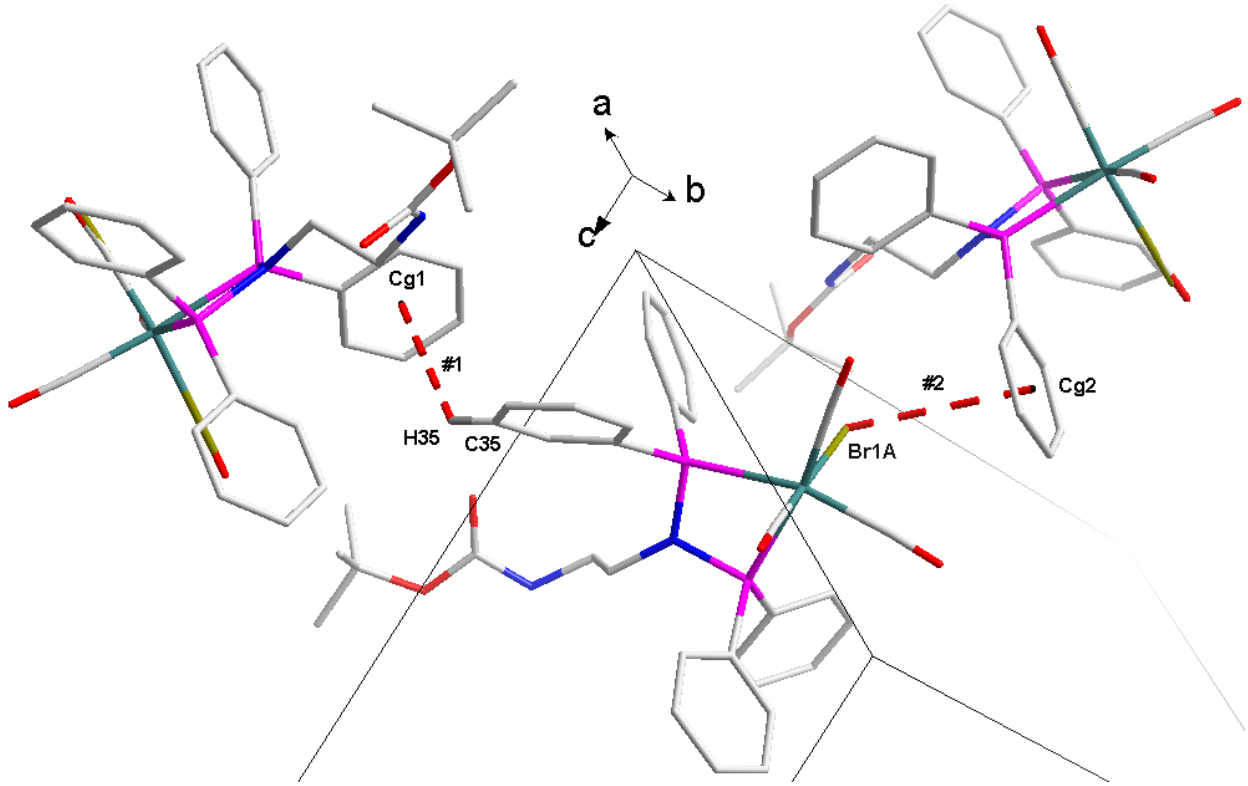

Figure 7.13 Graphic representation of some of the C-H···Cg and Re-Br···Cg interactions observed on *fac*-[Re(NBoc-PhPNP)$(CO)_3$Br] (**4c**) complex.

Figure 7.14 illustrates the packing manner of the *fac*-[Re(NBoc-PhPNP)$(CO)_3$Br] (**4c**) complex in the unit cell viewed along the *b*-axis.

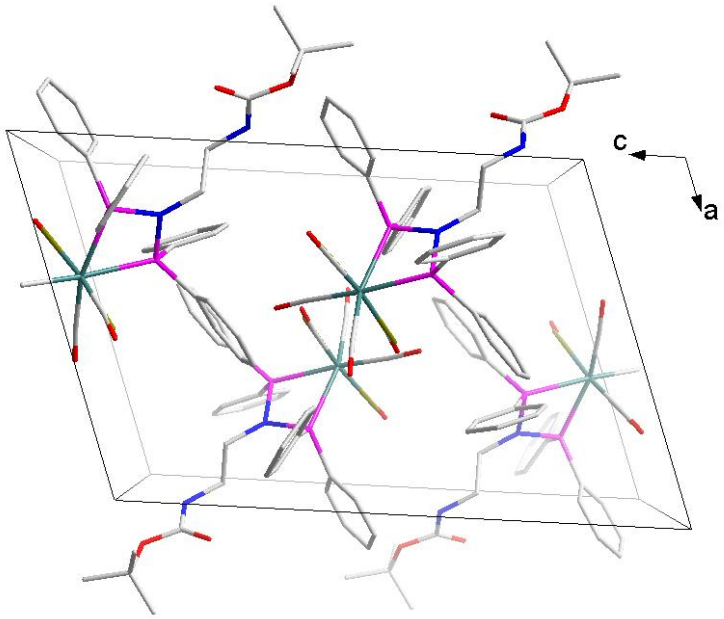

Figure 7.14 Crystal packing of *fac*-[Re(NBoc-PhPNP)$(CO)_3$Br] (**4c**) complex in the unit cell, viewed along the *b*-axis

7.6 Discussion

The solid state structures of *fac*-[Re(Chzyl-4-*p*-tolyl)$(CO)_3$Br] (**8c**), *fac*-[^{99}Tc(Chzyl-4-*p*-tolyl)$(CO)_3$Cl] (**8d**) and *fac*-[Re(NBoc-PhPNP)$(CO)_3$Br] (**4c**) were analyzed by X-ray diffraction. The first two complexes **8c** and **8d** are isostructural as inferred from the basic cell parameters. They (**8c** and **8d**) each contain two *para*-tolyl substituents on each P atom of the PNP backbone and a cyclohexyl group on the N atom.

There are however three main differences between complex **8c** and **8d**, the first one being that they have different metal centers: complex **8c** has a Re^I metal centre while complex **8d** contains a $^{99}Tc^I$. The second difference is that **8c** has a bromido moiety in the sixth position while **8d** contains a chlorido substituent. Thirdly, **8c** shows a statistical disorder of 85:15% on the Br-Re-CO axis while **8d** does not. The basic coordination modes as manifested by the M-C, P-M-P and the M-P (M = Re or ^{99}Tc) bonds/angle values illustrated in **Table 7.13** are also very similar.

Table 7.13 Selected bond distances and angles in complex **8c**, **8d** and **4c** illustrating the similarities between them.

Atoms (M = Re or ^{99}Tc)	Complex (8c)	Complex (8d)	Complex (4c)
		Bond length (Å)	
M – P1	2.4586(16)	2.4711(14)	2.4314(10)
M – P2	2.4635(15)	2.4523(14)	2.4636(10)
M – C7	1.956(6)	1.958(6)	1.948(3)
M – C8	1.945(6)	1.953(6)	1.968(3)
M – C9	1.947(9)	1.937(6)	1.897(6)
		Bond angles (°)	
P1 – M – P2	66.09(5)	66.16(4)	66.77(3)

The bond parameters illustrated in **Table 7.13** confirm that complex **8c** and **8d** are isostructural. In a typical biological system, this is very advantageous as this can further ensure that no secondary or metabolized compounds are produced when one changes from Re metal centre to a Tc one. This stability may further ensure that modification at the periphery of the ligand to increase the *in vivo* target selectivity of a drug is possible.

In both structures, the cyclohexyl substituent on the N atom is oriented in the chair conformation rather than the corresponding sterically demanding boat conformation. Moreover, the N atom adopts a distorted trigonal (sp^2) hybridization geometry to accommodate the resulting steric bulk on the N atom. Finally, an overlay of complex **8c** and **8d** was performed as illustrated in **Figure 7.15** and **Table 14** below which clearly indicates the isostructural behavior of these two complexes, as also manifested in the basic space group and unit cell parameters (**Table 7.1**).

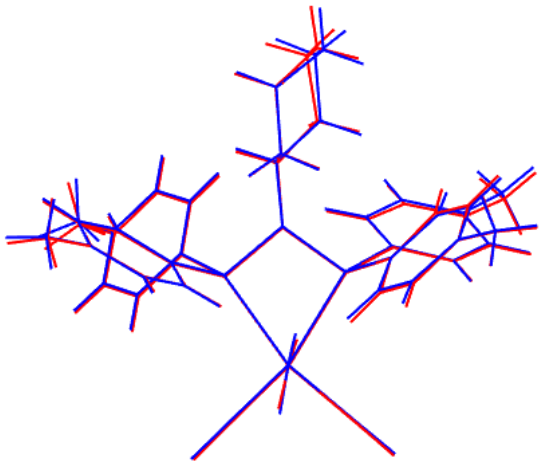

Figure 7.15 Graphical illustration of the overlay of **8c** (blue) and **8d** (red), RMS value = 0.00468.

Table 7.14 Selected information indicating the difference between complex **8c** and **8d**.

Complexes	C1-N1 (Å)	N-P_{ave} (Å)	P – M – P (°)	P – N – P (°)	Space group
fac-[Re(Chzyl-4-*p*-tolyl)$(CO)_3$Br] (**8c**)	1.502(7)	1.7055	66.09(5)	103.8(2)	*P*1
fac-[^{99}Tc(Chzyl-4-*p*-tolyl)$(CO)_3$Cl] (**8d**)	1.488(6)	1.7055	66.16(4)	104.0(2)	*P*1

Upon the synthesis of a homologous ^{99m}Tc complex with the same ligand as in complex **8c** and **8d**, a water solubility challenge, which is an inherent requirement for radiopharmaceuticals to have *in vivo* mobility, was encountered. To overcome this challenge, a new PNP ligand system described in **Chapter 3** was devised. Complex **4c** is the first product of this new system and its solubility study will be presented in **Chapter 8**. The crystal structure of complex (**4c**) differs from **8c** and **8d** in that it contains tetraphenyl PNP backbone instead of *para*-tolyl substituents on the P atoms. The most significant difference (and extremely important for potential future application of these PNP ligands in radiopharmacy) between **4c** and all the other structures described in this study however is the "NBoc" protected ethylenediamine moiety on the N atom of the PNP backbone. The other basic coordination geometry within **4c** is very similar to that of

8c and **8d** as manifested by comparison of bond distances and angles illustrated in **Table 7.13**, while the NBoc moiety provides the solubility, desperately required for application in vivo.

7.7 Conclusion

The solid state structures of *fac*-[Re(Chzyl-4-*p*-tolyl)$(CO)_3$Br] (**8c**), *fac*-[^{99}Tc(Chzyl-4-*p*-tolyl)$(CO)_3$Cl] (**8d**) and *fac*-[Re(NBoc-PhPNP)$(CO)_3$Br] (**4c**) were described whereby the identical ligand Chzyl-4-*p*-tolyl (**8**) was coordinated to non-radioactive rhenium and radioactive technetium-99 (weak β-emitter; E_{max} = 0.292 MeV; half-life = 212 000 years) in complex **8c** and **8d**. The two metals are valuable as model radiopharmaceutical nuclides. The solid state structures of **8c** and **8d** were confirmed to be isostructural.

As drug development ultimately involves the administration of pharmaceuticals to patients, it is critical to develop model drugs which are stable and soluble *in vivo*. Solubility studies should therefore form part of any investigation to determine whether the design complexes are soluble in the biological compatible solvents such as water, ethanol and dimethyl sulfoxide.

Indeed, it has also been the case with this PhD study. A challenge frequently encountered during ligand/complex design is the lack of solubility. This aspect has also been encountered in this study. These challenges lead to the synthesis of a promising NBoc-PhPNP (**4**) ligand which was later successfully coordinated to a $[Re(CO)_3]^+$ metal core, and indeed, the solid state structure of the resulting *fac*-[Re(NBoc-PhPNP)$(CO)_3$Br] (**4c**) complex has been enthusiastically described in this chapter. **Chapter 8** will focus on the solubility studies of all ligands and complexes synthesized during this PhD study.

8 Preliminary reactivity and solubility studies of PNP ligands and the corresponding Re(I) tricarbonyl complexes

What to expect!

A preliminary comparative study on reactivity behavior of NBoc-PhPNP and fac-[Re(NBoc-PhPNP)(CO)$_3$Br], followed by solubility studies of diphosphinoamine, diphosphinoamine oxide and Re(I) tricarbonyl complexes.

8.1 Introduction

In radiopharmaceutical drug development, the solubility and reactivity of the metallodrug and its coordinated ligands play a crucial role on the effectiveness of the drug on features such as *in vivo* stability, rate of uptake and compound excretion. This solubility parameter is driven by the desire to achieve a homogeneous drug concentration in a systemic circulation system, whereas the stability of the drug ensures that no secondary, or metabolized secondary compounds are produced.[1] Thus, the enhancement of both these parameters can increase the probability of receiving maximum anticipated pharmacological response. Consequently, considerable research in metallodrug development is consistently being directed to finding metal complexes that are stable and soluble both *in vivo* and *in vitro*.

The most convenient and commonly used route for drug administration is through oral administration. For an "oral ingested" drug to be absorbed, it must present itself in the form of a solution at the targeted site of absorption.[2] A challenge frequently encountered during

[1] Savjani, K. T., Gajjar A. K., Savjani, J. K., *ISRN Pharmaceutics*, **2012**, 1-10.

[2] Rahman, M. M., Khalipha, A. B. R., Azad, M. A. K., Hossain, S., Haque, S., *World J. Pharm. Pharm. Sci*, **2014**, 107-130.

metallodrug development is the lack of aqueous solubility and as mentioned in the previous chapters, this is a challenge constantly encountered by researchers. To address this stumbling block, the method of peripheral chemical modification was adopted and preliminary results will therefore be described in this chapter.

It flows from the above that it is therefore imperative to conduct experimental studies on reactivity and stability of any potential radiopharmaceutical agents. To first gain information regarding the stability of these Re^{I}-PNP tricarbonyl complexes, the complex formation and ligand substitution reactions on *fac*-[Re(NBoc-PhPNP)$(CO)_3$Br] (**4c**)[3] using ^{31}P NMR technique were investigated. The reason for choosing the ^{31}P nuclei instead of ^{1}H or ^{17}O was solely based on the more simple ^{31}P NMR spectra that one usually encounters when dealing with symmetrical phosphine bidentate ligands. The tricarbonyl tribromido complex of rhenium(I) (*fac*-$[Re^{I}(CO)_3Br_3]^{2-}$) was utilized as the precursor instead of the extensively used triaqua species due to the fact that all the rhenium complexes synthesized in this study had as reactant the tribromido species, and is thus preferable for comparison purposes. However, it is evident from previous studies that the *fac*-$[Re(CO)_3(H_2O)]^{+}$ is quite kinetically inert and that the three aqua molecules bound to the Re(I) can be readily displaced.[4,5,6,7] Therefore the next step in the near future should clearly be based on utilizing the tricarbonyl triaqua complex as the precursor.

While studies on reactivity and stability are of primary importance, the second aim of this chapter deals with the aqua solubility challenge that is frequently encountered in radiopharmaceutical studies. Peripheral chemical modification of the Re^{I}-PNP tricarbonyl complexes was again adopted, particularly modification on the periphery of the PNP ligand as a step to enhance the solubility of the complex. Solubility investigations on selected synthesized diphosphinoamine (PNP) ligands, diphosphinoamine oxide (PNPO) ligands and *fac*-[Re^{I}-PNP] tricarbonyl complexes in various solvents will therefore be presented in this chapter.

[3] **Chapter 3** and **Chapter 7** of this PhD thesis.

[4] Alberto, R., Schibli R., Waibel R., Abram U., Schubiger P. A., *Coord. Chem. Rev.* **1999**,*190-192*, 901-919.

[5] Schutte, M., Kemp, G., Visser, H. G., Roodt, A., *Inorg. Chem.* **2011**, *50*, 12486-12498.

[6] Schutte, M., Roodt, A., Visser, H. G., *Inorg. Chem.* **2012**, *51*, 11996-12006.

[7] Helm, L., *Coord. Chem. Rev*. **2008**, *252*, 2346-2361.

8.2 Experimental

8.2.1 Reagents

Synthetic procedures of diphosphinoamine (PNP) ligands, diphosphinoamine oxide (PNPO) ligands and the *fac*-[Re^{I}-PNP] tricarbonyl complexes are described in **Chapter 3**. All the other chemicals (with the exception of deuterated acetonitrile) were of analytical reagent grade, purchased from Sigma-Aldrich and were used without further purification. Deuterated acetonitrile (MeCN) was obtained from Cambridge Isotope Laboratories and was also used without further purification.

8.2.2 Equipment

- All ^{31}P NMR spectra were analyzed on a 400 MHz AVANCE III nuclear magnetic resonance spectrometer operating at a temperature of 25 °C using appropriate deuterated solvents. Chemical shifts (δ), are reported in parts per million (ppm), while the MestReNova program version 6.0.2-5475 program was used for drawing NMR spectra.

- UV-Visible measurements were performed on a Varian 50 Conc UV/Vis spectrophotometer. The temperature of the reaction mixture was maintained within ± 0.1 °C range by means of a Julabo F12-mV temperature cell regulator in a 1.000(1) cm tandem quartz cuvette cell. The Scientist Micromath program version 2.01was utilized for fitting data points to selected functions.

8.2.3 Reaction solutions

Unless stated otherwise, all the NMR and the UV/Vis experiments were performed under, or close to *pseudo* first-order conditions with the ligand in excess. Ligand and metal precursor stability studies in the reaction solvents were confirmed before the execution of each experiment. Fresh reaction solutions were prepared for every separate experiment.

For the *fac*-[Re(NBoc-PhPNP)$(CO)_3$Br] (**4c**) complex formation studies in 1.0 ml deuterated MeCN, the absolute metal concentration was kept at 0.005 M {$(NEt_4)_2[Re(CO)_3Br_3]$; 3.9 mg; 4.997×10^{-6} mol} while the ligand solution range was from 0.015 M (NBoc-PhPNP; 7.9 mg,

1.495×10^{-5} mol) to 0.05 M (NBoc-PhPNP; 26.4 mg, 4.995×10^{-5} mol). For the bromide ligand substitution reaction on *fac*-[Re(NBoc-PhPNP)$(CO)_3$Br] (**4c**), the metal final concentration was kept at 7.5×10^{-3} M (6.81 mg, 7.494×10^{-6} mol), while the maximum final entering nucleophile concentration was 10 times more (PTA, 11.8 mg, 7.494×10^{-5} mol; Pyridine, 6×10^{-3} ml, 7.494×10^{-5} mol; NaSCN, 6.1 mg, 7.494×10^{-5} mol). For solvent solubility tests, approximately 20 mg of a respective compound was dissolved in 5 ml of the respective solvent.

8.3 Formation of *fac*-[Re(NBoc-PhPNP)$(CO)_3$Br]

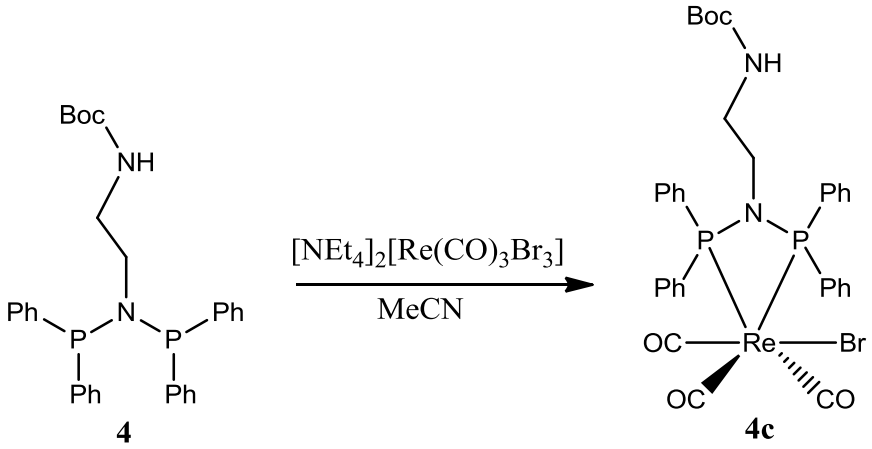

Scheme 8-1 Description of the formation of *fac*-[Re(NBoc-PhPNP)$(CO)_3$Br] complex from the reaction between NBoc-PhPNP and ReAA in acetonitrile.

The reaction of *N*,*N*-Bis(diphenylphosphino)-*N*-Boc-ethylenediamine (NBoc-PhPNP) with *fac*-$[NEt_4]_2[Re(CO)_3Br_3]$ (ReAA) in deuterated acetonitrile (MeCN) was investigated over a period of 4 hours at 25 °C using ^{31}P NMR on a 400 MHz AVANCE III NMR spectrometer. In **Figure 8.1** is shown the peak changes observed at a specific [NBoc-PNP] concentration value of 0.015M. The ^{31}P NMR spectra in this experiment showed two distinct singlet peaks which may be attributed to the free NBoc-PNP [peak (**ii**)] and the corresponding formation of the Re-NBoc-PNP species [peak (**i**)], see **Figure 8.1**(a).

It further served in confirming the following: (i) the absence of an oxidized NBoc-PhPNP which should appear at 31.69 ppm if present, (ii) the symmetric arrangement of the NBoc-PhPNP around the Re metal center, since no secondary coupling was observed on the product peak

resonating at 45.71 ppm, (iii) A significant peak intensity *decrease* for the free NBoc-PhPNP (63.67 ppm) and peak intensity increase of the *fac*-[Re(NBoc-PhPNP)$(CO)_3$Br] (45.71 ppm).

The results in **Figure 8.1**(a) clearly showed that the rates of peak *decrease* of the free NBoc-PNP and the *increase* of the Re-NBoc-PNP species were identical as illustrated in **Figure 8.1**(b). Thus, the formation of the *fac*-[Re(NBoc-PhPNP)$(CO)_3$Br] species could be conveniently studied as a function of time, see **Figure 8.1**(c). The pseudo first-order rate constants thus obtained are given in **Table 8.1** below.

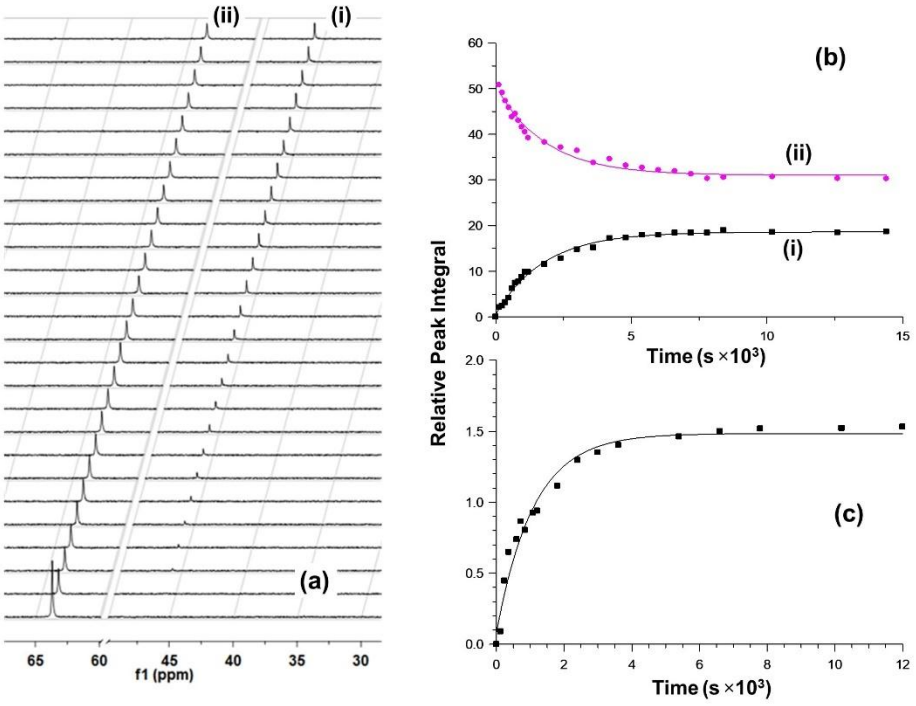

Figure 8.1 Graphic representation of the data obtained from analysis of the formation *fac*-[Re(NBoc-PhPNP)$(CO)_3$Br] by ^{31} P NMR in MeCN-d_4. The first spectrum denotes the undiluted starting concentration of the PNP-ligand. (**a**) ^{31}P stacked plot of the formation of the *fac*-[Re(NBoc-PhPNP)$(CO)_3$Br] and the decrease of the free PNP ligand for a 1: 3 ([Re]=0.005 M: [NBoc-PNP]=0.015M) ratio; (Δt= 140s) between spectra; (**b**) Typical correlation between the decrease and increase in the signals representing (**i**) *fac*-[Re(NBoc-PhPNP)$(CO)_3$Br] and (**ii**) the free NBoc-PNP ligand, respectively; formation of *fac*-[Re(NBoc-PhPNP)$(CO)_3$Br] in a 1:3 ratio ([Re]=0.005 M: [NBoc-PNP]=0.015M) showing the *decrease* (**ii**) of the free NBoc-PNP signal (at 63.7 ppm) and the *increase* (**i**) of the Re-NBoc-PNP signal at 45.7 ppm; (**c**) Kinetic trace for studying the formation of the Re-NBoc-PNP complex formation from the ^{31}P signal integrals, illustrating the formation of the product when a 1:10 ratio ([Re]=0.005 M: [NBoc-PNP]=0.05M) was utilized, yielding the *pseudo* first-order rate constant [line represents the least-squares fit to a first-order exponential; points indicate the experimental measurements observed].

Thus, although very expensive, with respect to use of deuterated solvents, and time consuming, the kinetics was investigated for four different values of [NBoc-PNP] concentration, see **Table 8.1** and are graphically illustrated in **Figure 8.2**.

Table 8.1 Pseudo first-order rate constants for the formation *fac*-[Re(NBoc-PhPNP)$(CO)_3$Br] from ^{31}P NMR in acetonitrile at 25 °C. [Re]=0.005M.

[NBoc-PNP] (M)	k_{obs} (s^{-1})
0.015	0.00056(3)
0.025	0.00075(3)
0.030	0.00084(8)
0.050	0.00091(9)

:

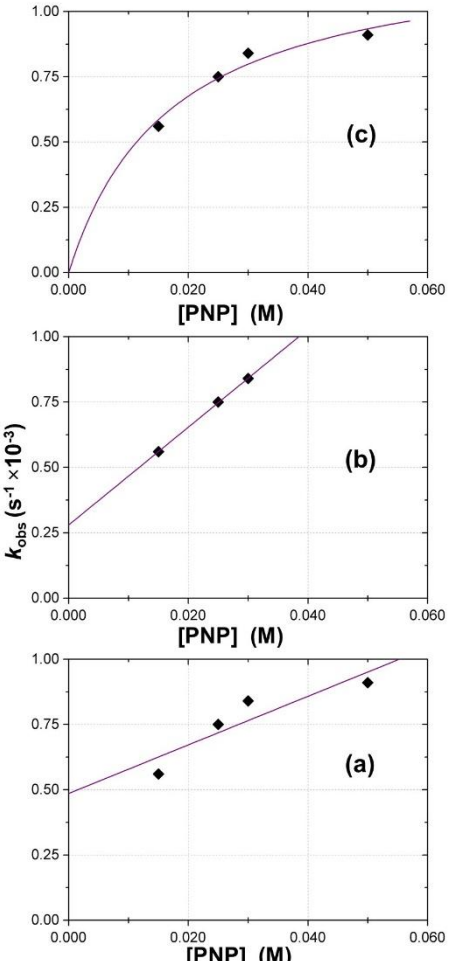

Figure 8.2 Plots of k_{obs} *vs*. entering PNP-ligand for the formation of the *fac*-[Re(NBoc-PhPNP)$(CO)_3$Br] complex as obtained from a ^{31}P NMR study as illustrated in **Figure 8.1**. (**a**) k_{obs} *vs.* [NBoc-PNP] in a linear relationship based on rate law given in **Eq. 8.2** below; (**b**) k_{obs} *vs.* [NBoc-PNP] in a linear relationship as from the same rate law given in **Eq. 8.2** but excluding the last [NBoc-PNP] where some precipitation started; (**c**) k_{obs} *vs.* [NBoc-PNP] in a pre-equilibrium limiting consecutive step rate law as given in **Eq. 8.5**.

8.4 Rate Laws for the formation of *fac*-[Re(NBoc-PhPNP)(CO)$_3$Br]

Although the data is limited for the formation of the *fac*-[Re(NBoc-PNP)(CO)$_3$(Br)] species as illustrated in Par. 8.3, a few speculations are justified with the current data in hand, as discussed in (**A**) and (**B**), yielding some preliminary conclusions as introduced below.

(**A**) **Pathway 1:**

First, if a simple single-step formation of the *fac*-[Re(NBoc-PNP)(CO)$_3$(Br)] species is envisaged upon reaction with a PNP entering nucleophile as shown in the equilibrium reaction in **Eq. 8.1**, then the simplified expression given in **Eq. 8.2** for the *pseudo* first-order rate constant holds (when [NBoc-PNP]>>[Re]):

$$fac\text{-}[Re(CO)_3(Br)_3]^{2-} + \text{NBoc-PNP} \underset{k_{-1}}{\overset{k_1,\ K_1}{\rightleftharpoons}} fac\text{-}[Re(CO)_3(\text{NBoc-PNP})Br] + 2Br^- \quad \ldots 8.1$$

$$k_{obs} = k_1[\text{NBoc-PNP}] + k_{-1} \quad \ldots 8.2$$

In this case, a plot of k_{obs} *vs*. [NBoc-PNP] should yield a linear relationship from which the two rate constants could be obtained.

The attempt to use **Eq. 8.2** is illustrated in **Fig. 8.2** (a) and (b), and the rate constants thus obtained are given in **Table 8.2**.

(**B**) **Pathway 2:**

However, if the coordination of the NBoc-PNP ligand to the Re(I) takes place in a consecutive two-step process, where the first step represents the mono-coordination as shown in **Eq. 8.3** in a rapid equilibrium, followed by a rate-determining ring-closure in the second step as in **Eq. 8.4**, then the simplified expression as given in **Eq. 8.5** for the *pseudo* first-order rate constant holds (when [NBoc-PNP]>>[Re]).

The data in **Table 8.1** was thus also fitted to **Eq. 8.5** and the corresponding rate and equilibrium constant as obtained therefrom, is reported in **Table 8.2**.

$$fac\text{-}[Re(CO)_3(Br)_3]^{2-} + \text{NBoc-PNP} \underset{k_{-1}}{\overset{k_1,\ K_1}{\rightleftharpoons}} fac\text{-}[Re(CO)_3(\text{NBoc-PNP}^1)Br] + 2Br^- \quad \ldots 8.3$$

$$fac\text{-}[Re(CO)_3(\text{NBoc-PNP}^1)Br] \xrightarrow{k_2} fac\text{-}[Re(CO)_3(\text{NBoc-PNP}^2)Br] \quad \ldots 8.4$$

$$k_{obs} = k_2 K_1 [\text{Nboc-PNP}]/(1 + K_1[\text{Nboc-PNP}]) \quad \ldots 8.5$$

In **Eq. 8.3** and **8.4** *fac*-[Re(CO)$_3$(NBoc-PNP^1)Br] and *fac*-[Re(CO)$_3$(NBoc-PNP^2)Br] indicates the mono-coordinated and the bidentate coordinated NBoc-PNP ligand, respectively.

It is clear that the fit of the *pseudo* first-order rate constants (from **Table 8.1**) to **Eq. 8.2**, shown in **Fig. 8.2**(a) is not good, as manifested also in the second and first-order rate constants obtained for the forward and reverse steps, k_1 and k_{-1}, (**Table 8.2**) respectively, indicating e.s.d's of some 30%.

However, some precipitation was observed at higher [NBoc-PNP], which might indicate that the k_{obs} value at [NBoc-PNP] = 0.05 M is less reliable and may potentially be discarded. In such a scenario **Fig. 8.2**(b) holds for the same fit of the data in **Table 8.1** to **Eq. 8.2**, which clearly yields a much better fit (although to only 3 data points!) and rate constants with much lower e.s.d.'s, only of the order or 10%, and seemingly quite acceptable.

On the other hand, Pathway 2 in (**B**) above also represents a very likely process, since it is known that the 2nd, and particularly the 3rd Br$^-$ is liberated from the starting *fac*-[Re(CO)$_3$(Br)$_3$]$^{2-}$ with much more difficulty, and potentially slower. Moreover, considering the rotation around the central N-atom in the PNP ligand, as was also illustrated and discussed in the structural work described in **Chapters 4** (in many cases the 2nd P-atom rotates very easily away by 180 °), implying that the ring-closure might well be a slower and indeed, the rate-determing step. Thus, when using this assumption and fitting the data in **Table 8.1** to **Eq. 8.5**, quite a reasonable fit is obtained, with rate and equilibrium constants (see **Table 8.2**) with very acceptable e.d.s.'s.

Thus, Pathway 2 is, with the current data in hand, considered as the most likely and acceptable representation of the process for the formation of the *fac*-[Re(CO)$_3$(NBoc-PNP)Br] complex. However, clearly, significant additional work not possible within this current PhD study, is required to make a more accurate assessment of the situation.

Table 8.2 Rate constants obtained from least-squares fitting of the date in Table 8.1 to respective kinetic functions in Pathway 1 and 2 for the formation *fac*-[Re(NBoc-PhPNP)(CO)$_3$Br] as monitored by ^{31}P NMR in acetonitrile at 25 C

Pathway: Figure (Rate Eq.)	**Rate Constant**	**Value**
1; Fig. 8.1(a)	k_1 ($M^{-1}s^{-1}$)	0.009(3)
(Eq. 8.1)	k_{-1} (s^{-1})	0.005(1)
1; Fig. 8.1(b)	k_1 ($M^{-1}s^{-1}$)	0.0187(2)
(Eq. 8.2)	k_{-1} (s^{-1})	0.00028(6)
2; Fig. 8.1(c)	K_1 (M^{-1})	58(16)
(Eq. 8.5)	k_2 (s^{-1})	0.0013(1)

8.5 Attempted Substitution reaction of the Bromido ion in *fac*-[Re(NBoc-PhPNP)(CO)$_3$Br]

Following up on the work reported in Par. 8.4, a kinetic investigation on the reaction between NBoc-PnPNP and the *fac*-[Re(CO)$_3$(Br)$_3$]$^{2-}$ as reactant at a temperature of 25 °C and various concentrations was attempted by UV/Vis techniques on a Varian 50 Conc UV/Vis spectrophotometer using dry MeCN. However, *no* significant absorption changes were observed; an aspect which have been predicted prior to the investigation considering the pale white colours exhibited by both the reactants, the PNP ligand and the *fac*-[Re(CO)$_3$(Br)$_3$]$^{2-}$ complex, as well as the product, *fac*-[Re(CO)$_3$(NBoc-PNP)Br]. Thus, using UV/Vis spectrophotometry could not be used to monitor the reaction progress which was clearly taking place, and were done by ^{31}P NMR as illustrated in **Par. 8.3** and **8.4**.

In yet a further attempt to use other ligands synthesized in **Chapter 3** of this PhD study, to study the formation reaction of a diphosphinoamine (PNP) ligand with ReAA were either prohibited by (i) the insolubility of the PNP ligand or (ii) produced similar results as those obtained upon using NBoc-PhPNP.

Thus, next, following up further on the work reported in Par. 8.4 and to study the *substitution* of the bromide ligand from the *fac*-[Re(NBoc-PhPNP)$(CO)_3$Br] by appropriate entering nucleophile(s), the following reactions were attempted.

8.5.1 1,3,5-triaza-7-phosphaadamantane (PTA) as the entering ligand

The potential substitution reaction of the bromido ligand from *fac*-[Re(NBoc-PhPNP)$(CO)_3$Br] with 1,3,5-triaza-7-phosphaadamantane (PTA) as proposed in **Scheme 8.2**, was investigated in deuterated acetonitrile (MeCN) for 4 hours at 25 °C using ^{31}P NMR on a 400 MHz AVANCE III NMR spectrometer under *pseudo* first-order conditions.

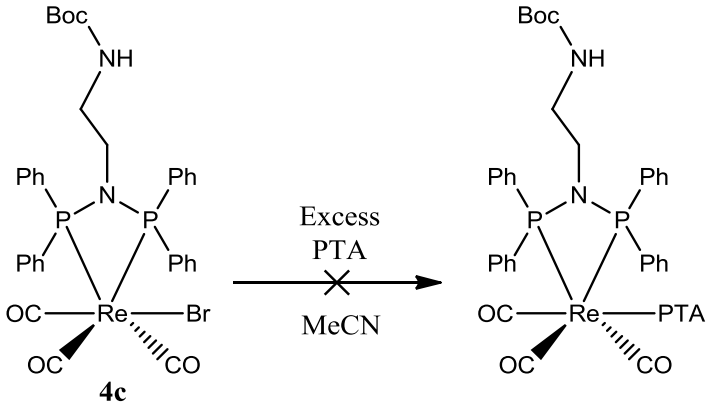

Scheme 8-2 Illustration of PTA as potential nucleophile to substitute Br^- from the *fac*-[Re(NBoc-PhPNP)$(CO)_3$Br] complex, in acetonitrile as solvent.

From the ^{31}P NMR results illustrated in **Figure 8.3**, two distinct singlet peaks were observed. However, unfortunately these peaks correspond only to *fac*-[Re(NBoc-PhPNP)$(CO)_3$Br] (46.15 ppm) and the entering ligand PTA (-102.10 ppm). Thus, it indicated clearly that no bromide substitution reaction was observed.

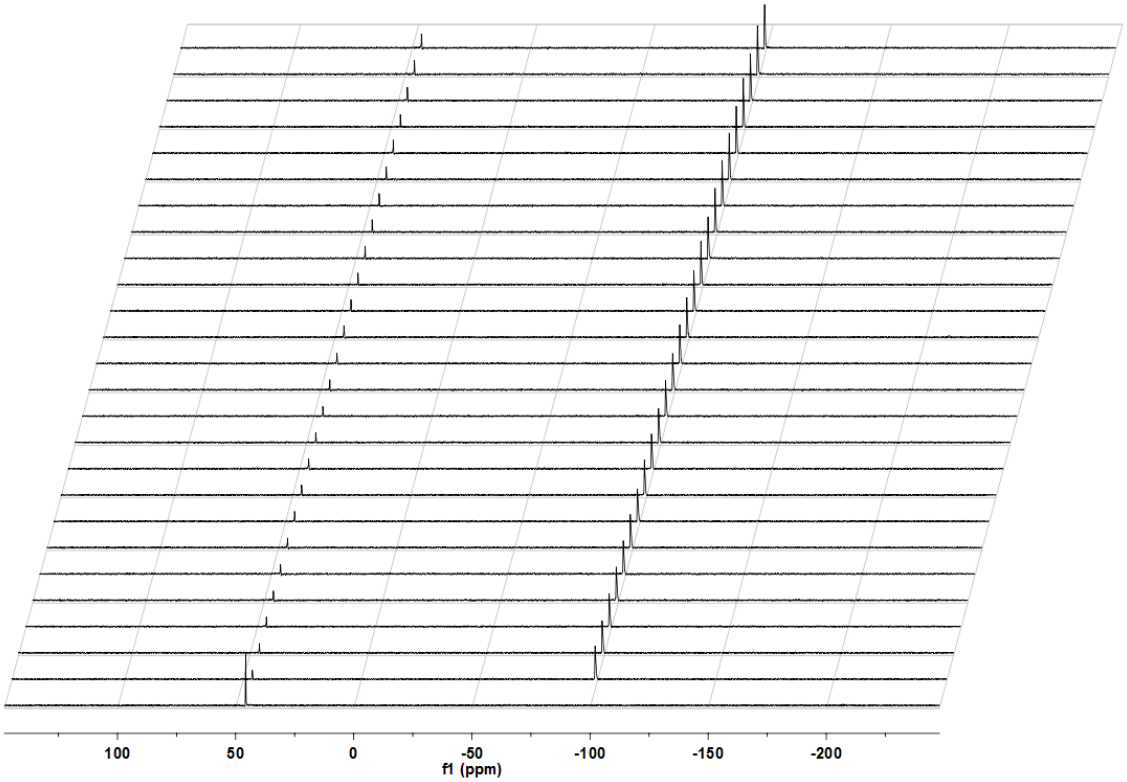

Figure 8.3 Stacked plot of ^{31}P NMR spectra as a function of time (Δt= 140 s) for the reaction between *fac*-[Re(NBoc-PhPNP)(CO)$_3$Br] and PTA.

For comparison purposes, the same substitution reaction was performed at various concentrations on a Varian 50 Conc UV/Vis spectrophotometer using dry MeCN. As anticipated, no absorbance change was observed. Both the ^{31}P NMR and the UV/Vis studies were performed in triplicate to confirm reproducibility.

8.5.2 Pyridine as the entering ligand

Similar to **8.5.1**, the substitution reaction of the bromide moiety in *fac*-[Re(NBoc-PhPNP)(CO)$_3$Br] by pyridine (**Scheme 8.3**) in deuterated acetonitrile (MeCN) was investigated for 4 hours at 25 °C using ^{31}P NMR technique on a 400 MHz AVANCE III NMR spectrometer under *pseudo* first-order conditions.

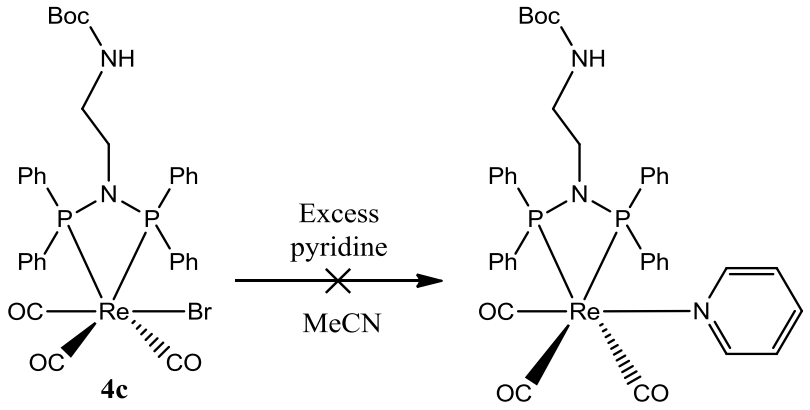

Scheme 8-3 Illustration of pyridine as potential nucleophile to substitute Br^- from the *fac*-[Re(NBoc-PhPNP)$(CO)_3$Br] complex, in acetonitrile as solvent.

Similar to **Par. 8.5.1**, again a distinct single peak at 46.15 ppm corresponding to only *fac*-[Re(NBoc-PhPNP)$(CO)_3$Br] was observed as illustrated in **Figure 8.4**, indicating that no substitution of the Br^- ligand took place.

For comparison purposes, the same substitution reaction was again performed at various concentrations on a Varian 50 Conc UV/Vis spectrophotometer using dry MeCN. As anticipated, no absorbance change was observed. Both the ^{31}P NMR and the UV/Vis studies were performed in triplicates to confirm reproducibility.

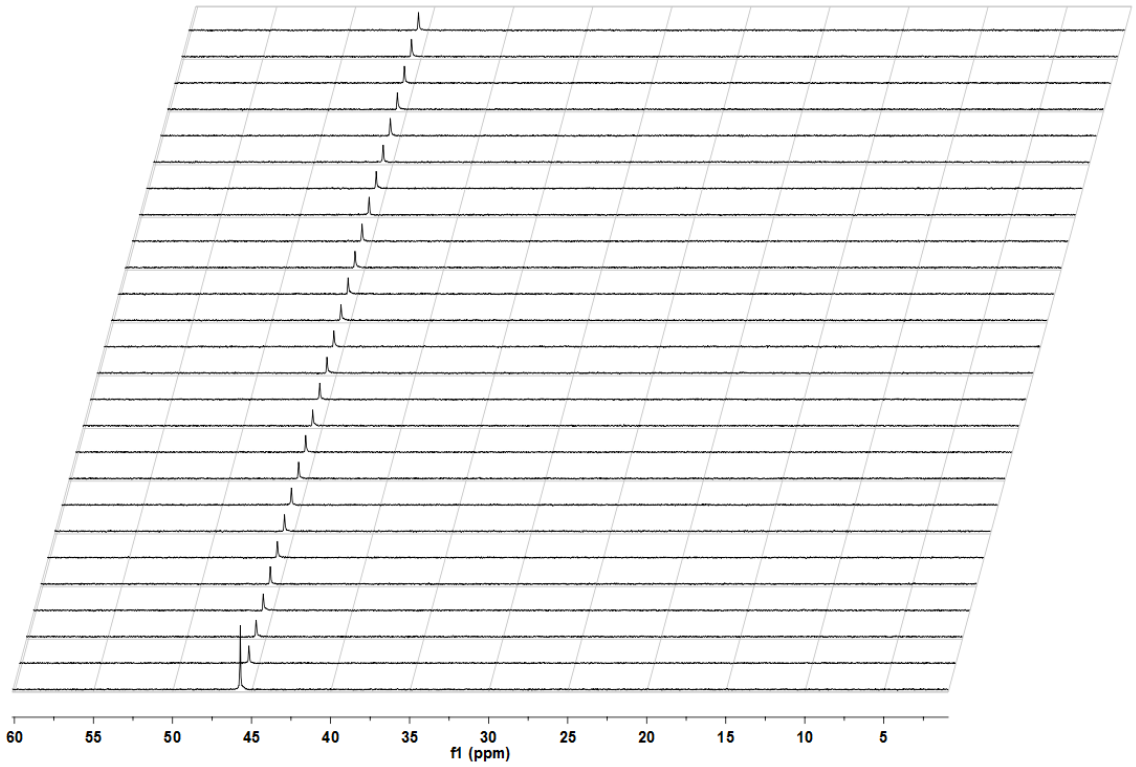

Figure 8.4 A stacked plot of ^{31}P NMR spectra as a function of time (Δt= 140 s) for monitoring the kinetics for the reaction between *fac*-[Re(NBoc-PhPNP)(CO)$_3$Br] and pyridine.

8.5.3 Thiocyanate anion (using NaSCN) as the entering ligand

Similar to the attempt in **Par. 8.5.1**, the substitution reaction of the bromide moiety in *fac*-[Re(NBoc-PhPNP)(CO)$_3$Br] with sodium thiocyanate (NaSCN) in deuterated acetonitrile (MeCN) was investigated for 4 hours at 25 °C using ^{31}P NMR on a 400 MHz AVANCE III NMR spectrometer under *pseudo* first-order conditions.

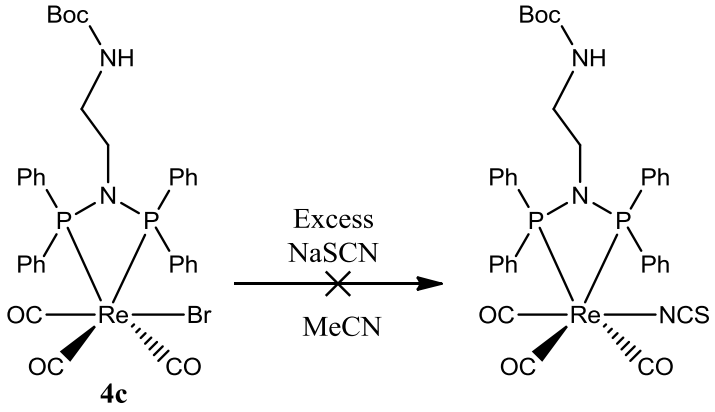

Scheme 8-4 Illustration of thiocyanate as potential nucleophile to substitute Br$^-$ from the *fac*-[Re(NBoc-PhPNP)(CO)$_3$Br] complex, in acetonitrile as solvent.

Again, only a distinct single peak at 45.69 ppm corresponding to *fac*-[Re(NBoc-PhPNP)$(CO)_3$Br] was observed as illustrated in **Figure 8.5** indicating that no substitution reaction took place.

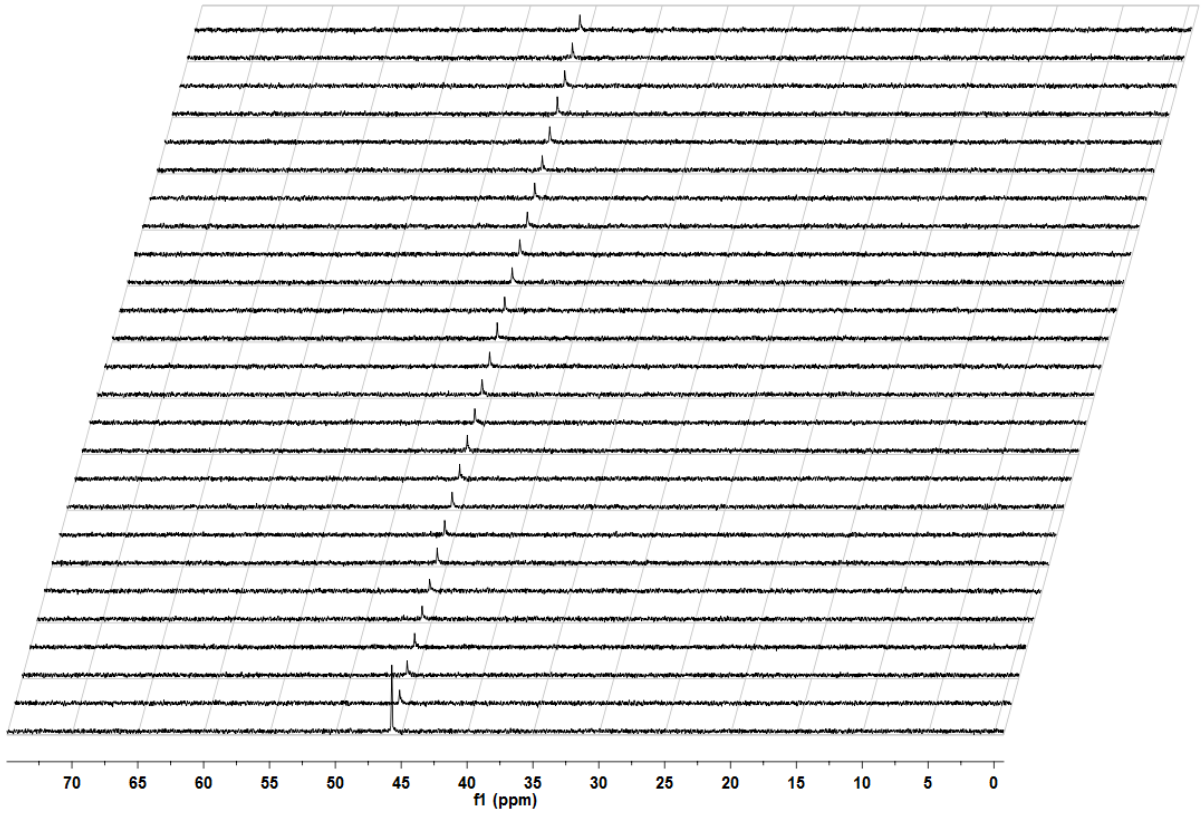

Figure 8.5 A stacked plot of ^{31}P NMR spectra as a function of time (Δt= 140 s) for monitoring the kinetics for the reaction between *fac*-[Re(NBoc-PhPNP)$(CO)_3$Br] and NaSCN.

As in the previous substitution reactions, the same attempted bromido substitution with NaSCN was performed at various concentrations on a Varian 50 Conc UV/Vis spectrophotometer using dry MeCN but no absorbance change was observed. Both the ^{31}P NMR and the UV/Vis studies were performed in triplicates to confirm reproducibility.

8.6 Solubility studies in solution

Solubility investigations of selected synthesized diphosphinoamine (PNP) ligands, diphosphinoamine oxide (PNPO) ligands and the *fac*-[Re^{I}-PNP] tricarbonyl described in **Chapter 3** were next conducted using biologically compatible solvents such as water (H_2O), ethanol (EtOH) and dimethyl sulfoxide (DMSO). At different times, aliquots were withdrawn and analyzed by ^{31}P NMR to ensure that no chemical degradations were taking place. The

solubility of compounds in this study will be classified into four categories namely: (i) very soluble, (ii) soluble, (iii) slightly soluble, and (iv) insoluble.

- Very soluble – dissolves immediately
- Soluble – dissolves slowly but completely
- Slightly soluble – heat and vigorous stirring needed for complete solubility.
- Insoluble – practically insoluble

Table 8.3 illustrates the results obtained in this study expressed in mg/ml. Except were specified, the solubility studies were conducted by dissolving approximately 20 mg of a compound in 5 ml of a solvent.

Table 8.3 Solubility study results on selected PNP, PNPO and Re^{I}-PNP compounds synthesized in this study.

Compound	**EtOH**	**DMSO**	**H_2O**
*p*Tol-PhPNP	slightly soluble	soluble	insoluble
*p*ClPh-PhPNP	slightly soluble	soluble	insoluble
*p*FPh-PhPNP	slightly soluble	soluble	insoluble
NBoc-PhPNP	very soluble[a]	very soluble[a]	insoluble
Chzyl-4-*p*-tolyl	slightly soluble	slightly soluble	insoluble
*p*Tol-PhPNPO	slightly soluble	slightly soluble	insoluble
*p*ClPh-PhPNPO	soluble	soluble	insoluble
*p*FPh-PhPNPO	soluble	soluble	insoluble
NBoc-PhPNPO	very soluble[a]	very soluble[a]	insoluble
Chzyl-4-*p*-tolyl-PNPO	soluble	soluble	insoluble
fac-[Re(*p*Tol-PhPNP)$(CO)_3$Br]	soluble	soluble	insoluble
fac-[Re(*p*ClPh-PhPNP)$(CO)_3$Br]	soluble	soluble	insoluble
fac-[Re(*p*FPh-PhPNP)$(CO)_3$Br]	soluble	soluble	insoluble
fac-[Re(NBoc-PhPNP)$(CO)_3$Br]	very soluble[a]	very soluble[a]	insoluble
fac-[Re(Chzyl-4-*p*-tolyl $CO)_3$Br]	slightly soluble	slightly soluble	insoluble

[a] – 20 mg dissolved in 1 mL of a respective solvent

Significant solubility enhancement of the poorly soluble diphosphinoamine (PNP) ligands was observed on the chemically modified NBoc-PhPNP ligand and its respective rhenium complex.

Although none of the selected compounds were water soluble, the next step would be to modify further the NBoc-PhPNP ligand and its respective Re complex. Other solvents that were tested includes solvents such methanol (MeOH) and acetonitrile (MeCN). In the MeOH/MeCN case, all the ligands and their respective rhenium complexes were in-between slightly soluble and insoluble, except for the NBoc-PhPNP ligand and its respective rhenium complex which were both very soluble in both solvents.

8.7 Discussion and conclusion

Preliminary formation kinetic studies of *fac*-[Re(NBoc-PhPNP)$(CO)_3$Br] from the reactants NBoc-PhPNP ligand and *fac*-$[NEt_4]_2[Re(CO)_3Br_3]$ metal precursor was described in par. **8.3**. From these results, it became evident that the reaction proceeds towards product formation without any significant side reaction. This was confirmed by the observation of two distinct singlet peaks corresponding to the un-reacted NBoc-PhPNP ligand and its respective rhenium complex. Furthermore, the calculated k_{obs} for the concentration lowering of the NBoc-PhPNP ligand and the concentration increment of *fac*-[Re(NBoc-PhPNP)$(CO)_3$Br] complex were equal within e.s.d, further confirming the absence of side reactions. However, due to the solubility challenge and the colourless nature of both the NBoc-PhPNP ligand and the *fac*-[Re(NBoc-PhPNP)$(CO)_3$Br] complex, UV/Vis studies were inconclusive.

Nevertheless, although limited data was available, acceptable rate laws were identified and proposed, the most acceptable consisting of a rapid pre-equilibrium followed by a rate-determining ring-closure by the PNP ligand.

The bromido ligand substitution studies from *fac*-[Re(NBoc-PhPNP)$(CO)_3$Br] were also preliminarily conducted both by the UV/Vis and ^{31}P NMR techniques using PTA, pyridine and NCS^- as the entering ligands. From these studies it was with the current data in hand, concluded that none of the entering ligands could displace the bromido ion in the *fac*-[Re(NBoc-PhPNP)$(CO)_3$Br].

This was an interesting observation from a radiopharmaceutical perspective. Firstly, this further confirms the stability that the PNP system brings to the rhenium tricarbonyl core. Secondly,

these results suggest that if one was to inject these complexes into a biological system, any information obtained can be attributed to the complex itself or the periphery of the coordinated ligand and not to metabolized secondary compounds. However, clearly further investigations are needed to confirm this phenomenon.

In addition, it is also evident that chemical modification on the periphery of the PNP ligand with organic groups such as carboxylic acids, amines and sugar moieties can improve the overall solubility of the complex. This was confirmed by the difference in solubility between all the other ligands synthesized in this study and the NBoc-PhPNP ligand which has a protected amine on its periphery. The idea behind this new PNP ligand system is illustrated in **Figure 8.6** whereby after removal of the protection group (step III), further functionalization can occur on the terminal end of the PNP ligand.

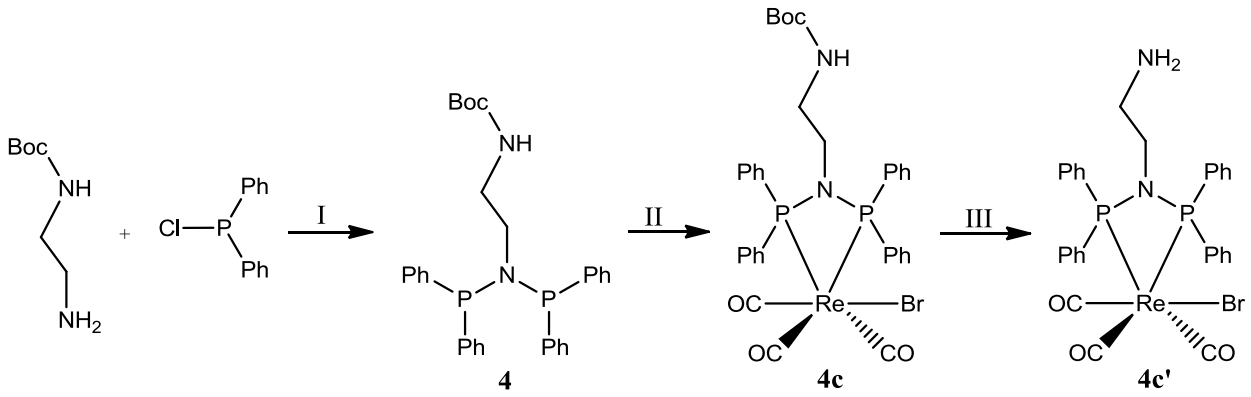

Figure 8.6 Schematic representation of the synthesis of the NBoc-PhPNP ligand (**4**) and its complexation to a fac-tricarbonyl rhenium moiety. Molecular numbering is reminiscent of that found in **Chapter 3**, except the "c" symbol which is meant to indicate a Re-PNP complex.

In conclusion, these preliminary results bring some interesting perspectives which should be further investigated thoroughly. Particularly, the stability and solubility of the new ligand system further proves the versatile nature of these phosphine ligand systems. The results from this study will thus contribute significantly towards the synthesis of water soluble diphosphinoamine ligands, to be further used as potential ligands in model radiopharmaceutical agents.

9 Preliminary biological evaluations

What to expect!

A preliminary anti-mitochondrial cytotoxicity evaluations of selected non-coordinated and rhenium metal coordinated diphosphinoamine (PNP) compounds synthesized in this study.

9.1 Introduction

Preliminary investigations were conducted on the potential growth inhibitor effect of selected PNP ligands, as well as their *fac*-[Re(PNP)$(CO)_3$Br] compounds synthesized in this study. Should they display significant *chemo*cytotoxic effects, larger concentrations when utilizing them in radiopharmacy may prove problematic, particularly in a carrier-added formulation where borderline concentrations are required.

Smaller *chemo*cytotoxicity will however render their concentrations in radiopharmaceutical studies less significant, and thus only the *radio*cytotoxicity delivered by the predesigned radioactive-PNP complex will be of prime importance. This is particularly relevant when one's interests lies on evaluating only the radiotoxic effects of certain compounds. The biological evaluation methodology using yeast organisms, as developed by Kock and co-workers,[1] was employed in this study and is also reported herein.

Yeasts are eukaryotic single-celled organisms widely used, not only in industry for food and beverage production, but also as model organisms to study, for example, ageing in humans (Bitterman *et al*., 2003).[2] In 2009, Kock and co-workers[1] developed a bio-assay where visual changes in indicator yeast color can be used as a rapid upstream screening method to determine if specific compounds have antifungal, anti-cancer and anti-malarial activity (collectively

[1] Kock, J. L. F., Swart, C. W., Ncango, D. M., Kock, J. L. F. (Jr), Munnik, I. A., Maartens, M. M. J., Pohl, C. H., Van Wyk, P. W. J., *Curr. Drug Discov. Technol*, **2009**, *6*, 186-191.

[2] Bitterman, K. J., Medvedik, O., Sinclair, D. A., *Microbiol. Mol. Biol. Rev*, ***2003***,*67*, 376- 399.

referred to as anti-mitochondrial activity). Compounds such as some non-steroidal anti-inflammatory (NSAID's) drugs, anti-malarial, antifungal and anti-cancer drugs inhibit sexual spore (biosensor) formation by cutting off the power supply (mitochondria) of the cell and can therefore be regarded as anti-mitochondrial. This forms the basis of this biological evaluation, where a positive hit using the bio-assay will cause the inhibition of sexual spore development leading to a visual color change in the indicator organism.

Below, we present a preliminary anti-mitochondrial cytotoxicity evaluations of four PNP ligands namely *p*Tol-PhPNP (**1**)[3], *p*ClPh-PhPNP (**2**)[3], *p*FPh-PhPNP (**3**)[3] Chzyl-4-*p*-tolyl (**8**)[3] and their respective *fac*-[Re-(PNP)$(CO)_3$Br] complexes (see **Figure 9.1**) presented in this study to further expand on this subject.

The first three ligands {*p*Tol-PhPNP (**1**), *p*ClPh-PhPNP (**2**), *p*FPh-PhPNP (**3**)} and their respective Re-tricarbonyl complexes were selected based on their subtle but systematically varied electronic properties on the nitrogen atom, whereas the last ligand Chzyl-4-*p*-tolyl (**8**) and its respective Re-tricarbonyl complex were chosen based on its distinct steric properties. The following paragraph will present in detail the experimental procedures used to carry out these evaluations.

[3] See Chapter **3**, **4** and **7** of this PhD thesis.

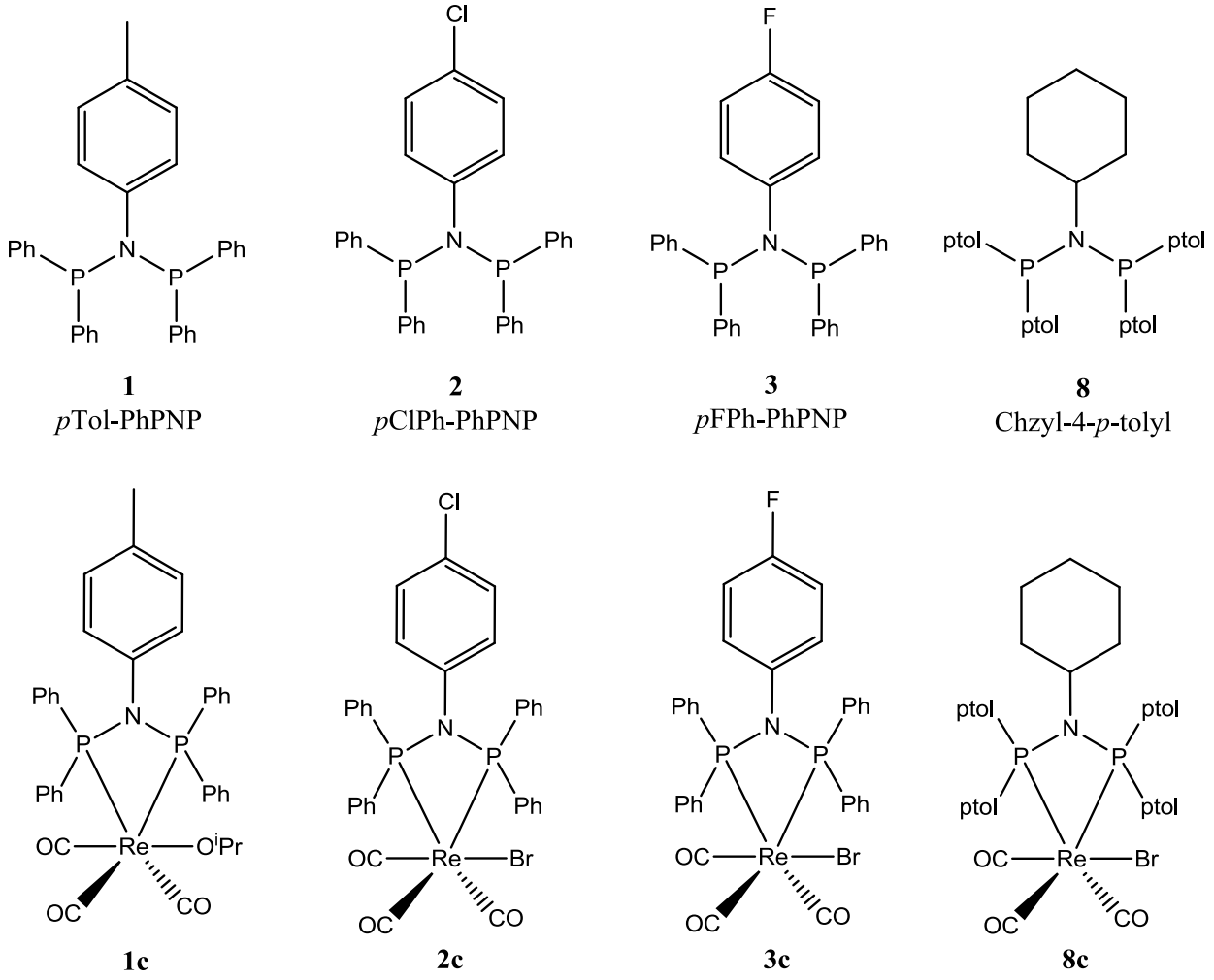

Figure 9.1 Selected PNP ligands and their respective Re-tricarbonyl complexes utilized on preliminary biological evaluations conducted in this study. *p*Tol-PhPNP (**1**), *p*ClPh-PhPNP (**2**), *p*FPh-PhPNP (**3**), Chzyl-4-*p*-tolyl (**8**), *fac*-[Re(*p*Tol-PhPNP)$(CO)_3(O^iPr)$] (**1c**), *fac*-[Re(*p*ClPh-PhPNP)$(CO)_3Br$] (**2c**), *fac*-[Re(*p*FPh-PhPNP)$(CO)_3Br$] (**3c**), *fac*-[Re(Chzyl-4-*p*-tolyl)$(CO)_3Br$] (**8c**).

9.2 Experimental

9.2.1 Biological evaluation

To obtain significant growth, *Eremothecium ashbyii* (UOFS-1122) and *Nadsonia fulvescens* (UOFS-0705), obtained from the yeast culture collection (stored at the University of the Free State, Department of Microbial, Biochemical and Food Biotechnology),[1] were streaked out on yeast malt (YM) agar plates and incubated for 48 hours at 25 ºC. The cultures were then scraped from the plates and suspended in 5 mL sterilized distilled water. From these suspensions, 100µL aliquots of *Eremothecium ashbyii* and *Nadsonia fulvescens* were placed on separate YM agar

plates and spread across the plate to form a homogenous lawn. A 0.5 mg sample of each of the eight compounds tested {*p*Tol-PhPNP (**1**), *p*ClPh-PhPNP (**2**), *p*FPh-PhPNP (**3**), Chzyl-4-*p*-tolyl (**8**), *fac*-[Re(*p*Tol-PhPNP)$(CO)_3(O^iPr)$] (**1c**), *fac*-[Re(*p*ClPh-PhPNP)$(CO)_3$Br] (**2c**), *fac*-[Re(*p*FPh-PhPNP)$(CO)_3$Br] (**3c**), *fac*-[Re(Chzyl-4-*p*-tolyl)$(CO)_3$Br] (**8c**)} were then placed in the middle of these agar plates and incubated at 25 ºC for 48 hours. The compounds will diffuse throughout the agar plate causing a high concentration near the middle of the plate with a decrease in concentration towards the border of the plate. In addition, two control plates, each containing only the cells of *Eremothecium ashbyii* and *Nadsonia fulvescens* respectively, were assembled for comparison purposes.

9.2.2 Results interpretation

A compound is considered positive for anti-mitochondrial activity if two distinct zones are observed on its experimental plate, *i.e.*:

- A white zone where only asexual growth can be observed (anti-mitochondrial inhibition caused inhibition of sexual structure formation).
- A yellow (*Eremothecium ashbyii*) or brown (*Nadsonia fulvescens*) zone near the border of the plate, where asexual and sexual growth took place.

The concentration of the compound is low near the border of the plate and as a result does not inhibit growth or sexual structure formation.[1] At the center of the plate, the compound's concentration is very high and thus if biologically active it can cause an inhibition zone where no growth occurs. The eight compounds shown in **Figure 9.1** were compared to *cis*-diamminedichloridoplatinum(II) (*cis*-platin), a well-known chemotherapeutic drug against different cancer cell lines,[4,5,6] which in principle should show limited anti-mitochondrial activity.

[4] Agudo-Lopez, A., Prieto-Garcia, E., Aleman, J., Perez, C., Diaz-Garcia, C. V., Parrilla-Rubio, L., Cabrera, S., Navarro-Ranninger, C., Cortes-Funes, H., Lopez-Martin, J. A., Agullo-Ortuno, M. T., *Molecular Cancer*. **2017,** *16*, 45.

[5] Sacht, C., Datt, M. S., Otto, S., Roodt, A., *J. Chem. Soc. Dalton Trans.* **2000**, 4579-4586.

[6] Sacht, C.; Datt, M. S.; Otto, S.; Roodt, A., *J. Chem. Soc. Dalton Trans.* **2000**, 727-733.

9.3 Results and Discussion

Upon analyzing the results obtained when *Eremothecium ashbyii* as indicator organism (**Figure 9.2** image 'A to C') was used, none of the eight compounds tested displayed a positive anti-mitochondrial activity except for cisplatin which was utilized for comparison purposes. This observation was concluded based on the lack of a white zone at the center of the representative experimental plate A (**Figure 9.2** image 'A'). This can be further supplemented by comparing Plate A to the control plate B (**Figure 9.2** image 'B') that does not contain any added compounds. A similar yellow color can be observed in both the test plate A and the control plate B. However, when comparing the intensity of the yellow color between these two plates, one can deduce that the compounds might actually be pro-mitochondrial, and thus stimulating the production of more sexual structures (hence a more intense yellow color is observed in plate A as compared to the control plate B). However, further investigations are needed to confirm this phenomenon. As anticipated, cisplatin caused a large inhibition zone (**Figure 9.2** image 'C') at the center of the plate, followed by a fading white zone in the direction away from the high compound concentration zone. At low concentration by the periphery of plate C, a yellow zone was formed. This shows that cisplatin does exhibit strong antifungal (owing to the large inhibition zone formed) and anti-mitochondrial activity.

From the results obtained when *Nadsonia fulvescens* as indicator organism (**Figure 9.2** image 'D to F') was used, only cisplatin (**Figure 9.2** image 'D') and the *p*Tol-PhPNP^3 (**1**) ligand (**Figure 9.2** image 'E') tested positive for anti-mitochondrial activity, with cisplatin exhibiting the largest activity. Cisplatin caused a large inhibition zone close to the center of the plate where the concentration of the compound was high, followed by a white zone, which is indicative of the antifungal and anti-mitochondrial (anti-cancer) property of this compound. Interestingly, the *p*Tol-PhPNP3 (**1**) ligand displayed no inhibition zone, but did cause significant white zones indicating anti-mitochondrial activity. The control plate (**Figure 9.2** image 'F') which does not contain any compound, displayed an intense brown color when compared to the plate D and E. Interestingly, cisplatin seemed to have a pro-mitochondrial effect at a certain concentration. This is indicated by the brown ring surrounding the inhibition zone at the centre of the plate. Nevertheless, white growth continues after the brown ring. This is an unexpected phenomenon

and it should definitely be further investigated given that cisplatin is a well-known chemotherapeutic drug.

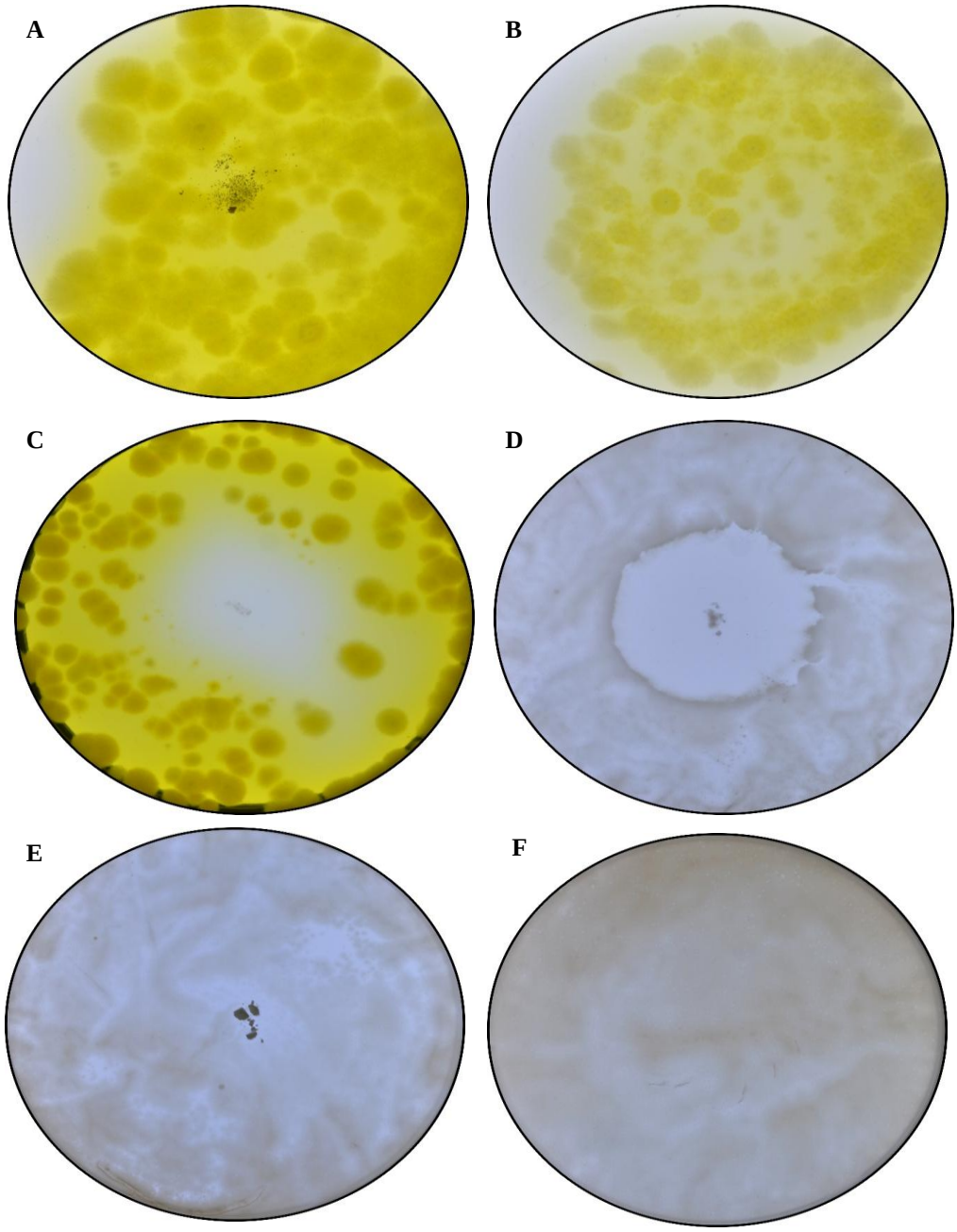

Figure 9.2: Determination of anti-mitochondrial activity using a yeast bio-assay with *Eremothecium ashbyii* and *Nadsonia fulvescens* as indicator organisms. (**A**) Representative plate of the compounds tested using *Eremothecium ashbyii*. (**B**) Control plate containing no compounds, only yeast cells of *Eremothecium ashbyii*. (**C**) Cisplatin using *Eremothecium ashbyii* as indicator organism. (**D**) Cisplatin using *Nadsonia fulvescens* as indicator organism. **E**) ***p*Tol-PhPNP3** (**1**) using *Nadsonia fulvescens* as indicator organism. (**F**) Control plate containing only cells of *Nadsonia fulvescens*.

9.4 Conclusion

Anti-mitochondrial and antifungal activities of four PNP ligands and four *fac*-[Re-PNP] tricarbonyl complexes were investigated. With the exception of *p*Tol-PhPNP (**1**)**,** none of the tested compounds displayed any cytotoxicity to the *Eremothecium ashbyii* and *Nadsonia fulvescens* yeast cells used. Cisplatin was investigated for comparison purposes and displayed the highest inhibition on both yeast cells.

Interesting phenomenona were observed in some experiments. The first one is that the investigated compounds (except cisplatin) might in actual fact be pro-mitochondrial to the *Eremothecium ashbyii* cells. The second one is that cisplatin seemed to have a pro-mitochondrial effect on *Nadsonia fulvescens* yeast cells at a specific concentration. However, further investigation will be carried out in the near future to confirm these two unexpected results.

From these preliminary biological evaluations, it is clear that these compounds may not display any anti-mitochondrial activity. Further quantitative evaluations will be carried out in the near future to additionally supplement these findings. Anti-mitochondrial evaluations of the remaining compounds are still being conducted and all the compounds will be further evaluated on selected cell lines in the near future.

In final conclusion, diphosphinoamine ligand system presented in this study, seems to present themselves as excellent models in radiopharmaceutical studies, particularly studies where the interests are only in evaluating the *radiotoxic effects* of radio-isotopes such as $^{99/99m}$Tc and $^{186/188}$Re.

10 Evaluation and Future research

What to expect!

A brief discussion on the relevant success of this PhD study with respect to the aims and objectives stated in Chapter 1, followed by a proposal of potential future research will be described in this chapter.

10.1 Evaluation of the study

The first overarching aim of this study was to synthesize systematically altered diphosphinoamine (PNP) ligands and evaluate crystallographically their spatial arrangements. This was successfully achieved and as a result paved a way for the successful synthesis and characterization of various aminediphosphineoxide (PNPO) ligands presented in **Chapter 3** and **5**. A significant potential problem with applying these ligands in water systems is the lack of solubility. Thus, further manipulations of this ligand system resulted in the successful synthesis of a promising water-soluble ligand NBoc-PhPNP (**4**)[1] that contains a protected amine which can be de-protected, at a later stage, to increase the water solubility. A challenge encountered for these systems was the *unsuccessful* attempts of coordinating the PNPO ligands to various metal centers such as rhenium, niobium or tantalum metal precursors. The second challenge was encountered upon product isolation of a reaction whereby *gamma*-Aminobutyric acid was used in an attempt to synthesize a PNP ligand containing a protected carboxylic acid on its periphery similar to the NBoc-PhPNP (**4**)[1] ligand. A feasible solution to the above challenges has not yet been obtained but further attempts are still ongoing.

From the above achievements with respect to ligand design, the project's focus was then shifted towards the synthesis of model radiopharmaceutical agents utilizing the *fac*-$[M^{I}(CO)_3]^+$ (M = Re or ^{99}Tc] cores. The primary aim of this follow-up section was to first evaluate the coordinating

[1] See **Chapter 3** and C**hapter 7** of this PhD study.

ability of various PNP ligands to *fac*-$[Re(CO)_3]^+$. This was successfully achieved with the characterization of various Re-PNP complexes as illustrated in Chapter **3**, **6** and **7**. To conclude this section, two *fac*-$[^{99}Tc(CO)_3(PNP)Cl]$ complexes were in addition successfully synthesized utilizing the Cbutyl-4-*p*-tolyl (**7**) (see **Chapter 3**) and Chzyl-4-*p*-tolyl (**8**)[1] PNP ligands. Valuable information in terms of structural geometry were obtained when the Re and ^{99}Tc homologous complexes bearing the Chzyl-4-*p*-tolyl (**8**) PNP ligand were crystallographically compared. These two structures were in fact found to be isostructural further confirming why the two metal (Re^I/Tc^I) centers are often described as a *matched* pair. Unfortunately, coordination of these PNP ligands to the ^{99m}Tc metal center was not successful due to the lack of aqueous solubility of these ligands. However, these challenge lead to the ongoing investigations of water soluble promising ligands such as the NBoc-PhPNP (**4**)[1] PNP ligand.

Reactivity and solubility studies of these ligands and their respective rhenium complexes (i.e. *fac*-$[Re(CO)_3(PNP)Br]$) were also conducted. ^{31}P NMR evaluations in terms of the complex formation proved that the reaction proceeded successfully without any significant side reactions. This is particularly important in radiopharmaceuticals where > 98 % final product purity is a critical requirement. Although limited data was available for this section, acceptable rate laws were identified and proposed, with the most feasible with current data in hand consisting of a rapid pre-equilibrium followed by a rate-determining ring-closure by the PNP ligand. Moreover, preliminary substitution reactions of the bromido ligand in *fac*-$[Re(CO)_3(PNP)Br]$ complexes with entering ligands such as PTA, pyridine and SCN^- ions proved that none of the entering ligands could displace the bromido ion, further proving the stability that these PNP ligand systems brings to the rhenium tricarbonyl core.

To conclude the PhD study, preliminary anti-mitochondrial activity of selected non-coordinated PNP ligands, as well as the corresponding *fac*-$[Re(CO)_3(PNP)Br]$ complexes were tested on *Eremothecium ashbyii* and *Nadsonia fulvescens* yeast cells. This was done to ensure that when the actual radiolabeled complexes are prepared, that only *radio-cytotoxicity* is evaluated. With the exception of *p*Tol-PhPNP (**1**) (see **Chapter 3**), none of the tested free PNP ligands and rhenium complexes displayed any cytotoxicity towards the *Eremothecium ashbyii* and *Nadsonia fulvescens* yeast cells. In fact, with the data in hand, it suggests that both the free and the rhenium

coordinated PNP compounds might actually be pro-mitochondrial. However, further biological investigations will be conducted in the near future to confirm this interesting phenomenon.
Overall, the aims and objectives of this research project have been well attained and resulted in many interesting features which require additional exploration.

10.2 Future research

In terms of structural investigations, the next step is to synthesize a *fac*-[^{99}Tc(CO)$_3$(NBoc-PhPNP)Cl] complex. The follow-up experiment thereafter would then be to de-protect the amine and conduct thorough biological, solubility and kinetic evaluations on both the Re and the ^{99}Tc-NBoc-PhPNP complexes. If successful, further research can be directed into synthesizing the model radionuclide agents utilizing $^{188/186}$Re and ^{99m}Tc metal centers.

A detail formation and substitution kinetic study should be expanded by investigating additional *fac*-[Re(CO)$_3$(PNP)Br] complexes and other possible entering ligands. To increase the substitution ability, the bromido ligand in *fac*-[Re(CO)$_3$(PNP)Br] should be replaced by a more labile leaving group such as H_2O or any other good leaving solvento species. This will provide further valuable information needed not only for *in vivo* and *in vitro* evaluations but also for cases were a [2+1] labeling approach is of valuable interest. Moreover, this will also potentially increase the water solubility of the complexes.

One more future work would be to fully investigate the potential application of diphosphinoamineoxide ligands in the field of f-block elements (lanthanides and actinides) photoluminescence and liquid-liquid extraction studies. Extensive studies will also be directed towards possible application of these diphosphinoamineoxide ligands on the separation of niobium and tantalum.

A definite aim in future is to synthesize more water soluble promising PNP ligands using amine precursors such as *gamma*-aminobutyric acid. The first step would be to protect these water soluble functional groups to limit the possibility of other side reactions. The second step would be to de-protect these functional groups and add other water soluble groups such as sugar moieties in cases were further manipulations are possible.

Since the phosphorus fraction of the PNP ligand geometrically provides the biggest part of the molecule, typical PNP ligands that may yield interesting results in future will include water soluble phosphorus fractions such as the derivatives of PTA, tris(2-carboxyethyl)phosphine hydrochloride (TCEP) and tris(3-sulfonatophenyl)phosphine (TPPTS). Thus, another future goal is to synthesize water soluble PNP ligands by manipulating the phosphorus fraction of the PNP ligand systematically.

As soon as the above mentioned goals are met, a number of projects can be pursued. The first one will be the synthesis of model radiopharmaceutical agents utilizing the *fac*-$[M^{I}(CO)_3(H_2O)_3]^+$ (M = Re or ^{99}Tc] cores. This will enable the design of better water soluble agents that can be translated to relevant radiopharmaceutical agents utilizing ^{188}Re and ^{99m}Tc metal centers. A follow-up step from thereon will be to proceed with thorough kinetic evaluations particularly in media which are closer to *in vivo* conditions to better capture the pharmacokinetic profiles of these model agents.

Finally, effects of these ligand systems on the chemistry of neighboring elements such as the platinum group metals particularly in the field of catalysis should also be pursued. Although the uses of PNP ligands in catalytic reactions such as ethylene tri- and tetramerization is well-known in literature, to the best of knowledge very few ligand systems utilized were water soluble. Thus, this may yield interesting results in future if one can modify catalysts in such a way as to make the entire complex water soluble. Similarly, a follow-up investigation on utilizing the PNP-phosphineoxide ligands on *early* transition metal modalities (V and Ti-triads), should also be pursued in more depth.

Summary

The research project presents the synthesis and evaluation of the radiopharmaceutical model type of *fac*-$[M^{I}(CO)_3]^+$ (M = Re or ^{99}Tc] cores bearing neutral bidentate diphosphinoamine (PNP) ligands. A range of PNP ligands and *fac*-$[M(CO)_3(PNP)]^+$ (M = Re or ^{99}Tc) complexes were prepared using methods described in literature and characterized by means of NMR, IR and X-ray crystallography. These ligands were systematically altered in terms of electronic and steric properties. A total of sixteen ligands were evaluated during this study, namely *N*,*N*-Bis-(di-phenylphosphino)-*p*-toluidine (**1**), *N*,*N*-Bis(diphenylphosphino)-4-chloroaniline (**2**), *N*,*N*-Bis(diphenyl-phosphino)-4-fluoroaniline (**3**), *N*,*N*-Bis(diphenylphosphino)-*N*-Boc-ethylenediamine (**4**), *N*,*N*-Bis(di-*p*-tolylphosphino)-*p*-toluidine (**5**), *N*,*N*-Bis(di-*p*-tolylphosphino)-*o*-toluidine (**6**), *N*,*N*-Bis(di-*p*-tolyl-phosphino)cyclobutylamine (**7**), *N*,*N*-Bis(di-*p*-tolylphosphino)cyclohexylamine (**8**), *N*,*N*-Bis(diphenyl-phosphineoxide)-*p*-toluidine (**1a**), *N*,*N*-Bis(diphenylphosphineoxide)-4-chloroaniline (**2a**), *N*,*N*-Bis(di-phenylphosphineoxide)-4-fluoroaniline (**3a**), *N*,*N*-Bis(diphenylphosphineoxide)-*N*-Boc-ethylene-diamine (**4a**), *N*,*N*-Bis(di-*p*-tolylphosphineoxide)-*p*-toluidine (**5a**), *N*,*N*-Bis(di-*p*-tolylphosphineoxide)-*o*-toluidine (**6a**), *N*,*N*-Bis(di-*p*-tolylphosphineoxide)cyclobutylamine (**7a**) and *N*,*N*-Bis(di-*p*-tolylphosphine-oxide)cyclohexylamine (**8a**).

The solid state crystal structures of the ligands *p*FPh-PhPNP (**3**), Cbutyl-4-*p*-tolyl (**7**), Chzyl-4-*p*-tolyl (**8**), *p*FPh-PhPNPO (**3a**), 5-*p*-tolyl-PNPO (**5a**) and Chzyl-4-*p*-tolyl-PNPO (**8a**) were reported and described, and revealed various interesting structural conformations. The reported X-ray crystallographic structure determinations further included six rhenium(I) and one technetium-99(I) tricarbonyl complexes namely: *fac*-[Re(*p*Tol-PhPNP)$(CO)_3(O^{i}Pr)$] (**1c**), *fac*-[Re(*p*ClPh-PhPNP)$(CO)_3$Br] (**2c**), *fac*-[Re(*p*FPh-PhPNP)$(CO)_3$Br] (**3c**), *fac*-[Re(NBoc-PhPNP)$(CO)_3$Br] (**4c**), *fac*-[Re(Cbutyl-4-p-tolyl)$(CO)_3$Br] (**7c**), *fac*-[Re(Chzyl-4-*p*-tolyl)$(CO)_3$Br] (**8c**) and *fac*-[^{99}Tc(Chzyl-4-*p*-tolyl)$(CO)_3$Cl] (**8d**) respectively. Four of the reported solid-state rhenium complex structures showed a statistical disorder of the bromido ligand on the apical Br-Re-CO axes.

Summary

A kinetic study of the formation of *fac*-[Re(NBoc-PhPNP)$(CO)_3$Br] was conducted utilizing ^{31}P time-resolved NMR. Experimental evidence indicated that the reaction proceeded towards product formation without any significant side reactions. Although limited data was available for this section, acceptable rate laws were identified and proposed, the most feasible consisting of a rapid pre-equilibrium followed by a rate-determining ring-closure by the PNP ligand (K_1 = 58(16) M^{-1}, k_2 = 0.0013(1) s^{-1}). Preliminary substitution reactions of the bromido ligand in *fac*-[Re$(CO)_3$(PNP)Br] complexes with entering ligands such as PTA, pyridine and SCN^- ions were conducted and the results illustrated that none of the entering ligands could displace the bromine ligand.

Preliminary anti-mitochondrial activity of selected non-coordinated PNP ligand namely *p*Tol-PhPNP (**1**), *p*ClPh-PhPNP (**2**), *p*FPh-PhPNP (**3**) Chzyl-4-*p*-tolyl (**8**) and their respective *fac*-[Re$(CO)_3$(PNP)Br] complexes were tested on *Eremothecium ashbyii* and *Nadsonia fulvescens* yeast cells. With the exception of *p*Tol-PhPNP (**1**), none of the compounds evaluated displayed any cytotoxicity towards the *Eremothecium ashbyii* and *Nadsonia fulvescens* yeast cells.

Keywords: Radiopharmaceutical models, Rhenium, Technetium, Diphosphinoamine, anti-Mitochondrial, Tricarbonyl complexes, Formation, Substitution, Phosphine oxide, X-ray crystallography.

Opsomming

Die navorsingsprojek bied die sintese en evaluasie van die radiofaramaseutiese model tipes met *fas*-$[M^{I}(CO)_3]^+$ (M = Re of ^{99}Tc] kerne draende neutrale difosfinoamien (PNP) ligande aan. ’n Reeks PNP ligande en *fas*-$[M(CO)_3(PNP)]^+$ (M = Re of ^{99}Tc) komplekse is voorberei volgens metodes soos in die literatuur beskryf, en is gekarakteriseer deur middel van KMR, IR, en X-straal kristallografie. Hierdie ligande is sistematies verander ten opsigte van elektroniese en steriese eienskappe. ’n Totaal van sestien ligande naamlik *N*,*N*-bis-(di-fenielfosfino)-*p*-toluïdien (**1**), *N*,*N*-bis(difenielfosfino)-4-chloroanilien (**2**), *N*,*N*-bis(difeniel-fosfino)-4-fluoroanilien (**3**), *N*,*N*-bis(difenielfosfino)-*N*-boc-etileendiamien (**4**), *N*,*N*-bis(di-*p*-tolielfosfino)-*p*-toluïdien (**5**), *N*,*N*-bis(di-*p*-tolielfosfino)-*o*-toluïdien (**6**), *N*,*N*-bis(di-*p*-toliel-fosfino)siklobutielamien (**7**), *N*,*N*-bis(di-*p*-tolielfosfino)sikloheksielamien (**8**), *N*,*N*-bis(difeniel-fosfienoksied)-*p*-toluïdien (**1a**), *N*,*N*-bis(difenielfosfienoksied)-4-chloroaniline (**2a**), *N*,*N*-bis(di-fenielfosfienoksied)-4-fluoro-aniline (**3a**), *N*,*N*-bis(difenielfosfienoksied)-*N*-boc-etileendiamien (**4a**), *N*,*N*-bis(di-*p*-tolielfosfienoksied)-*p*-toluïdien (**5a**), *N*,*N*-bis(di-*p*-tolielfosfienoksied)-*o*-toluïdien (**6a**), *N*,*N*-bis(di-*p*-tolielfosfienoksied)siklobutielamien (**7a**), en *N*,*N*-bis(di-*p*-tolielfosfienoksied)siklo-heksielamien (**8a**) is gedurende hierdie studie geëvalueer.

Die vaste toestand kristalstrukture van die ligande *p*FPh-PhPNP (**3**), Cbutiel-4-*p*-toliel (**7**), Chzyl-4-*p*-toliel (**8**), *p*FPh-PhPNPO (**3a**), 5-*p*-toliel-PNPO (**5a**) en Chzyl-4-*p*-toliel-PNPO (**8a**) is gerapporteer en beskryf, en verskeie interessante strukturele konformasies is onthul. Die gerapporteerde X-straal kristallografiese struktuurbepalings het verder ses renium(I) en een tegnesium-99(I) trikarboniel komplekse ingesluit naamlik: *fas*-[Re(*p*Tol-PhPNP)$(CO)_3(O^{i}Pr)$] (**1c**), *fas*-[Re(*p*ClPh-PhPNP)$(CO)_3$Br] (**2c**), *fas*-[Re(*p*FPh-PhPNP)$(CO)_3$Br] (**3c**), *fas*-[Re(NBoc-PhPNP)$(CO)_3$Br] (**4c**), *fas*-[Re(Cbutiel-4-p-toliel)$(CO)_3$Br] (**7c**), *fas*-[Re(Chziel-4-*p*-toliel)$(CO)_3$Br] (**8c**), en *fas*-[^{99}Tc(Chziel-4-*p*-toliel)$(CO)_3$Cl] (**8d**). Vier van die gerapporteerde vaste toestand renium kompleks strukture het ’n statistiese wanorde van die bromido ligand op die apikale Br-Re-CO as vertoon.

Opsomming

'n Kinetiese studie van die vorming van *fas*-[Re(NBoc-PhPNP)$(CO)_3$Br] is uitgevoer deur ^{31}P tydgeskeide KMR te benut. Eksperimentele bewyse dui daarop dat die reaksie voortgaan na produkvorming sonder enige beduidende newereaksies. Ten spyte daarvan dat beperkte data vir hierdie afdeling beskikbaar was is aanvaarbare tempowette geïdentifiseer en voorgestel waarvan die mees waarskynlike bestaan uit 'n vinnige pre-ekwilibrium gevolg deur 'n tempobepalende ringsluitings deur die PNP ligand (K_1 = 58(16) M^{-1}, k_2 = 0.0013(1) s^{-1}). Voorlopige substitusiereaksies van die bromido ligand in *fas*-[Re$(CO)_3$(PNP)Br] komplekse met inkomende ligande soos PTA, piridien en SCN^- ione is uitgevoer en die resultate illustreer dat geen van die inkomende ligande die broom ligand kon verplaas nie.

Voorlopige antimitokondriale aktiwiteit van uitgesoekte ongekoördineerde PNP ligande naamlik *p*Tol-PhPNP (**1**), *p*ClPh-PhPNP (**2**), *p*FPh-PhPNP (**3**), en chziel-4-*p*-toliel (**8**), asook hulle onderskeie *fas*-[Re$(CO)_3$(PNP)Br] komplekse is op *Eremothecium ashbyii* en *Nadsonia fulvescens* gisselle getoets. Met die uitsondering van *p*Tol-PhPNP (**1**) toon geen van die geëvalueerde stowwe enige sitotoksisiteit teenoor die *Eremothecium ashbyii* en *Nadsonia fulvescens* gisselle nie.

Sleutelwoorde: Radiofarmaseutiese modelle, Renium, Tegnesium, Difosfinoamien, Antimitokondriaal, Trikarboniel komplekse, Vorming, Substitusie, Fosfienoksied, X-straal kristallografie.

Appendix

Supplementary Data

A. Crystal data of *N,N*-Bis(diphenylphosphino)-4-fluoroaniline

Table A.1 Fractional Atomic Coordinates ($\times 10^4$) and Equivalent Isotropic Displacement Parameters ($Å^2 \times 10^3$) for *p*FPh-PhPNP. U_{eq} is defined as 1/3 of of the trace of the orthogonalised U_{IJ} tensor.

Atom	*x*	*y*	*z*	U(eq)
C1	-70.0(13)	3111.1(10)	2331.9(7)	13.2(3)
C2	483.5(14)	3957.9(10)	2115.1(8)	17.0(3)
C3	151.8(15)	4307.1(10)	1352.8(8)	19.4(3)
C4	-733.6(15)	3793.1(11)	823.1(8)	19.2(3)
C5	-1312.3(15)	2958.5(10)	1013.6(8)	19.5(3)
C6	-981.0(14)	2620.4(10)	1780.9(8)	17.4(3)
C11	2545.7(13)	1753.5(10)	2760.0(8)	14.3(3)
C12	3851.9(14)	1706.3(10)	3173.4(8)	15.9(3)
C13	4933.9(14)	1618.3(11)	2783.2(9)	20.1(3)
C14	4722.5(15)	1589.7(11)	1969.6(9)	23.2(3)
C15	3436.8(16)	1646.5(12)	1548.3(9)	25.3(3)
C16	2351.0(15)	1725.0(11)	1936.6(8)	20.9(3)
C21	197.7(13)	749.8(10)	2960.5(8)	14.5(3)
C22	750.3(15)	-34.9(11)	2636.1(9)	22.0(3)
C23	17.0(17)	-867.4(11)	2453.7(10)	26.5(3)
C24	-1282.7(16)	-928.6(11)	2589.2(9)	23.2(3)
C25	-1849.4(15)	-154.3(11)	2910.4(8)	21.3(3)
C26	-1116.5(14)	674.1(10)	3099.9(8)	18.0(3)
C31	-914.0(14)	2661.6(11)	4458.1(8)	17.3(3)
C32	-2307.5(15)	2662.2(13)	4377.9(8)	24.9(3)
C33	-2956.2(17)	1989.1(15)	4770.4(10)	34.1(4)
C34	-2222.5(18)	1312.1(14)	5245(1)	34.7(4)
C35	-837.2(17)	1316.5(12)	5347.0(9)	27.4(3)
C36	-186.6(15)	1991.1(11)	4960.7(8)	19.9(3)
C41	1396.8(14)	3786(1)	4479.1(8)	15.8(3)
C42	1340.7(16)	4159.5(10)	5226.8(8)	19.3(3)
C43	2496.4(17)	4449.2(11)	5719.6(9)	25.3(3)
C44	3723.0(17)	4363.5(11)	5480.3(9)	27.2(4)
C45	3793.1(16)	4011.8(11)	4737.6(10)	25.9(3)
C46	2633.7(15)	3735.3(10)	4236.6(8)	19.6(3)
N1	290.4(11)	2764.5(8)	3125.0(6)	13.6(2)
F1	-1049.4(10)	4126.1(7)	72.2(5)	29.8(2)
P1	1243.8(3)	1753.7(2)	3377.2(2)	12.96(9)
P2	-176.1(3)	3500.1(3)	3836.6(2)	14.62(9)

Table A.2 Anisotropic Displacement Parameters ($Å^2 \times 10^3$) for *p*FPh-PhPNP. The Anisotropic displacement factor exponent takes the form: $-2\pi^2[h^2a^{*2}U_{11}+...+2hka\times b\times U_{12}]$

Atom	U_{11}	U_{22}	U_{33}	U_{23}	U_{13}	U_{12}
C1	13.1(6)	15.9(6)	10.8(6)	0.0(5)	2.6(5)	2.8(5)
C2	17.9(7)	18.7(7)	14.8(6)	-2.2(5)	3.9(5)	-2.7(5)
C3	25.6(7)	17.3(7)	17.5(6)	1.7(5)	9.7(6)	-0.3(6)
C4	26.9(8)	20.4(7)	10.5(6)	1.5(5)	3.9(5)	7.9(6)
C5	22.3(7)	18.9(7)	15.0(6)	-2.3(5)	-3.1(5)	2.4(6)
C6	18.8(7)	15.1(6)	17.4(6)	0.2(5)	-0.1(5)	-0.5(5)
C11	15.1(6)	13.7(6)	14.7(6)	1.3(5)	4.3(5)	0.5(5)
C12	16.8(6)	15.5(6)	15.2(6)	0.2(5)	2.5(5)	0.5(5)
C13	14.2(7)	20.9(7)	25.2(7)	-1.0(6)	3.6(5)	1.6(5)
C14	21.5(7)	26.1(8)	25.0(8)	-0.5(6)	12.4(6)	1.9(6)
C15	27.3(8)	34.5(9)	15.8(7)	2.4(6)	8.5(6)	4.3(7)
C16	18.7(7)	29.0(8)	14.8(6)	1.5(6)	2.6(5)	2.8(6)
C21	16.1(6)	14.7(6)	12.7(6)	2.7(5)	2.9(5)	-0.5(5)
C22	20.4(7)	18.5(7)	29.3(8)	-1.4(6)	10.4(6)	0.7(6)
C23	33.8(9)	15.6(7)	32.7(8)	-4.8(6)	13.2(7)	-0.7(6)
C24	29.6(8)	19.1(7)	20.5(7)	-0.5(6)	2.8(6)	-7.1(6)
C25	17.5(7)	25.2(8)	21.5(7)	2.6(6)	4.0(5)	-4.6(6)
C26	17.2(7)	19.3(7)	18.1(6)	0.1(5)	5.2(5)	0.4(5)
C31	17.2(7)	24.3(7)	11.1(6)	-3.6(5)	4.4(5)	-2.9(5)
C32	17.7(7)	41.7(9)	15.0(7)	-3.1(6)	2.0(5)	-2.8(6)
C33	18.5(8)	60.5(12)	24.0(8)	-4.3(8)	5.4(6)	-15.0(8)
C34	34.8(9)	46.2(11)	25.3(8)	0.0(8)	11.4(7)	-20.5(8)
C35	33.3(9)	30.6(9)	19.3(7)	2.5(6)	7.4(6)	-6.4(7)
C36	19.6(7)	26.4(8)	14.4(6)	-1.2(6)	4.5(5)	-2.8(6)
C41	20.9(7)	12.6(6)	13.7(6)	0.5(5)	1.9(5)	-2.0(5)
C42	27.2(8)	15.2(7)	15.3(6)	-0.8(5)	2.9(5)	0.9(6)
C43	40.7(9)	15.8(7)	16.7(7)	-1.1(5)	-2.9(6)	-4.1(6)
C44	30.8(8)	20.0(7)	26.6(8)	2.9(6)	-7.6(6)	-11.2(6)
C45	20.5(7)	23.8(8)	32.5(8)	3.1(6)	2.1(6)	-7.1(6)
C46	22.7(7)	17.9(7)	18.6(7)	-0.5(5)	4.6(6)	-4.3(6)
N1	16.2(5)	15.0(5)	9.6(5)	-0.3(4)	2.1(4)	1.9(4)
F1	48.7(6)	28.3(5)	11.3(4)	5.3(3)	2.4(4)	6.2(4)
P1	12.46(17)	15.50(17)	11.11(16)	1.18(12)	2.58(12)	0.50(12)
P2	15.47(18)	17.40(18)	11.10(16)	-1.33(12)	2.61(12)	1.93(13)

Table A.3 Bond Lengths for *p*FPh-PhPNP.

Atom	Atom	Length/Å	Atom	Atom	Length/Å
C1	C2	1.391(2)	C23	C24	1.382(2)
C1	C6	1.3907(19)	C24	C25	1.387(2)
C1	N1	1.4401(16)	C25	C26	1.387(2)
C2	C3	1.3908(19)	C31	C32	1.399(2)

C3	C4	1.372(2)	C31	C36	1.401(2)
C4	C5	1.373(2)	C31	P2	1.8344(15)
C4	F1	1.3637(16)	C32	C33	1.391(2)
C5	C6	1.3931(19)	C33	C34	1.385(3)
C11	C12	1.397(2)	C34	C35	1.388(3)
C11	C16	1.4022(19)	C35	C36	1.387(2)
C11	P1	1.8340(15)	C41	C42	1.4029(19)
C12	C13	1.389(2)	C41	C46	1.392(2)
C13	C14	1.385(2)	C41	P2	1.8278(15)
C14	C15	1.385(2)	C42	C43	1.388(2)
C15	C16	1.389(2)	C43	C44	1.383(3)
C21	C22	1.394(2)	C44	C45	1.387(2)
C21	C26	1.400(2)	C45	C46	1.392(2)
C21	P1	1.8338(15)	N1	P1	1.7283(13)
C22	C23	1.390(2)	N1	P2	1.7300(12)

Table A.4 Bond Angles for *p*FPh-PhPNP.

Atom	**Atom**	**Atom**	**Angle/°**	**Atom**	**Atom**	**Atom**	**Angle/°**
C2	C1	C6	119.31(12)	C32	C31	C36	118.68(14)
C2	C1	N1	119.63(12)	C32	C31	P2	116.68(11)
C6	C1	N1	121.06(12)	C36	C31	P2	124.51(11)
C1	C2	C3	120.71(13)	C33	C32	C31	120.45(16)
C4	C3	C2	118.17(13)	C34	C33	C32	120.03(16)
C3	C4	C5	123.05(13)	C33	C34	C35	120.26(16)
F1	C4	C3	118.41(13)	C36	C35	C34	119.84(16)
F1	C4	C5	118.54(13)	C35	C36	C31	120.68(14)
C4	C5	C6	118.23(13)	C42	C41	P2	118.17(11)
C1	C6	C5	120.51(13)	C46	C41	C42	118.41(13)
C12	C11	C16	118.33(13)	C46	C41	P2	123.14(11)
C12	C11	P1	114.77(10)	C43	C42	C41	120.70(15)
C16	C11	P1	126.72(11)	C44	C43	C42	120.16(15)
C13	C12	C11	121.15(13)	C43	C44	C45	119.85(14)
C14	C13	C12	119.71(14)	C44	C45	C46	120.15(15)
C15	C14	C13	120.06(14)	C41	C46	C45	120.67(14)
C14	C15	C16	120.40(14)	C1	N1	P1	123.82(9)
C15	C16	C11	120.33(14)	C1	N1	P2	114.74(9)
C22	C21	C26	118.05(13)	P1	N1	P2	121.20(7)
C22	C21	P1	121.06(11)	C21	P1	C11	101.46(6)
C26	C21	P1	119.76(10)	N1	P1	C11	106.39(6)
C23	C22	C21	121.01(14)	N1	P1	C21	105.46(7)
C24	C23	C22	120.26(15)	C41	P2	C31	100.78(7)
C23	C24	C25	119.51(14)	N1	P2	C31	102.88(6)
C24	C25	C26	120.37(14)	N1	P2	C41	104.17(6)
C25	C26	C21	120.79(14)				

Table A.5 Torsion Angles for *p*FPh-PhPNP.

A	B	C	D	Angle/°	A	B	C	D	Angle/°
C1	C2	C3	C4	0.0(2)	C31	C32	C33	C34	0.0(3)
C1	N1	P1	C11	39.21(12)	C32	C31	C36	C35	2.5(2)
C1	N1	P1	C21	-68.02(12)	C32	C31	P2	C41	147.64(12)
C1	N1	P2	C31	134.05(10)	C32	C31	P2	N1	-104.96(12)
C1	N1	P2	C41	-121.15(10)	C32	C33	C34	C35	1.6(3)
C2	C1	C6	C5	1.6(2)	C33	C34	C35	C36	-1.2(3)
C2	C1	N1	P1	-110.78(13)	C34	C35	C36	C31	-0.9(2)
C2	C1	N1	P2	63.58(15)	C36	C31	C32	C33	-2.1(2)
C2	C3	C4	C5	0.6(2)	C36	C31	P2	C41	-36.64(13)
C2	C3	C4	F1	-179.19(12)	C36	C31	P2	N1	70.76(13)
C3	C4	C5	C6	-0.1(2)	C41	C42	C43	C44	-0.6(2)
C4	C5	C6	C1	-1.1(2)	C42	C41	C46	C45	2.6(2)
C6	C1	C2	C3	-1.1(2)	C42	C41	P2	C31	-56.93(12)
C6	C1	N1	P1	70.27(16)	C42	C41	P2	N1	-163.31(11)
C6	C1	N1	P2	-115.37(13)	C42	C43	C44	C45	1.8(2)
C11	C12	C13	C14	0.9(2)	C43	C44	C45	C46	-0.7(2)
C12	C11	C16	C15	0.3(2)	C44	C45	C46	C41	-1.5(2)
C12	C11	P1	C21	-125.55(11)	C46	C41	C42	C43	-1.6(2)
C12	C11	P1	N1	124.38(10)	C46	C41	P2	C31	129.25(12)
C12	C13	C14	C15	-0.2(2)	C46	C41	P2	N1	22.87(13)
C13	C14	C15	C16	-0.5(2)	N1	C1	C2	C3	179.97(12)
C14	C15	C16	C11	0.4(2)	N1	C1	C6	C5	-179.42(12)
C16	C11	C12	C13	-1.0(2)	F1	C4	C5	C6	179.74(13)
C16	C11	P1	C21	49.44(14)	P1	C11	C12	C13	174.44(11)
C16	C11	P1	N1	-60.63(14)	P1	C11	C16	C15	-174.49(12)
C21	C22	C23	C24	0.3(2)	P1	C21	C22	C23	168.00(12)
C22	C21	C26	C25	-0.8(2)	P1	C21	C26	C25	-168.77(11)
C22	C21	P1	C11	31.54(13)	P1	N1	P2	C31	-51.43(9)
C22	C21	P1	N1	142.32(11)	P1	N1	P2	C41	53.38(9)
C22	C23	C24	C25	-0.2(2)	P2	C31	C32	C33	173.89(12)
C23	C24	C25	C26	-0.4(2)	P2	C31	C36	C35	-173.10(12)
C24	C25	C26	C21	0.9(2)	P2	C41	C42	C43	-175.68(11)
C26	C21	C22	C23	0.2(2)	P2	C41	C46	C45	176.44(12)
C26	C21	P1	C11	-160.89(11)	P2	N1	P1	C11	-134.80(8)
C26	C21	P1	N1	-50.11(12)	P2	N1	P1	C21	117.96(8)

Table A.6 Hydrogen Atom Coordinates (Å×10^4) and Isotropic Displacement Parameters (Å^2×10^3) for *p*FPh-PhPNP.

Atom	*x*	*y*	*z*	U(eq)
H16	1082	4294	2484	20
H21	520	4873	1206	23
H20	-1910	2628	640	23
H8	-1372	2062	1926	21

H12	3999	1734	3720	19
H10	5797	1579	3067	24
H30	5445	1532	1706	28
H29	3300	1632	1002	30
H28	1491	1759	1649	25
H11	1623	-1	2540	26
H32	403	-1385	2240	32
H18	-1774	-1485	2466	28
H15	-2726	-191	2999	26
H13	-1503	1185	3322	22
H25	-2804	3116	4060	30
H31	-3883	1993	4714	41
H34	-2660	853	5496	42
H33	-347	868	5674	33
H26	742	1998	5036	24
H5	520	4213	5394	23
H24	2446	4702	6212	30
H22	4499	4541	5817	33
H23	4616	3961	4574	31
H7	2686	3515	3735	24

B. Crystal data of *N*,*N*-Bis(di-*p*-tolylphosphino)cyclobutylamine

Table B.1 Fractional Atomic Coordinates ($\times 10^4$) and Equivalent Isotropic Displacement Parameters ($Å^2 \times 10^3$) for Cbutyl-4-*p*-tolyl. U_{eq} is defined as 1/3 of of the trace of the orthogonalised U_{IJ} tensor.

Atom	***x***	***y***	***z***	**U(eq)**
C1	95.6(15)	2288.6(16)	7666.3(15)	22.4(3)
C2	-856.9(16)	3331.6(17)	8066.9(16)	26.5(4)
C3	-1866.5(17)	3397.3(19)	7306.9(18)	33.3(4)
C4	-800.3(17)	2795(2)	6589.5(17)	32.1(4)
C11	2813.7(15)	3851.8(15)	6976.9(15)	21.4(3)
C12	2893.6(17)	3503.4(17)	8220.5(15)	26.5(4)
C13	3654.2(19)	3880.7(18)	8668.7(16)	31.0(4)
C14	4361.6(18)	4626.4(18)	7908.9(17)	30.0(4)
C15	4283.6(18)	4979.2(18)	6667.1(17)	30.1(4)
C16	3523.4(17)	4605.7(17)	6210.4(15)	26.1(4)
C17	5168(2)	5054(2)	8405(2)	42.3(5)
C21	2513.0(15)	3041.6(15)	5189.7(14)	19.9(3)
C22	1817.8(16)	3280.3(16)	4211.9(15)	23.5(3)
C23	2384.8(17)	2818.7(17)	3335.8(15)	26.1(4)
C24	3663.5(16)	2113.8(16)	3399.6(15)	24.2(3)
C25	4363.0(16)	1878.9(17)	4373.3(16)	26.7(4)
C26	3801.8(16)	2334.1(16)	5253.0(15)	23.8(3)
C27	4284.9(19)	1631(2)	2440.9(17)	34.0(4)

C31	2135.5(15)	-351.6(16)	7835.9(15)	22.3(3)
C32	1749.8(19)	-18.5(18)	6666.0(16)	31.6(4)
C33	1373.3(19)	-852.4(19)	6419.4(17)	34.1(4)
C34	1390.0(17)	-2065.9(18)	7312.1(18)	29.5(4)
C35	1808.8(18)	-2420.3(18)	8466.4(18)	31.1(4)
C36	2166.1(17)	-1575.7(17)	8733.0(16)	26.2(4)
C37	944(2)	-2944(2)	7026(2)	44.1(5)
C41	2609.2(15)	253.9(15)	9703.9(14)	20.7(3)
C42	3729.8(16)	-621.5(17)	10353.5(15)	25.3(4)
C43	3815.5(17)	-1065.3(19)	11602.7(16)	29.6(4)
C44	2784.6(17)	-624.3(19)	12244.3(16)	27.4(4)
C45	1674.6(18)	246.4(19)	11605.4(16)	32.8(4)
C46	1578.1(17)	681.6(19)	10359.4(16)	31.8(4)
C47	2874(2)	-1081(2)	13599.9(17)	41.4(5)
N1	1413.3(12)	2238.7(13)	7462.1(12)	21.2(3)
P1	1633.3(4)	3617.8(4)	6327.5(4)	20.39(11)
P2	2668.2(4)	803.9(4)	8055.8(4)	19.92(11)

Table B.2 Anisotropic Displacement Parameters ($Å^2 \times 10^3$) for Cbutyl-4-*p*-tolyl. The Anisotropic displacement factor exponent takes the form: $-2\pi^2[h^2a^{*2}U_{11}+...+2hka \times b \times U_{12}]$

Atom	**U_{11}**	**U_{22}**	**U_{33}**	**U_{12}**	**U_{13}**	**U_{23}**
C1	18.6(8)	20.0(8)	24.1(8)	-6.6(6)	5.6(6)	-6.6(7)
C2	21.3(8)	24.8(9)	26.8(9)	-5.8(7)	7.5(7)	-8.7(7)
C3	19.8(9)	31.9(10)	38.1(10)	-8.1(7)	4.5(7)	-7.5(8)
C4	26.3(9)	39.3(11)	31.0(9)	-15.8(8)	4.7(7)	-12.6(8)
C11	23.1(8)	17.5(7)	22.2(8)	-6.0(6)	6.1(6)	-9.4(6)
C12	35.7(10)	22.3(8)	21.7(8)	-12.6(7)	9.6(7)	-9.8(7)
C13	43.6(11)	28.9(9)	22.5(8)	-13.3(8)	5.3(8)	-13.1(7)
C14	33.3(10)	30.3(9)	31.7(9)	-11.2(8)	5.5(8)	-18.9(8)
C15	33.3(10)	32.6(10)	29.7(9)	-17.8(8)	11.8(8)	-15.6(8)
C16	30.3(9)	27.7(9)	21.0(8)	-13.0(7)	7.4(7)	-10.4(7)
C17	47.2(13)	52.1(13)	42.7(12)	-23.3(11)	7.7(10)	-29.8(11)
C21	20.9(8)	17.3(7)	18.3(7)	-8.2(6)	5.0(6)	-4.7(6)
C22	19.6(8)	22.4(8)	24.1(8)	-6.7(7)	2.7(6)	-7.1(7)
C23	27.2(9)	30.2(9)	21.0(8)	-11.6(7)	1.1(7)	-9.3(7)
C24	28.8(9)	22.1(8)	22.6(8)	-10.7(7)	5.2(7)	-10.0(7)
C25	21.8(8)	27.4(9)	27.2(9)	-4.7(7)	3.8(7)	-12.3(7)
C26	21.6(8)	26.0(8)	20.8(8)	-7.0(7)	1.4(6)	-8.4(7)
C27	36.7(10)	40.1(11)	31.6(10)	-14.0(9)	8.9(8)	-22.4(9)
C31	22.3(8)	19.9(8)	22.5(8)	-4.9(6)	6.4(6)	-10.4(7)
C32	43.3(11)	26.4(9)	23.5(9)	-12.4(8)	5.3(8)	-10.1(7)
C33	41.3(11)	37(1)	27.0(9)	-9.6(9)	3.1(8)	-19.8(8)
C34	23.8(9)	30.0(9)	41.1(10)	-6.2(7)	7.7(8)	-24.9(8)
C35	33.6(10)	21.2(9)	35.9(10)	-9.8(8)	3.8(8)	-10.3(8)

C36	28.5(9)	21.5(8)	24.4(8)	-6.6(7)	0.7(7)	-7.7(7)
C37	37.8(12)	42.1(12)	66.3(15)	-12(1)	1.5(10)	-36.2(11)
C41	22.6(8)	16.8(7)	22.0(8)	-8.7(6)	4.1(6)	-7.0(6)
C42	19.5(8)	32.6(9)	26.6(9)	-8.5(7)	3.8(7)	-16.1(7)
C43	20.9(8)	40.3(10)	27.6(9)	-9.9(8)	-2.8(7)	-13.9(8)
C44	28.9(9)	36.7(10)	24.2(8)	-18.6(8)	3.9(7)	-14.3(8)
C45	27.4(9)	39.9(11)	25.3(9)	-6.2(8)	8.2(7)	-15.2(8)
C46	23.6(9)	31.8(10)	24.6(9)	2.1(7)	1.1(7)	-8.1(8)
C47	34.8(11)	69.2(15)	25.8(9)	-22.9(11)	3.1(8)	-21.5(10)
N1	17.9(7)	16.8(6)	22.2(7)	-5.0(5)	5.4(5)	-4.5(5)
P1	20.6(2)	16.8(2)	19.3(2)	-5.86(16)	5.66(16)	-5.57(16)
P2	19.7(2)	16.9(2)	18.9(2)	-4.88(16)	4.93(16)	-6.12(16)

Table B.3 Bond Lengths for Cbutyl-4-*p*-tolyl.

Atom	**Atom**	**Length/Å**	**Atom**	**Atom**	**Length/Å**
C1	C2	1.542(2)	C25	C26	1.390(2)
C1	C4	1.541(3)	C31	C32	1.396(2)
C1	N1	1.481(2)	C31	C36	1.393(2)
C2	C3	1.542(3)	C31	P2	1.8364(17)
C3	C4	1.546(3)	C32	C33	1.379(3)
C11	C12	1.398(2)	C33	C34	1.386(3)
C11	C16	1.401(2)	C34	C35	1.385(3)
C11	P1	1.8207(18)	C34	C37	1.507(3)
C12	C13	1.381(3)	C35	C36	1.392(3)
C13	C14	1.390(3)	C41	C42	1.394(2)
C14	C15	1.395(3)	C41	C46	1.398(2)
C14	C17	1.505(3)	C41	P2	1.8286(17)
C15	C16	1.384(3)	C42	C43	1.387(2)
C21	C22	1.394(2)	C43	C44	1.392(2)
C21	C26	1.399(2)	C44	C45	1.380(3)
C21	P1	1.8354(16)	C44	C47	1.509(2)
C22	C23	1.392(2)	C45	C46	1.385(3)
C23	C24	1.389(2)	N1	P1	1.7184(14)
C24	C25	1.395(2)	N1	P2	1.7133(14)
C24	C27	1.508(2)			

Table B.4 Bond Angles for Cbutyl-4-*p*-tolyl.

Atom	**Atom**	**Atom**	**Angle/°**	**Atom**	**Atom**	**Atom**	**Angle/°**
C4	C1	C2	88.59(13)	P2	C31	C36	124.76(13)
N1	C1	C2	119.74(14)	C33	C32	C31	121.13(17)
N1	C1	C4	120.78(13)	C34	C33	C32	121.57(18)
C3	C2	C1	87.87(13)	C35	C34	C33	117.58(17)
C4	C3	C2	88.41(13)	C37	C34	C33	120.51(18)
C3	C4	C1	87.74(13)	C37	C34	C35	121.89(18)

C16	C11	C12	117.33(16)	C36	C35	C34	121.39(17)
P1	C11	C12	121.99(13)	C35	C36	C31	120.81(17)
P1	C11	C16	119.72(13)	C46	C41	C42	117.35(15)
C13	C12	C11	120.96(16)	P2	C41	C42	116.10(12)
C14	C13	C12	121.76(17)	P2	C41	C46	126.43(13)
C15	C14	C13	117.54(17)	C43	C42	C41	121.42(15)
C17	C14	C13	121.28(17)	C44	C43	C42	120.68(17)
C17	C14	C15	121.18(17)	C45	C44	C43	118.13(16)
C16	C15	C14	121.07(16)	C47	C44	C43	121.13(17)
C15	C16	C11	121.34(16)	C47	C44	C45	120.74(16)
C26	C21	C22	117.73(15)	C46	C45	C44	121.48(16)
P1	C21	C22	116.60(12)	C45	C46	C41	120.91(17)
P1	C21	C26	125.60(13)	P1	N1	C1	115.86(10)
C23	C22	C21	121.09(15)	P2	N1	C1	122.70(10)
C24	C23	C22	121.21(16)	P2	N1	P1	119.92(8)
C25	C24	C23	117.86(15)	C21	P1	C11	102.68(7)
C27	C24	C23	121.36(16)	N1	P1	C11	103.58(7)
C27	C24	C25	120.78(16)	N1	P1	C21	104.08(7)
C26	C25	C24	121.22(16)	C41	P2	C31	102.10(7)
C25	C26	C21	120.90(16)	N1	P2	C31	101.36(7)
C36	C31	C32	117.47(16)	N1	P2	C41	106.15(7)
P2	C31	C32	117.63(13)				

Table B.5 Hydrogen Atom Coordinates (Å×10^4) and Isotropic Displacement Parameters (Å^2×10^3) for Cbutyl-4-*p*-tolyl.

Atom	***x***	***y***	***z***	**U(eq)**
H1	92.0(15)	1397.9(16)	8258.8(15)	26.9(4)
H2a	-1005.0(16)	2995.3(17)	8950.0(16)	31.8(4)
H2b	-679.9(16)	4160.2(17)	7768.6(16)	31.8(4)
H3a	-2361.6(17)	2827.6(19)	7780.7(18)	40.0(5)
H3b	-2421.4(17)	4304.3(19)	6810.5(18)	40.0(5)
H4a	-605.7(17)	3455(2)	5827.2(17)	38.5(5)
H4b	-911.0(17)	2088(2)	6449.7(17)	38.5(5)
H12	2417.9(17)	2999.8(17)	8765.3(15)	31.8(4)
H13	3695.1(19)	3623.9(18)	9518.7(16)	37.2(5)
H15	4760.0(18)	5484.1(18)	6125.8(17)	36.1(5)
H16	3482.2(17)	4865.9(17)	5359.8(15)	31.3(4)
H17a	4631(2)	5698(12)	8715(13)	63.5(8)
H17b	5714(11)	4287(3)	9066(10)	63.5(8)
H17c	5683(11)	5456(14)	7758(4)	63.5(8)
H22	942.6(16)	3766.1(16)	4142.5(15)	28.2(4)
H23	1888.1(17)	2988.8(17)	2682.1(15)	31.4(4)
H25	5239.3(16)	1398.9(17)	4436.4(16)	32.0(4)
H26	4300.0(16)	2162.6(16)	5906.1(15)	28.6(4)

H27a	3640.2(19)	1723(13)	1927(8)	51.0(6)
H27b	4800(11)	2154(9)	1940(8)	51.0(6)
H27c	4819(10)	702(4)	2832.3(17)	51.0(6)
H32	1746.7(19)	796.7(18)	6028.8(16)	37.9(5)
H33	1095.8(19)	-589.1(19)	5618.8(17)	41.0(5)
H35	1853.2(18)	-3257.4(18)	9089.3(18)	37.3(5)
H36	2434.1(17)	-1837.2(17)	9536.6(16)	31.4(4)
H37a	1578(7)	-3349(13)	6557(13)	66.2(8)
H37b	810(15)	-3636(10)	7784(2)	66.2(8)
H37c	153(8)	-2420(4)	6551(13)	66.2(8)
H42	4450.1(16)	-920.3(17)	9931.3(15)	30.4(4)
H43	4585.8(17)	-1676.7(19)	12024.8(16)	35.5(5)
H45	960.4(18)	554.5(19)	12029.3(16)	39.3(5)
H46	800.3(17)	1278.8(19)	9945.0(16)	38.2(5)
H47a	3299(13)	-602(11)	13777.2(18)	62.0(8)
H47b	2028(2)	-910(14)	13927(3)	62.0(8)
H47c	3353(12)	-2028(4)	13976(2)	62.0(8)

C. Crystal data of *N*,*N*-Bis(di-*p*-tolylphosphino)cyclohexylamine

Table C.1 Fractional Atomic Coordinates ($\times 10^4$) and Equivalent Isotropic Displacement Parameters ($Å^2 \times 10^3$) for Chzyl-4-*p*-tolyl. U_{eq} is defined as 1/3 of of the trace of the orthogonalised U_{IJ} tensor.

Atom	***x***	***y***	***z***	**U(eq)**
C1	3489(4)	3545(3)	6775(2)	20.4(7)
C2	2009(4)	4543(3)	6992(3)	28.2(8)
C3	1929(4)	5491(3)	6029(3)	34.6(9)
C4	2216(5)	4987(4)	5020(3)	40.6(10)
C5	3682(4)	3999(3)	4818(3)	31.3(9)
C6	3751(4)	3046(3)	5767(3)	25.9(8)
C11	4283(4)	4045(3)	8710(3)	20.8(7)
C12	3399(4)	4321(3)	9730(3)	22.5(7)
C13	2942(4)	5441(3)	9992(3)	25.4(8)
C14	3339(4)	6330(3)	9248(3)	22.2(7)
C15	4228(4)	6053(3)	8237(3)	24.2(8)
C16	4697(4)	4936(3)	7971(3)	22.6(7)
C17	2868(4)	7552(3)	9523(3)	27.7(8)
C21	6581(4)	2307(3)	7488(3)	22.9(7)
C22	7650(4)	2689(3)	7588(3)	24.9(8)
C23	9078(4)	2387(3)	6923(3)	27.6(8)
C24	9501(4)	1711(3)	6121(3)	27.6(8)
C25	8449(4)	1331(3)	6017(3)	28.8(8)
C26	7029(4)	1607(3)	6693(3)	25.4(8)
C27	11059(4)	1402(4)	5376(3)	40(1)
C31	4113(4)	260(3)	7883(3)	21.2(7)

C32	5026(4)	-299(3)	8556(3)	23.8(8)
C33	6156(4)	-1344(3)	8354(3)	24.2(8)
C34	6421(4)	-1881(3)	7478(3)	24.1(8)
C35	5521(4)	-1320(3)	6807(3)	25.2(8)
C36	4377(4)	-272(3)	7006(3)	23.4(7)
C37	7618(4)	-3043(3)	7297(3)	31.4(9)
C41	1789(4)	1659(3)	9449(3)	23.4(7)
C42	1663(4)	616(3)	10103(3)	32.0(9)
C43	827(4)	632(3)	11154(3)	31.1(9)
C44	77(4)	1672(3)	11599(3)	27.4(8)
C45	204(4)	2700(3)	10951(3)	26.4(8)
C46	1032(4)	2705(3)	9900(3)	22.8(7)
C47	-848(5)	1674(4)	12754(3)	41.1(10)
N1	3617(3)	2657(2)	7718(2)	20.3(6)
P1	4753.5(10)	2538.9(7)	8466.9(7)	20.5(3)
P2	2655.8(10)	1696.5(8)	8015.9(7)	23.3(3)

Table C.2 Anisotropic Displacement Parameters ($Å^2×10^3$) for Chzyl-4-*p*-tolyl. The Anisotropic displacement factor exponent takes the form: $-2\pi^2[h^2a^{*2}U_{11}+...+2hka×b×U_{12}]$

Atom	**U_{11}**	**U_{22}**	**U_{33}**	**U_{23}**	**U_{13}**	**U_{12}**
C1	27.2(17)	14.9(16)	19.9(16)	-0.1(13)	-8.8(14)	-7.1(14)
C2	27.8(19)	23.8(19)	27.9(19)	-2.4(15)	-4.4(15)	-6.6(15)
C3	34(2)	21.1(19)	37(2)	2.3(16)	-9.0(17)	-0.4(16)
C4	43(2)	42(3)	32(2)	6.9(19)	-17.5(19)	-10(2)
C5	43(2)	31(2)	24.7(19)	-1.8(16)	-10.7(16)	-17.0(18)
C6	37(2)	19.3(18)	24.4(18)	-2.8(14)	-11.4(15)	-9.9(15)
C11	28.0(18)	18.2(17)	20.0(16)	0.4(13)	-10.2(14)	-10.1(14)
C12	31.8(18)	19.0(17)	21.1(17)	0.0(13)	-8.4(14)	-14.0(15)
C13	31.3(19)	24.0(19)	22.7(17)	-4.8(14)	-6.8(15)	-10.7(15)
C14	25.8(17)	19.8(17)	26.1(18)	-1.2(14)	-12.4(14)	-9.4(14)
C15	31.7(19)	19.9(18)	24.4(18)	1.1(14)	-9.0(15)	-13.6(15)
C16	33.0(19)	18.5(17)	20.3(16)	-2.8(13)	-6.9(14)	-13.1(15)
C17	35(2)	21.6(19)	29.1(19)	-4.5(15)	-9.5(16)	-11.1(16)
C21	28.5(18)	18.8(17)	23.8(17)	0.9(14)	-10.7(14)	-9.6(14)
C22	32.9(19)	23.5(18)	24.1(17)	-1.2(14)	-11.1(15)	-13.9(15)
C23	31.4(19)	29(2)	28.2(19)	4.4(16)	-13.4(15)	-16.2(16)
C24	30.3(19)	28(2)	26.5(18)	2.1(15)	-10.0(15)	-13.0(16)
C25	31.3(19)	28(2)	28.8(19)	-8.6(16)	-6.9(15)	-10.3(16)
C26	28.7(18)	21.7(18)	29.2(19)	-5.7(15)	-8.4(15)	-10.3(15)
C27	29(2)	50(3)	40(2)	-7(2)	-4.1(17)	-16.0(19)
C31	25.6(17)	18.0(17)	21.7(16)	-2.4(13)	-4.0(13)	-11.5(14)
C32	34.1(19)	20.0(18)	20.2(17)	-4.2(14)	-5.4(14)	-12.9(15)
C33	28.9(18)	21.6(18)	24.4(18)	0.4(14)	-9.1(14)	-11.3(15)
C34	25.1(17)	19.0(17)	25.2(18)	-2.8(14)	-0.5(14)	-10.0(14)

C35	30.5(19)	23.3(18)	22.8(17)	-7.1(14)	-3.2(15)	-11.2(15)
C36	31.1(18)	20.6(18)	20.8(17)	-1.4(14)	-7.7(14)	-11.2(15)
C37	28.9(19)	28(2)	31(2)	-6.1(16)	-4.7(16)	-4.6(16)
C41	24.4(17)	18.5(17)	28.1(18)	-3.8(14)	-5.5(14)	-9.0(14)
C42	38(2)	18.5(18)	32(2)	-3.7(16)	-1.1(17)	-9.9(16)
C43	36(2)	22.7(19)	31(2)	-1.5(16)	-4.0(17)	-12.8(16)
C44	25.3(18)	25.5(19)	28.7(19)	-4.3(15)	-6.6(15)	-5.9(15)
C45	23.3(18)	24.4(19)	32(2)	-12.5(16)	-6.7(15)	-4.3(15)
C46	22.9(17)	19.4(17)	26.9(18)	-3.9(14)	-6.7(14)	-7.5(14)
C47	42(2)	42(3)	30(2)	-7.7(19)	-1.2(18)	-10(2)
N1	27.7(15)	17.0(14)	18.4(14)	1.5(11)	-7.4(11)	-11.3(12)
P1	28.2(5)	16.6(5)	19.5(5)	-1.4(3)	-8.0(4)	-10.0(4)
P2	27.3(5)	17.7(5)	25.5(5)	-4.4(4)	-4.0(4)	-10.3(4)

Table C.3 Bond Lengths for Chzyl-4-*p*-tolyl.

Atom	**Atom**	**Length/Å**	**Atom**	**Atom**	**Length/Å**
C1	C2	1.526(5)	C24	C27	1.509(5)
C1	C6	1.531(4)	C25	C26	1.375(5)
C1	N1	1.478(4)	C31	C32	1.396(5)
C2	C3	1.532(5)	C31	C36	1.393(5)
C3	C4	1.528(6)	C31	P2	1.835(4)
C4	C5	1.511(6)	C32	C33	1.377(5)
C5	C6	1.522(5)	C33	C34	1.395(5)
C11	C12	1.400(5)	C34	C35	1.385(5)
C11	C16	1.391(4)	C34	C37	1.500(5)
C11	P1	1.833(3)	C35	C36	1.384(5)
C12	C13	1.384(5)	C41	C42	1.407(5)
C13	C14	1.387(5)	C41	C46	1.398(5)
C14	C15	1.390(5)	C41	P2	1.824(4)
C14	C17	1.510(5)	C42	C43	1.378(5)
C15	C16	1.382(5)	C43	C44	1.388(5)
C21	C22	1.396(4)	C44	C45	1.389(5)
C21	C26	1.390(5)	C44	C47	1.515(5)
C21	P1	1.829(3)	C45	C46	1.376(5)
C22	C23	1.375(5)	N1	P1	1.726(3)
C23	C24	1.382(5)	N1	P2	1.713(3)
C24	C25	1.381(5)			

Table C.4 Bond Angles for Chzyl-4-*p*-tolyl.

Atom	**Atom**	**Atom**	**Angle/°**	**Atom**	**Atom**	**Atom**	**Angle/°**
C2	C1	C6	110.2(3)	C36	C31	C32	118.0(3)
N1	C1	C2	112.0(3)	C36	C31	P2	116.9(3)
N1	C1	C6	114.0(3)	C33	C32	C31	120.8(3)
C1	C2	C3	111.4(3)	C32	C33	C34	121.2(3)

C4	C3	C2	111.8(3)	C33	C34	C37	120.4(3)
C5	C4	C3	110.3(3)	C35	C34	C33	117.8(3)
C4	C5	C6	111.9(3)	C35	C34	C37	121.8(3)
C5	C6	C1	111.1(3)	C36	C35	C34	121.4(3)
C12	C11	P1	116.4(2)	C35	C36	C31	120.7(3)
C16	C11	C12	117.4(3)	C42	C41	P2	121.7(3)
C16	C11	P1	126.1(3)	C46	C41	C42	117.7(3)
C13	C12	C11	121.3(3)	C46	C41	P2	119.9(3)
C12	C13	C14	121.1(3)	C43	C42	C41	120.8(3)
C13	C14	C15	117.6(3)	C42	C43	C44	121.3(3)
C13	C14	C17	121.8(3)	C43	C44	C45	117.7(3)
C15	C14	C17	120.6(3)	C43	C44	C47	120.6(3)
C16	C15	C14	121.7(3)	C45	C44	C47	121.7(3)
C15	C16	C11	120.9(3)	C46	C45	C44	121.9(3)
C22	C21	P1	121.7(3)	C45	C46	C41	120.5(3)
C26	C21	C22	117.0(3)	C1	N1	P1	121.6(2)
C26	C21	P1	120.7(2)	C1	N1	P2	117.7(2)
C23	C22	C21	121.2(3)	P2	N1	P1	120.58(16)
C22	C23	C24	121.2(3)	C21	P1	C11	101.47(15)
C23	C24	C27	121.3(3)	N1	P1	C11	104.18(14)
C25	C24	C23	117.9(3)	N1	P1	C21	103.02(15)
C25	C24	C27	120.9(3)	C41	P2	C31	103.44(16)
C26	C25	C24	121.2(3)	N1	P2	C31	104.08(15)
C25	C26	C21	121.4(3)	N1	P2	C41	104.32(14)
C32	C31	P2	124.9(3)				

Table C.5 Torsion Angles for Chzyl-4-*p*-tolyl.

A	**B**	**C**	**D**	**Angle/°**	**A**	**B**	**C**	**D**	**Angle/°**
C1	C2	C3	C4	55.2(4)	C31	C32	C33	C34	-0.4(5)
C1	N1	P1	C11	48.5(3)	C32	C31	C36	C35	-0.5(5)
C1	N1	P1	C21	-57.1(3)	C32	C31	P2	C41	-40.7(3)
C1	N1	P2	C31	117.2(2)	C32	C31	P2	N1	68.1(3)
C1	N1	P2	C41	-134.7(2)	C32	C33	C34	C35	0.8(5)
C2	C1	C6	C5	56.1(4)	C32	C33	C34	C37	-177.5(3)
C2	C1	N1	P1	-106.3(3)	C33	C34	C35	C36	-1.1(5)
C2	C1	N1	P2	76.5(3)	C34	C35	C36	C31	1.0(5)
C2	C3	C4	C5	-54.8(4)	C36	C31	C32	C33	0.2(5)
C3	C4	C5	C6	55.9(4)	C36	C31	P2	C41	143.3(2)
C4	C5	C6	C1	-57.2(4)	C36	C31	P2	N1	-107.9(3)
C6	C1	C2	C3	-55.2(4)	C37	C34	C35	C36	177.2(3)
C6	C1	N1	P1	127.8(3)	C41	C42	C43	C44	0.4(6)
C6	C1	N1	P2	-49.5(3)	C42	C41	C46	C45	0.4(5)
C11	C12	C13	C14	0.4(5)	C42	C41	P2	C31	-33.6(3)
C12	C11	C16	C15	-1.0(5)	C42	C41	P2	N1	-142.2(3)

C12	C11	P1	C21	-148.9(3)	C42	C43	C44	C45	-0.3(6)
C12	C11	P1	N1	104.3(3)	C42	C43	C44	C47	179.4(4)
C12	C13	C14	C15	-0.9(5)	C43	C44	C45	C46	0.3(5)
C12	C13	C14	C17	-179.1(3)	C44	C45	C46	C41	-0.4(5)
C13	C14	C15	C16	0.5(5)	C46	C41	C42	C43	-0.4(6)
C14	C15	C16	C11	0.4(5)	C46	C41	P2	C31	156.1(3)
C16	C11	C12	C13	0.6(5)	C46	C41	P2	N1	47.5(3)
C16	C11	P1	C21	32.5(3)	C47	C44	C45	C46	-179.4(3)
C16	C11	P1	N1	-74.3(3)	N1	C1	C2	C3	176.8(3)
C17	C14	C15	C16	178.8(3)	N1	C1	C6	C5	-177.0(3)
C21	C22	C23	C24	1.1(6)	P1	C11	C12	C13	-178.1(3)
C22	C21	C26	C25	-1.8(5)	P1	C11	C16	C15	177.6(3)
C22	C21	P1	C11	42.1(3)	P1	C21	C22	C23	172.0(3)
C22	C21	P1	N1	149.8(3)	P1	C21	C26	C25	-173.6(3)
C22	C23	C24	C25	-1.0(6)	P1	N1	P2	C31	-60.1(2)
C22	C23	C24	C27	178.6(4)	P1	N1	P2	C41	48.0(2)
C23	C24	C25	C26	-0.5(6)	P2	C31	C32	C33	-175.7(2)
C24	C25	C26	C21	2.0(6)	P2	C31	C36	C35	175.8(2)
C26	C21	C22	C23	0.2(5)	P2	C41	C42	C43	-170.9(3)
C26	C21	P1	C11	-146.5(3)	P2	C41	C46	C45	171.1(3)
C26	C21	P1	N1	-38.8(3)	P2	N1	P1	C11	-134.29(19)
C27	C24	C25	C26	179.8(4)	P2	N1	P1	C21	120.12(19)

Table C.6 Hydrogen Atom Coordinates (Å×10^4) and Isotropic Displacement Parameters (Å^2×10^3) for Chzyl-4-*p*-tolyl.

Atom	***x***	***y***	***z***	**U(eq)**
H13	4270	3889	6627	24
H16A	1888	4886	7604	34
H16B	1201	4235	7160	34
H32A	953	6085	6176	41
H32B	2661	5863	5916	41
H21A	1417	4700	5097	49
H21B	2233	5598	4418	49
H24A	4486	4307	4668	38
H24B	3822	3663	4197	38
H33A	4718	2441	5616	31
H33B	3001	2691	5882	31
H12	3113	3741	10243	27
H14	2360	5599	10678	30
H10	4515	6633	7727	29
H5	5297	4778	7289	27
H23A	1901	7732	10030	42
H23B	2832	8104	8890	42
H23C	3572	7598	9824	42

H19	7391	3157	8113	30
H28	9772	2643	7016	33
H27	8706	881	5478	35
H11	6353	1319	6618	30
H37A	11628	619	5599	60
H37B	11521	1939	5389	60
H37C	11018	1450	4666	60
H4	4869	39	9149	29
H34	6755	-1698	8811	29
H30	5688	-1655	6210	30
H8	3779	80	6548	28
H17A	8428	-3093	7538	47
H17B	7967	-3120	6551	47
H17C	7224	-3660	7686	47
H35	2150	-93	9823	38
H25	764	-69	11573	37
H18	-286	3406	11236	32
H7	1089	3409	9487	27
H36A	-1474	1207	12899	62
H36B	-1455	2462	12886	62
H36C	-202	1353	13207	62

D. Crystal data of *N*,*N*-Bis(diphenylphosphino oxide)-4-fluoroaniline

Table D.1 Fractional Atomic Coordinates ($\times 10^4$) and Equivalent Isotropic Displacement Parameters ($Å^2 \times 10^3$) for *p*FPh-PhPNPO. U_{eq} is defined as 1/3 of of the trace of the orthogonalised U_{IJ} tensor.

Atom	***x***	***y***	***z***	**U(eq)**
C1	5000	-893.0(8)	2500	12.5(3)
C2	4990.9(12)	-1240.7(6)	1483.4(12)	15.3(2)
C3	4981.0(13)	-1947.4(7)	1479.6(13)	19.4(3)
C4	5000	-2281.6(9)	2500	19.9(4)
C11	7629.4(11)	-302.9(6)	3999.8(11)	13.5(2)
C12	7829.9(12)	-558.3(6)	3016.9(12)	16.6(2)
C13	8918.6(14)	-941.8(7)	3308.3(15)	24.4(3)
C14	9810.7(14)	-1072.3(7)	4569.3(17)	29.4(3)
C15	9622.2(13)	-816.4(8)	5542.6(15)	26.6(3)
C16	8535.3(12)	-432.1(7)	5265.4(12)	19.0(3)
C21	6500.5(11)	1023.4(6)	3096.3(11)	13.1(2)
C22	6731.6(12)	1054.6(6)	2055.9(12)	16.1(2)
C23	7003.8(13)	1675.6(7)	1686.0(13)	21.1(3)
C24	7008.7(14)	2267.3(7)	2321.7(14)	24.3(3)
C25	6758.3(14)	2240.5(7)	3340.8(14)	24.2(3)
C26	6527.1(13)	1618.1(7)	3745.5(12)	18.2(3)
N1	5000	-155.9(7)	2500	11.5(3)

O1	6188.9(9)	333.6(5)	4898.9(8)	17.5(2)
F1	5000	-2971.7(6)	2500	30.3(3)
P1	6282.3(3)	231.1(2)	3720.3(3)	10.91(10)

Table D.2 Anisotropic Displacement Parameters ($Å^2×10^3$) for *p*FPh-PhPNPO. The Anisotropic displacement factor exponent takes the form: $-2\pi^2[h^2a^{*2}U_{11}+...+2hka×b×U_{12}]$

Atom	U_{11}	U_{22}	U_{33}	U_{23}	U_{13}	U_{12}
C1	10.2(7)	11.3(8)	14.0(7)	0	4.3(6)	0
C2	14.9(6)	16.3(6)	14.3(5)	-0.1(4)	6.6(5)	0.5(4)
C3	19.6(6)	17.1(6)	19.9(6)	-4.2(5)	8.3(5)	1.3(5)
C4	17.9(9)	10.4(8)	27.6(9)	0	7.8(8)	0
C11	10.5(5)	12.7(5)	15.9(6)	2.0(4)	5.2(5)	-0.9(4)
C12	14.7(6)	15.5(6)	20.5(6)	-0.7(5)	9.2(5)	-1.1(5)
C13	19.8(7)	18.4(6)	40.2(8)	-4.0(6)	18.4(6)	-0.8(5)
C14	14.6(6)	19.3(7)	50.8(10)	5.9(6)	12.9(6)	5.0(5)
C15	14.8(6)	24.0(7)	29.9(7)	12.2(6)	1.9(6)	0.9(5)
C16	14.7(6)	20.8(6)	17.8(6)	4.7(5)	4.8(5)	-2.3(5)
C21	10.1(5)	13.0(5)	13.4(5)	-0.6(4)	3.4(4)	-1.1(4)
C22	15.4(6)	15.9(6)	16.3(6)	0.1(4)	7.1(5)	-0.3(5)
C23	19.0(6)	22.3(7)	20.6(6)	5.1(5)	8.4(5)	-1.9(5)
C24	20.9(7)	16.0(6)	28.0(7)	4.2(5)	5.4(6)	-4.3(5)
C25	24.9(7)	13.8(6)	26.9(7)	-4.8(5)	6.6(6)	-2.7(5)
C26	17.1(6)	17.2(6)	17.3(6)	-3.6(5)	5.8(5)	-0.9(5)
N1	10.7(6)	10.8(7)	11.1(6)	0	3.7(5)	0
O1	19.2(5)	23.1(5)	11.6(4)	-2.8(3)	8.5(4)	-1.8(4)
F1	37.3(7)	10.0(5)	41.5(7)	0	17.2(6)	0
P1	10.42(16)	12.71(16)	9.02(15)	-0.55(10)	4.20(12)	-0.41(10)

Table D.3 Bond Lengths for *p*FPh-PhPNPO.

Atom	Atom	Length/Å	Atom	Atom	Length/Å
C1	C2	1.3910(15)	C14	C15	1.382(2)
C1	C2[1]	1.3909(15)	C15	C16	1.389(2)
C1	N1	1.450(2)	C21	C22	1.3980(17)
C2	C3	1.3896(18)	C21	C26	1.3959(17)
C3	C4	1.3774(17)	C21	P1	1.7990(13)
C4	C3[1]	1.3774(17)	C22	C23	1.3884(18)
C4	F1	1.357(2)	C23	C24	1.389(2)
C11	C12	1.3997(18)	C24	C25	1.387(2)
C11	C16	1.3975(18)	C25	C26	1.3907(19)
C11	P1	1.8022(14)	N1	P1[1]	1.7011(8)
C12	C13	1.3863(19)	N1	P1	1.7011(8)
C13	C14	1.390(2)	O1	P1	1.4803(11)

[1]1-X,+Y,1/2-Z

Table D.4 Bond Angles for *p*FPh-PhPNPO.

Atom	Atom	Atom	Angle/°	Atom	Atom	Atom	Angle/°
C2[1]	C1	C2	121.12(16)	C26	C21	C22	119.79(12)
C2	C1	N1	119.44(8)	C26	C21	P1	117.64(10)
C2[1]	C1	N1	119.44(8)	C23	C22	C21	119.79(12)
C3	C2	C1	119.40(12)	C22	C23	C24	120.20(13)
C4	C3	C2	118.54(13)	C25	C24	C23	120.21(13)
C3[1]	C4	C3	122.99(17)	C24	C25	C26	120.01(13)
F1	C4	C3	118.50(9)	C25	C26	C21	119.95(13)
F1	C4	C3[1]	118.50(9)	C1	N1	P1[1]	116.57(4)
C12	C11	P1	122.97(9)	C1	N1	P1	116.57(4)
C16	C11	C12	119.62(12)	P1	N1	P1[1]	126.86(9)
C16	C11	P1	117.33(10)	C21	P1	C11	106.94(6)
C13	C12	C11	119.68(13)	N1	P1	C11	104.22(6)
C12	C13	C14	120.36(14)	N1	P1	C21	106.12(6)
C15	C14	C13	120.15(13)	O1	P1	C11	111.45(6)
C14	C15	C16	120.14(13)	O1	P1	C21	111.63(6)
C15	C16	C11	120.04(13)	O1	P1	N1	115.83(5)
C22	C21	P1	122.41(9)				

[1]1-X,+Y,1/2-Z

Table D.5 Torsion Angles for *p*FPh-PhPNPO.

A	B	C	D	Angle/°	A	B	C	D	Angle/°
C1	C2	C3	C4	-0.95(17)	C16	C11	P1	O1	-12.64(12)
C1	N1	P1	C11	36.99(4)	C21	C22	C23	C24	-2.0(2)
C1	N1	P1	C21	149.70(4)	C22	C21	C26	C25	1.24(19)
C1	N1	P1	O1	-85.82(5)	C22	C21	P1	C11	51.90(11)
C2[1]	C1	C2	C3	0.49(9)	C22	C21	P1	N1	-58.92(11)
C2	C1	N1	P1	-119.27(7)	C22	C21	P1	O1	174.04(10)
C2[1]	C1	N1	P1	60.73(7)	C22	C23	C24	C25	0.9(2)
C2[1]	C1	N1	P1[1]	-119.27(7)	C23	C24	C25	C26	1.3(2)
C2	C1	N1	P1[1]	60.73(7)	C24	C25	C26	C21	-2.3(2)
C2	C3	C4	C3[1]	0.48(9)	C26	C21	C22	C23	0.90(18)
C2	C3	C4	F1	-179.52(9)	C26	C21	P1	C11	-123.48(10)
C11	C12	C13	C14	-0.1(2)	C26	C21	P1	N1	125.71(10)
C12	C11	C16	C15	-0.50(19)	C26	C21	P1	O1	-1.34(12)
C12	C11	P1	C21	-67.09(11)	N1	C1	C2	C3	-179.51(9)
C12	C11	P1	N1	45.03(11)	P1	C11	C12	C13	177.21(10)
C12	C11	P1	O1	170.66(10)	P1	C11	C16	C15	-177.31(10)
C12	C13	C14	C15	-0.4(2)	P1	C21	C22	C23	-174.38(10)
C13	C14	C15	C16	0.5(2)	P1	C21	C26	C25	176.75(10)
C14	C15	C16	C11	0.0(2)	P1[1]	N1	P1	C11	-143.01(4)
C16	C11	C12	C13	0.58(18)	P1[1]	N1	P1	C21	-30.30(4)
C16	C11	P1	C21	109.61(10)	P1[1]	N1	P1	O1	94.18(5)

C16 C11 P1 N1 -138.27(10)
[1]1-X,+Y,1/2-Z

Table D.6 Hydrogen Atom Coordinates (Å×10^4) and Isotropic Displacement Parameters (Å^2×10^3) for *p*FPh-PhPNPO.

Atom	*x*	*y*	*z*	U(eq)
H12	4991	-1002	812	18
H14	4962	-2189	803	23
H10	7236	-471	2172	20
H17	9053	-1113	2657	29
H18	10536	-1332	4758	35
H15	10224	-902	6385	32
H16	8410	-261	5922	23
H6	6703	661	1613	19
H5	7183	1695	1010	25
H9	7180	2683	2063	29
H19	6745	2639	3754	29
H20	6390	1598	4448	22

E. Crystal data of *N,N*-Bis(di-*p*-tolylphosphino oxide)-*p*-toluidine

Table E.1 Fractional Atomic Coordinates (×10^4) and Equivalent Isotropic Displacement Parameters (Å^2×10^3) for 5-*p*-tolyl-PNPO. U_{eq} is defined as 1/3 of of the trace of the orthogonalised U_{IJ} tensor.

Atom	*x*	*y*	*z*	U(eq)
C1	3288(2)	6650.3(17)	849.2(18)	12.8(4)
C2	2574(2)	7312.6(19)	1153(2)	17.5(4)
C3	3227(2)	8589(2)	1854(2)	22.3(4)
C4	4574(2)	9217(2)	2247(2)	23.1(5)
C5	5248(2)	8528(2)	1908(2)	21.0(4)
C6	4625(2)	7254.7(19)	1223(2)	15.9(4)
C7	5272(3)	10604(2)	3005(3)	36.7(6)
C11	1808.6(19)	5574.1(17)	-2115.0(18)	12.1(3)
C12	2320(2)	5809(2)	-2847(2)	17.6(4)
C13	1800(2)	6410(2)	-3575(2)	20.9(4)
C14	769(2)	6777(2)	-3599(2)	19.9(4)
C15	266(2)	6541(2)	-2863(2)	18.4(4)
C16	776(2)	5947.0(19)	-2127(2)	15.6(4)
C17	203(3)	7426(2)	-4392(3)	30.9(5)
C21	989(2)	3179.6(18)	-2228.4(18)	13.4(4)
C22	1214(2)	2145.1(19)	-2755.7(19)	17.9(4)
C23	143(3)	988(2)	-3503(2)	23.4(5)
C24	-1164(2)	845(2)	-3778(2)	23.6(5)
C25	-1385(2)	1889(2)	-3271(2)	22.6(4)
C26	-312(2)	3049.5(19)	-2483.4(19)	16.3(4)
C27	-2319(3)	-422(2)	-4577(3)	39.1(7)

C31	2411(2)	3137.9(17)	407.4(18)	13.1(4)
C32	1320(2)	2072(2)	-31(2)	20.0(4)
C33	1445(2)	945(2)	-361(2)	24.8(5)
C34	2648(3)	869(2)	-230(2)	24.7(5)
C35	3737(2)	1950(2)	237(2)	20.9(4)
C36	3618(2)	3071.2(18)	538.8(19)	15.5(4)
C37	2777(4)	-349(2)	-621(3)	40.3(7)
C41	3610(2)	5495.7(18)	2628.3(19)	13.6(4)
C42	3245(2)	5733.3(19)	3544(2)	17.0(4)
C43	4262(2)	6327(2)	4872(2)	19.6(4)
C44	5639(2)	6677.9(18)	5309.9(19)	16.9(4)
C45	5995(2)	6440.2(19)	4391(2)	17.3(4)
C46	4994(2)	5856.1(18)	3062.1(19)	14.2(4)
C47	6732(3)	7307(2)	6747(2)	26.5(5)
N1	2638.5(16)	5313.2(14)	152.7(15)	11.4(3)
O1	3617.4(14)	4530.9(13)	-1329.8(14)	16.1(3)
O2	884.2(15)	4406.4(14)	748.7(14)	18.6(3)
P1	2405.9(5)	4651.6(4)	-1335.1(5)	10.48(12)
P2	2236.3(5)	4581.4(4)	931.3(5)	11.43(12)

Table E.2 Anisotropic Displacement Parameters ($Å^2 \times 10^3$) for 5-*p*-tolyl-PNPO. The Anisotropic displacement factor exponent takes the form: $-2\pi^2[h^2a^{*2}U_{11}+...+2hka\times b\times U_{12}]$

Atom	$\mathbf{U_{11}}$	$\mathbf{U_{22}}$	$\mathbf{U_{33}}$	$\mathbf{U_{23}}$	$\mathbf{U_{13}}$	$\mathbf{U_{12}}$
C1	15.5(9)	12.4(9)	10.4(8)	5.4(7)	7.1(7)	4.9(7)
C2	19.7(10)	17.6(10)	18.8(10)	8.5(8)	12.5(8)	9.3(8)
C3	30.0(11)	17.4(10)	25.5(11)	9.2(9)	18.3(10)	13.7(9)
C4	29.4(12)	15.1(10)	21.1(10)	7.1(8)	12.3(9)	7.9(9)
C5	19.3(10)	16(1)	21.3(10)	6.5(8)	9.6(9)	2.6(8)
C6	15.7(9)	16.2(9)	17.5(9)	8.1(8)	9.7(8)	7.3(8)
C7	42.5(15)	15.1(11)	37.8(15)	4.5(10)	18.0(12)	7.1(10)
C11	12.8(8)	12.4(8)	11.0(8)	6.1(7)	6.3(7)	4.2(7)
C12	19.4(9)	21.2(10)	18.7(10)	11.4(8)	13.2(8)	9.5(8)
C13	25.2(11)	26.1(11)	20.8(10)	16.0(9)	16.0(9)	10.1(9)
C14	20.2(10)	18.5(10)	15.1(9)	9.6(8)	5.3(8)	4.6(8)
C15	17.4(9)	20.4(10)	20.4(10)	11.8(8)	9.7(8)	10.3(8)
C16	15.5(9)	18.0(9)	16.5(9)	9.9(8)	9.9(8)	6.9(7)
C17	35.8(13)	33.8(13)	28.6(12)	23.9(11)	14.2(11)	16.4(11)
C21	16.3(9)	13.5(9)	8.7(8)	5.6(7)	5.5(7)	5.3(7)
C22	26.6(11)	16.2(9)	13.2(9)	7.6(8)	10.9(8)	11.2(8)
C23	38.7(13)	13.6(10)	14.2(9)	6.0(8)	12.2(9)	9.9(9)
C24	32.8(12)	13.5(10)	11.5(9)	4.6(8)	7.4(9)	-0.1(9)
C25	19.1(10)	21.8(11)	16.9(10)	7.4(9)	6.8(8)	0.4(8)
C26	18.0(9)	14.4(9)	14.4(9)	6.2(8)	8.3(8)	5.0(8)
C27	44.9(16)	18.3(12)	27.1(13)	3.7(10)	12.1(12)	-6.0(11)

C31	16.5(9)	11.7(8)	9.1(8)	5.8(7)	5.9(7)	3.2(7)
C32	20.3(10)	18.4(10)	14.7(9)	8.4(8)	7.0(8)	1.0(8)
C33	31.1(12)	13.1(10)	16.7(10)	6.6(8)	7.8(9)	-1.8(8)
C34	42.2(13)	13.8(10)	14.9(10)	8.0(8)	13(1)	10.0(9)
C35	30.0(11)	19.1(10)	16.9(10)	9.0(8)	13.5(9)	13.0(9)
C36	19.2(9)	12.8(9)	12.7(9)	5.7(7)	7.9(8)	5.0(7)
C37	67(2)	16.0(11)	31.3(14)	9.4(10)	22.9(14)	16.5(12)
C41	17.4(9)	14.7(9)	11.7(8)	6.8(7)	9.1(7)	7.8(7)
C42	17.3(9)	20.5(10)	15.9(9)	7.8(8)	11.2(8)	8.0(8)
C43	27.9(11)	21.6(10)	13.9(9)	7.6(8)	14.3(9)	11.9(9)
C44	23.9(10)	13.3(9)	11.3(9)	5.8(7)	7.6(8)	8.3(8)
C45	15.8(9)	16.6(9)	14.9(9)	5.6(8)	6.3(8)	5.8(8)
C46	15.5(9)	16.4(9)	12.0(9)	5.8(7)	8.7(7)	6.7(7)
C47	31.1(12)	27.3(12)	12.3(10)	7.8(9)	6.8(9)	10.2(10)
N1	13.1(7)	10.9(7)	10.0(7)	4.4(6)	6.6(6)	4.3(6)
O1	13.9(7)	19.4(7)	16.9(7)	8.6(6)	8.6(6)	9.2(6)
O2	14.9(7)	27.3(8)	15.8(7)	10.4(6)	9.1(6)	9.8(6)
P1	10.9(2)	12.2(2)	10.1(2)	5.48(18)	6.48(18)	5.34(18)
P2	10.6(2)	13.9(2)	10.3(2)	5.84(18)	6.22(18)	4.22(18)

Table E.3 Bond Lengths for 5-*p*-tolyl-PNPO.

Atom	**Atom**	**Length/Å**	**Atom**	**Atom**	**Length/Å**
C1	C2	1.393(3)	C24	C27	1.514(3)
C1	C6	1.388(3)	C25	C26	1.392(3)
C1	N1	1.456(2)	C31	C32	1.397(3)
C2	C3	1.392(3)	C31	C36	1.391(3)
C3	C4	1.397(3)	C31	P2	1.809(2)
C4	C5	1.389(3)	C32	C33	1.398(3)
C4	C7	1.512(3)	C33	C34	1.388(4)
C5	C6	1.387(3)	C34	C35	1.396(3)
C11	C12	1.398(3)	C34	C37	1.511(3)
C11	C16	1.393(3)	C35	C36	1.388(3)
C11	P1	1.805(2)	C41	C42	1.400(3)
C12	C13	1.391(3)	C41	C46	1.394(3)
C13	C14	1.383(3)	C41	P2	1.804(2)
C14	C15	1.397(3)	C42	C43	1.392(3)
C14	C17	1.510(3)	C43	C44	1.384(3)
C15	C16	1.387(3)	C44	C45	1.396(3)
C21	C22	1.400(3)	C44	C47	1.506(3)
C21	C26	1.391(3)	C45	C46	1.390(3)
C21	P1	1.799(2)	N1	P1	1.6984(17)
C22	C23	1.390(3)	N1	P2	1.6997(17)
C23	C24	1.388(4)	O1	P1	1.4745(15)
C24	C25	1.400(3)	O2	P2	1.4733(16)

Table E.4 Bond Angles for 5-*p*-tolyl-PNPO.

Atom	Atom	Atom	Angle/°	Atom	Atom	Atom	Angle/°
C2	C1	N1	119.84(17)	C31	C32	C33	119.4(2)
C6	C1	C2	120.50(19)	C34	C33	C32	121.3(2)
C6	C1	N1	119.65(17)	C33	C34	C35	118.3(2)
C3	C2	C1	119.0(2)	C33	C34	C37	121.6(2)
C2	C3	C4	121.5(2)	C35	C34	C37	120.1(2)
C3	C4	C7	121.0(2)	C36	C35	C34	121.2(2)
C5	C4	C3	117.9(2)	C35	C36	C31	120.04(19)
C5	C4	C7	121.0(2)	C42	C41	P2	117.28(16)
C6	C5	C4	121.6(2)	C46	C41	C42	119.25(18)
C5	C6	C1	119.39(19)	C46	C41	P2	123.11(15)
C12	C11	P1	117.30(15)	C43	C42	C41	119.90(19)
C16	C11	C12	119.25(18)	C44	C43	C42	121.19(19)
C16	C11	P1	123.11(14)	C43	C44	C45	118.57(19)
C13	C12	C11	120.02(19)	C43	C44	C47	120.9(2)
C14	C13	C12	121.10(19)	C45	C44	C47	120.6(2)
C13	C14	C15	118.51(19)	C46	C45	C44	121.06(19)
C13	C14	C17	121.0(2)	C45	C46	C41	120.02(18)
C15	C14	C17	120.4(2)	C1	N1	P1	116.32(12)
C16	C15	C14	121.17(19)	C1	N1	P2	116.65(12)
C15	C16	C11	119.93(18)	P1	N1	P2	127.01(10)
C22	C21	P1	117.03(16)	C21	P1	C11	106.47(9)
C26	C21	C22	119.94(18)	N1	P1	C11	105.35(9)
C26	C21	P1	122.87(15)	N1	P1	C21	105.86(8)
C23	C22	C21	119.8(2)	O1	P1	C11	111.23(9)
C24	C23	C22	120.9(2)	O1	P1	C21	111.48(9)
C23	C24	C25	118.8(2)	O1	P1	N1	115.82(8)
C23	C24	C27	120.5(2)	C41	P2	C31	105.92(9)
C25	C24	C27	120.7(2)	N1	P2	C31	106.42(9)
C26	C25	C24	120.9(2)	N1	P2	C41	104.80(9)
C21	C26	C25	119.6(2)	O2	P2	C31	112.01(9)
C32	C31	P2	117.37(16)	O2	P2	C41	111.39(9)
C36	C31	C32	119.72(19)	O2	P2	N1	115.58(8)
C36	C31	P2	122.63(14)				

Table E.5 Torsion Angles for 5-*p*-tolyl-PNPO.

A	B	C	D	Angle/°	A	B	C	D	Angle/°
C1	C2	C3	C4	0.5(3)	C27	C24	C25	C26	176.8(2)
C1	N1	P1	C11	-42.47(15)	C31	C32	C33	C34	1.8(3)
C1	N1	P1	C21	-155.03(14)	C32	C31	C36	C35	-0.1(3)
C1	N1	P1	O1	80.89(15)	C32	C31	P2	C41	118.62(16)
C1	N1	P2	C31	-147.80(14)	C32	C31	P2	N1	-130.22(15)
C1	N1	P2	C41	-35.87(15)	C32	C31	P2	O2	-3.01(18)

C1	N1	P2	O2	87.14(15)	C32	C33	C34	C35	-0.3(3)
C2	C1	C6	C5	0.2(3)	C32	C33	C34	C37	-178.3(2)
C2	C1	N1	P1	117.86(17)	C33	C34	C35	C36	-1.3(3)
C2	C1	N1	P2	-63.8(2)	C34	C35	C36	C31	1.6(3)
C2	C3	C4	C5	0.5(3)	C36	C31	C32	C33	-1.5(3)
C2	C3	C4	C7	179.9(2)	C36	C31	P2	C41	-55.35(18)
C3	C4	C5	C6	-1.2(3)	C36	C31	P2	N1	55.81(18)
C4	C5	C6	C1	0.9(3)	C36	C31	P2	O2	-176.98(15)
C6	C1	C2	C3	-0.9(3)	C37	C34	C35	C36	176.6(2)
C6	C1	N1	P1	-63.1(2)	C41	C42	C43	C44	-0.8(3)
C6	C1	N1	P2	115.18(17)	C42	C41	C46	C45	0.2(3)
C7	C4	C5	C6	179.4(2)	C42	C41	P2	C31	-111.46(16)
C11	C12	C13	C14	-0.5(3)	C42	C41	P2	N1	136.24(16)
C12	C11	C16	C15	0.2(3)	C42	C41	P2	O2	10.57(19)
C12	C11	P1	C21	-107.67(17)	C42	C43	C44	C45	0.9(3)
C12	C11	P1	N1	140.20(16)	C42	C43	C44	C47	-179.3(2)
C12	C11	P1	O1	13.96(19)	C43	C44	C45	C46	-0.5(3)
C12	C13	C14	C15	0.6(3)	C44	C45	C46	C41	-0.1(3)
C12	C13	C14	C17	-179.8(2)	C46	C41	C42	C43	0.2(3)
C13	C14	C15	C16	-0.3(3)	C46	C41	P2	C31	61.65(19)
C14	C15	C16	C11	-0.1(3)	C46	C41	P2	N1	-50.65(19)
C16	C11	C12	C13	0.1(3)	C46	C41	P2	O2	-176.32(16)
C16	C11	P1	C21	65.66(19)	C47	C44	C45	C46	179.8(2)
C16	C11	P1	N1	-46.46(18)	N1	C1	C2	C3	178.10(18)
C16	C11	P1	O1	-172.71(16)	N1	C1	C6	C5	-178.80(18)
C17	C14	C15	C16	-179.9(2)	P1	C11	C12	C13	173.72(17)
C21	C22	C23	C24	2.6(3)	P1	C11	C16	C15	-173.03(16)
C22	C21	C26	C25	-0.5(3)	P1	C21	C22	C23	-177.27(15)
C22	C21	P1	C11	123.00(16)	P1	C21	C26	C25	174.75(16)
C22	C21	P1	N1	-125.22(15)	P1	N1	P2	C31	30.30(14)
C22	C21	P1	O1	1.53(18)	P1	N1	P2	C41	142.24(12)
C22	C23	C24	C25	-1.1(3)	P1	N1	P2	O2	-94.75(13)
C22	C23	C24	C27	-179.1(2)	P2	C31	C32	C33	-175.68(16)
C23	C24	C25	C26	-1.2(3)	P2	C31	C36	C35	173.73(15)
C24	C25	C26	C21	2.0(3)	P2	C41	C42	C43	173.61(16)
C26	C21	C22	C23	-1.8(3)	P2	C41	C46	C45	-172.75(15)
C26	C21	P1	C11	-52.36(18)	P2	N1	P1	C11	139.41(12)
C26	C21	P1	N1	59.41(18)	P2	N1	P1	C21	26.86(14)
C26	C21	P1	O1	-173.83(15)	P2	N1	P1	O1	-97.22(13)

Table E.6 Hydrogen Atom Coordinates (Å×10^4) and Isotropic Displacement Parameters (Å^2×10^3) for 5-*p*-tolyl-PNPO.

Atom	***x***	***y***	***z***	**U(eq)**
H15	1674	6908	892	21
H28	2756	9034	2065	27
H23	6139	8931	2147	25
H9	5098	6810	1016	19
H38A	6248	10857	3425	55
H38B	5060	10881	3652	55
H38C	4952	10954	2420	55
H20	3007	5563	-2848	21
H32	2151	6569	-4054	25
H26	-424	6786	-2866	22
H22	430	5798	-1642	19
H37A	-711	6884	-5131	46
H37B	779	7662	-4688	46
H37C	179	8146	-3862	46
H34	2077	2232	-2607	21
H35	305	299	-3822	28
H25	-2261	1806	-3464	27
H6	-464	3733	-2130	20
H39A	-2207	-839	-4048	59
H39B	-2298	-884	-5314	59
H39C	-3183	-346	-4877	59
H30	516	2111	-102	24
H36	709	233	-676	30
H18	4557	1917	349	25
H7	4347	3779	829	19
H40A	2530	-677	-1508	60
H40B	2176	-913	-542	60
H40C	3708	-232	-60	60
H12	2324	5495	3267	20
H21	4013	6491	5475	24
H19	6916	6676	4672	21
H16	5249	5706	2462	17
H31A	7333	6885	6921	40
H31B	6309	7294	7229	40
H31C	7252	8143	7006	40

F. Crystal data of *N*,*N*-Bis(di-*p*-tolylphosphino oxide)cyclohexylamine

Table F.1 Fractional Atomic Coordinates ($\times 10^4$) and Equivalent Isotropic Displacement Parameters ($Å^2 \times 10^3$) for Chzyl-4-*p*-tolyl-PNPO. U_{eq} is defined as 1/3 of of the trace of the orthogonalised U_{IJ} tensor.

Atom	***x***	***y***	***z***	**U(eq)**
P1	5695.6(8)	2370.0(5)	6593.6(3)	10.2(3)
P2	5076.7(8)	1120.3(5)	6128.8(4)	11.2(3)
Cl1	8303.4(18)	9221.6(8)	5224.7(6)	55.5(6)
Cl2	8748.9(17)	10590.6(10)	5442.5(11)	75.2(8)
O2	5096(2)	793.9(15)	5622.4(11)	17.0(7)
O1	5388(2)	1991.1(15)	7047.9(10)	15.0(6)
N1	5573(3)	1883.8(17)	6079.9(12)	10.2(7)
C8	7046(3)	2651(2)	6635.2(14)	13.3(8)
C9	5750(3)	2206(2)	5574.7(14)	11.7(8)
C10	7232(4)	-173(2)	7113.6(16)	19.2(9)
C12	1593(4)	1214(2)	6626.4(17)	18.6(9)
C13	3733(3)	1157(2)	6354.9(15)	13.8(8)
C14	4751(3)	2244(2)	5250.4(15)	15.8(8)
C15	2958(3)	1196(2)	5987.6(16)	16.7(9)
C16	5484(4)	153(2)	6840.0(17)	20.1(9)
C17	3051(3)	3412(2)	6352.4(17)	19.7(9)
C18	7570(3)	2465(2)	7073.6(16)	16.2(8)
C19	6976(3)	769(2)	6564.5(15)	17.1(9)
C20	3767(3)	2927(2)	6465.8(17)	17.6(9)
C21	9156(3)	3017(2)	6804.6(17)	19.5(9)
C22	4842(3)	3058(2)	6470.8(15)	13.3(8)
C23	7585(3)	3036(2)	6277.3(16)	16.9(9)
C24	1888(4)	1239(2)	6121.4(16)	19.0(9)
C25	3433(3)	1143(2)	6863.2(16)	14.9(8)
C26	8619(4)	2639(2)	7152.8(17)	21.3(10)
C27	5887(4)	2297(2)	4476.8(16)	21(1)
C28	4981(4)	2624(2)	4760.6(16)	20.5(10)
C29	2373(4)	1170(2)	6995.4(17)	19.0(9)
C30	8626(3)	3218(2)	6360.7(16)	18.7(9)
C31	7635(4)	346(2)	6829.5(17)	21.0(9)
C32	3377(4)	4051(3)	6240(2)	26.4(11)
C33	6682(3)	1896(2)	5290.5(16)	16.8(9)
C34	4444(4)	4185(2)	6263(3)	37.1(14)
C35	10298(4)	3207(3)	6886(2)	29.9(12)
C36	437(4)	1226(3)	6775(2)	30.4(12)
C38	6142(4)	-260(2)	7112.0(17)	21.8(10)
C39	6884(4)	2267(3)	4801.2(17)	23.2(10)
C40	5168(4)	3694(2)	6380(2)	28.0(11)
C41	2598(5)	4568(3)	6097(3)	47.0(17)

C42	5897(3)	671(2)	6566.1(15)	13.9(8)
C43	2936(5)	-617(3)	7594(2)	31.4(12)
C44	7766(7)	9981(4)	5417(4)	77(3)

Table F.2 Anisotropic Displacement Parameters ($Å^2 \times 10^3$) for Chzyl-4-*p*-tolyl-PNPO. The Anisotropic displacement factor exponent takes the form: $-2\pi^2[h^2a^{*2}U_{11}+...+2hka \times b \times U_{12}]$

Atom	**U_{11}**	**U_{22}**	**U_{33}**	**U_{23}**	**U_{13}**	**U_{12}**
P1	9.8(5)	12.0(6)	8.7(5)	-0.7(3)	0.3(3)	-1.2(4)
P2	12.0(6)	10.2(5)	11.5(6)	0.1(3)	-0.6(3)	-1.0(4)
Cl1	95.1(15)	39.5(10)	31.9(8)	-5.5(6)	-6.1(8)	11.0(9)
Cl2	53.1(12)	39.9(10)	132(2)	-5.6(11)	29.9(12)	-1.2(9)
O2	23.3(17)	14.0(15)	13.6(14)	-3.9(11)	-1.0(11)	-3.0(12)
O1	15.1(15)	18.3(15)	11.7(13)	0.6(11)	3.3(11)	-3.0(12)
N1	10.3(16)	12.1(16)	8.1(14)	0.8(12)	0.0(11)	-2.5(12)
C8	12.1(19)	16(2)	12.2(18)	-3.5(14)	-0.4(14)	-0.8(15)
C9	12.8(19)	13.4(19)	9.1(17)	1.3(14)	2.2(14)	-1.8(14)
C10	23(2)	16(2)	19(2)	-1.4(16)	-4.8(17)	4.9(17)
C12	15(2)	18(2)	23(2)	-1.7(16)	2.0(16)	-2.9(17)
C13	14.5(19)	11.0(19)	16(2)	0.3(14)	1.2(15)	-2.6(15)
C14	13(2)	21(2)	13.4(19)	1.2(15)	-0.9(15)	2.1(16)
C15	17(2)	18(2)	15.0(18)	3.0(15)	-1.2(16)	-4.7(16)
C16	17(2)	16(2)	27(2)	8.2(17)	-2.1(17)	-1.3(17)
C17	15(2)	20(2)	23(2)	-3.9(17)	3.6(16)	4.6(17)
C18	14(2)	20(2)	14.8(18)	2.6(15)	-1.2(15)	0.1(16)
C19	15(2)	21(2)	15.5(19)	2.1(15)	2.5(15)	2.3(17)
C20	14(2)	15(2)	24(2)	-0.7(17)	-0.5(16)	-2.0(16)
C21	11(2)	24(2)	23(2)	-9.0(18)	-0.2(16)	-3.9(17)
C22	13.5(19)	16(2)	10.8(17)	-0.5(15)	0.0(14)	-0.7(15)
C23	14(2)	22(2)	14.7(19)	0.7(16)	-3.0(15)	-2.4(16)
C24	17(2)	22(2)	18(2)	1.1(16)	-5.1(16)	1.1(17)
C25	16(2)	15(2)	13.8(19)	2.1(14)	-4.2(15)	-1.9(16)
C26	17(2)	28(2)	19(2)	-3.3(17)	-9.5(16)	1.9(18)
C27	32(3)	21(2)	10.2(18)	2.2(16)	3.2(17)	-7.4(19)
C28	25(2)	20(2)	16(2)	4.4(17)	-3.9(16)	-2.0(18)
C29	19(2)	19(2)	19(2)	1.2(16)	2.4(16)	-4.3(17)
C30	14(2)	23(2)	19(2)	-3.0(16)	1.0(16)	-6.5(17)
C31	18(2)	21(2)	24(2)	-0.6(17)	0.8(17)	4.8(18)
C32	25(2)	20(2)	35(3)	2(2)	4(2)	11.8(19)
C33	10.2(19)	24(2)	16.6(19)	-1.5(16)	1.7(15)	-1.1(16)
C34	30(3)	8(2)	73(4)	5(2)	4(3)	-3.9(19)
C35	11(2)	44(3)	35(3)	-10(2)	-5.0(19)	-4(2)
C36	16(2)	40(3)	35(3)	-5(2)	4(2)	0(2)
C38	26(2)	16(2)	23(2)	5.3(17)	-3.5(18)	0.4(18)

C39	24(2)	30(3)	16(2)	-1.6(18)	5.6(17)	-9(2)
C40	16(2)	17(2)	52(3)	0(2)	3(2)	-1.7(18)
C41	36(3)	24(3)	81(5)	17(3)	8(3)	13(3)
C42	16(2)	8.9(19)	16.9(19)	-1.2(14)	-0.8(15)	0.6(15)
C43	37(3)	29(3)	29(3)	0(2)	14(2)	13(2)
C44	65(5)	56(5)	109(7)	-42(5)	43(5)	-17(4)

Table F.3 Bond Lengths for Chzyl-4-*p*-tolyl-PNPO.

Atom	**Atom**	**Length/Å**	**Atom**	**Atom**	**Length/Å**
P1	O1	1.481(3)	C14	C28	1.538(6)
P1	N1	1.690(3)	C15	C24	1.402(6)
P1	C8	1.806(4)	C16	C38	1.386(6)
P1	C22	1.800(4)	C16	C42	1.383(6)
P2	O2	1.497(3)	C17	C20	1.374(6)
P2	N1	1.683(4)	C17	C32	1.397(7)
P2	C13	1.805(4)	C18	C26	1.391(6)
P2	C42	1.805(4)	C19	C31	1.390(6)
Cl1	C44	1.766(8)	C19	C42	1.381(6)
Cl2	C44	1.759(9)	C20	C22	1.388(6)
N1	C9	1.507(5)	C21	C26	1.380(7)
C8	C18	1.390(6)	C21	C30	1.414(6)
C8	C23	1.407(6)	C21	C35	1.512(6)
C9	C14	1.531(6)	C22	C40	1.381(6)
C9	C33	1.535(6)	C23	C30	1.387(6)
C10	C31	1.395(7)	C25	C29	1.388(6)
C10	C38	1.391(7)	C27	C28	1.524(7)
C10	C43[1]	1.488(6)	C27	C39	1.529(7)
C12	C24	1.389(6)	C32	C34	1.379(8)
C12	C29	1.393(6)	C32	C41	1.492(7)
C12	C36	1.515(7)	C33	C39	1.521(6)
C13	C15	1.384(6)	C34	C40	1.391(7)
C13	C25	1.399(6)	C43	C10[2]	1.488(6)

[1]1/2+X,+Y,3/2-Z; [2]-1/2+X,+Y,3/2-Z

Table F.4 Bond Angles for Chzyl-4-*p*-tolyl-PNPO.

Atom	**Atom**	**Atom**	**Angle/°**	**Atom**	**Atom**	**Atom**	**Angle/°**
O1	P1	N1	108.88(17)	C42	C16	C38	120.6(4)
O1	P1	C8	111.40(18)	C20	C17	C32	121.4(4)
O1	P1	C22	113.25(19)	C8	C18	C26	120.9(4)
N1	P1	C8	108.80(18)	C42	C19	C31	120.2(4)
N1	P1	C22	104.85(18)	C17	C20	C22	120.7(4)
C22	P1	C8	109.4(2)	C26	C21	C30	118.9(4)
O2	P2	N1	109.64(17)	C26	C21	C35	121.2(4)
O2	P2	C13	109.31(19)	C30	C21	C35	119.9(4)

O2	P2	C42	109.85(18)	C20	C22	P1	116.1(3)
N1	P2	C13	109.83(18)	C40	C22	P1	125.7(3)
N1	P2	C42	107.70(18)	C40	C22	C20	118.2(4)
C42	P2	C13	110.5(2)	C30	C23	C8	120.2(4)
P2	N1	P1	120.97(19)	C12	C24	C15	120.1(4)
C9	N1	P1	116.4(3)	C29	C25	C13	120.3(4)
C9	N1	P2	121.8(3)	C21	C26	C18	120.8(4)
C18	C8	P1	114.6(3)	C28	C27	C39	111.3(4)
C18	C8	C23	118.8(4)	C27	C28	C14	109.8(4)
C23	C8	P1	126.5(3)	C25	C29	C12	120.8(4)
N1	C9	C14	113.4(3)	C23	C30	C21	120.4(4)
N1	C9	C33	111.7(3)	C19	C31	C10	121.5(4)
C14	C9	C33	112.4(3)	C17	C32	C41	121.1(5)
C31	C10	C43[1]	121.5(5)	C34	C32	C17	117.7(4)
C38	C10	C31	117.2(4)	C34	C32	C41	121.2(5)
C38	C10	C43[1]	121.3(4)	C39	C33	C9	110.1(4)
C24	C12	C29	119.1(4)	C32	C34	C40	120.8(5)
C24	C12	C36	120.6(4)	C16	C38	C10	121.4(4)
C29	C12	C36	120.3(4)	C33	C39	C27	111.0(4)
C15	C13	P2	116.0(3)	C22	C40	C34	121.1(4)
C15	C13	C25	119.0(4)	C16	C42	P2	120.4(3)
C25	C13	P2	125.0(3)	C19	C42	P2	119.5(3)
C9	C14	C28	110.0(3)	C19	C42	C16	119.1(4)
C13	C15	C24	120.7(4)	Cl2	C44	Cl1	110.9(5)

[1]1/2+X,+Y,3/2-Z

Table F.5 Torsion Angles for Chzyl-4-*p*-tolyl-PNPO.

A	**B**	**C**	**D**	**Angle/°**	**A**	**B**	**C**	**D**	**Angle/°**
P1	N1	C9	C14	-113.0(3)	C13	C25	C29	C12	-0.3(7)
P1	N1	C9	C33	118.8(3)	C14	C9	C33	C39	55.3(5)
P1	C8	C18	C26	179.1(4)	C15	C13	C25	C29	-0.2(6)
P1	C8	C23	C30	179.8(3)	C17	C20	C22	P1	-177.0(3)
P1	C22	C40	C34	176.7(5)	C17	C20	C22	C40	2.7(7)
P2	N1	C9	C14	56.8(4)	C17	C32	C34	C40	2.0(9)
P2	N1	C9	C33	-71.5(4)	C18	C8	C23	C30	0.7(6)
P2	C13	C15	C24	-178.8(3)	C20	C17	C32	C34	-2.2(8)
P2	C13	C25	C29	-179.6(3)	C20	C17	C32	C41	177.5(5)
O2	P2	N1	P1	-177.9(2)	C20	C22	C40	C34	-2.9(8)
O2	P2	N1	C9	12.8(4)	C22	P1	N1	P2	-117.2(2)
O2	P2	C13	C15	-29.7(4)	C22	P1	N1	C9	52.7(3)
O2	P2	C13	C25	149.7(3)	C22	P1	C8	C18	126.7(3)
O2	P2	C42	C16	-87.5(4)	C22	P1	C8	C23	-52.5(4)
O2	P2	C42	C19	81.4(4)	C23	C8	C18	C26	-1.8(7)
O1	P1	N1	P2	4.3(3)	C24	C12	C29	C25	-0.8(7)

O1	P1	N1	C9	174.2(3)	C25	C13	C15	C24	1.7(6)
O1	P1	C8	C18	0.7(4)	C26	C21	C30	C23	-0.2(7)
O1	P1	C8	C23	-178.4(4)	C28	C27	C39	C33	58.1(5)
O1	P1	C22	C20	-50.5(4)	C29	C12	C24	C15	2.4(7)
O1	P1	C22	C40	129.9(4)	C30	C21	C26	C18	-0.8(7)
N1	P1	C8	C18	-119.3(3)	C31	C10	C38	C16	-0.1(7)
N1	P1	C8	C23	61.5(4)	C31	C19	C42	P2	-168.2(3)
N1	P1	C22	C20	68.1(4)	C31	C19	C42	C16	0.9(6)
N1	P1	C22	C40	-111.5(4)	C32	C17	C20	C22	-0.1(7)
N1	P2	C13	C15	90.6(4)	C32	C34	C40	C22	0.5(10)
N1	P2	C13	C25	-90.0(4)	C33	C9	C14	C28	-56.3(5)
N1	P2	C42	C16	153.1(3)	C35	C21	C26	C18	-179.8(5)
N1	P2	C42	C19	-37.9(4)	C35	C21	C30	C23	178.8(4)
N1	C9	C14	C28	175.8(3)	C36	C12	C24	C15	-177.0(4)
N1	C9	C33	C39	-175.9(3)	C36	C12	C29	C25	178.5(4)
C8	P1	N1	P2	125.9(2)	C38	C10	C31	C19	1.4(7)
C8	P1	N1	C9	-64.2(3)	C38	C16	C42	P2	169.4(4)
C8	P1	C22	C20	-175.4(3)	C38	C16	C42	C19	0.4(7)
C8	P1	C22	C40	5.0(5)	C39	C27	C28	C14	-58.4(5)
C8	C18	C26	C21	1.8(7)	C41	C32	C34	C40	-177.7(6)
C8	C23	C30	C21	0.3(7)	C42	P2	N1	P1	-58.4(3)
C9	C14	C28	C27	56.9(5)	C42	P2	N1	C9	132.3(3)
C9	C33	C39	C27	-55.3(5)	C42	P2	C13	C15	-150.7(3)
C13	P2	N1	P1	62.0(3)	C42	P2	C13	C25	28.7(4)
C13	P2	N1	C9	-107.3(3)	C42	C16	C38	C10	-0.8(7)
C13	P2	C42	C16	33.2(4)	C42	C19	C31	C10	-1.9(7)
C13	P2	C42	C19	-157.9(3)	C43[1]	C10	C31	C19	-178.6(4)
C13	C15	C24	C12	-2.9(7)	C43[1]	C10	C38	C16	180.0(5)

[1]1/2+X,+Y,3/2-Z

Table F.6 Hydrogen Atom Coordinates (Å×10^4) and Isotropic Displacement Parameters (Å^2×10^3) for Chzyl-4-*p*-tolyl-PNPO.

Atom	***x***	***y***	***z***	**U(eq)**
H9	5956	2660	5646	14
H14A	4195	2464	5438	19
H14B	4510	1805	5169	19
H15	3148	1194	5648	20
H16	4758	81	6842	24
H17	2334	3313	6350	24
H18	7215	2221	7317	19
H19	7262	1119	6386	21
H20	3528	2506	6540	21
H23	7243	3169	5984	20
H24	1377	1285	5872	23
H25	3946	1115	7114	18

H26	8963	2500	7444	26
H27A	6034	2542	4171	25
H27B	5681	1856	4381	25
H28A	4355	2631	4550	25
H28B	5168	3074	4841	25
H29	2182	1158	7335	23
H30	8977	3474	6123	22
H31	8362	410	6817	25
H33A	7309	1910	5501	20
H33B	6525	1440	5216	20
H34	4682	4609	6201	45
H35A	10397	3340	7231	45
H35B	10477	3564	6666	45
H35C	10744	2838	6814	45
H36A	27	1402	6501	46
H36B	347	1496	7069	46
H36C	204	788	6848	46
H38	5849	-602	7297	26
H39A	7442	2049	4614	28
H39B	7118	2709	4878	28
H40	5883	3796	6396	34
H41A	1981	4365	5955	71
H41B	2909	4856	5852	71
H41C	2403	4814	6391	71
H43A	3658	-535	7685	47
H43B	2843	-538	7239	47
H43C	2762	-1066	7669	47
H44A	7220	10114	5181	92
H44B	7445	9933	5748	92

G. Crystal data of *fac*-[Re(*p*Tol-PhPNP)(CO)$_3$(O^{i}Pr)]

Table G.1 Fractional Atomic Coordinates ($\times 10^4$) and Equivalent Isotropic Displacement Parameters ($Å^2 \times 10^3$) for *fac*-[Re(*p*Tol-PhPNP)(CO)$_3$(O^{i}Pr)]. U_{eq} is defined as 1/3 of of the trace of the orthogonalised U_{IJ} tensor.

Atom	***x***	***y***	***z***	**U(eq)**
C1	8133(4)	3077.9(18)	1026.8(19)	21.0(6)
C2	6682(4)	3094(2)	601(2)	30.1(8)
C3	6042(5)	3651(2)	66(2)	38.5(10)
C4	6831(5)	4198(2)	-59(2)	37.4(9)
C5	8282(5)	4174(2)	368(3)	37.0(9)
C6	8936(4)	3624.3(19)	911(2)	29.5(8)
C10	6121(6)	4801(3)	-648(3)	58.4(15)
C7	10328(4)	1139.4(19)	3987(2)	23.8(7)
C8	10929(4)	367.8(19)	2857(2)	24.1(7)

C9	11894(3)	1726.1(19)	3295.7(19)	22.3(6)
C11	7361(3)	2694.9(17)	2655(2)	19.8(6)
C12	6919(4)	2217(2)	3093(2)	28.4(7)
C13	5700(4)	2361(2)	3199(3)	40.3(10)
C14	4922(4)	2964(2)	2860(3)	39.8(10)
C15	5355(4)	3447(2)	2432(3)	35.3(9)
C16	6579(4)	3316(2)	2334(2)	27.1(7)
C21	10087(3)	3277.4(17)	3054.4(18)	18.0(6)
C22	9841(4)	3700.8(18)	3607(2)	23.8(7)
C23	10716(4)	4277(2)	3970(2)	29.2(8)
C24	11843(4)	4434.8(19)	3784(2)	26.4(7)
C25	12098(4)	4011.3(19)	3241(2)	27.0(7)
C26	11232(3)	3430.6(19)	2879(2)	23.1(7)
C31	10886(3)	1832.4(18)	1179.0(19)	20.5(6)
C36	10761(4)	2273(2)	534(2)	29.0(8)
C35	11874(5)	2324(2)	307(3)	38.5(9)
C34	13092(4)	1933(2)	708(3)	37.4(9)
C33	13219(4)	1485(3)	1335(3)	36.4(9)
C32	12118(4)	1439(2)	1573(2)	28.7(8)
C41	8074(3)	1293.1(16)	619.5(19)	17.5(6)
C42	8363(4)	952.6(17)	24.7(19)	21.0(6)
C43	7296(4)	592(2)	-602(2)	27.7(7)
C44	5948(4)	567.6(19)	-642(2)	28.1(7)
C45	5649(4)	909.4(19)	-56(2)	26.7(7)
C46	6707(3)	1264.8(17)	579(2)	21.2(6)
N1	8790(3)	2512.3(14)	1611.2(15)	17.1(5)
O1	10562(3)	1055.0(16)	4647.2(16)	36.7(6)
O2	11528(3)	-141.7(15)	2861.8(17)	37.9(6)
O3	12995(3)	1963.7(16)	3587.9(17)	35.4(6)
O4	7925(2)	897.5(13)	2358.3(14)	24.5(5)
P1	9006.4(8)	2501.0(4)	2593.0(5)	15.68(15)
P2	9461.3(8)	1707.5(4)	1487.1(5)	15.78(15)
Re01	10054.4(2)	1301.6(2)	2870.0(2)	16.25(5)
C1B	6210(3)	260.0(17)	2356.6(18)	17.5(5)
C1A	7403(3)	428.6(16)	2645.8(16)	20.7(6)
C1C	8349(3)	73.4(18)	3328.4(18)	27.4(7)

Table G.2 Anisotropic Displacement Parameters ($Å^2 \times 10^3$) for *fac*-[Re(*p*Tol-PhPNP)$(CO)_3$(O^iPr)]. The Anisotropic displacement factor exponent takes the form: $-2\pi^2[h^2a^{*2}U_{11}+...+2hka\times b\times U_{12}]$

Atom	**U_{11}**	**U_{22}**	**U_{33}**	**U_{23}**	**U_{13}**	**U_{12}**
C1	27.5(16)	18.2(16)	18.4(14)	-1.3(12)	10.9(13)	4.2(13)
C2	28.4(18)	25.3(18)	29.1(18)	-0.7(14)	4.8(15)	2.6(14)
C3	39(2)	37(2)	27.5(19)	-0.6(16)	1.8(17)	10.8(17)
C4	59(3)	31(2)	25.5(18)	6.2(15)	20.1(18)	18.8(19)

C5	56(3)	24.3(19)	45(2)	10.5(17)	35(2)	11.2(18)
C6	31.6(19)	23.7(18)	39(2)	3.1(15)	20.6(17)	4.2(14)
C10	87(4)	49(3)	44(3)	24(2)	32(3)	36(3)
C7	25.6(17)	19.2(16)	26.5(17)	-2.2(13)	10.9(14)	-3.1(13)
C8	25.4(16)	24.3(17)	20.5(15)	0.4(13)	7.5(13)	0.3(13)
C9	21.8(16)	25.8(17)	21.3(15)	2.2(13)	10.9(13)	2.6(13)
C11	15.8(14)	20.4(16)	24.7(15)	-5.6(12)	9.8(12)	-1.7(12)
C12	27.7(18)	24.4(18)	40(2)	-2.7(15)	21.1(16)	-2.9(14)
C13	38(2)	35(2)	64(3)	-2(2)	38(2)	-5.4(17)
C14	25.4(19)	41(2)	63(3)	-11(2)	28(2)	-3.2(16)
C15	25.5(18)	33(2)	47(2)	-5.1(18)	14.9(17)	7.0(16)
C16	24.3(17)	27.1(18)	31.7(18)	-2.9(14)	13.5(15)	1.1(14)
C21	16.9(14)	17.7(15)	17.5(14)	-1.3(11)	5.2(12)	-2.2(11)
C22	28.1(17)	23.1(17)	23.2(16)	-4.0(12)	13.8(14)	-6.6(13)
C23	35.9(19)	26.5(18)	25.6(17)	-9.2(14)	13.3(15)	-7.4(15)
C24	23.8(16)	18.4(16)	30.2(18)	-2.5(13)	4.7(14)	-5.6(13)
C25	18.3(15)	23.4(18)	37.2(19)	-2.0(15)	9.5(14)	-4.7(13)
C26	19.3(15)	21.5(16)	30.0(17)	-5.2(13)	11.7(13)	-2.5(13)
C31	16.9(14)	22.6(16)	23.1(15)	-5.4(12)	9.7(12)	-2.2(12)
C36	29.4(18)	24.4(18)	41(2)	5.4(15)	22.2(16)	4.3(14)
C35	45(2)	30(2)	57(3)	5.6(18)	38(2)	1.1(17)
C34	31.3(19)	41(2)	53(2)	-6.5(19)	31.0(19)	-4.7(17)
C33	20.0(17)	52(2)	37(2)	-5.2(19)	12.1(16)	7.5(17)
C32	23.5(17)	38(2)	24.7(17)	0.5(15)	10.3(14)	6.6(15)
C41	18.5(15)	14.8(15)	16.8(14)	0.1(11)	5.1(12)	-0.3(11)
C42	25.3(16)	19.0(16)	18.4(14)	0.9(12)	8.8(13)	-0.8(12)
C43	36.4(19)	26.3(18)	17.7(15)	-2.8(13)	8.6(14)	-1.3(15)
C44	28.7(17)	22.9(17)	21.5(16)	-1.9(13)	-0.5(14)	-3.8(14)
C45	18.9(15)	23.9(17)	29.0(17)	0.4(14)	1.9(13)	-0.9(13)
C46	19.0(15)	18.4(16)	23.6(16)	-0.1(12)	6.3(13)	0.7(11)
N1	17.7(12)	15.7(13)	18.1(12)	-1.5(10)	7.7(10)	0.2(10)
O1	49.7(17)	41.0(16)	23.9(13)	-1.9(12)	19.8(12)	-6.9(14)
O2	45.4(16)	27.9(15)	38.7(15)	0.6(12)	16.0(13)	12.0(13)
O3	21.5(13)	41.6(16)	38.5(15)	1.9(12)	7.9(11)	-1.3(11)
O4	22.8(12)	23.4(12)	25.2(12)	0.5(10)	7.9(10)	-3.0(9)
P1	14.0(3)	15.3(4)	18.5(4)	-2.7(3)	7.5(3)	-2.3(3)
P2	14.3(3)	16.0(4)	16.9(3)	-2.1(3)	6.4(3)	-0.2(3)
Re01	16.34(7)	15.02(7)	17.30(7)	-1.11(4)	6.96(5)	-0.63(4)
C1B	16.5(10)	16.6(14)	20.1(13)	-4.9(11)	8.3(9)	-8.4(11)
C1A	18.9(11)	20.4(15)	22.2(14)	-5.6(11)	8(1)	-7.8(11)
C1C	23.2(14)	28.2(18)	23.6(15)	6.5(12)	2.8(10)	-17.7(13)

Table G.3 Bond Lengths for *fac*-[Re(*p*Tol-PhPNP)$(CO)_3(O^iPr)$].

Atom	Atom	Length/Å	Atom	Atom	Length/Å
C1	C2	1.386(5)	C23	C24	1.389(5)
C1	C6	1.389(5)	C24	C25	1.378(5)
C1	N1	1.450(4)	C25	C26	1.386(5)
C2	C3	1.388(5)	C31	C36	1.397(5)
C3	C4	1.388(6)	C31	C32	1.391(5)
C4	C5	1.386(6)	C31	P2	1.816(3)
C4	C10	1.514(6)	C36	C35	1.393(5)
C5	C6	1.388(5)	C35	C34	1.380(6)
C7	O1	1.139(4)	C34	C33	1.379(6)
C7	Re01	1.964(4)	C33	C32	1.393(5)
C8	O2	1.133(4)	C41	C42	1.397(4)
C8	Re01	1.967(4)	C41	C46	1.401(5)
C9	O3	1.136(4)	C41	P2	1.813(3)
C9	Re01	1.917(3)	C42	C43	1.392(5)
C11	C12	1.399(5)	C43	C44	1.382(5)
C11	C16	1.393(5)	C44	C45	1.390(5)
C11	P1	1.808(3)	C45	C46	1.390(5)
C12	C13	1.394(5)	N1	P1	1.714(3)
C13	C14	1.371(6)	N1	P2	1.707(3)
C14	C15	1.385(6)	O4	Re01	2.157(3)
C15	C16	1.387(5)	O4	C1A	1.255(4)
C21	C22	1.387(4)	P1	Re01	2.4412(10)
C21	C26	1.394(4)	P2	Re01	2.4571(10)
C21	P1	1.808(3)	C1B	C1A	1.175(4)
C22	C23	1.384(5)	C1A	C1C	1.3918(11)

Table G.4 Bond Angles for *fac*-[Re(*p*Tol-PhPNP)$(CO)_3(O^iPr)$].

Atom	Atom	Atom	Angle/°	Atom	Atom	Atom	Angle/°
C2	C1	C6	119.2(3)	C43	C42	C41	119.9(3)
C2	C1	N1	119.9(3)	C44	C43	C42	120.5(3)
C6	C1	N1	120.8(3)	C43	C44	C45	120.0(3)
C1	C2	C3	120.2(4)	C44	C45	C46	120.2(3)
C2	C3	C4	121.3(4)	C45	C46	C41	120.0(3)
C3	C4	C10	120.7(4)	C1	N1	P1	126.5(2)
C5	C4	C3	117.9(4)	C1	N1	P2	129.1(2)
C5	C4	C10	121.3(4)	P2	N1	P1	104.34(14)
C4	C5	C6	121.5(4)	C1A	O4	Re01	127.7(2)
C5	C6	C1	119.9(4)	C11	P1	C21	103.68(15)
O1	C7	Re01	176.3(3)	C11	P1	Re01	121.69(11)
O2	C8	Re01	174.6(3)	C21	P1	Re01	119.55(11)
O3	C9	Re01	176.3(3)	N1	P1	C11	110.63(14)
C12	C11	P1	117.5(3)	N1	P1	C21	105.16(14)

C16	C11	C12	119.4(3)	N1	P1	Re01	94.54(9)
C16	C11	P1	123.0(3)	C31	P2	Re01	118.24(11)
C13	C12	C11	120.0(4)	C41	P2	C31	104.02(15)
C14	C13	C12	119.9(4)	C41	P2	Re01	122.33(11)
C13	C14	C15	120.8(3)	N1	P2	C31	111.49(14)
C14	C15	C16	119.8(4)	N1	P2	C41	105.40(14)
C15	C16	C11	120.1(4)	N1	P2	Re01	94.14(9)
C22	C21	C26	119.5(3)	C7	Re01	C8	90.68(14)
C22	C21	P1	121.5(2)	C7	Re01	O4	94.09(12)
C26	C21	P1	119.0(2)	C7	Re01	P1	102.29(10)
C23	C22	C21	120.1(3)	C7	Re01	P2	169.11(10)
C22	C23	C24	120.2(3)	C8	Re01	O4	95.09(12)
C25	C24	C23	119.8(3)	C8	Re01	P1	166.84(10)
C24	C25	C26	120.3(3)	C8	Re01	P2	100.13(10)
C25	C26	C21	120.1(3)	C9	Re01	C7	87.53(14)
C36	C31	P2	122.6(3)	C9	Re01	C8	88.58(14)
C32	C31	C36	118.9(3)	C9	Re01	O4	175.96(12)
C32	C31	P2	118.3(3)	C9	Re01	P1	89.74(11)
C35	C36	C31	119.8(4)	C9	Re01	P2	93.95(10)
C34	C35	C36	120.5(4)	O4	Re01	P1	86.31(7)
C33	C34	C35	120.3(3)	O4	Re01	P2	83.76(7)
C34	C33	C32	119.5(4)	P1	Re01	P2	66.96(3)
C31	C32	C33	120.9(4)	O4	C1A	C1C	115.8(3)
C42	C41	C46	119.4(3)	C1B	C1A	O4	124.2(3)
C42	C41	P2	121.3(2)	C1B	C1A	C1C	119.9(3)
C46	C41	P2	119.1(2)				

Table G.5 Torsion Angles for *fac*-[Re(*p*Tol-PhPNP)$(CO)_3$(O^iPr)].

A	**B**	**C**	**D**	**Angle/°**	**A**	**B**	**C**	**D**	**Angle/°**
C1	C2	C3	C4	0.2(6)	C31	C36	C35	C34	1.0(6)
C1	N1	P1	C11	50.7(3)	C36	C31	C32	C33	0.5(6)
C1	N1	P1	C21	-60.7(3)	C36	C31	P2	C41	62.4(3)
C1	N1	P1	Re01	177.0(2)	C36	C31	P2	N1	-50.7(3)
C1	N1	P2	C31	60.5(3)	C36	C31	P2	Re01	-158.1(3)
C1	N1	P2	C41	-51.8(3)	C36	C35	C34	C33	0.3(7)
C1	N1	P2	Re01	-177.0(3)	C35	C34	C33	C32	-1.2(7)
C2	C1	C6	C5	-0.6(5)	C34	C33	C32	C31	0.8(6)
C2	C1	N1	P1	-83.8(4)	C32	C31	C36	C35	-1.4(6)
C2	C1	N1	P2	93.9(4)	C32	C31	P2	C41	-113.7(3)
C2	C3	C4	C5	0.0(6)	C32	C31	P2	N1	133.2(3)
C2	C3	C4	C10	179.8(4)	C32	C31	P2	Re01	25.8(3)
C3	C4	C5	C6	-0.5(6)	C41	C42	C43	C44	0.1(5)
C4	C5	C6	C1	0.8(6)	C42	C41	C46	C45	-1.0(5)
C6	C1	C2	C3	0.1(5)	C42	C41	P2	C31	19.1(3)

C6	C1	N1	P1	93.4(4)	C42	C41	P2	N1	136.5(3)
C6	C1	N1	P2	-89.0(4)	C42	C41	P2	Re01	-118.2(2)
C10	C4	C5	C6	179.7(4)	C42	C43	C44	C45	0.4(5)
C11	C12	C13	C14	1.3(6)	C43	C44	C45	C46	-1.1(5)
C12	C11	C16	C15	-1.6(5)	C44	C45	C46	C41	1.4(5)
C12	C11	P1	C21	-119.3(3)	C46	C41	C42	C43	0.2(5)
C12	C11	P1	N1	128.4(3)	C46	C41	P2	C31	-166.0(3)
C12	C11	P1	Re01	19.0(3)	C46	C41	P2	N1	-48.6(3)
C12	C13	C14	C15	-2.0(7)	C46	C41	P2	Re01	56.6(3)
C13	C14	C15	C16	0.8(7)	N1	C1	C2	C3	177.3(3)
C14	C15	C16	C11	1.0(6)	N1	C1	C6	C5	-177.8(3)
C16	C11	C12	C13	0.5(5)	P1	C11	C12	C13	176.4(3)
C16	C11	P1	C21	56.4(3)	P1	C11	C16	C15	-177.3(3)
C16	C11	P1	N1	-55.9(3)	P1	C21	C22	C23	177.8(3)
C16	C11	P1	Re01	-165.3(2)	P1	C21	C26	C25	-178.3(3)
C21	C22	C23	C24	0.0(6)	P1	N1	P2	C31	-121.51(15)
C22	C21	C26	C25	-1.4(5)	P1	N1	P2	C41	126.24(15)
C22	C21	P1	C11	24.5(3)	P1	N1	P2	Re01	1.06(12)
C22	C21	P1	N1	140.7(3)	P2	C31	C36	C35	-177.4(3)
C22	C21	P1	Re01	-115.0(3)	P2	C31	C32	C33	176.7(3)
C22	C23	C24	C25	-0.6(6)	P2	C41	C42	C43	175.0(3)
C23	C24	C25	C26	0.2(6)	P2	C41	C46	C45	-175.9(3)
C24	C25	C26	C21	0.8(5)	P2	N1	P1	C11	-127.44(15)
C26	C21	C22	C23	1.0(5)	P2	N1	P1	C21	121.22(15)
C26	C21	P1	C11	-158.7(3)	P2	N1	P1	Re01	-1.07(12)
C26	C21	P1	N1	-42.5(3)	Re01	O4	C1A	C1B	175.7(3)
C26	C21	P1	Re01	61.9(3)	Re01	O4	C1A	C1C	-7.7(4)

Table G.6 Hydrogen Atom Coordinates (Å×10^4) and Isotropic Displacement Parameters (Å^2×10^3) for *fac*-[Re(*p*Tol-PhPNP)$(CO)_3$(O^iPr)].

Atom	***x***	***y***	***z***	**U(eq)**
H2	6134	2732	675	36
H3	5067	3657	-215	46
H5	8829	4534	290	44
H6	9910	3622	1197	35
H10A	5137	4811	-764	88
H10B	6231	4721	-1137	88
H10C	6544	5252	-415	88
H12	7438	1803	3313	34
H13	5415	2049	3499	48
H14	4094	3051	2919	48
H15	4825	3857	2211	42
H16	6878	3643	2054	33
H22	9088	3597	3734	29

H23	10549	4560	4341	35
H24	12423	4825	4024	32
H25	12854	4116	3117	32
H26	11415	3143	2518	28
H36	9937	2532	256	35
H35	11795	2623	-117	46
H34	13831	1972	553	45
H33	14033	1215	1598	44
H32	12209	1142	2000	34
H42	9268	967	47	25
H43	7491	365	-997	33
H44	5241	323	-1060	34
H45	4738	900	-88	32
H46	6509	1484	977	25
H1BA	5587	479	1884	21
H1BB	5890	-92	2600	21
H1CA	9265	71	3326	41
H1CB	8038	-413	3329	41
H1CC	8396	317	3802	41

H. Crystal data of *fac*-[Re(*p*ClPh-PhPNP)(CO)$_3$Br]

Table H.1 Fractional Atomic Coordinates ($\times 10^4$) and Equivalent Isotropic Displacement Parameters ($Å^2 \times 10^3$) for *fac*-[Re(*p*ClPh-PhPNP)(CO)$_3$Br]. U_{eq} is defined as 1/3 of of the trace of the orthogonalised U_{IJ} tensor.

Atom	***x***	***y***	***z***	**U(eq)**
C1	1239(3)	2808(2)	3375.0(14)	17.7(6)
C6	147(3)	3187(2)	3548.9(15)	21.1(6)
C5	-549(3)	2777(2)	4049.6(15)	23.5(7)
C4	-161(3)	1984(2)	4373.4(15)	23.1(7)
C3	919(3)	1598(2)	4207.3(15)	24.0(7)
C2	1609(3)	2010(2)	3707.2(14)	21.2(6)
C8	3062(3)	4574(2)	724.6(17)	25.2(7)
C7	4733(3)	5110(2)	1779.5(15)	22.7(7)
C9	2347(5)	5380(3)	1961(4)	22.5(12)
C31	114(3)	3463(2)	1850.3(14)	17.9(6)
C32	-326(3)	4334(2)	1716.9(16)	23.5(7)
C33	-1539(3)	4473(2)	1652.2(18)	30.3(8)
C34	-2315(3)	3744(2)	1713.6(16)	26.3(7)
C35	-1882(3)	2877(2)	1849.5(15)	22.9(7)
C36	-672(3)	2738(2)	1923.2(15)	20.1(6)
C41	1880(3)	2124(2)	1615.5(14)	19.8(6)
C42	1480(3)	1954(2)	929.7(16)	28.4(7)
C43	1699(3)	1128(3)	612.8(19)	38.6(9)
C44	2299(4)	448(3)	976(2)	43.4(10)

C45	2703(4)	612(3)	1656(2)	44.8(10)
C46	2501(3)	1446(2)	1967.3(17)	32.4(8)
C11	4334(3)	3213(2)	3417.0(14)	19.2(6)
C16	4152(3)	2862(2)	4091.5(15)	25.6(7)
C15	5018(3)	2335(2)	4423.7(17)	30.8(8)
C14	6084(3)	2186(2)	4095.9(18)	33.1(8)
C13	6299(3)	2559(2)	3443.9(17)	32.1(8)
C12	5423(3)	3067(2)	3104.4(16)	26.5(7)
C21	2949(3)	4776(2)	3619.5(14)	18.9(6)
C22	3929(3)	5141(2)	3972.7(16)	29.4(8)
C23	3809(3)	5889(2)	4411.8(18)	34.0(8)
C24	2713(3)	6266(2)	4513.3(17)	32.8(8)
C25	1728(3)	5902(2)	4171.2(18)	32.8(8)
C26	1846(3)	5168(2)	3715.6(16)	25.9(7)
N1	1961(2)	3252.2(17)	2854.4(12)	18.1(5)
O2	2940(2)	4691.6(18)	135.7(12)	39.4(6)
O3	1808(15)	5992(8)	2084(9)	23.1(15)
O1	5572(2)	5535.1(16)	1815.8(13)	33.7(6)
P2	1694.0(7)	3275.0(5)	1963.2(4)	16.88(16)
P1	3220.9(7)	3892.4(5)	2968.4(4)	16.98(16)
Cl1	-1026.4(8)	1467.8(6)	5009.5(4)	34.0(2)
Br1A	4599.0(12)	2953.3(9)	1350.2(9)	23.05(15)
Br1	1991(5)	5774(3)	2052(3)	31.4(4)
Re1	3296.8(2)	4352.7(2)	1735.2(2)	16.53(4)
C9A	4266(10)	3349(6)	1475(6)	34(3)
O3A	4778(18)	2770(11)	1270(13)	33(4)

Table H.2 Anisotropic Displacement Parameters ($Å^2 \times 10^3$) for *fac*-[Re(*p*ClPh-PhPNP)$(CO)_3$Br]. The Anisotropic displacement factor exponent takes the form: $-2\pi^2[h^2a^{*2}U_{11}+...+2hka\times b\times U_{12}]$

Atom	$\mathbf{U_{11}}$	$\mathbf{U_{22}}$	$\mathbf{U_{33}}$	$\mathbf{U_{23}}$	$\mathbf{U_{13}}$	$\mathbf{U_{12}}$
C1	18.6(15)	21.1(16)	13.3(12)	-3.1(11)	-0.8(11)	-5.0(13)
C6	22.5(16)	21.6(16)	19.2(14)	0.5(12)	-2.7(12)	0.3(13)
C5	21.2(16)	30.6(18)	18.8(14)	-1.5(13)	1.6(12)	-3.5(14)
C4	25.9(17)	27.3(17)	16.1(13)	0.8(12)	-0.2(12)	-10.8(14)
C3	29.1(18)	22.8(17)	19.9(14)	3.1(12)	-2.4(13)	-4.2(14)
C2	22.2(16)	20.7(16)	20.6(14)	-3.1(12)	-0.3(12)	-0.4(13)
C8	21.7(17)	26.1(18)	27.6(17)	2.0(13)	1.1(13)	-0.7(14)
C7	23.8(17)	23.9(17)	20.5(14)	0.5(12)	0.5(13)	-1.9(14)
C9	17(4)	21(4)	29(3)	1(3)	-7(3)	-11(3)
C31	20.1(16)	19.2(15)	14.5(13)	-1.9(11)	1.6(11)	0.0(12)
C32	21.5(16)	18.6(16)	30.6(16)	0.5(13)	4.8(13)	-2.0(13)
C33	25.0(18)	23.2(18)	43(2)	6.8(14)	5.8(15)	5.7(14)
C34	15.5(16)	32.6(19)	30.9(16)	0.7(14)	4.8(13)	2.1(14)
C35	22.0(17)	21.0(16)	25.8(15)	0.4(12)	4.2(13)	-6.3(13)

C36	19.6(16)	19.2(16)	21.5(14)	0.7(12)	0.4(12)	-1.8(13)
C41	17.9(15)	22.4(16)	19.2(14)	-3.2(12)	1.7(12)	-0.8(13)
C42	28.0(18)	34.9(19)	22.2(15)	-7.1(14)	-2.5(13)	2.4(16)
C43	36(2)	46(2)	34.3(19)	-19.0(17)	-1.4(16)	0.0(18)
C44	50(3)	34(2)	46(2)	-19.2(18)	9.8(19)	3.7(19)
C45	62(3)	32(2)	41(2)	-3.1(17)	8.8(19)	20(2)
C46	46(2)	29.3(19)	21.9(15)	-3.8(14)	-0.1(15)	12.2(17)
C11	20.5(16)	20.7(16)	16.3(13)	-3.1(11)	-2.6(12)	-1.3(13)
C16	25.6(18)	29.4(18)	21.7(15)	-0.7(13)	-0.5(13)	-6.1(15)
C15	38(2)	31.3(19)	22.5(15)	2.4(14)	-8.4(14)	-5.3(16)
C14	34(2)	25.8(19)	39.6(19)	-3.7(15)	-15.9(16)	6.8(16)
C13	24.2(18)	38(2)	33.9(18)	-10.2(16)	-3.3(15)	10.6(16)
C12	26.1(18)	31.3(18)	21.9(15)	-5.4(13)	-0.6(13)	2.8(15)
C21	21.5(16)	16.9(15)	18.3(13)	1.1(12)	2.5(12)	-1.9(13)
C22	29.3(19)	29.6(19)	29.3(17)	-9.4(14)	2.1(14)	1.2(15)
C23	41(2)	30.1(19)	30.9(18)	-9.6(15)	-3.0(16)	-2.7(17)
C24	55(2)	19.2(17)	24.2(16)	-2.2(13)	6.1(16)	-0.6(17)
C25	37(2)	22.2(18)	39.7(19)	1.6(15)	11.5(16)	12.0(16)
C26	26.1(18)	22.1(17)	29.6(16)	1.3(13)	2.5(14)	1.9(14)
N1	17.5(13)	21.1(13)	15.9(11)	-1.4(10)	-1(1)	-5.4(11)
O2	45.3(16)	51.0(16)	21.8(12)	5.0(11)	-4.9(11)	-1.8(13)
O3	14(4)	22(5)	34(3)	-7(4)	-1(3)	-7(3)
O1	23.5(13)	32.4(14)	45.2(14)	2.2(11)	-3.6(11)	-7.6(11)
P2	16.6(4)	18.8(4)	15.2(3)	-0.2(3)	-0.9(3)	-1.7(3)
P1	16.2(4)	18.9(4)	15.8(3)	-2.1(3)	0.9(3)	-2.2(3)
Cl1	30.9(5)	45.6(5)	25.7(4)	12.2(4)	4.4(3)	-8.8(4)
Br1A	19.4(4)	28.0(5)	21.8(6)	-9.0(4)	3.5(3)	1.5(3)
Br1	34(2)	27(2)	32.8(13)	4.1(14)	-1.3(12)	-2.2(11)
Re1	15.72(6)	18.23(7)	15.65(6)	-0.01(4)	0.78(4)	-1.52(5)
C9A	44(8)	37(8)	23(5)	-8(5)	-2(5)	3(6)
O3A	46(9)	41(9)	12(5)	-12(5)	11(5)	4(5)

Table H.3 Bond Lengths for *fac*-[Re(*p*ClPh-PhPNP)$(CO)_3$Br].

Atom	**Atom**	**Length/Å**	**Atom**	**Atom**	**Length/Å**
C1	C6	1.396(4)	C43	C44	1.383(5)
C1	C2	1.389(4)	C44	C45	1.386(5)
C1	N1	1.446(4)	C45	C46	1.376(5)
C6	C5	1.381(4)	C11	C16	1.399(4)
C5	C4	1.380(4)	C11	C12	1.390(4)
C4	C3	1.384(4)	C11	P1	1.807(3)
C4	Cl1	1.739(3)	C16	C15	1.389(5)
C3	C2	1.377(4)	C15	C14	1.381(5)
C8	O2	1.139(4)	C14	C13	1.379(5)
C8	Re1	1.963(3)	C13	C12	1.388(5)

C7	O1	1.135(4)	C21	C22	1.391(4)
C7	Re1	1.964(3)	C21	C26	1.386(4)
C9	O3	1.108(2)	C21	P1	1.818(3)
C9	Br1	0.725(3)	C22	C23	1.385(4)
C9	Re1	1.899(2)	C23	C24	1.370(5)
C31	C32	1.390(4)	C24	C25	1.387(5)
C31	C36	1.392(4)	C25	C26	1.388(5)
C31	P2	1.814(3)	N1	P2	1.717(2)
C32	C33	1.388(4)	N1	P1	1.714(3)
C33	C34	1.385(5)	P2	Re1	2.4431(10)
C34	C35	1.382(4)	P1	Re1	2.4425(9)
C35	C36	1.387(4)	Br1A	Re1	2.6300(12)
C41	C42	1.396(4)	Br1A	C9A	0.732(3)
C41	C46	1.380(4)	Br1	Re1	2.6237(18)
C41	P2	1.822(3)	Re1	C9A	1.900(2)
C42	C43	1.373(5)	C9A	O3A	1.100(2)

Table H.4 Bond Angles for *fac*-[Re(*p*ClPh-PhPNP)$(CO)_3$Br].

Atom	**Atom**	**Atom**	**Angle/°**	**Atom**	**Atom**	**Atom**	**Angle/°**
C6	C1	N1	119.5(3)	C1	N1	P2	126.29(19)
C2	C1	C6	119.2(3)	C1	N1	P1	129.34(19)
C2	C1	N1	121.3(3)	P1	N1	P2	104.34(12)
C5	C6	C1	120.3(3)	C31	P2	C41	102.46(14)
C4	C5	C6	119.5(3)	C31	P2	Re1	127.62(10)
C5	C4	C3	121.0(3)	C41	P2	Re1	116.23(10)
C5	C4	Cl1	119.8(2)	N1	P2	C31	106.14(12)
C3	C4	Cl1	119.2(2)	N1	P2	C41	108.70(13)
C2	C3	C4	119.2(3)	N1	P2	Re1	93.89(9)
C3	C2	C1	120.8(3)	C11	P1	C21	101.08(14)
O2	C8	Re1	178.8(3)	C11	P1	Re1	124.83(10)
O1	C7	Re1	178.5(3)	C21	P1	Re1	117.82(10)
O3	C9	Re1	178.4(14)	N1	P1	C11	109.24(13)
Br1	C9	O3	1.8(12)	N1	P1	C21	109.04(13)
Br1	C9	Re1	179.1(8)	N1	P1	Re1	94.00(8)
C32	C31	C36	119.3(3)	C9A	Br1A	Re1	3.8(10)
C32	C31	P2	120.6(2)	C9	Br1	Re1	0.7(6)
C36	C31	P2	120.0(2)	C8	Re1	C7	92.79(13)
C33	C32	C31	120.0(3)	C8	Re1	P2	100.97(10)
C34	C33	C32	120.3(3)	C8	Re1	P1	168.32(10)
C35	C34	C33	120.0(3)	C8	Re1	Br1A	85.62(10)
C34	C35	C36	119.9(3)	C8	Re1	Br1	91.49(15)
C35	C36	C31	120.5(3)	C7	Re1	P2	165.72(9)
C42	C41	P2	117.8(2)	C7	Re1	P1	98.90(9)
C46	C41	C42	118.7(3)	C7	Re1	Br1A	89.21(10)

C46	C41	P2	123.2(2)	C7	Re1	Br1	90.57(18)
C43	C42	C41	120.6(3)	C9	Re1	C8	91.3(2)
C42	C43	C44	120.2(3)	C9	Re1	C7	90.7(2)
C43	C44	C45	119.6(3)	C9	Re1	P2	92.8(2)
C46	C45	C44	120.0(4)	C9	Re1	P1	88.4(2)
C45	C46	C41	120.9(3)	C9	Re1	Br1	0.2(2)
C16	C11	P1	121.6(2)	C9	Re1	C9A	177.7(5)
C12	C11	C16	118.6(3)	P2	Re1	Br1A	88.05(5)
C12	C11	P1	119.7(2)	P2	Re1	Br1	92.87(15)
C15	C16	C11	120.6(3)	P1	Re1	P2	67.38(3)
C14	C15	C16	119.6(3)	P1	Re1	Br1A	94.61(5)
C13	C14	C15	120.6(3)	P1	Re1	Br1	88.29(12)
C14	C13	C12	119.8(3)	C9A	Re1	C8	86.7(4)
C13	C12	C11	120.8(3)	C9A	Re1	C7	88.2(4)
C22	C21	P1	117.4(2)	C9A	Re1	P2	88.8(4)
C26	C21	C22	119.1(3)	C9A	Re1	P1	93.8(4)
C26	C21	P1	123.0(2)	C9A	Re1	Br1A	1.5(4)
C23	C22	C21	120.7(3)	C9A	Re1	Br1	177.7(4)
C24	C23	C22	119.9(3)	Br1A	C9A	Re1	174.8(14)
C23	C24	C25	120.0(3)	Br1A	C9A	O3A	2.3(14)
C24	C25	C26	120.4(3)	O3A	C9A	Re1	174(2)
C21	C26	C25	119.8(3)				

Table H.5 Torsion Angles for *fac*-[Re(*p*ClPh-PhPNP)$(CO)_3$Br].

A	**B**	**C**	**D**	**Angle**/°	**A**	**B**	**C**	**D**	**Angle**/°
C1	C6	C5	C4	-0.5(4)	C16	C11	C12	C13	2.0(5)
C1	N1	P2	C31	41.6(3)	C16	C11	P1	C21	53.8(3)
C1	N1	P2	C41	-67.9(3)	C16	C11	P1	N1	-61.0(3)
C1	N1	P2	Re1	172.7(2)	C16	C11	P1	Re1	-170.5(2)
C1	N1	P1	C11	58.3(3)	C16	C15	C14	C13	0.3(5)
C1	N1	P1	C21	-51.3(3)	C15	C14	C13	C12	-1.9(5)
C1	N1	P1	Re1	-172.6(2)	C14	C13	C12	C11	0.7(5)
C6	C1	C2	C3	-0.7(4)	C12	C11	C16	C15	-3.7(5)
C6	C1	N1	P2	-72.7(3)	C12	C11	P1	C21	-123.0(3)
C6	C1	N1	P1	105.1(3)	C12	C11	P1	N1	122.1(3)
C6	C5	C4	C3	0.4(5)	C12	C11	P1	Re1	12.7(3)
C6	C5	C4	Cl1	179.5(2)	C21	C22	C23	C24	1.4(5)
C5	C4	C3	C2	-0.5(5)	C22	C21	C26	C25	-1.3(5)
C4	C3	C2	C1	0.6(4)	C22	C21	P1	C11	42.0(3)
C2	C1	C6	C5	0.6(4)	C22	C21	P1	N1	157.0(2)
C2	C1	N1	P2	107.3(3)	C22	C21	P1	Re1	-97.6(2)
C2	C1	N1	P1	-74.9(4)	C22	C23	C24	C25	-0.6(5)
C31	C32	C33	C34	-0.6(5)	C23	C24	C25	C26	-1.2(5)
C32	C31	C36	C35	1.3(4)	C24	C25	C26	C21	2.1(5)

C32	C31	P2	C41	-148.2(2)	C26	C21	C22	C23	-0.4(5)
C32	C31	P2	N1	97.9(2)	C26	C21	P1	C11	-145.8(3)
C32	C31	P2	Re1	-10.3(3)	C26	C21	P1	N1	-30.8(3)
C32	C33	C34	C35	0.9(5)	C26	C21	P1	Re1	74.6(3)
C33	C34	C35	C36	-0.1(5)	N1	C1	C6	C5	-179.4(3)
C34	C35	C36	C31	-1.0(4)	N1	C1	C2	C3	179.4(3)
C36	C31	C32	C33	-0.5(4)	O3	C9	Br1	Re1	-116(77)
C36	C31	P2	C41	34.3(2)	P2	C31	C32	C33	-178.1(2)
C36	C31	P2	N1	-79.7(2)	P2	C31	C36	C35	178.9(2)
C36	C31	P2	Re1	172.13(17)	P2	C41	C42	C43	173.5(3)
C41	C42	C43	C44	1.4(6)	P2	C41	C46	C45	-174.4(3)
C42	C41	C46	C45	-1.3(5)	P2	N1	P1	C11	-123.58(14)
C42	C41	P2	C31	55.6(3)	P2	N1	P1	C21	126.79(14)
C42	C41	P2	N1	167.6(2)	P2	N1	P1	Re1	5.52(12)
C42	C41	P2	Re1	-88.1(3)	P1	C11	C16	C15	179.5(2)
C42	C43	C44	C45	-1.6(6)	P1	C11	C12	C13	179.0(3)
C43	C44	C45	C46	0.3(6)	P1	C21	C22	C23	172.1(3)
C44	C45	C46	C41	1.1(6)	P1	C21	C26	C25	-173.4(2)
C46	C41	C42	C43	0.1(5)	P1	N1	P2	C31	-136.56(14)
C46	C41	P2	C31	-131.3(3)	P1	N1	P2	C41	113.86(15)
C46	C41	P2	N1	-19.2(3)	P1	N1	P2	Re1	-5.52(12)
C46	C41	P2	Re1	85.0(3)	Cl1	C4	C3	C2	-179.5(2)
C11	C16	C15	C14	2.5(5)	Re1	Br1A	C9A	O3A	-77(38)

Table H.6 Hydrogen Atom Coordinates (Å×10^4) and Isotropic Displacement Parameters (Å^2×10^3) for *fac*-[Re(*p*ClPh-PhPNP)$(CO)_3$Br].

Atom	***x***	***y***	***z***	**U(eq)**
H6	-113	3719	3327	25
H5	-1274	3032	4168	28
H3	1175	1067	4431	29
H2	2332	1750	3590	25
H32	192	4825	1671	28
H33	-1832	5058	1567	36
H34	-3126	3839	1663	32
H35	-2403	2388	1892	27
H36	-384	2155	2022	24
H42	1062	2403	685	34
H43	1443	1027	152	46
H44	2430	-117	765	52
H45	3110	158	1903	54
H46	2786	1555	2421	39
H16	3446	2983	4319	31
H15	4880	2083	4864	37
H14	6663	1831	4317	40

H13	7028	2471	3233	39
H12	5567	3312	2663	32
H22	4671	4879	3913	35
H23	4471	6136	4638	41
H24	2631	6765	4812	39
H25	983	6152	4248	39
H26	1187	4939	3475	31

I. Crystal data of *fac*-[Re(*p*FPh-PhPNP)(CO)$_3$Br]

Table I.1 Fractional Atomic Coordinates ($\times 10^4$) and Equivalent Isotropic Displacement Parameters ($Å^2 \times 10^3$) for *fac*-[Re(*p*FPh-PhPNP)(CO)$_3$Br]. U_{eq} is defined as 1/3 of of the trace of the orthogonalised U_{IJ} tensor.

Atom	***x***	***y***	***z***	**U(eq)**
C1	7058(3)	4500(2)	3138.6(15)	17.2(6)
C2	7948(3)	5147(2)	3210.4(19)	25.6(7)
C3	7764(4)	5816(2)	3689(2)	32.5(8)
C4	6682(4)	5818(2)	4076.4(18)	29.3(8)
C5	5769(4)	5192(2)	4021.0(18)	28.9(8)
C6	5963(3)	4529(2)	3543.6(17)	23.0(7)
C7	7144(3)	1826(2)	723.1(17)	19.9(6)
C8	8524(3)	1140(2)	1885.9(18)	22.2(7)
C11	7591(3)	4620.5(19)	1340.8(15)	13.8(5)
C12	8883(3)	4760(2)	1458.6(18)	22.7(7)
C13	9504(3)	5400(2)	1087(2)	32.4(8)
C14	8854(3)	5894(2)	590(2)	27.6(7)
C15	7568(3)	5765(2)	477.4(17)	21.8(7)
C16	6933(3)	5134.4(19)	851.0(15)	16.4(6)
C21	5173(3)	3900.8(19)	1683.8(15)	13.8(5)
C22	4641(3)	4677(2)	1904.8(16)	18.5(6)
C23	3344(3)	4803(2)	1838.1(18)	25.5(7)
C24	2571(3)	4162(2)	1554.0(19)	27.1(7)
C25	3087(3)	3401(2)	1326.6(18)	23.5(7)
C26	4392(3)	3271(2)	1385.2(16)	16.6(6)
C31	7250(3)	2378.0(19)	3588.4(16)	16.3(6)
C32	5929(3)	2384(2)	3595.2(17)	18.7(6)
C33	5280(3)	1941(2)	4117.0(18)	24.0(7)
C34	5952(3)	1472(2)	4624.3(17)	25.0(7)
C35	7261(3)	1456(2)	4621.4(17)	23.7(7)
C36	7913(3)	1909(2)	4107.6(16)	19.1(6)
C41	9614(3)	3130(2)	3242.4(17)	21.9(7)
C42	9714(3)	3545(2)	3904.4(19)	28.3(8)
C43	10908(4)	3694(3)	4208(2)	40.1(10)
C44	11984(4)	3443(4)	3858(2)	51.8(13)
C45	11887(4)	3033(4)	3211(2)	54.5(14)

C46	10702(3)	2874(3)	2897(2)	38(1)
N1	7275(2)	3793.0(16)	2657.9(13)	14.6(5)
O1	6818(3)	1545.3(17)	187.3(13)	32.8(6)
O2	9013(2)	514.1(17)	2036.5(16)	35.6(6)
F5	6490(3)	6472.2(14)	4542.4(12)	42.9(6)
P1	6860.1(7)	3704.0(5)	1772.0(4)	11.88(14)
P2	8074.7(7)	2870.5(5)	2850.8(4)	14.41(15)
Br1	9748.0(3)	2729.8(2)	1028.1(2)	23.80(8)
Re1	7680.8(2)	2224.3(2)	1680.3(2)	13.49(4)
C9	6131(2)	1755.8(18)	2034.8(15)	19.7(7)
O3	5279(3)	1478.8(14)	2201.5(12)	24.6(5)

Table I.2 Anisotropic Displacement Parameters ($Å^2×10^3$) for *fac*-[Re(*p*FPh-PhPNP)$(CO)_3$Br]. The Anisotropic displacement factor exponent takes the form: $-2\pi^2[h^2a^{*2}U_{11}+...+2hka×b×U_{12}]$

Atom	**U_{11}**	**U_{22}**	**U_{33}**	**U_{23}**	**U_{13}**	**U_{12}**
C1	22.5(15)	14.0(15)	14.9(13)	0.1(11)	-5.1(11)	1.9(12)
C2	22.1(16)	21.8(17)	32.7(18)	-2.5(14)	-1.5(13)	-3.5(13)
C3	36(2)	17.3(17)	44(2)	-8.1(15)	-11.4(16)	-3.8(15)
C4	47(2)	19.5(17)	21.0(16)	-6.4(13)	-9.4(15)	7.6(15)
C5	42(2)	25.3(18)	19.5(15)	-0.6(13)	6.6(14)	4.7(16)
C6	29.7(17)	19.3(17)	20.1(15)	2.8(12)	3.4(13)	-2.4(13)
C7	21.2(15)	15.9(16)	22.4(15)	2.4(12)	1.4(12)	-1.2(12)
C8	19.7(15)	18.0(16)	28.9(16)	0.9(13)	4.3(12)	1.0(13)
C11	16.2(14)	12.5(14)	12.8(12)	0.5(10)	2.6(10)	-0.8(11)
C12	17.0(15)	20.1(17)	30.9(17)	9.5(13)	0.2(12)	-0.5(12)
C13	17.5(16)	29(2)	51(2)	16.3(17)	-1.0(15)	-6.6(14)
C14	26.9(17)	19.1(17)	36.9(19)	11.6(14)	7.7(14)	-2.5(14)
C15	27.8(17)	19.2(16)	18.4(14)	6.1(12)	3.3(12)	4.4(13)
C16	18.7(14)	15.5(15)	14.9(13)	-0.3(11)	0.6(11)	1.5(11)
C21	12.8(13)	15.5(14)	13.2(12)	3.3(11)	0.7(10)	0.3(11)
C22	16.8(14)	20.4(16)	18.5(14)	-2.9(12)	-0.4(11)	2.3(12)
C23	20.8(16)	26.3(18)	29.5(17)	-3.6(14)	2.9(13)	7.7(14)
C24	12.3(14)	36(2)	33.5(18)	5.0(15)	1.6(13)	2.9(13)
C25	16.5(15)	26.1(18)	27.7(16)	6.3(14)	-4.8(12)	-6.1(13)
C26	15.3(14)	14.4(15)	20.0(14)	2.6(11)	-0.5(11)	2.4(11)
C31	19.8(15)	12.6(15)	16.4(14)	2.9(11)	1.0(11)	-1.2(11)
C32	19.6(15)	15.0(15)	21.6(15)	2.0(12)	1.2(12)	-0.8(12)
C33	22.4(16)	22.0(17)	27.7(17)	0.6(13)	6.9(13)	-2.0(13)
C34	36.5(19)	19.8(17)	19.1(15)	3.4(12)	7.9(13)	-7.8(14)
C35	37.1(19)	16.8(16)	17.0(15)	4.5(12)	-2.5(13)	-0.6(14)
C36	22.4(15)	15.7(15)	19.0(14)	1.8(12)	-2.0(12)	1.4(12)
C41	16.5(14)	25.7(18)	23.3(15)	10.3(13)	-4.8(12)	-3.6(13)
C42	23.9(17)	28.6(19)	32.0(18)	0.4(15)	-8.1(14)	-2.1(14)
C43	36(2)	49(3)	35(2)	2.5(18)	-15.5(17)	-12.7(19)

C44	24(2)	94(4)	38(2)	18(2)	-14.7(17)	-20(2)
C45	14.9(18)	115(5)	34(2)	14(3)	-1.7(15)	-5(2)
C46	19.4(17)	72(3)	22.6(17)	6.7(18)	-1.7(14)	-1.8(18)
N1	15.6(12)	13.5(12)	14.5(11)	2.1(9)	-2.8(9)	-1.3(9)
O1	49.4(16)	26.0(14)	23.0(12)	-4.4(10)	-0.9(11)	-9.9(12)
O2	28.2(13)	23.7(14)	55.1(17)	10.6(12)	6.9(12)	9.5(11)
F5	68.0(17)	26.4(12)	33.8(12)	-15.9(10)	-10.6(11)	12.1(11)
P1	11.3(3)	10.7(3)	13.6(3)	1.3(3)	-0.3(3)	-1.1(3)
P2	12.6(3)	14.7(4)	15.9(3)	3.7(3)	-1.2(3)	-0.6(3)
Br1	18.06(15)	28.95(18)	24.48(16)	4.00(13)	3.01(12)	-0.50(12)
Re1	12.79(6)	12.16(7)	15.54(6)	1.64(4)	0.70(4)	0.88(4)
C9	30.7(18)	15.8(16)	12.4(13)	-1.3(11)	-7.3(12)	16.1(14)
O3	46.4(16)	9.9(11)	17.0(11)	1.5(8)	-13.4(10)	6.5(10)

Table I.3 Bond Lengths for *fac*-[Re(*p*FPh-PhPNP)$(CO)_3$Br].

Atom	**Atom**	**Length/Å**	**Atom**	**Atom**	**Length/Å**
C1	C2	1.384(5)	C24	C25	1.378(5)
C1	C6	1.391(5)	C25	C26	1.393(4)
C1	N1	1.444(4)	C31	C32	1.392(4)
C2	C3	1.391(5)	C31	C36	1.395(4)
C3	C4	1.360(6)	C31	P2	1.813(3)
C4	C5	1.374(5)	C32	C33	1.385(4)
C4	F5	1.361(4)	C33	C34	1.384(5)
C5	C6	1.385(5)	C34	C35	1.381(5)
C7	O1	1.141(4)	C35	C36	1.384(4)
C7	Re1	1.968(3)	C41	C42	1.399(5)
C8	O2	1.138(4)	C41	C46	1.384(5)
C8	Re1	1.949(3)	C41	P2	1.815(3)
C11	C12	1.393(4)	C42	C43	1.392(5)
C11	C16	1.393(4)	C43	C44	1.376(7)
C11	P1	1.820(3)	C44	C45	1.370(7)
C12	C13	1.387(5)	C45	C46	1.394(5)
C13	C14	1.381(5)	N1	P1	1.711(2)
C14	C15	1.383(5)	N1	P2	1.706(3)
C15	C16	1.386(4)	P1	Re1	2.4754(10)
C21	C22	1.401(4)	P2	Re1	2.4383(10)
C21	C26	1.394(4)	Br1	Re1	2.6350(10)
C21	P1	1.810(3)	Re1	C9	1.9179(19)
C22	C23	1.385(4)	C9	O3	1.049(3)
C23	C24	1.390(5)			

Table I.4 Bond Angles for *fac*-[Re(*p*FPh-PhPNP)(CO)$_3$Br].

Atom	Atom	Atom	Angle/°	Atom	Atom	Atom	Angle/°
C2	C1	C6	119.3(3)	C46	C41	P2	119.3(3)
C2	C1	N1	120.4(3)	C43	C42	C41	119.6(4)
C6	C1	N1	120.3(3)	C44	C43	C42	120.3(4)
C1	C2	C3	120.7(3)	C45	C44	C43	120.2(4)
C4	C3	C2	118.1(3)	C44	C45	C46	120.6(4)
C3	C4	C5	123.4(3)	C41	C46	C45	119.7(4)
C3	C4	F5	118.5(3)	C1	N1	P1	128.6(2)
F5	C4	C5	118.1(3)	C1	N1	P2	126.69(19)
C4	C5	C6	118.0(3)	P2	N1	P1	104.67(14)
C5	C6	C1	120.5(3)	C11	P1	Re1	123.60(10)
O1	C7	Re1	175.6(3)	C21	P1	C11	104.37(13)
O2	C8	Re1	177.1(3)	C21	P1	Re1	119.76(10)
C12	C11	C16	119.2(3)	N1	P1	C11	105.13(13)
C12	C11	P1	118.2(2)	N1	P1	C21	108.03(13)
C16	C11	P1	122.3(2)	N1	P1	Re1	93.37(9)
C13	C12	C11	120.1(3)	C31	P2	C41	103.01(14)
C14	C13	C12	120.4(3)	C31	P2	Re1	115.42(10)
C13	C14	C15	119.7(3)	C41	P2	Re1	126.32(12)
C14	C15	C16	120.5(3)	N1	P2	C31	106.13(13)
C15	C16	C11	120.1(3)	N1	P2	C41	109.39(14)
C22	C21	P1	121.2(2)	N1	P2	Re1	94.82(9)
C26	C21	C22	119.5(3)	C7	Re1	P1	105.23(10)
C26	C21	P1	119.3(2)	C7	Re1	P2	171.23(10)
C23	C22	C21	119.7(3)	C7	Re1	Br1	84.39(9)
C22	C23	C24	120.3(3)	C8	Re1	C7	91.59(14)
C25	C24	C23	120.5(3)	C8	Re1	P1	163.18(10)
C24	C25	C26	119.8(3)	C8	Re1	P2	96.47(10)
C25	C26	C21	120.3(3)	C8	Re1	Br1	88.50(10)
C32	C31	C36	119.1(3)	P1	Re1	Br1	92.55(3)
C32	C31	P2	119.7(2)	P2	Re1	P1	66.78(3)
C36	C31	P2	120.7(2)	P2	Re1	Br1	99.24(3)
C33	C32	C31	120.6(3)	C9	Re1	C7	87.66(13)
C34	C33	C32	119.6(3)	C9	Re1	C8	89.34(13)
C35	C34	C33	120.5(3)	C9	Re1	P1	91.84(9)
C34	C35	C36	120.0(3)	C9	Re1	P2	88.97(9)
C35	C36	C31	120.2(3)	C9	Re1	Br1	171.70(9)
C42	C41	P2	120.9(3)	O3	C9	Re1	176.7(3)
C46	C41	C42	119.7(3)				

Table I.5 Torsion Angles for *fac*-[Re(*p*FPh-PhPNP)$(CO)_3$Br].

A	B	C	D	Angle/°	A	B	C	D	Angle/°
C1	C2	C3	C4	-0.7(5)	C31	C32	C33	C34	-1.7(5)
C1	N1	P1	C11	56.5(3)	C32	C31	C36	C35	0.0(5)
C1	N1	P1	C21	-54.5(3)	C32	C31	P2	C41	155.6(3)
C1	N1	P1	Re1	-177.4(2)	C32	C31	P2	N1	40.7(3)
C1	N1	P2	C31	59.0(3)	C32	C31	P2	Re1	-62.8(3)
C1	N1	P2	C41	-51.5(3)	C32	C33	C34	C35	1.2(5)
C1	N1	P2	Re1	177.2(2)	C33	C34	C35	C36	-0.2(5)
C2	C1	C6	C5	-0.8(5)	C34	C35	C36	C31	-0.5(5)
C2	C1	N1	P1	-90.0(3)	C36	C31	C32	C33	1.0(5)
C2	C1	N1	P2	86.9(3)	C36	C31	P2	C41	-31.7(3)
C2	C3	C4	C5	0.3(6)	C36	C31	P2	N1	-146.6(3)
C2	C3	C4	F5	-179.6(3)	C36	C31	P2	Re1	109.8(2)
C3	C4	C5	C6	-0.2(5)	C41	C42	C43	C44	0.5(6)
C4	C5	C6	C1	0.5(5)	C42	C41	C46	C45	-0.2(6)
C6	C1	C2	C3	0.9(5)	C42	C41	P2	C31	-47.8(3)
C6	C1	N1	P1	91.1(3)	C42	C41	P2	N1	64.7(3)
C6	C1	N1	P2	-91.9(3)	C42	C41	P2	Re1	176.4(2)
C11	C12	C13	C14	-1.0(6)	C42	C43	C44	C45	-0.9(7)
C12	C11	C16	C15	1.2(4)	C43	C44	C45	C46	0.7(8)
C12	C11	P1	C21	165.7(2)	C44	C45	C46	C41	-0.2(8)
C12	C11	P1	N1	52.1(3)	C46	C41	C42	C43	0.0(6)
C12	C11	P1	Re1	-52.6(3)	C46	C41	P2	C31	128.8(3)
C12	C13	C14	C15	1.7(6)	C46	C41	P2	N1	-118.6(3)
C13	C14	C15	C16	-1.0(5)	C46	C41	P2	Re1	-7.0(4)
C14	C15	C16	C11	-0.5(5)	N1	C1	C2	C3	-178.0(3)
C16	C11	C12	C13	-0.5(5)	N1	C1	C6	C5	178.1(3)
C16	C11	P1	C21	-20.3(3)	F5	C4	C5	C6	179.7(3)
C16	C11	P1	N1	-133.9(2)	P1	C11	C12	C13	173.7(3)
C16	C11	P1	Re1	121.5(2)	P1	C11	C16	C15	-172.8(2)
C21	C22	C23	C24	0.1(5)	P1	C21	C22	C23	-179.2(2)
C22	C21	C26	C25	-2.0(4)	P1	C21	C26	C25	178.6(2)
C22	C21	P1	C11	-52.5(3)	P1	N1	P2	C31	-123.47(14)
C22	C21	P1	N1	59.0(3)	P1	N1	P2	C41	126.03(15)
C22	C21	P1	Re1	164.0(2)	P1	N1	P2	Re1	-5.25(12)
C22	C23	C24	C25	-0.9(5)	P2	C31	C32	C33	173.8(3)
C23	C24	C25	C26	0.3(5)	P2	C31	C36	C35	-172.7(2)
C24	C25	C26	C21	1.1(5)	P2	C41	C42	C43	176.6(3)
C26	C21	C22	C23	1.3(4)	P2	C41	C46	C45	-176.8(4)
C26	C21	P1	C11	127.0(2)	P2	N1	P1	C11	-121.00(14)
C26	C21	P1	N1	-121.5(2)	P2	N1	P1	C21	127.99(14)
C26	C21	P1	Re1	-16.6(3)	P2	N1	P1	Re1	5.16(12)

Table I.6 Hydrogen Atom Coordinates (Å×10^4) and Isotropic Displacement Parameters (Å^2×10^3) for *fac*-[Re(*p*FPh-PhPNP)$(CO)_3$Br].

Atom	*x*	*y*	*z*	U(eq)
H2	8676	5135	2936	31
H3	8363	6249	3743	39
H5	5042	5214	4296	35
H6	5357	4100	3493	28
H12	9330	4424	1787	27
H13	10363	5496	1173	39
H14	9279	6312	333	33
H15	7126	6103	149	26
H16	6067	5054	775	20
H22	5156	5106	2096	22
H23	2988	5318	1984	31
H24	1699	4248	1517	33
H25	2567	2976	1135	28
H26	4744	2762	1224	20
H32	5479	2687	3246	22
H33	4399	1959	4126	29
H34	5518	1166	4970	30
H35	7706	1140	4965	28
H36	8795	1900	4109	23
H42	8988	3719	4140	34
H43	10978	3965	4650	48
H44	12779	3551	4061	62
H45	12618	2859	2980	65
H46	10643	2596	2457	46

J. Crystal data of *fac*-[Re(Cbutyl-4-p-tolyl)$(CO)_3$Br]

Table J.1 Fractional Atomic Coordinates (×10^4) and Equivalent Isotropic Displacement Parameters (Å^2×10^3) for *fac*-[Re(Cbutyl-4-p-tolyl)$(CO)_3$Br]. U_{eq} is defined as 1/3 of of the trace of the orthogonalised U_{IJ} tensor.

Atom	*x*	*y*	*z*	U(eq)
Re01	-1148.7(11)	762.1(2)	-3067.8(2)	12.88(7)
Br1	-1406(4)	1210(3)	-4276.4(8)	22.8(7)
Br1A	-1172.5(17)	411.3(7)	-1832.2(5)	18.1(2)
P2	1085.3(19)	91.3(8)	-3108.5(8)	12.4(3)
P1	-1419(2)	-635.9(8)	-3312.5(8)	12.9(3)
O1	-4223(6)	1334(3)	-3110(3)	33.1(13)
O2	117(6)	2344(2)	-2578(3)	36.7(13)
O3	-1443(17)	1275(9)	-4507(5)	8.1(19)
O3A	-1199(14)	352(7)	-1584(2)	12(2)
N1	341(5)	-800(3)	-3297(3)	14.9(10)
C1	1089(7)	-1496(3)	-3488(3)	18.0(12)

C2	1287(8)	-1626(4)	-4234(4)	24.1(14)
C4	376(7)	-2307(4)	-3487(4)	25.0(15)
C3	1075(10)	-2497(4)	-4114(5)	41(2)
C7	-3099(8)	1120(4)	-3082(4)	19.8(15)
C8	-393(7)	1772(4)	-2771(3)	23.3(14)
C9	-1242(10)	1055(7)	-3957.2(16)	12(2)
C9A	-1010(30)	464(13)	-2159(3)	56(6)
C11	-2075(7)	-1216(3)	-2668(3)	16.5(12)
C12	-1254(7)	-1734(4)	-2257(3)	21.4(13)
C13	-1834(9)	-2153(4)	-1775(4)	29.9(17)
C14	-3242(9)	-2082(4)	-1688(4)	30.8(18)
C15	-4057(8)	-1562(4)	-2092(4)	28.1(16)
C16	-3477(7)	-1124(4)	-2570(4)	24.2(14)
C17	-3881(11)	-2559(5)	-1172(4)	48(2)
C21	-2305(6)	-1055(3)	-4077(3)	15.4(12)
C22	-3175(7)	-1702(4)	-4076(4)	22.6(14)
C23	-3826(8)	-2005(4)	-4660(4)	28.5(16)
C24	-3636(7)	-1674(4)	-5275(4)	25.9(15)
C25	-2767(8)	-1032(4)	-5276(3)	25.7(15)
C26	-2115(7)	-723(4)	-4693(3)	21.8(14)
C27	-4354(9)	-2008(5)	-5921(4)	37.0(19)
C31	2248(6)	334(4)	-3732(3)	14.2(12)
C32	2094(7)	1032(4)	-4078(3)	19.9(13)
C33	2968(7)	1217(4)	-4556(3)	21.6(13)
C34	4001(7)	702(4)	-4717(3)	18.9(13)
C35	4190(7)	16(4)	-4354(4)	21.8(14)
C36	3345(7)	-158(4)	-3867(3)	20.4(13)
C37	4876(8)	873(5)	-5272(4)	28.4(16)
C41	2337(6)	-35(3)	-2373(3)	14.9(12)
C42	3548(7)	423(4)	-2307(4)	21.7(14)
C43	4547(7)	350(4)	-1764(4)	25.5(15)
C44	4370(7)	-181(4)	-1261(3)	21.6(13)
C45	3139(7)	-626(4)	-1319(3)	20.6(13)
C46	2129(7)	-553(4)	-1864(3)	17.6(12)
C47	5506(8)	-293(5)	-689(4)	30.3(16)
Re02	4373.9(11)	5708.7(2)	-2889.4(2)	14.12(7)
Br2	4401.5(19)	6244.7(9)	-4078.6(7)	18.9(3)
Br2A	4445(2)	5320.6(10)	-1649.7(8)	25.5(3)
P4	4477(2)	4320.6(9)	-3200.9(9)	14.5(3)
P3	2082(2)	5121.5(9)	-3174.0(8)	12.9(3)
O1B	3283(6)	7307(3)	-2477(3)	33.9(13)
O2B	7489(6)	6203(4)	-2578(3)	42.4(16)
O3B	4433(10)	6314(5)	-4321(2)	13.0(17)
O3C	4350(20)	5236(10)	-1411(3)	22(3)

N2	2704(6)	4255(3)	-3411(3)	15.2(10)
C1B	1979(7)	3583(4)	-3759(3)	19.2(13)
C41B	4946(7)	3609(4)	-2546(3)	17.6(12)
C2B	2066(7)	3490(4)	-4520(3)	25.2(15)
C3B	523(8)	3224(5)	-4596(4)	29.0(16)
C4B	356(7)	3564(4)	-3899(3)	23.2(14)
C7B	3726(7)	6721(4)	-2639(3)	21.0(13)
C8B	6352(8)	6006(4)	-2702(4)	23.3(15)
C9B	4390(15)	6033(8)	-3786(3)	17(3)
C9C	4349(18)	5386(10)	-1993(3)	30(3)
C11B	1063(6)	4988(3)	-2484(3)	14.8(11)
C12B	518(7)	4266(3)	-2319(3)	18.7(13)
C13B	-267(7)	4204(4)	-1782(4)	24.1(15)
C14B	-565(7)	4848(5)	-1410(4)	25.5(15)
C15B	2(8)	5552(4)	-1562(4)	25.1(15)
C16B	814(8)	5633(4)	-2089(4)	21.7(14)
C17B	-1481(9)	4776(6)	-854(4)	40(2)
C21B	806(6)	5464(3)	-3841(3)	14.3(11)
C22B	-525(7)	5711(3)	-3707(4)	18.4(14)
C23B	-1521(7)	5935(4)	-4225(3)	20.5(13)
C24B	-1229(7)	5910(4)	-4887(3)	21.8(14)
C25B	117(7)	5687(3)	-5010(3)	18.8(13)
C26B	1129(7)	5479(4)	-4498(3)	17.9(12)
C27B	-2346(8)	6130(5)	-5440(4)	33.8(17)
C31B	5324(6)	3910(3)	-3882(3)	16.5(12)
C32B	5920(8)	4386(4)	-4330(4)	23.6(14)
C33B	6526(8)	4063(4)	-4866(4)	27.8(15)
C34B	6544(7)	3263(4)	-4963(4)	24.3(14)
C35B	6000(8)	2788(4)	-4498(4)	25.3(15)
C36B	5397(7)	3104(4)	-3969(4)	23.8(14)
C37B	7141(8)	2915(4)	-5556(4)	30.2(16)
C42B	6358(8)	3403(5)	-2397(4)	35.6(19)
C43B	6755(8)	2887(5)	-1884(4)	39(2)
C44B	5791(8)	2563(4)	-1507(4)	27.8(15)
C45B	4384(9)	2757(5)	-1674(4)	37.6(19)
C46B	3977(8)	3272(5)	-2181(4)	33.4(18)
C47B	6242(10)	2023(5)	-925(4)	38.1(19)

Table J.2 Anisotropic Displacement Parameters ($Å^2 \times 10^3$) for *fac*-[Re(Cbutyl-4-p-tolyl)$(CO)_3$Br]. The Anisotropic displacement factor exponent takes the form: $-2\pi^2[h^2a^{*2}U_{11}+...+2hka\times b\times U_{12}]$

Atom	**U_{11}**	**U_{22}**	**U_{33}**	**U_{23}**	**U_{13}**	**U_{12}**
Re01	14.09(13)	8.98(11)	15.94(14)	0.33(9)	3.4(1)	-0.37(9)
Br1	19.9(12)	27.1(16)	20(2)	0.6(18)	-2.0(19)	3(1)
Br1A	25.8(6)	17.7(6)	11.5(6)	-0.2(5)	4.5(5)	-2.5(4)

P2	13.5(7)	8.5(7)	15.1(7)	1.2(6)	1.7(6)	-0.7(5)
P1	13.1(7)	9.5(7)	15.7(8)	-1.0(5)	0.4(6)	-0.5(5)
O1	20(3)	32(3)	48(4)	9(3)	11(2)	6(2)
O2	60(4)	18(3)	31(3)	-2(2)	1(3)	-14(2)
O3	8(3)	7(4)	8(6)	1(5)	-6(5)	1(3)
O3A	24(5)	5(4)	8.7(18)	-1.0(18)	5.4(19)	-1(3)
N1	13(2)	10(2)	22(3)	0.3(19)	3(2)	-0.5(18)
C1	19(3)	12(3)	24(3)	1(2)	2(2)	1(2)
C2	26(3)	20(3)	26(4)	-9(3)	5(3)	3(3)
C4	21(3)	9(3)	46(4)	-4(3)	4(3)	2(2)
C3	51(5)	18(4)	57(6)	-17(4)	20(4)	-5(3)
C7	25(4)	15(3)	21(4)	5(3)	8(3)	-6(3)
C8	35(4)	16(3)	20(3)	2(3)	7(3)	-2(3)
C9	7(5)	12(5)	15(3)	-3(3)	-3(3)	2(4)
C9A	96(15)	61(12)	17(3)	6(4)	28(5)	-1(11)
C11	24(3)	11(3)	15(3)	-2(2)	7(2)	0(2)
C12	21(3)	18(3)	25(3)	0(3)	0(3)	-5(2)
C13	48(5)	20(4)	20(4)	6(3)	-2(3)	-5(3)
C14	50(5)	25(4)	20(4)	-5(3)	14(3)	-22(3)
C15	34(4)	23(4)	31(4)	-7(3)	18(3)	-11(3)
C16	27(3)	22(3)	25(4)	-4(3)	9(3)	0(3)
C17	71(6)	52(6)	23(4)	3(4)	12(4)	-33(5)
C21	14(3)	14(3)	18(3)	-1(2)	0(2)	0(2)
C22	23(3)	18(3)	25(4)	1(3)	-2(3)	-8(3)
C23	29(4)	19(3)	35(4)	-2(3)	-6(3)	-8(3)
C24	26(3)	20(3)	29(4)	-9(3)	-8(3)	7(3)
C25	35(4)	23(3)	18(3)	2(3)	1(3)	4(3)
C26	25(3)	20(3)	20(3)	1(2)	2(3)	-9(3)
C27	40(4)	36(4)	31(4)	-9(3)	-16(3)	6(4)
C31	15(3)	15(3)	13(3)	-1(2)	2(2)	-3(2)
C32	20(3)	16(3)	24(3)	0(3)	0(3)	1(2)
C33	24(3)	20(3)	21(3)	5(3)	1(3)	-1(3)
C34	19(3)	22(3)	15(3)	-2(2)	1(2)	-8(2)
C35	15(3)	23(3)	27(4)	-2(3)	4(3)	3(3)
C36	20(3)	18(3)	22(3)	4(3)	1(3)	-1(2)
C37	28(4)	38(4)	20(4)	1(3)	7(3)	-11(3)
C41	17(3)	13(3)	15(3)	0(2)	2(2)	1(2)
C42	22(3)	23(4)	20(3)	6(3)	0(3)	-6(3)
C43	20(3)	33(4)	23(4)	2(3)	1(3)	-7(3)
C44	20(3)	27(3)	18(3)	-1(3)	3(3)	5(3)
C45	23(3)	23(3)	16(3)	5(2)	1(3)	4(3)
C46	16(3)	17(3)	20(3)	3(2)	1(2)	-2(2)
C47	24(4)	46(5)	20(4)	5(3)	-3(3)	4(3)
Re02	13.50(13)	12.63(13)	15.79(15)	-0.33(9)	-0.26(10)	-0.33(9)

Br2	20.9(7)	20.5(8)	16.2(8)	11.5(7)	5.6(7)	-2.1(5)
Br2A	29.8(8)	26.2(9)	20.0(9)	-0.5(8)	0.0(8)	2.0(7)
P4	15.1(7)	11.2(7)	16.8(8)	-0.8(6)	0.0(6)	0.5(5)
P3	15.8(7)	10.7(7)	12.8(7)	0.1(6)	4.3(6)	-0.6(5)
O1B	35(3)	18(3)	47(3)	-9(2)	-4(2)	5(2)
O2B	17(3)	62(4)	49(4)	-25(3)	4(2)	-6(3)
O3B	14(4)	12(4)	13.4(19)	11.1(18)	3.3(18)	-3(3)
O3C	26(6)	21(6)	18(2)	-1(3)	0(3)	5(5)
N2	16(2)	13(2)	16(3)	-3.9(19)	2(2)	2.7(19)
C1B	21(3)	10(3)	26(3)	-3(2)	-2(3)	-2(2)
C41B	24(3)	14(3)	14(3)	0(2)	0(2)	3(2)
C2B	26(3)	25(3)	24(4)	-11(3)	3(3)	0(3)
C3B	26(4)	33(4)	26(4)	-7(3)	-6(3)	-3(3)
C4B	20(3)	22(3)	27(4)	-6(3)	1(3)	-5(3)
C7B	24(3)	17(3)	20(3)	-1(3)	-6(3)	-9(3)
C8B	19(3)	27(4)	23(4)	-11(3)	3(3)	3(3)
C9B	23(6)	15(5)	13(3)	11(3)	7(3)	1(5)
C9C	36(8)	36(8)	19(2)	2(3)	3(2)	14(6)
C11B	18(3)	15(3)	12(3)	1(2)	2(2)	0(2)
C12B	19(3)	14(3)	23(3)	-1(2)	4(3)	-2(2)
C13B	21(3)	27(4)	25(4)	7(3)	3(3)	-7(3)
C14B	18(3)	40(4)	19(3)	1(3)	2(3)	-2(3)
C15B	32(4)	26(3)	19(3)	-2(3)	7(3)	4(3)
C16B	29(4)	18(3)	19(4)	-1(3)	6(3)	-2(3)
C17B	36(4)	63(6)	23(4)	2(4)	11(3)	-5(4)
C21B	17(3)	12(3)	14(3)	1(2)	3(2)	1(2)
C22B	18(3)	18(3)	20(3)	1(2)	7(3)	1(2)
C23B	18(3)	18(3)	26(4)	1(3)	4(3)	6(2)
C24B	26(3)	15(3)	24(3)	1(3)	0(3)	1(3)
C25B	27(3)	17(3)	13(3)	0(2)	6(3)	2(2)
C26B	18(3)	15(3)	21(3)	-4(2)	5(2)	1(2)
C27B	35(4)	34(4)	30(4)	3(3)	-4(3)	7(3)
C31B	14(3)	14(3)	21(3)	0(2)	1(2)	3(2)
C32B	29(4)	17(3)	26(4)	-1(3)	9(3)	-1(3)
C33B	31(4)	28(4)	26(4)	3(3)	12(3)	-3(3)
C34B	18(3)	29(4)	25(4)	-4(3)	2(3)	4(3)
C35B	28(4)	19(3)	29(4)	-3(3)	5(3)	5(3)
C36B	30(4)	16(3)	26(4)	2(3)	5(3)	-2(3)
C37B	28(4)	32(4)	31(4)	-8(3)	7(3)	4(3)
C42B	24(4)	41(5)	40(5)	21(4)	-3(3)	-7(3)
C43B	25(4)	42(5)	47(5)	21(4)	-13(3)	-4(3)
C44B	39(4)	22(3)	21(4)	4(3)	-1(3)	-1(3)
C45B	39(4)	39(5)	39(5)	17(4)	24(4)	11(4)
C46B	23(4)	41(4)	38(4)	16(4)	12(3)	9(3)

C47B	57(5)	27(4)	28(4)	10(3)	-3(4)	2(4)

Table J.3 Bond Lengths for *fac*-[Re(Cbutyl-4-p-tolyl)$(CO)_3$Br].

Atom	Atom	Length/Å	Atom	Atom	Length/Å
Re01	Br1	2.5481(12)	Re02	Br2A	2.5877(15)
Re01	Br1A	2.5729(10)	Re02	P4	2.4732(15)
Re01	P2	2.4459(16)	Re02	P3	2.4322(16)
Re01	P1	2.4617(15)	Re02	C7B	1.935(7)
Re01	C7	1.969(7)	Re02	C8B	1.963(7)
Re01	C8	1.951(7)	Re02	C9B	1.898(3)
Re01	C9	1.8604(3)	Re02	C9C	1.898(3)
Re01	C9A	1.899(3)	Br2	O3B	0.509(3)
Br1	C9	0.700(3)	Br2	C9B	0.696(4)
Br1A	O3A	0.516(3)	Br2A	O3C	0.521(4)
Br1A	C9A	0.700(8)	Br2A	C9C	0.700(5)
P2	N1	1.716(5)	P4	P3	2.687(2)
P2	C31	1.824(6)	P4	N2	1.712(6)
P2	C41	1.817(6)	P4	C41B	1.822(6)
P1	N1	1.710(5)	P4	C31B	1.819(7)
P1	C11	1.810(6)	P3	N2	1.694(5)
P1	C21	1.827(6)	P3	C11B	1.807(6)
O1	C7	1.137(9)	P3	C21B	1.816(6)
O2	C8	1.147(7)	O1B	C7B	1.155(8)
O3	C9	1.169(9)	O2B	C8B	1.144(9)
O3A	C9A	1.211(7)	O3B	C9B	1.191(4)
N1	C1	1.470(8)	O3C	C9C	1.204(4)
C1	C2	1.558(9)	N2	C1B	1.486(8)
C1	C4	1.553(9)	C1B	C2B	1.558(9)
C2	C3	1.535(10)	C1B	C4B	1.554(9)
C4	C3	1.534(11)	C41B	C42B	1.402(10)
C11	C12	1.399(9)	C41B	C46B	1.379(10)
C11	C16	1.392(9)	C2B	C3B	1.542(10)
C12	C13	1.379(10)	C3B	C4B	1.550(10)
C13	C14	1.388(12)	C11B	C12B	1.401(8)
C14	C15	1.392(12)	C11B	C16B	1.403(9)
C14	C17	1.510(10)	C12B	C13B	1.395(10)
C15	C16	1.390(10)	C13B	C14B	1.387(10)
C21	C22	1.391(9)	C14B	C15B	1.377(10)
C21	C26	1.401(9)	C14B	C17B	1.508(10)
C22	C23	1.376(10)	C15B	C16B	1.395(10)
C23	C24	1.398(11)	C21B	C22B	1.403(9)
C24	C25	1.384(10)	C21B	C26B	1.398(9)
C24	C27	1.520(10)	C22B	C23B	1.392(10)
C25	C26	1.377(9)	C23B	C24B	1.399(10)

C31	C32	1.389(9)	C24B	C25B	1.398(10)
C31	C36	1.402(9)	C24B	C27B	1.509(10)
C32	C33	1.386(9)	C25B	C26B	1.385(9)
C33	C34	1.396(9)	C31B	C32B	1.392(9)
C34	C35	1.390(9)	C31B	C36B	1.400(9)
C34	C37	1.505(9)	C32B	C33B	1.401(10)
C35	C36	1.377(9)	C33B	C34B	1.390(10)
C41	C42	1.399(9)	C34B	C35B	1.391(10)
C41	C46	1.393(9)	C34B	C37B	1.509(10)
C42	C43	1.380(10)	C35B	C36B	1.385(10)
C43	C44	1.392(10)	C42B	C43B	1.386(10)
C44	C45	1.402(10)	C43B	C44B	1.381(11)
C44	C47	1.510(9)	C44B	C45B	1.396(11)
C45	C46	1.389(9)	C44B	C47B	1.524(10)
Re02	Br2	2.5783(13)	C45B	C46B	1.378(11)

Table J.4 Bond Angles for *fac*-[Re(Cbutyl-4-p-tolyl)$(CO)_3$Br].

Atom	**Atom**	**Atom**	**Angle/°**	**Atom**	**Atom**	**Atom**	**Angle/°**
P2	Re01	Br1	95.81(11)	C7B	Re02	Br2	87.7(2)
P2	Re01	Br1A	91.46(5)	C7B	Re02	Br2A	87.3(2)
P2	Re01	P1	66.79(5)	C7B	Re02	P4	163.33(19)
P1	Re01	Br1	96.07(11)	C7B	Re02	P3	97.25(19)
P1	Re01	Br1A	87.37(5)	C7B	Re02	C8B	92.8(3)
C7	Re01	Br1	84.4(2)	C8B	Re02	Br2	88.6(2)
C7	Re01	Br1A	88.6(2)	C8B	Re02	Br2A	87.7(2)
C7	Re01	P2	169.7(2)	C8B	Re02	P4	103.6(2)
C7	Re01	P1	102.9(2)	C8B	Re02	P3	170.0(2)
C8	Re01	Br1	91.0(2)	C9B	Re02	Br2	3.9(4)
C8	Re01	Br1A	87.4(2)	C9B	Re02	P4	92.0(4)
C8	Re01	P2	97.6(2)	C9B	Re02	P3	90.0(4)
C8	Re01	P1	163.4(2)	C9B	Re02	C7B	91.3(5)
C8	Re01	C7	92.7(3)	C9B	Re02	C8B	89.8(5)
C9	Re01	Br1	3.4(4)	C9C	Re02	Br2A	3.0(6)
C9	Re01	P2	92.4(4)	C9C	Re02	P4	88.0(5)
C9	Re01	P1	94.5(4)	C9C	Re02	P3	89.8(6)
C9	Re01	C7	87.6(4)	C9C	Re02	C7B	88.6(6)
C9	Re01	C8	91.8(4)	C9C	Re02	C8B	90.5(6)
C9A	Re01	Br1A	4.9(8)	O3B	Br2	Re02	172.1(13)
C9A	Re01	P2	86.6(8)	O3B	Br2	C9B	161.8(16)
C9A	Re01	P1	85.7(7)	C9B	Br2	Re02	10.6(12)
C9A	Re01	C7	93.4(8)	O3C	Br2A	Re02	169(2)
C9A	Re01	C8	87.7(8)	O3C	Br2A	C9C	161(2)
C9	Br1	Re01	9.0(9)	C9C	Br2A	Re02	8.3(15)
O3A	Br1A	Re01	176.9(15)	Re02	P4	P3	56.06(5)

O3A	Br1A	C9A	170(2)	N2	P4	Re02	93.42(17)
C9A	Br1A	Re01	13(2)	N2	P4	P3	37.68(17)
N1	P2	Re01	94.77(18)	N2	P4	C41B	107.1(3)
N1	P2	C31	108.8(3)	N2	P4	C31B	107.7(3)
N1	P2	C41	107.2(3)	C41B	P4	Re02	118.5(2)
C31	P2	Re01	121.5(2)	C41B	P4	P3	118.1(2)
C41	P2	Re01	122.1(2)	C31B	P4	Re02	127.0(2)
C41	P2	C31	101.1(3)	C31B	P4	P3	132.2(2)
N1	P1	Re01	94.35(17)	C31B	P4	C41B	101.2(3)
N1	P1	C11	108.6(3)	Re02	P3	P4	57.52(5)
N1	P1	C21	108.5(3)	N2	P3	Re02	95.33(19)
C11	P1	Re01	115.5(2)	N2	P3	P4	38.14(18)
C11	P1	C21	103.0(3)	N2	P3	C11B	110.2(3)
C21	P1	Re01	125.7(2)	N2	P3	C21B	107.8(3)
Br1A	O3A	C9A	6.0(14)	C11B	P3	Re02	115.1(2)
P1	N1	P2	104.1(3)	C11B	P3	P4	119.3(2)
C1	N1	P2	125.6(4)	C11B	P3	C21B	103.7(3)
C1	N1	P1	129.8(4)	C21B	P3	Re02	123.9(2)
N1	C1	C2	119.2(5)	C21B	P3	P4	131.2(2)
N1	C1	C4	120.1(5)	Br2	O3B	C9B	10.5(9)
C4	C1	C2	88.5(5)	Br2A	O3C	C9C	10.8(14)
C3	C2	C1	87.3(5)	P3	N2	P4	104.2(3)
C3	C4	C1	87.5(5)	C1B	N2	P4	124.7(4)
C4	C3	C2	90.1(5)	C1B	N2	P3	131.0(4)
O1	C7	Re01	177.9(7)	N2	C1B	C2B	118.3(5)
O2	C8	Re01	176.0(6)	N2	C1B	C4B	120.7(5)
Br1	C9	Re01	167.6(13)	C4B	C1B	C2B	89.0(5)
Br1	C9	O3	5.1(10)	C42B	C41B	P4	118.7(5)
O3	C9	Re01	172.5(14)	C46B	C41B	P4	123.0(5)
Br1A	C9A	Re01	162(3)	C46B	C41B	C42B	118.3(6)
Br1A	C9A	O3A	4.4(10)	C3B	C2B	C1B	88.4(5)
O3A	C9A	Re01	166(2)	C2B	C3B	C4B	89.7(5)
C12	C11	P1	124.0(5)	C3B	C4B	C1B	88.2(5)
C16	C11	P1	117.4(5)	O1B	C7B	Re02	176.5(6)
C16	C11	C12	118.5(6)	O2B	C8B	Re02	177.3(7)
C13	C12	C11	120.5(7)	Br2	C9B	Re02	165.5(16)
C12	C13	C14	121.4(7)	Br2	C9B	O3B	7.7(7)
C13	C14	C15	118.2(7)	O3B	C9B	Re02	172.9(13)
C13	C14	C17	121.2(8)	Br2A	C9C	O3C	8.0(11)
C15	C14	C17	120.6(8)	C12B	C11B	P3	123.0(5)
C16	C15	C14	120.9(7)	C12B	C11B	C16B	118.2(6)
C15	C16	C11	120.4(7)	C16B	C11B	P3	118.8(5)
C22	C21	P1	122.5(5)	C13B	C12B	C11B	120.2(6)
C22	C21	C26	117.7(6)	C14B	C13B	C12B	121.6(6)

C26	C21	P1	119.8(5)	C13B	C14B	C17B	120.8(7)
C23	C22	C21	121.1(7)	C15B	C14B	C13B	118.0(7)
C22	C23	C24	121.2(7)	C15B	C14B	C17B	121.2(7)
C23	C24	C27	121.3(7)	C14B	C15B	C16B	121.8(7)
C25	C24	C23	117.7(6)	C15B	C16B	C11B	120.1(6)
C25	C24	C27	121.1(7)	C22B	C21B	P3	120.5(5)
C26	C25	C24	121.5(7)	C26B	C21B	P3	120.6(5)
C25	C26	C21	120.8(6)	C26B	C21B	C22B	118.9(6)
C32	C31	P2	120.5(5)	C23B	C22B	C21B	120.2(6)
C32	C31	C36	117.6(6)	C22B	C23B	C24B	121.1(6)
C36	C31	P2	121.9(5)	C23B	C24B	C27B	119.9(6)
C33	C32	C31	120.7(6)	C25B	C24B	C23B	117.9(6)
C32	C33	C34	121.3(6)	C25B	C24B	C27B	122.2(7)
C33	C34	C37	121.4(6)	C26B	C25B	C24B	121.6(6)
C35	C34	C33	118.0(6)	C25B	C26B	C21B	120.2(6)
C35	C34	C37	120.6(6)	C32B	C31B	P4	121.1(5)
C36	C35	C34	120.6(6)	C32B	C31B	C36B	118.1(6)
C35	C36	C31	121.7(6)	C36B	C31B	P4	120.8(5)
C42	C41	P2	118.5(5)	C31B	C32B	C33B	120.5(6)
C46	C41	P2	123.0(5)	C34B	C33B	C32B	121.0(7)
C46	C41	C42	118.4(6)	C33B	C34B	C35B	118.3(7)
C43	C42	C41	121.4(6)	C33B	C34B	C37B	121.1(7)
C42	C43	C44	120.7(6)	C35B	C34B	C37B	120.6(6)
C43	C44	C45	117.9(6)	C36B	C35B	C34B	120.9(6)
C43	C44	C47	120.4(6)	C35B	C36B	C31B	121.1(7)
C45	C44	C47	121.7(6)	C43B	C42B	C41B	120.1(7)
C46	C45	C44	121.6(6)	C44B	C43B	C42B	121.7(7)
C45	C46	C41	119.9(6)	C43B	C44B	C45B	117.5(7)
P4	Re02	Br2	95.88(5)	C43B	C44B	C47B	121.5(7)
P4	Re02	Br2A	90.02(6)	C45B	C44B	C47B	121.0(7)
P3	Re02	Br2	91.80(5)	C46B	C45B	C44B	121.3(7)
P3	Re02	Br2A	92.68(6)	C45B	C46B	C41B	121.1(7)
P3	Re02	P4	66.43(5)				

Table J.5 Torsion Angles for *fac*-[Re(Cbutyl-4-p-tolyl)$(CO)_3$Br].

A	**B**	**C**	**D**	**Angle/°**	**A**	**B**	**C**	**D**	**Angle/°**
Re01	Br1	C9	O3	168(12)	Re02	Br2A	O3C	C9C	15(7)
Re01	Br1A	C9A	O3A	175(8)	Re02	Br2A	C9C	O3C	-159(10)
Re01	P2	N1	P1	-1.2(3)	Re02	P4	N2	P3	-7.0(3)
Re01	P2	N1	C1	171.2(5)	Re02	P4	N2	C1B	169.7(5)
Re01	P2	C31	C32	17.7(6)	Re02	P4	C41B	C42B	-91.9(6)
Re01	P2	C31	C36	-164.2(4)	Re02	P4	C41B	C46B	87.0(6)
Re01	P2	C41	C42	-105.6(5)	Re02	P4	C31B	C32B	-5.1(6)
Re01	P2	C41	C46	72.5(6)	Re02	P4	C31B	C36B	174.8(4)

Re01	P1	N1	P2	1.2(3)	Re02	P3	N2	P4	7.2(3)
Re01	P1	N1	C1	-170.8(5)	Re02	P3	N2	C1B	-169.3(6)
Re01	P1	C11	C12	-107.2(5)	Re02	P3	C11B	C12B	-124.7(5)
Re01	P1	C11	C16	71.3(5)	Re02	P3	C11B	C16B	54.6(6)
Re01	P1	C21	C22	-138.9(5)	Re02	P3	C21B	C22B	-120.8(5)
Re01	P1	C21	C26	41.2(6)	Re02	P3	C21B	C26B	59.9(6)
Br1A	Re01	C9A	O3A	-2(3)	P4	Re02	C9B	Br2	-176(6)
Br1A	O3A	C9A	Re01	7(10)	P4	P3	N2	C1B	-176.4(8)
P2	Re01	C9	Br1	-175(6)	P4	P3	C11B	C12B	-59.3(6)
P2	Re01	C9A	Br1A	-177(9)	P4	P3	C11B	C16B	120.0(5)
P2	Re01	C9A	O3A	-178(9)	P4	P3	C21B	C22B	164.9(4)
P2	N1	C1	C2	-87.2(7)	P4	P3	C21B	C26B	-14.4(6)
P2	N1	C1	C4	165.9(5)	P4	N2	C1B	C2B	-75.6(7)
P2	C31	C32	C33	-179.6(5)	P4	N2	C1B	C4B	177.3(5)
P2	C31	C36	C35	177.8(5)	P4	C41B	C42B	C43B	177.4(7)
P2	C41	C42	C43	-179.3(6)	P4	C41B	C46B	C45B	-177.7(7)
P2	C41	C46	C45	179.2(5)	P4	C31B	C32B	C33B	-177.8(6)
P1	Re01	C9	Br1	118(6)	P4	C31B	C36B	C35B	177.9(5)
P1	Re01	C9A	Br1A	-110(9)	P3	Re02	C9B	Br2	118(6)
P1	Re01	C9A	O3A	-111(9)	P3	P4	N2	C1B	176.7(7)
P1	N1	C1	C2	83.2(7)	P3	P4	C41B	C42B	-156.4(5)
P1	N1	C1	C4	-23.7(9)	P3	P4	C41B	C46B	22.5(7)
P1	C11	C12	C13	179.7(5)	P3	P4	C31B	C32B	69.8(6)
P1	C11	C16	C15	178.8(5)	P3	P4	C31B	C36B	-110.3(5)
P1	C21	C22	C23	-179.9(6)	P3	N2	C1B	C2B	100.2(7)
P1	C21	C26	C25	179.6(5)	P3	N2	C1B	C4B	-7.0(9)
O3A	Br1A	C9A	Re01	-175(8)	P3	C11B	C12B	C13B	-179.6(5)
N1	P2	C31	C32	125.9(5)	P3	C11B	C16B	C15B	178.4(5)
N1	P2	C31	C36	-56.0(6)	P3	C21B	C22B	C23B	-176.7(5)
N1	P2	C41	C42	147.1(5)	P3	C21B	C26B	C25B	175.3(5)
N1	P2	C41	C46	-34.7(6)	O3B	Br2	C9B	Re02	170(5)
N1	P1	C11	C12	-2.8(6)	N2	P4	C41B	C42B	164.3(6)
N1	P1	C11	C16	175.8(5)	N2	P4	C41B	C46B	-16.8(7)
N1	P1	C21	C22	111.3(6)	N2	P4	C31B	C32B	103.5(6)
N1	P1	C21	C26	-68.6(6)	N2	P4	C31B	C36B	-76.6(6)
N1	C1	C2	C3	-143.2(6)	N2	P3	C11B	C12B	-18.3(6)
N1	C1	C4	C3	142.5(6)	N2	P3	C11B	C16B	161.0(5)
C1	C2	C3	C4	19.3(6)	N2	P3	C21B	C22B	129.7(5)
C1	C4	C3	C2	-19.4(6)	N2	P3	C21B	C26B	-49.6(6)
C2	C1	C4	C3	19.1(6)	N2	C1B	C2B	C3B	-141.1(6)
C4	C1	C2	C3	-19.1(5)	N2	C1B	C4B	C3B	139.1(6)
C7	Re01	C9	Br1	16(6)	C1B	C2B	C3B	C4B	16.4(5)
C7	Re01	C9A	Br1A	-7(9)	C41B	P4	N2	P3	114.2(3)
C7	Re01	C9A	O3A	-9(9)	C41B	P4	N2	C1B	-69.1(6)

C8	Re01	C9	Br1	-77(6)	C41B	P4	C31B	C32B	-144.3(5)
C8	Re01	C9A	Br1A	86(9)	C41B	P4	C31B	C36B	35.6(6)
C8	Re01	C9A	O3A	84(9)	C41B	C42B	C43B	C44B	0.0(14)
C11	P1	N1	P2	-117.6(3)	C2B	C1B	C4B	C3B	16.3(5)
C11	P1	N1	C1	70.5(6)	C2B	C3B	C4B	C1B	-16.5(5)
C11	P1	C21	C22	-3.7(6)	C4B	C1B	C2B	C3B	-16.4(5)
C11	P1	C21	C26	176.4(5)	C7B	Re02	C9B	Br2	21(6)
C11	C12	C13	C14	0.8(11)	C8B	Re02	C9B	Br2	-72(6)
C12	C11	C16	C15	-2.6(10)	C11B	P3	N2	P4	-112.1(3)
C12	C13	C14	C15	-1.3(11)	C11B	P3	N2	C1B	71.5(6)
C12	C13	C14	C17	178.3(7)	C11B	P3	C21B	C22B	12.8(6)
C13	C14	C15	C16	-0.1(11)	C11B	P3	C21B	C26B	-166.5(5)
C14	C15	C16	C11	2.1(10)	C11B	C12B	C13B	C14B	1.9(10)
C16	C11	C12	C13	1.1(10)	C12B	C11B	C16B	C15B	-2.3(10)
C17	C14	C15	C16	-179.7(7)	C12B	C13B	C14B	C15B	-3.5(11)
C21	P1	N1	P2	131.2(3)	C12B	C13B	C14B	C17B	176.7(7)
C21	P1	N1	C1	-40.8(6)	C13B	C14B	C15B	C16B	2.2(11)
C21	P1	C11	C12	112.1(6)	C14B	C15B	C16B	C11B	0.7(11)
C21	P1	C11	C16	-69.4(5)	C16B	C11B	C12B	C13B	1.1(10)
C21	C22	C23	C24	0.1(11)	C17B	C14B	C15B	C16B	-177.9(7)
C22	C21	C26	C25	-0.3(10)	C21B	P3	N2	P4	135.4(3)
C22	C23	C24	C25	0.1(11)	C21B	P3	N2	C1B	-41.0(6)
C22	C23	C24	C27	180.0(7)	C21B	P3	C11B	C12B	96.8(6)
C23	C24	C25	C26	-0.4(11)	C21B	P3	C11B	C16B	-83.9(6)
C24	C25	C26	C21	0.5(11)	C21B	C22B	C23B	C24B	1.0(10)
C26	C21	C22	C23	0.0(10)	C22B	C21B	C26B	C25B	-4.0(9)
C27	C24	C25	C26	179.7(7)	C22B	C23B	C24B	C25B	-3.0(10)
C31	P2	N1	P1	-126.9(3)	C22B	C23B	C24B	C27B	177.8(6)
C31	P2	N1	C1	45.5(6)	C23B	C24B	C25B	C26B	1.5(10)
C31	P2	C41	C42	33.2(6)	C24B	C25B	C26B	C21B	2.0(10)
C31	P2	C41	C46	-148.7(5)	C26B	C21B	C22B	C23B	2.6(9)
C31	C32	C33	C34	1.8(10)	C27B	C24B	C25B	C26B	-179.3(6)
C32	C31	C36	C35	-4.0(9)	C31B	P4	N2	P3	-137.7(3)
C32	C33	C34	C35	-4.1(10)	C31B	P4	N2	C1B	39.0(6)
C32	C33	C34	C37	175.1(6)	C31B	P4	C41B	C42B	51.7(6)
C33	C34	C35	C36	2.3(10)	C31B	P4	C41B	C46B	-129.4(6)
C34	C35	C36	C31	1.7(10)	C31B	C32B	C33B	C34B	0.2(11)
C36	C31	C32	C33	2.2(9)	C32B	C31B	C36B	C35B	-2.2(10)
C37	C34	C35	C36	-176.8(6)	C32B	C33B	C34B	C35B	-2.8(11)
C41	P2	N1	P1	124.5(3)	C32B	C33B	C34B	C37B	177.3(7)
C41	P2	N1	C1	-63.1(6)	C33B	C34B	C35B	C36B	2.9(11)
C41	P2	C31	C32	-121.5(5)	C34B	C35B	C36B	C31B	-0.4(11)
C41	P2	C31	C36	56.7(6)	C36B	C31B	C32B	C33B	2.3(10)
C41	C42	C43	C44	-0.6(12)	C37B	C34B	C35B	C36B	-177.2(7)

C42	C41	C46	C45	-2.6(10)	C42B	C41B	C46B	C45B	1.2(12)
C42	C43	C44	C45	-1.1(11)	C42B	C43B	C44B	C45B	1.8(13)
C42	C43	C44	C47	176.3(7)	C42B	C43B	C44B	C47B	-177.4(8)
C43	C44	C45	C46	0.9(10)	C43B	C44B	C45B	C46B	-2.1(13)
C44	C45	C46	C41	1.0(10)	C44B	C45B	C46B	C41B	0.6(14)
C46	C41	C42	C43	2.4(10)	C46B	C41B	C42B	C43B	-1.5(12)
C47	C44	C45	C46	-176.5(6)	C47B	C44B	C45B	C46B	177.1(8)
Re02	Br2	C9B	O3B	-170(5)					

Table J.6 Hydrogen Atom Coordinates ($Å \times 10^4$) and Isotropic Displacement Parameters ($Å^2 \times 10^3$) for *fac*-[Re(Cbutyl-4-p-tolyl)$(CO)_3$Br].

Atom	***x***	***y***	***z***	**U(eq)**
H1	2004	-1522	-3221	22
H3A	562	-1393	-4544	29
H3B	2213	-1494	-4347	29
H4A	698	-2626	-3105	30
H4B	-639	-2290	-3560	30
H6A	453	-2748	-4461	49
H6B	1944	-2785	-4024	49
H12	-312	-1796	-2310	26
H13	-1271	-2489	-1503	36
H15	-5003	-1507	-2042	34
H16	-4030	-767	-2826	29
H17A	-4603	-2887	-1388	72
H17B	-4277	-2217	-867	72
H17C	-3170	-2874	-932	72
H22	-3318	-1934	-3673	27
H23	-4404	-2437	-4646	34
H25	-2619	-804	-5679	31
H26	-1543	-289	-4709	26
H27A	-5115	-1675	-6090	56
H27B	-4709	-2517	-5840	56
H27C	-3692	-2043	-6242	56
H32	1396	1379	-3988	24
H33	2864	1694	-4773	26
H35	4894	-329	-4440	26
H36	3506	-613	-3622	24
H37A	4709	482	-5611	43
H37B	5849	872	-5101	43
H37C	4626	1374	-5459	43
H42	3682	785	-2636	26
H43	5346	659	-1734	31
H45	2996	-979	-985	25
H46	1314	-849	-1887	21

H47A	5652	186	-447	45
H47B	6359	-444	-859	45
H47C	5228	-691	-398	45
H1B	2303	3102	-3532	23
H2BA	2223	3974	-4746	30
H2BB	2717	3091	-4629	30
H3BA	407	2664	-4623	35
H3BB	-53	3481	-4956	35
H4BA	-91	3213	-3613	28
H4BB	-78	4074	-3911	28
H12B	681	3828	-2569	22
H13B	-599	3718	-1670	29
H15B	-162	5986	-1308	30
H16B	1192	6115	-2177	26
H17D	-1858	5277	-763	60
H17E	-934	4584	-461	60
H17F	-2234	4421	-983	60
H22B	-743	5724	-3270	22
H23B	-2396	6105	-4130	25
H25B	339	5678	-5446	23
H26B	2026	5349	-4592	22
H27D	-2239	6666	-5555	51
H27E	-3254	6052	-5295	51
H27F	-2257	5810	-5823	51
H32B	5915	4923	-4274	28
H33B	6923	4388	-5161	33
H35B	6041	2250	-4544	30
H36B	5034	2775	-3665	29
H37D	7784	2507	-5410	45
H37E	7623	3311	-5776	45
H37F	6394	2706	-5860	45
H42B	7029	3613	-2643	43
H43B	7696	2756	-1791	47
H45B	3708	2534	-1438	45
H46B	3033	3394	-2279	40
H47D	5427	1808	-759	57
H47E	6777	2311	-578	57
H47F	6806	1610	-1071	57

K. Crystal data of *fac*-[Re(Chzyl-4-*p*-tolyl)(CO)$_3$Br]

Table K.1 Fractional Atomic Coordinates (×10^4) and Equivalent Isotropic Displacement Parameters (Å^2×10^3) for *fac*-[Re(Chzyl-4-*p*-tolyl)(CO)$_3$Br]. U_{eq} is defined as 1/3 of of the trace of the orthogonalised U_{IJ} tensor.

Atom	*x*	*y*	*z*	U(eq)
C1	7781(6)	778(6)	2816(5)	19.6(11)
C2	9208(8)	1593(7)	4083(6)	24.7(14)
C3	8759(8)	2183(7)	5183(6)	37.4(16)
C4	7714(10)	3093(8)	4620(7)	50(2)
C5	6245(9)	2231(9)	3427(7)	44.4(18)
C6	6645(7)	1640(7)	2285(6)	26.7(13)
C8	9442(7)	-2864(6)	-900(6)	20.9(11)
C7	10012(7)	-169(6)	-1778(6)	23.1(12)
C9	7226(11)	-1528(9)	-1678(9)	24.0(17)
C41	9469(6)	-1766(5)	3187(5)	18.3(10)
C46	11062(6)	-1133(6)	3830(5)	21.5(11)
C45	11889(7)	-1416(6)	5108(6)	24.7(12)
C44	11168(7)	-2319(6)	5787(6)	23.7(12)
C43	9586(8)	-2917(7)	5174(7)	27.9(15)
C42	8729(7)	-2658(6)	3871(6)	25.5(12)
C47	12082(8)	-2622(8)	7185(7)	35.2(15)
C31	6569(6)	-2744(5)	931(5)	18.5(10)
C36	6526(7)	-4118(6)	505(6)	26.4(12)
C35	5159(7)	-5199(6)	16(6)	30.6(14)
C34	3769(6)	-4959(6)	-101(5)	24.8(12)
C33	3812(6)	-3593(6)	334(6)	24.1(12)
C32	5190(6)	-2491(6)	845(5)	19.4(11)
C37	2253(8)	-6130(7)	-723(7)	38.8(16)
C21	7262(6)	1603(6)	-668(5)	18.1(10)
C26	5735(6)	832(6)	-992(5)	20.2(11)
C25	4528(7)	1194(6)	-1991(6)	24.1(12)
C24	4836(7)	2301(6)	-2691(5)	25.1(12)
C23	6366(7)	3051(6)	-2394(5)	26.1(12)
C22	7582(7)	2706(6)	-1395(6)	24.4(12)
C27	3527(8)	2716(8)	-3746(7)	40.5(17)
C11	10273(6)	2760(5)	1514(5)	17.3(10)
C16	9930(7)	4032(6)	1631(6)	25.0(12)
C15	11068(7)	5260(6)	2369(6)	27.5(13)
C14	12594(6)	5276(6)	3024(6)	23.0(11)
C13	12938(6)	4006(6)	2924(6)	24.4(12)
C12	11806(6)	2762(6)	2186(5)	22.7(12)
C17	13851(7)	6625(6)	3815(7)	34.6(15)
N1	8189(5)	223(4)	1694(4)	15.4(9)
O2	9466(6)	-3976(5)	-1230(5)	35.7(11)

O1	10424(6)	324(5)	-2587(5)	36.2(11)
Br1B	6631(10)	-1857(9)	-2222(9)	28.6(16)
P2	8417.8(16)	-1409.0(15)	1476.7(15)	15.7(3)
P1	8845.8(16)	1090.7(15)	569.9(14)	14.9(3)
Br1A	12367.5(10)	-460.5(8)	1084.3(9)	24.19(17)
Re1	9367.0(2)	-968.1(2)	-369.0(2)	15.62(5)
O3	5998(10)	-1897(12)	-2489(10)	51(3)

Table K.2 Anisotropic Displacement Parameters ($Å^2 \times 10^3$) for *fac*-[Re(Chzyl-4-*p*-tolyl)$(CO)_3$Br]. The Anisotropic displacement factor exponent takes the form: $-2\pi^2[h^2a^{*2}U_{11}+...+2hka\times b\times U_{12}]$

Atom	**U_{11}**	**U_{22}**	**U_{33}**	**U_{23}**	**U_{13}**	**U_{12}**
C1	17(3)	22(3)	19(3)	-1(2)	4(2)	8(2)
C2	23(3)	26(3)	20(3)	-5(3)	4(2)	9(3)
C3	39(4)	43(4)	25(3)	-7(3)	7(3)	12(3)
C4	75(6)	51(4)	40(4)	-3(3)	32(4)	34(4)
C5	47(4)	64(5)	39(4)	4(3)	23(3)	35(4)
C6	23(3)	36(3)	25(3)	2(2)	10(2)	15(3)
C8	18(3)	20(3)	25(3)	3(2)	10(2)	2(2)
C7	23(3)	21(3)	27(3)	4(2)	10(2)	10(2)
C9	30(5)	23(4)	24(4)	0(3)	16(4)	8(4)
C41	18(3)	16(2)	19(2)	-0.5(19)	4(2)	9(2)
C46	19(3)	22(3)	23(3)	4(2)	9(2)	4(2)
C45	18(3)	28(3)	23(3)	-3(2)	4(2)	7(2)
C44	25(3)	27(3)	18(3)	3(2)	4(2)	12(2)
C43	31(4)	28(4)	24(3)	8(3)	9(3)	9(3)
C42	19(3)	28(3)	26(3)	6(2)	6(2)	5(2)
C47	36(4)	42(4)	33(3)	18(3)	13(3)	18(3)
C31	16(3)	17(2)	18(2)	-0.8(19)	2(2)	2(2)
C36	24(3)	20(3)	36(3)	-3(2)	13(2)	6(2)
C35	34(3)	18(3)	37(3)	-7(2)	18(3)	-1(2)
C34	20(3)	27(3)	21(3)	1(2)	8(2)	-4(2)
C33	12(3)	32(3)	28(3)	8(2)	7(2)	5(2)
C32	17(3)	21(3)	21(2)	6(2)	8(2)	7(2)
C37	29(3)	40(4)	32(3)	-7(3)	11(3)	-14(3)
C21	17(3)	20(2)	18(2)	1.5(19)	6(2)	9(2)
C26	20(3)	19(2)	23(3)	3(2)	7(2)	8(2)
C25	16(3)	27(3)	22(3)	-1(2)	0(2)	6(2)
C24	23(3)	35(3)	17(2)	2(2)	4(2)	16(3)
C23	27(3)	33(3)	22(3)	10(2)	9(2)	13(3)
C22	21(3)	30(3)	26(3)	7(2)	11(2)	11(2)
C27	30(4)	57(4)	31(3)	13(3)	2(3)	21(3)
C11	19(3)	16(2)	20(2)	3.1(19)	9(2)	7(2)
C16	18(3)	22(3)	34(3)	0(2)	7(2)	8(2)
C15	24(3)	21(3)	36(3)	-4(2)	10(3)	9(2)

C14	21(3)	21(3)	25(3)	0(2)	8(2)	5(2)
C13	16(3)	27(3)	27(3)	0(2)	4(2)	8(2)
C12	20(3)	20(3)	24(3)	0(2)	2(2)	9(2)
C17	28(3)	26(3)	42(4)	-6(3)	8(3)	5(3)
N1	17(2)	14.5(19)	15.2(19)	1.1(15)	5.2(17)	6.3(17)
O2	40(3)	17(2)	57(3)	2(2)	26(2)	8(2)
O1	43(3)	40(3)	36(2)	14(2)	27(2)	12(2)
Br1B	36(6)	24(3)	21(4)	-7(2)	8(4)	8(4)
P2	13.4(7)	14.8(6)	18.2(6)	0.9(5)	4.7(5)	5.8(5)
P1	11.8(7)	16.3(7)	16.4(6)	1.9(5)	4.5(5)	5.3(5)
Br1A	15.4(4)	26.7(4)	30.3(4)	0.3(3)	7.2(3)	9.3(3)
Re1	14.46(9)	14.95(8)	18.70(8)	1.83(6)	6.98(7)	5.73(6)
O3	45(6)	57(5)	41(5)	1(4)	10(5)	12(5)

Table K.3 Bond Lengths for *fac*-[Re(Chzyl-4-*p*-tolyl)$(CO)_3$Br].

Atom	**Atom**	**Length/Å**	**Atom**	**Atom**	**Length/Å**
C1	C2	1.531(8)	C34	C33	1.390(8)
C1	C6	1.524(7)	C34	C37	1.517(8)
C1	N1	1.502(7)	C33	C32	1.397(8)
C2	C3	1.522(9)	C21	C26	1.390(8)
C3	C4	1.504(10)	C21	C22	1.401(8)
C4	C5	1.524(11)	C21	P1	1.821(5)
C5	C6	1.529(9)	C26	C25	1.400(7)
C8	O2	1.145(7)	C25	C24	1.383(8)
C8	Re1	1.956(6)	C24	C23	1.392(9)
C7	O1	1.150(7)	C24	C27	1.516(8)
C7	Re1	1.945(6)	C23	C22	1.397(7)
C9	Br1B	0.644(8)	C11	C16	1.390(7)
C9	Re1	1.947(9)	C11	C12	1.394(7)
C9	O3	1.138(10)	C11	P1	1.823(5)
C41	C46	1.396(8)	C16	C15	1.381(8)
C41	C42	1.394(8)	C15	C14	1.383(8)
C41	P2	1.826(5)	C14	C13	1.386(8)
C46	C45	1.381(7)	C14	C17	1.516(8)
C45	C44	1.385(9)	C13	C12	1.390(7)
C44	C43	1.381(9)	N1	P2	1.698(4)
C44	C47	1.510(7)	N1	P1	1.713(5)
C43	C42	1.400(8)	Br1B	Re1	2.554(9)
C31	C36	1.395(7)	Br1B	O3	0.565(9)
C31	C32	1.394(8)	P2	P1	2.684(2)
C31	P2	1.810(5)	P2	Re1	2.4586(16)
C36	C35	1.380(8)	P1	Re1	2.4635(15)
C35	C34	1.390(9)	Br1A	Re1	2.6489(10)

Table K.4 Bond Angles for *fac*-[Re(Chzyl-4-*p*-tolyl)$(CO)_3$Br].

Atom	Atom	Atom	Angle/°	Atom	Atom	Atom	Angle/°
C6	C1	C2	112.1(5)	C13	C14	C17	120.9(5)
N1	C1	C2	112.6(5)	C14	C13	C12	121.8(5)
N1	C1	C6	111.4(4)	C13	C12	C11	120.4(5)
C3	C2	C1	111.4(6)	C1	N1	P2	125.1(4)
C4	C3	C2	111.1(5)	C1	N1	P1	130.2(4)
C3	C4	C5	110.1(6)	P2	N1	P1	103.8(2)
C4	C5	C6	110.3(6)	C9	Br1B	Re1	16.8(12)
C1	C6	C5	111.7(5)	O3	Br1B	C9	140(3)
O2	C8	Re1	178.9(6)	O3	Br1B	Re1	157(2)
O1	C7	Re1	178.4(6)	C41	P2	P1	126.72(18)
Br1B	C9	Re1	157.8(15)	C41	P2	Re1	127.44(19)
Br1B	C9	O3	18.5(13)	C31	P2	C41	102.7(2)
O3	C9	Re1	176.2(10)	C31	P2	P1	124.28(17)
C46	C41	P2	119.3(4)	C31	P2	Re1	113.82(18)
C42	C41	C46	118.8(5)	N1	P2	C41	106.7(2)
C42	C41	P2	121.9(4)	N1	P2	C31	109.9(2)
C45	C46	C41	120.3(5)	N1	P2	P1	38.31(16)
C46	C45	C44	121.3(5)	N1	P2	Re1	95.31(16)
C45	C44	C47	120.9(5)	Re1	P2	P1	57.04(5)
C43	C44	C45	118.7(5)	C21	P1	C11	104.6(2)
C43	C44	C47	120.4(6)	C21	P1	P2	122.23(19)
C44	C43	C42	120.9(6)	C21	P1	Re1	113.31(17)
C41	C42	C43	119.9(6)	C11	P1	P2	127.15(17)
C36	C31	P2	116.6(4)	C11	P1	Re1	126.25(18)
C32	C31	C36	118.2(5)	N1	P1	C21	108.3(2)
C32	C31	P2	125.1(4)	N1	P1	C11	108.1(2)
C35	C36	C31	121.1(6)	N1	P1	P2	37.92(14)
C36	C35	C34	121.5(5)	N1	P1	Re1	94.73(15)
C35	C34	C37	121.3(6)	Re1	P1	P2	56.87(5)
C33	C34	C35	117.5(5)	C8	Re1	Br1B	82.8(2)
C33	C34	C37	121.1(6)	C8	Re1	P2	100.14(19)
C34	C33	C32	121.6(5)	C8	Re1	P1	165.50(19)
C31	C32	C33	120.1(5)	C8	Re1	Br1A	84.73(17)
C26	C21	C22	119.2(5)	C7	Re1	C8	94.0(3)
C26	C21	P1	120.8(4)	C7	Re1	C9	89.7(3)
C22	C21	P1	119.7(4)	C7	Re1	Br1B	87.2(3)
C21	C26	C25	120.4(5)	C7	Re1	P2	165.66(18)
C24	C25	C26	120.6(5)	C7	Re1	P1	99.64(18)
C25	C24	C23	119.1(5)	C7	Re1	Br1A	84.61(17)
C25	C24	C27	120.5(6)	C9	Re1	C8	87.5(3)
C23	C24	C27	120.3(6)	C9	Re1	Br1B	5.5(4)
C24	C23	C22	120.9(5)	C9	Re1	P2	88.4(3)

C23	C22	C21	119.7(5)	C9	Re1	P1	87.6(3)
C16	C11	C12	117.6(5)	P2	Re1	Br1B	92.0(2)
C16	C11	P1	124.3(4)	P2	Re1	P1	66.09(5)
C12	C11	P1	118.2(4)	P2	Re1	Br1A	99.18(4)
C15	C16	C11	121.4(5)	P1	Re1	Br1B	92.84(19)
C16	C15	C14	121.4(5)	P1	Re1	Br1A	101.44(4)
C15	C14	C13	117.4(5)	Br1B	O3	C9	21.2(15)
C15	C14	C17	121.6(5)				

Table K.5 Torsion Angles for *fac*-[Re(Chzyl-4-*p*-tolyl)$(CO)_3$Br].

A	**B**	**C**	**D**	**Angle**/°	**A**	**B**	**C**	**D**	**Angle**/°
C1	C2	C3	C4	-55.8(8)	C26	C21	C22	C23	2.5(8)
C1	N1	P2	C41	-41.2(5)	C26	C21	P1	C11	-142.4(5)
C1	N1	P2	C31	69.4(4)	C26	C21	P1	N1	-27.2(5)
C1	N1	P2	P1	-170.1(5)	C26	C21	P1	P2	12.1(5)
C1	N1	P2	Re1	-172.9(4)	C26	C21	P1	Re1	76.5(5)
C1	N1	P1	C21	-71.4(5)	C26	C25	C24	C23	0.2(9)
C1	N1	P1	C11	41.5(5)	C26	C25	C24	C27	-178.4(6)
C1	N1	P1	P2	169.3(6)	C25	C24	C23	C22	-0.5(9)
C1	N1	P1	Re1	172.1(4)	C24	C23	C22	C21	-0.8(9)
C2	C1	C6	C5	-51.8(8)	C22	C21	C26	C25	-2.8(8)
C2	C1	N1	P2	92.6(5)	C22	C21	P1	C11	43.4(5)
C2	C1	N1	P1	-74.7(6)	C22	C21	P1	N1	158.6(4)
C2	C3	C4	C5	59.7(8)	C22	C21	P1	P2	-162.1(4)
C3	C4	C5	C6	-59.3(8)	C22	C21	P1	Re1	-97.7(4)
C4	C5	C6	C1	55.4(8)	C27	C24	C23	C22	178.1(5)
C6	C1	C2	C3	51.6(7)	C11	C16	C15	C14	-0.1(10)
C6	C1	N1	P2	-140.5(4)	C16	C11	C12	C13	-0.9(8)
C6	C1	N1	P1	52.2(6)	C16	C11	P1	C21	23.3(5)
C41	C46	C45	C44	-0.5(9)	C16	C11	P1	N1	-92.1(5)
C46	C41	C42	C43	-0.7(9)	C16	C11	P1	P2	-129.6(4)
C46	C41	P2	C31	167.0(4)	C16	C11	P1	Re1	157.6(4)
C46	C41	P2	N1	-77.5(5)	C16	C15	C14	C13	-0.7(9)
C46	C41	P2	P1	-40.4(5)	C16	C15	C14	C17	179.0(6)
C46	C41	P2	Re1	33.1(5)	C15	C14	C13	C12	0.7(9)
C46	C45	C44	C43	-1.3(9)	C14	C13	C12	C11	0.1(9)
C46	C45	C44	C47	-180.0(6)	C12	C11	C16	C15	0.9(9)
C45	C44	C43	C42	2.2(10)	C12	C11	P1	C21	-158.0(4)
C44	C43	C42	C41	-1.1(10)	C12	C11	P1	N1	86.7(5)
C42	C41	C46	C45	1.5(8)	C12	C11	P1	P2	49.2(5)
C42	C41	P2	C31	-12.9(5)	C12	C11	P1	Re1	-23.6(5)
C42	C41	P2	N1	102.7(5)	C17	C14	C13	C12	-179.0(6)
C42	C41	P2	P1	139.7(4)	N1	C1	C2	C3	178.2(5)
C42	C41	P2	Re1	-146.7(4)	N1	C1	C6	C5	-179.0(5)

C47	C44	C43	C42	-179.2(6)	P2	C41	C46	C45	-178.3(4)
C31	C36	C35	C34	1.5(9)	P2	C41	C42	C43	179.1(5)
C36	C31	C32	C33	-0.5(8)	P2	C31	C36	C35	-177.3(5)
C36	C31	P2	C41	-76.4(5)	P2	C31	C32	C33	176.3(4)
C36	C31	P2	N1	170.4(4)	P2	N1	P1	C21	119.3(2)
C36	C31	P2	P1	130.1(4)	P2	N1	P1	C11	-127.9(2)
C36	C31	P2	Re1	64.9(4)	P2	N1	P1	Re1	2.8(2)
C36	C35	C34	C33	-1.9(9)	P1	C21	C26	C25	-177.0(4)
C36	C35	C34	C37	176.1(6)	P1	C21	C22	C23	176.8(4)
C35	C34	C33	C32	1.2(8)	P1	C11	C16	C15	179.7(5)
C34	C33	C32	C31	-0.1(8)	P1	C11	C12	C13	-179.8(4)
C32	C31	C36	C35	-0.2(8)	P1	N1	P2	C41	128.9(2)
C32	C31	P2	C41	106.8(5)	P1	N1	P2	C31	-120.5(2)
C32	C31	P2	N1	-6.4(5)	P1	N1	P2	Re1	-2.8(2)
C32	C31	P2	P1	-46.7(5)	Re1	C9	Br1B	O3	-179(3)
C32	C31	P2	Re1	-112.0(4)	Re1	Br1B	O3	C9	-1(2)
C37	C34	C33	C32	-176.8(5)	O3	C9	Br1B	Re1	179(3)
C21	C26	C25	C24	1.5(9)					

Table K.6 Hydrogen Atom Coordinates (Å×10^4) and Isotropic Displacement Parameters (Å^2×10^3) for *fac*-[Re(Chzyl-4-*p*-tolyl)$(CO)_3$Br].

Atom	***x***	***y***	***z***	**U(eq)**
H1	7248	-47	3110	24
H2A	9832	968	4458	30
H2B	9828	2365	3814	30
H3A	8236	1407	5524	45
H3B	9684	2739	5947	45
H4A	8246	3888	4306	60
H4B	7449	3463	5339	60
H5A	5577	2825	3070	53
H5B	5693	1458	3750	53
H6A	5705	1046	1560	32
H6B	7091	2416	1895	32
H12	11568	-518	3396	26
H13	12951	-992	5521	30
H15	9083	-3500	5633	33
H16	7667	-3081	3463	31
H17A	12052	-1988	7886	53
H17B	13134	-2489	7290	53
H17C	11639	-3581	7267	53
H22	7433	-4308	551	32
H23	5168	-6109	-241	37
H25	2901	-3409	283	29
H26	5188	-1586	1128	23

H27A	2428	-7014	-482	58
H27B	1844	-6190	-1705	58
H27C	1529	-5927	-375	58
H32	5513	72	-543	24
H33	3509	685	-2185	29
H35	6582	3791	-2866	31
H36	8600	3206	-1213	29
H37A	2555	2117	-3800	61
H37B	3592	2611	-4628	61
H37C	3606	3684	-3479	61
H42	8914	4057	1204	30
H43	10801	6095	2426	33
H45	13954	3986	3364	29
H46	12073	1926	2139	27
H47A	14839	6519	3911	52
H47B	13838	6813	4709	52
H47C	13671	7399	3326	52

L. Crystal data of *fac*-[Re(NBoc-PhPNP)(CO)$_3$Br]

Table L.1 Fractional Atomic Coordinates ($\times 10^4$) and Equivalent Isotropic Displacement Parameters ($Å^2 \times 10^3$) for *fac*-[Re(NBoc-PhPNP)(CO)$_3$Br]. U_{eq} is defined as 1/3 of of the trace of the orthogonalised U_{IJ} tensor.

Atom	***x***	***y***	***z***	**U(eq)**
Re1	6125.1(2)	1799.3(2)	417.9(2)	14.45(4)
Br1	4704(2)	821.8(13)	794.7(18)	28.2(4)
Br1A	7437.9(7)	2746.1(4)	-104.5(4)	21.0(2)
P1	6726.2(7)	2247.8(4)	1836.4(4)	14.19(14)
P2	8061.5(7)	1247.1(4)	1335.4(4)	14.78(14)
O1	3735(2)	2728.4(13)	-219.6(15)	32.1(5)
O2	5534(2)	961.9(13)	-1249.9(14)	31.5(5)
O3	4439(9)	658(5)	797(7)	48(2)
O3A	7689(16)	2927(9)	-214(11)	53(7)
O4	11552(2)	822.4(13)	3909.8(14)	30.7(5)
O5	11821(2)	1121.4(11)	5253.6(13)	22.8(4)
N1	7987(2)	1696.9(12)	2193.1(15)	17.3(5)
N2	10588(2)	1792.6(14)	4242.6(16)	26.0(6)
C1	8695(3)	1562.5(16)	3082.0(18)	19.7(6)
C2	9918(3)	1977.6(17)	3382.1(19)	23.8(6)
C3	11343(3)	1204.3(16)	4425.7(19)	21.3(6)
C4	11947(4)	-213.3(19)	5341(3)	40.9(9)
C5	13812(3)	541(2)	5380(2)	37.5(8)
C6	12942(4)	627(2)	6538(2)	38.7(9)
C7	4635(3)	2396.7(16)	-9.8(18)	21.1(6)
C8	5797(3)	1273.0(16)	-638.3(19)	20.4(6)

C9	5111(5)	1089(3)	691(3)	27.7(11)
C9A	7063(10)	2509(5)	35(7)	14(3)
C10	12646(3)	498.1(16)	5612.1(19)	23.6(6)
C11	7167(3)	3180.3(14)	2173.5(18)	17.2(5)
C12	7612(3)	3354.3(15)	3014.1(19)	21.1(6)
C13	7904(3)	4074.8(17)	3266(2)	25.5(7)
C14	7708(3)	4620.8(17)	2677(2)	28.2(7)
C15	7267(3)	4453.8(16)	1846(2)	26.0(7)
C16	7007(3)	3732.0(15)	1589.4(19)	21.1(6)
C21	5702(3)	2004.5(15)	2409.7(17)	17.2(5)
C22	4889(3)	2525.2(17)	2545.3(19)	22.9(6)
C23	3990(3)	2310.3(19)	2885(2)	28.8(7)
C24	3892(3)	1585(2)	3087(2)	32.3(8)
C25	4699(3)	1074.7(19)	2968(2)	30.6(7)
C26	5598(3)	1278.2(17)	2627(2)	24.7(6)
C31	8249(3)	281.4(14)	1577.3(18)	17.6(6)
C32	7372(3)	-207.1(16)	1109(2)	25.0(7)
C33	7526(3)	-957.3(17)	1267(2)	32.1(8)
C34	8534(3)	-1212.9(16)	1894(2)	29.5(7)
C35	9421(3)	-733.1(16)	2367(2)	25.8(7)
C36	9296(3)	13.4(16)	2207.4(19)	21.6(6)
C41	9526(3)	1484.0(16)	1197.3(18)	19.7(6)
C42	10133(3)	985.8(18)	844(2)	28.8(7)
C43	11196(4)	1192(2)	673(3)	42.1(9)
C44	11674(3)	1887(2)	870(2)	44.4(10)
C45	11083(3)	2383(2)	1216(2)	38.5(9)
C46	10005(3)	2190.0(18)	1377.9(19)	27.1(7)

Table L.2 Anisotropic Displacement Parameters ($Å^2 \times 10^3$) for *fac*-[Re(NBoc-PhPNP)$(CO)_3$Br]. The Anisotropic displacement factor exponent takes the form: $-2\pi^2[h^2a^{*2}U_{11}+...+2hka \times b \times U_{12}]$

Atom	**U_{11}**	**U_{22}**	**U_{33}**	**U_{23}**	**U_{13}**	**U_{12}**
Re1	15.29(6)	13.73(6)	13.59(6)	0.08(4)	3.73(4)	-0.43(4)
Br1	30.0(12)	27.0(11)	26.3(8)	-4.1(8)	7.7(8)	0.5(8)
Br1A	26.9(4)	19.1(4)	18.5(3)	1.0(2)	9.6(2)	-4.3(3)
P1	15.6(3)	12.1(3)	14.2(3)	0.8(2)	3.8(3)	0.8(3)
P2	15.0(3)	12.9(3)	16.1(3)	-0.2(3)	4.6(3)	-0.7(3)
O1	28.3(13)	32.9(12)	33.3(13)	4(1)	8(1)	12(1)
O2	41.4(14)	32.2(12)	22.7(12)	-7.4(10)	12.9(11)	-4.4(10)
O3	46(5)	46(5)	47(3)	-7(3)	9(3)	-4(3)
O3A	65(11)	33(8)	82(12)	2(6)	52(8)	-20(6)
O4	33.8(13)	33.3(12)	23.2(12)	-3.3(10)	7(1)	11.9(10)
O5	25.1(11)	21.7(10)	18.2(10)	-0.4(8)	2.4(9)	7.3(8)
N1	17.9(12)	15.3(11)	16.3(12)	0.3(9)	2.5(10)	4.0(9)
N2	25.1(14)	27.2(13)	20.3(13)	-6.4(11)	0.0(11)	7.0(11)

C1	21.8(15)	18.8(13)	17.7(14)	1.7(11)	5.6(12)	2.0(11)
C2	23.9(16)	22.6(14)	22.1(15)	2.1(12)	3.8(13)	1.5(12)
C3	18.4(15)	21.9(14)	21.6(15)	-0.7(12)	3.7(12)	1.1(11)
C4	54(2)	23.9(17)	45(2)	2.2(15)	15.5(19)	-3.3(16)
C5	29.2(19)	45(2)	37(2)	14.4(17)	9.7(16)	12.7(16)
C6	52(2)	36.7(19)	23.4(17)	4.7(14)	6.9(16)	16.1(17)
C7	25.0(16)	18.7(13)	18.8(14)	-1.4(11)	6.0(12)	-1.7(12)
C8	19.3(15)	21.6(14)	20.2(15)	2.0(12)	6.5(12)	0.1(11)
C9	37(3)	24(3)	23(2)	1(2)	10(2)	4(2)
C9A	16(7)	16(7)	13(6)	-4(5)	7(5)	-1(5)
C10	26.6(16)	19.5(14)	23.9(16)	3.8(12)	7.1(13)	6.0(12)
C11	16.5(13)	12.8(12)	22.0(14)	0.4(11)	6.0(11)	0.3(10)
C12	21.9(15)	17.8(13)	23.9(15)	0.5(11)	8.0(12)	1.2(11)
C13	21.6(16)	25.8(15)	28.5(17)	-10.6(13)	7.4(13)	-3.1(12)
C14	23.5(16)	16.4(14)	44(2)	-7.2(13)	11.1(15)	-4.4(12)
C15	27.6(17)	14.9(13)	35.5(18)	5.2(12)	10.5(14)	-0.4(12)
C16	21.0(15)	18.4(13)	24.2(15)	0.3(11)	7.9(12)	0.9(11)
C21	18.1(14)	19.5(13)	12.8(13)	-0.3(10)	3.3(11)	-1.6(11)
C22	20.5(15)	25.1(15)	21.9(15)	-1.9(12)	5.5(12)	0.1(12)
C23	20.4(16)	39.8(18)	27.3(17)	-5.6(14)	9.4(13)	-1.5(14)
C24	23.9(17)	49(2)	25.4(17)	2.3(15)	9.8(14)	-12.3(15)
C25	26.8(17)	31.8(17)	31.3(18)	11.6(14)	6.9(14)	-6.6(14)
C26	19.8(15)	21.7(14)	30.1(17)	6.3(12)	4.8(13)	0.3(12)
C31	18.6(14)	14.1(12)	23.4(15)	-2.5(11)	11.3(12)	-0.8(10)
C32	20.9(15)	19.1(14)	32.2(17)	-3.7(12)	4.9(13)	0.8(12)
C33	28.2(18)	19.6(15)	46(2)	-6.7(14)	9.4(16)	-5.1(13)
C34	26.4(17)	15.9(14)	50(2)	3.1(14)	18.4(16)	3.0(12)
C35	19.4(15)	22.4(15)	36.0(18)	7.7(13)	9.6(14)	5.4(12)
C36	17.8(14)	19.3(14)	27.8(16)	1.2(12)	7.6(12)	-0.2(11)
C41	16.3(14)	22.7(14)	19.3(14)	3.4(11)	4.6(11)	-2.7(11)
C42	29.0(18)	30.6(17)	31.8(18)	6.3(14)	16.9(15)	3.1(13)
C43	36(2)	55(2)	45(2)	16.0(19)	26.6(18)	10.6(18)
C44	24.2(18)	72(3)	38(2)	22(2)	11.6(16)	-9.8(18)
C45	33(2)	50(2)	26.4(18)	10.8(16)	1.8(15)	-22.0(17)
C46	32.0(18)	28.3(16)	19.4(15)	2.2(12)	6.2(13)	-8.9(13)

Table L.3 Bond Lengths for *fac*-[Re(NBoc-PhPNP)$(CO)_3$Br].

Atom	Atom	Length/Å	Atom	Atom	Length/Å
Re1	Br1	2.6310(17)	C5	C10	1.510(5)
Re1	Br1A	2.6291(11)	C6	C10	1.522(5)
Re1	P1	2.4314(10)	C11	C12	1.392(4)
Re1	P2	2.4636(10)	C11	C16	1.388(4)
Re1	C7	1.948(3)	C12	C13	1.392(4)
Re1	C8	1.968(3)	C13	C14	1.381(5)

Re1	C9	1.897(6)	C14	C15	1.374(5)
Re1	C9A	1.928(2)	C15	C16	1.391(4)
P1	P2	2.6935(11)	C21	C22	1.400(4)
P1	N1	1.696(2)	C21	C26	1.394(4)
P1	C11	1.817(3)	C22	C23	1.391(4)
P1	C21	1.809(3)	C23	C24	1.384(5)
P2	N1	1.706(2)	C24	C25	1.372(5)
P2	C31	1.810(3)	C25	C26	1.386(4)
P2	C41	1.814(3)	C31	C32	1.382(4)
O1	C7	1.144(4)	C31	C36	1.406(4)
O2	C8	1.139(4)	C32	C33	1.398(4)
O3	C9	1.153(2)	C33	C34	1.369(5)
O3A	C9A	1.213(15)	C34	C35	1.381(5)
O4	C3	1.208(4)	C35	C36	1.390(4)
O5	C3	1.345(4)	C41	C42	1.396(4)
O5	C10	1.476(3)	C41	C46	1.396(4)
N1	C1	1.486(4)	C42	C43	1.389(5)
N2	C2	1.455(4)	C43	C44	1.380(6)
N2	C3	1.348(4)	C44	C45	1.375(6)
C1	C2	1.520(4)	C45	C46	1.391(5)
C4	C10	1.516(5)			

Table L.4 Bond Angles for *fac*-[Re(NBoc-PhPNP)$(CO)_3$Br].

Atom	**Atom**	**Atom**	**Angle/°**	**Atom**	**Atom**	**Atom**	**Angle/°**
P1	Re1	Br1	88.85(7)	C3	N2	C2	120.2(3)
P1	Re1	Br1A	96.34(3)	N1	C1	C2	113.0(2)
P1	Re1	P2	66.77(3)	N2	C2	C1	110.0(2)
P2	Re1	Br1	93.52(7)	O4	C3	O5	126.3(3)
P2	Re1	Br1A	89.68(4)	O4	C3	N2	123.8(3)
C7	Re1	Br1	86.62(11)	O5	C3	N2	109.9(3)
C7	Re1	Br1A	91.57(9)	O1	C7	Re1	175.4(3)
C7	Re1	P1	96.26(9)	O2	C8	Re1	175.8(3)
C7	Re1	P2	163.01(9)	O3	C9	Re1	175.0(9)
C7	Re1	C8	92.96(12)	O3A	C9A	Re1	176.6(16)
C8	Re1	Br1	86.86(11)	O5	C10	C4	109.7(3)
C8	Re1	Br1A	88.22(9)	O5	C10	C5	110.3(3)
C8	Re1	P1	169.58(9)	O5	C10	C6	101.8(2)
C8	Re1	P2	104.02(9)	C4	C10	C6	111.4(3)
C9	Re1	Br1A	174.71(17)	C5	C10	C4	112.6(3)
C9	Re1	P1	88.90(16)	C5	C10	C6	110.6(3)
C9	Re1	P2	93.11(17)	C12	C11	P1	120.7(2)
C9	Re1	C7	87.08(19)	C16	C11	P1	119.8(2)
C9	Re1	C8	86.74(18)	C16	C11	C12	119.4(3)
C9A	Re1	Br1	174.6(4)	C13	C12	C11	120.2(3)

C9A	Re1	P1	96.0(4)	C14	C13	C12	119.7(3)
C9A	Re1	P2	90.6(4)	C15	C14	C13	120.4(3)
C9A	Re1	C7	90.5(4)	C14	C15	C16	120.2(3)
C9A	Re1	C8	88.7(4)	C11	C16	C15	119.9(3)
Re1	P1	P2	57.19(2)	C22	C21	P1	120.2(2)
N1	P1	Re1	94.87(9)	C26	C21	P1	120.3(2)
N1	P1	P2	37.77(8)	C26	C21	C22	119.0(3)
N1	P1	C11	109.30(13)	C23	C22	C21	119.7(3)
N1	P1	C21	106.36(13)	C24	C23	C22	120.4(3)
C11	P1	Re1	126.15(10)	C25	C24	C23	120.1(3)
C11	P1	P2	127.73(10)	C24	C25	C26	120.3(3)
C21	P1	Re1	115.81(10)	C25	C26	C21	120.4(3)
C21	P1	P2	122.54(10)	C32	C31	P2	119.4(2)
C21	P1	C11	102.70(13)	C32	C31	C36	119.2(3)
Re1	P2	P1	56.04(3)	C36	C31	P2	121.4(2)
N1	P2	Re1	93.46(8)	C31	C32	C33	120.1(3)
N1	P2	P1	37.50(8)	C34	C33	C32	120.4(3)
N1	P2	C31	108.06(12)	C33	C34	C35	120.3(3)
N1	P2	C41	107.74(13)	C34	C35	C36	120.1(3)
C31	P2	Re1	123.95(10)	C35	C36	C31	119.9(3)
C31	P2	P1	128.81(9)	C42	C41	P2	120.6(2)
C31	P2	C41	102.61(13)	C42	C41	C46	119.0(3)
C41	P2	Re1	119.35(10)	C46	C41	P2	120.1(2)
C41	P2	P1	121.32(10)	C43	C42	C41	120.3(3)
C3	O5	C10	120.3(2)	C44	C43	C42	120.0(4)
P1	N1	P2	104.73(13)	C45	C44	C43	120.2(3)
C1	N1	P1	125.19(19)	C44	C45	C46	120.5(3)
C1	N1	P2	129.26(19)	C45	C46	C41	119.9(3)

Table L.5 Torsion Angles for *fac*-[Re(NBoc-PhPNP)$(CO)_3$Br].

A	**B**	**C**	**D**	**Angle/°**	**A**	**B**	**C**	**D**	**Angle/°**
Re1	P1	N1	P2	3.74(12)	C3	O5	C10	C6	-179.8(3)
Re1	P1	N1	C1	-166.7(2)	C3	N2	C2	C1	86.6(3)
Re1	P1	C11	C12	-173.54(19)	C10	O5	C3	O4	-2.9(5)
Re1	P1	C11	C16	9.4(3)	C10	O5	C3	N2	177.9(3)
Re1	P1	C21	C22	-104.1(2)	C11	P1	N1	P2	-127.34(14)
Re1	P1	C21	C26	67.5(3)	C11	P1	N1	C1	62.2(3)
Re1	P2	N1	P1	-3.68(11)	C11	P1	C21	C22	37.2(3)
Re1	P2	N1	C1	166.2(2)	C11	P1	C21	C26	-151.1(2)
Re1	P2	C31	C32	13.6(3)	C11	C12	C13	C14	2.3(5)
Re1	P2	C31	C36	-169.30(19)	C12	C11	C16	C15	-1.4(4)
Re1	P2	C41	C42	-106.3(2)	C12	C13	C14	C15	-2.2(5)
Re1	P2	C41	C46	68.1(3)	C13	C14	C15	C16	0.3(5)
P1	P2	N1	C1	169.9(3)	C14	C15	C16	C11	1.5(5)

P1	P2	C31	C32	84.8(3)	C16	C11	C12	C13	-0.5(4)
P1	P2	C31	C36	-98.1(2)	C21	P1	N1	P2	122.44(14)
P1	P2	C41	C42	-172.3(2)	C21	P1	N1	C1	-48.0(2)
P1	P2	C41	C46	2.2(3)	C21	P1	C11	C12	50.6(3)
P1	N1	C1	C2	-103.4(3)	C21	P1	C11	C16	-126.5(2)
P1	C11	C12	C13	-177.6(2)	C21	C22	C23	C24	-0.2(5)
P1	C11	C16	C15	175.8(2)	C22	C21	C26	C25	0.3(5)
P1	C21	C22	C23	171.2(2)	C22	C23	C24	C25	1.3(5)
P1	C21	C26	C25	-171.5(3)	C23	C24	C25	C26	-1.5(5)
P2	P1	N1	C1	-170.4(3)	C24	C25	C26	C21	0.7(5)
P2	P1	C11	C12	-100.0(2)	C26	C21	C22	C23	-0.6(4)
P2	P1	C11	C16	82.9(2)	C31	P2	N1	P1	-131.14(13)
P2	P1	C21	C22	-170.2(2)	C31	P2	N1	C1	38.8(3)
P2	P1	C21	C26	1.5(3)	C31	P2	C41	C42	35.1(3)
P2	N1	C1	C2	88.6(3)	C31	P2	C41	C46	-150.4(2)
P2	C31	C32	C33	177.6(3)	C31	C32	C33	C34	1.0(5)
P2	C31	C36	C35	-178.8(2)	C32	C31	C36	C35	-1.7(4)
P2	C41	C42	C43	174.4(3)	C32	C33	C34	C35	-1.2(5)
P2	C41	C46	C45	-175.5(2)	C33	C34	C35	C36	-0.2(5)
N1	P1	C11	C12	-62.0(3)	C34	C35	C36	C31	1.6(5)
N1	P1	C11	C16	120.9(2)	C36	C31	C32	C33	0.4(5)
N1	P1	C21	C22	152.0(2)	C41	P2	N1	P1	118.66(14)
N1	P1	C21	C26	-36.3(3)	C41	P2	N1	C1	-71.4(3)
N1	P2	C31	C32	120.8(2)	C41	P2	C31	C32	-125.5(2)
N1	P2	C31	C36	-62.1(3)	C41	P2	C31	C36	51.6(3)
N1	P2	C41	C42	149.0(2)	C41	C42	C43	C44	1.4(6)
N1	P2	C41	C46	-36.5(3)	C42	C41	C46	C45	-1.0(5)
N1	C1	C2	N2	-177.2(2)	C42	C43	C44	C45	-1.6(6)
C2	N2	C3	O4	3.3(5)	C43	C44	C45	C46	0.5(6)
C2	N2	C3	O5	-177.4(3)	C44	C45	C46	C41	0.8(5)
C3	O5	C10	C4	-61.7(4)	C46	C41	C42	C43	-0.1(5)
C3	O5	C10	C5	62.9(4)					

Table L.6 Hydrogen Atom Coordinates (Å×10^4) and Isotropic Displacement Parameters (Å^2×10^3) for *fac*-[Re(NBoc-PhPNP)(CO)$_3$Br].

Atom	***x***	***y***	***z***	**U(eq)**
H2	10503	2059	4635	31
H1A	8863	1043	3165	24
H1B	8189	1705	3415	24
H2A	10419	1853	3039	29
H2B	9758	2499	3334	29
H4A	11223	-218	5510	61
H4B	12475	-617	5593	61
H4C	11700	-256	4748	61

H5A	13598	520	4787	56
H5B	14347	138	5626	56
H5C	14234	993	5580	56
H6A	13309	1102	6681	58
H6B	13512	260	6843	58
H6C	12190	601	6674	58
H12	7715	2988	3409	25
H13	8230	4188	3827	31
H14	7876	5105	2844	34
H15	7141	4824	1454	31
H16	6727	3619	1027	25
H22	4950	3013	2409	27
H23	3451	2656	2977	35
H24	3278	1443	3304	39
H25	4643	590	3116	37
H26	6136	928	2542	30
H32	6678	-36	688	30
H33	6940	-1285	945	39
H34	8622	-1712	2001	35
H35	10104	-910	2792	31
H36	9904	335	2517	26
H42	9823	514	722	35
H43	11586	861	426	50
H44	12397	2020	768	53
H45	11406	2852	1343	46
H46	9604	2530	1606	33

M. Crystal data of *fac*-[^{99}Tc(Chzyl-4-*p*-tolyl)(CO)$_3$Cl]

Table M.1 Fractional Atomic Coordinates ($\times 10^4$) and Equivalent Isotropic Displacement Parameters ($Å^2 \times 10^3$) for *fac*-[^{99}Tc(Chzyl-4-*p*-tolyl)(CO)$_3$Cl]. U_{eq} is defined as 1/3 of of the trace of the orthogonalised U_{IJ} tensor.

Atom	***x***	***y***	***z***	**U(eq)**
C1	9685(6)	9106(6)	7830(5)	34.8(12)
C2	8461(8)	9878(8)	7313(6)	55.4(17)
C3	8007(9)	10340(11)	8454(8)	93(3)
C4	9459(11)	11251(11)	9644(9)	98(3)
C5	10608(9)	10458(9)	10183(6)	68(2)
C6	11085(7)	9902(7)	9097(6)	42.2(15)
C7	11997(7)	8202(6)	3337(6)	38.7(13)
C8	11397(6)	5499(6)	4194(6)	38.8(13)
C9	9178(7)	6833(6)	3386(6)	36.7(13)
C11	12223(5)	11081(5)	6601(5)	31.0(11)
C12	13775(6)	11099(6)	7216(5)	37.2(12)
C13	14900(6)	12329(6)	7941(6)	42.3(13)

C14	14551(6)	13575(6)	8091(6)	40.1(13)
C15	13009(7)	13558(6)	7496(6)	49.6(15)
C16	11855(6)	12328(6)	6774(6)	42.0(13)
C17	15824(7)	14919(7)	8870(7)	59.4(18)
C21	9213(5)	9988(5)	4428(5)	28.2(10)
C22	9522(6)	11088(6)	3715(5)	39.2(12)
C23	8322(7)	11448(6)	2717(5)	44.0(13)
C24	6775(6)	10702(6)	2376(5)	40.4(13)
C25	6468(6)	9596(6)	3053(6)	42.2(13)
C26	7663(6)	9210(6)	4071(5)	35.5(12)
C27	5481(8)	11106(9)	1298(7)	70(2)
C31	8457(5)	5599(5)	5959(5)	30.2(10)
C32	7077(6)	5850(6)	5862(5)	35.5(12)
C33	5698(6)	4780(7)	5362(6)	43.6(13)
C34	5663(6)	3428(7)	4929(5)	43.9(14)
C35	7054(7)	3163(6)	5050(6)	50.4(16)
C36	8452(7)	4247(6)	5549(6)	45.2(14)
C37	4134(8)	2258(8)	4306(7)	68(2)
C41	11386(6)	6551(5)	8211(5)	33.2(11)
C42	10666(6)	5648(6)	8894(6)	43.1(13)
C43	11508(8)	5382(7)	10173(7)	52.1(18)
C44	13109(7)	6005(6)	10801(6)	44.7(14)
C45	13812(6)	6907(6)	10137(5)	41.6(13)
C46	12985(6)	7197(6)	8857(5)	37.3(12)
C47	14028(9)	5686(8)	12170(7)	65(2)
N1	10102(5)	8549(5)	6744(4)	29.0(9)
O1	12408(6)	8664(5)	2555(5)	62.8(13)
O2	11419(5)	4423(5)	3863(5)	59.3(12)
O3	8017(5)	6486(5)	2586(5)	60.4(13)
P1	10784.7(14)	9441.3(14)	5649.4(13)	28.1(3)
P2	10333.8(14)	6926.1(13)	6523.7(13)	27.4(3)
Cl1	14160.7(17)	7852.9(17)	6182.0(17)	46.3(4)
Tc1	11308.8(2)	7381.6(2)	4717.7(2)	30.74(12)

Table M.2 Anisotropic Displacement Parameters ($Å^2 \times 10^3$) for *fac*-[^{99}Tc(Chzyl-4-*p*-tolyl)$(CO)_3$Cl]. The Anisotropic displacement factor exponent takes the form: $-2\pi^2[h^2a^{*2}U_{11}+...+2hka\times b\times U_{12}]$

Atom	**U_{11}**	**U_{22}**	**U_{33}**	**U_{23}**	**U_{13}**	**U_{12}**
C1	31(3)	40(3)	34(3)	-2(2)	10(2)	15(2)
C2	49(4)	69(5)	52(4)	-2(3)	17(3)	28(3)
C3	66(5)	144(9)	75(5)	-31(5)	26(4)	52(5)
C4	109(7)	120(8)	77(6)	-26(5)	39(5)	58(6)
C5	69(5)	83(6)	41(3)	-10(3)	12(3)	23(4)
C6	38(3)	53(4)	32(3)	-4(3)	10(2)	15(3)
C7	39(3)	32(3)	45(3)	4(3)	18(3)	8(2)

C8	32(3)	33(3)	49(3)	5(3)	15(2)	8(2)
C9	42(3)	33(3)	41(3)	0(2)	21(3)	15(3)
C11	24(2)	33(3)	36(3)	4(2)	10(2)	10(2)
C12	28(3)	38(3)	42(3)	4(2)	7(2)	14(2)
C13	27(3)	43(3)	49(3)	2(3)	7(2)	10(2)
C14	35(3)	37(3)	43(3)	-5(2)	15(2)	4(2)
C15	39(3)	33(3)	69(4)	-6(3)	16(3)	7(2)
C16	29(3)	35(3)	56(3)	1(3)	11(2)	9(2)
C17	41(3)	50(4)	71(4)	-18(3)	16(3)	-1(3)
C21	25(2)	29(3)	29(2)	0.7(19)	7.2(19)	10.3(19)
C22	33(3)	45(3)	41(3)	13(2)	15(2)	11(2)
C23	46(3)	50(4)	42(3)	16(3)	19(3)	19(3)
C24	35(3)	54(4)	30(3)	5(2)	4(2)	22(3)
C25	25(3)	47(3)	40(3)	-3(3)	0(2)	7(2)
C26	33(3)	31(3)	38(3)	6(2)	11(2)	7(2)
C27	58(4)	90(6)	49(4)	21(4)	-2(3)	31(4)
C31	27(2)	33(3)	28(2)	1(2)	8.6(19)	8(2)
C32	33(3)	40(3)	35(3)	5(2)	13(2)	14(2)
C33	26(3)	54(4)	49(3)	14(3)	15(2)	7(2)
C34	30(3)	56(4)	34(3)	3(3)	12(2)	-6(3)
C35	53(4)	32(3)	59(4)	-10(3)	26(3)	-5(3)
C36	39(3)	39(3)	57(4)	-8(3)	23(3)	6(2)
C37	53(4)	66(5)	55(4)	-8(3)	17(3)	-27(3)
C41	26(2)	32(3)	36(3)	-1(2)	6(2)	10(2)
C42	31(3)	48(3)	43(3)	9(3)	10(2)	6(2)
C43	42(4)	52(4)	54(4)	22(3)	12(3)	6(3)
C44	46(3)	47(4)	37(3)	3(3)	9(3)	18(3)
C45	30(3)	48(3)	38(3)	1(2)	5(2)	9(2)
C46	32(3)	37(3)	38(3)	3(2)	13(2)	5(2)
C47	57(4)	78(6)	55(4)	21(4)	13(3)	24(4)
N1	24(2)	31(2)	32(2)	-0.4(17)	9.3(17)	11.1(17)
O1	69(3)	70(4)	61(3)	17(3)	37(2)	20(3)
O2	55(3)	38(3)	87(3)	-7(2)	34(3)	9(2)
O3	48(3)	64(3)	60(3)	-9(2)	14(2)	14(2)
P1	21.4(6)	30.2(7)	31.0(7)	1.1(5)	8.0(5)	8.3(5)
P2	22.2(6)	25.7(7)	31.3(7)	-0.1(5)	7.2(5)	7.4(5)
Cl1	29.4(8)	48.3(9)	59.5(10)	-1.6(7)	15.0(7)	13.6(7)
Tc1	24.7(2)	29.7(2)	36.2(2)	1.33(15)	10.55(15)	7.71(15)

Table M.3 Bond Lengths for *fac*-[^{99}Tc(Chzyl-4-*p*-tolyl)$(CO)_3$Cl].

Atom	**Atom**	**Length/Å**	**Atom**	**Atom**	**Length/Å**
C1	C2	1.509(8)	C24	C25	1.369(8)
C1	C6	1.519(7)	C24	C27	1.504(8)
C1	N1	1.488(6)	C25	C26	1.407(7)

C2	C3	1.527(9)	C31	C32	1.377(7)
C3	C4	1.533(11)	C31	C36	1.388(7)
C4	C5	1.471(10)	C31	P2	1.818(5)
C5	C6	1.525(9)	C32	C33	1.379(7)
C7	O1	1.119(7)	C33	C34	1.385(9)
C7	Tc1	1.958(6)	C34	C35	1.387(9)
C8	O2	1.115(7)	C34	C37	1.522(7)
C8	Tc1	1.953(6)	C35	C36	1.397(7)
C9	O3	1.084(7)	C41	C42	1.391(8)
C9	Tc1	1.937(6)	C41	C46	1.394(7)
C11	C12	1.386(7)	C41	P2	1.819(5)
C11	C16	1.389(7)	C42	C43	1.383(8)
C11	P1	1.815(5)	C43	C44	1.391(9)
C12	C13	1.379(7)	C44	C45	1.367(9)
C13	C14	1.373(8)	C44	C47	1.499(8)
C14	C15	1.377(8)	C45	C46	1.389(7)
C14	C17	1.520(7)	N1	P1	1.717(5)
C15	C16	1.389(7)	N1	P2	1.693(4)
C21	C22	1.390(7)	P1	P2	2.6873(19)
C21	C26	1.396(7)	P1	Tc1	2.4712(14)
C21	P1	1.813(5)	P2	Tc1	2.4525(14)
C22	C23	1.387(7)	Cl1	Tc1	2.5152(15)
C23	C24	1.387(8)			

Table M.4 Bond Angles for *fac*-[^{99}Tc(Chzyl-4-*p*-tolyl)$(CO)_3$Cl].

Atom	**Atom**	**Atom**	**Angle/°**	**Atom**	**Atom**	**Atom**	**Angle/°**
C2	C1	C6	113.6(5)	C42	C43	C44	120.3(6)
N1	C1	C2	113.2(5)	C43	C44	C47	120.3(6)
N1	C1	C6	113.9(4)	C45	C44	C43	118.4(6)
C1	C2	C3	110.8(6)	C45	C44	C47	121.3(6)
C2	C3	C4	109.9(6)	C44	C45	C46	122.1(5)
C5	C4	C3	110.7(7)	C45	C46	C41	119.7(5)
C4	C5	C6	112.5(6)	C1	N1	P1	129.1(4)
C1	C6	C5	112.3(5)	C1	N1	P2	126.0(4)
O1	C7	Tc1	179.1(6)	P2	N1	P1	104.0(2)
O2	C8	Tc1	178.2(6)	C11	P1	P2	127.00(17)
O3	C9	Tc1	175.4(5)	C11	P1	Tc1	126.27(16)
C12	C11	C16	117.5(5)	C21	P1	C11	104.4(2)
C12	C11	P1	118.9(4)	C21	P1	P2	122.65(17)
C16	C11	P1	123.6(4)	C21	P1	Tc1	113.62(16)
C13	C12	C11	120.4(5)	N1	P1	C11	108.3(2)
C14	C13	C12	122.5(5)	N1	P1	C21	108.6(2)
C13	C14	C15	117.3(5)	N1	P1	P2	37.70(14)
C13	C14	C17	121.1(5)	N1	P1	Tc1	94.23(15)

C15	C14	C17	121.6(5)	Tc1	P1	P2	56.59(4)
C14	C15	C16	121.2(5)	C31	P2	C41	103.0(2)
C15	C16	C11	121.1(5)	C31	P2	P1	124.29(17)
C22	C21	C26	118.2(5)	C31	P2	Tc1	113.66(16)
C22	C21	P1	121.0(4)	C41	P2	P1	126.36(17)
C26	C21	P1	120.4(4)	C41	P2	Tc1	127.17(17)
C23	C22	C21	121.1(5)	N1	P2	C31	109.8(2)
C22	C23	C24	121.1(5)	N1	P2	C41	106.6(2)
C23	C24	C27	120.7(6)	N1	P2	P1	38.32(15)
C25	C24	C23	118.0(5)	N1	P2	Tc1	95.52(16)
C25	C24	C27	121.3(6)	Tc1	P2	P1	57.26(4)
C24	C25	C26	122.1(5)	C7	Tc1	P1	99.60(17)
C21	C26	C25	119.4(5)	C7	Tc1	P2	165.72(17)
C32	C31	C36	119.3(5)	C7	Tc1	Cl1	85.96(18)
C32	C31	P2	125.4(4)	C8	Tc1	C7	93.8(3)
C36	C31	P2	115.3(4)	C8	Tc1	P1	165.84(17)
C31	C32	C33	120.9(5)	C8	Tc1	P2	100.29(18)
C32	C33	C34	120.8(5)	C8	Tc1	Cl1	85.43(17)
C33	C34	C35	118.5(5)	C9	Tc1	C7	89.3(2)
C33	C34	C37	121.2(6)	C9	Tc1	C8	87.0(2)
C35	C34	C37	120.3(6)	C9	Tc1	P1	88.73(16)
C34	C35	C36	120.8(6)	C9	Tc1	P2	89.41(17)
C31	C36	C35	119.7(5)	C9	Tc1	Cl1	170.73(16)
C42	C41	C46	118.1(5)	P1	Tc1	Cl1	99.89(5)
C42	C41	P2	122.9(4)	P2	Tc1	P1	66.16(4)
C46	C41	P2	118.9(4)	P2	Tc1	Cl1	97.17(5)
C43	C42	C41	121.3(5)				

Table M.5 Torsion Angles for *fac*-[^{99}Tc(Chzyl-4-*p*-tolyl)(CO)$_3$Cl].

A	**B**	**C**	**D**	**Angle**/°	**A**	**B**	**C**	**D**	**Angle**/°
C1	C2	C3	C4	56.5(10)	C27	C24	C25	C26	-179.5(6)
C1	N1	P1	C11	41.9(5)	C31	C32	C33	C34	-0.7(8)
C1	N1	P1	C21	-70.9(4)	C32	C31	C36	C35	-0.2(8)
C1	N1	P1	P2	169.4(5)	C32	C31	P2	C41	106.8(5)
C1	N1	P1	Tc1	172.4(4)	C32	C31	P2	N1	-6.4(5)
C1	N1	P2	C31	69.6(4)	C32	C31	P2	P1	-46.6(5)
C1	N1	P2	C41	-41.4(4)	C32	C31	P2	Tc1	-112.1(4)
C1	N1	P2	P1	-169.8(5)	C32	C33	C34	C35	2.0(8)
C1	N1	P2	Tc1	-172.8(4)	C32	C33	C34	C37	-176.7(5)
C2	C1	C6	C5	48.2(8)	C33	C34	C35	C36	-2.4(9)
C2	C1	N1	P1	56.9(6)	C34	C35	C36	C31	1.5(9)
C2	C1	N1	P2	-135.9(5)	C36	C31	C32	C33	-0.2(8)
C2	C3	C4	C5	-59.8(11)	C36	C31	P2	C41	-75.9(4)
C3	C4	C5	C6	56.9(11)	C36	C31	P2	N1	170.8(4)

C4	C5	C6	C1	-50.9(9)	C36	C31	P2	P1	130.6(4)
C6	C1	C2	C3	-51.7(8)	C36	C31	P2	Tc1	65.2(4)
C6	C1	N1	P1	-74.9(6)	C37	C34	C35	C36	176.3(6)
C6	C1	N1	P2	92.3(6)	C41	C42	C43	C44	-0.7(10)
C11	C12	C13	C14	0.1(9)	C42	C41	C46	C45	1.2(8)
C12	C11	C16	C15	2.2(8)	C42	C41	P2	C31	-12.2(5)
C12	C11	P1	C21	-154.4(4)	C42	C41	P2	N1	103.4(5)
C12	C11	P1	N1	90.0(5)	C42	C41	P2	P1	140.5(4)
C12	C11	P1	P2	52.6(5)	C42	C41	P2	Tc1	-146.0(4)
C12	C11	P1	Tc1	-19.8(5)	C42	C43	C44	C45	1.5(10)
C12	C13	C14	C15	0.7(9)	C42	C43	C44	C47	-178.3(6)
C12	C13	C14	C17	-178.6(6)	C43	C44	C45	C46	-1.0(9)
C13	C14	C15	C16	0.1(9)	C44	C45	C46	C41	-0.4(9)
C14	C15	C16	C11	-1.5(10)	C46	C41	C42	C43	-0.7(9)
C16	C11	C12	C13	-1.5(8)	C46	C41	P2	C31	168.0(4)
C16	C11	P1	C21	26.8(5)	C46	C41	P2	N1	-76.4(5)
C16	C11	P1	N1	-88.8(5)	C46	C41	P2	P1	-39.3(5)
C16	C11	P1	P2	-126.2(4)	C46	C41	P2	Tc1	34.2(5)
C16	C11	P1	Tc1	161.4(4)	C47	C44	C45	C46	178.8(6)
C17	C14	C15	C16	179.3(6)	N1	C1	C2	C3	176.4(6)
C21	C22	C23	C24	-1.4(9)	N1	C1	C6	C5	179.8(6)
C22	C21	C26	C25	-2.8(8)	P1	C11	C12	C13	179.6(4)
C22	C21	P1	C11	43.6(5)	P1	C11	C16	C15	-179.0(5)
C22	C21	P1	N1	159.0(4)	P1	C21	C22	C23	175.7(4)
C22	C21	P1	P2	-161.9(4)	P1	C21	C26	C25	-175.6(4)
C22	C21	P1	Tc1	-97.6(4)	P1	N1	P2	C31	-120.7(2)
C22	C23	C24	C25	-0.2(8)	P1	N1	P2	C41	128.4(2)
C22	C23	C24	C27	179.6(6)	P1	N1	P2	Tc1	-3.04(19)
C23	C24	C25	C26	0.3(9)	P2	C31	C32	C33	177.0(4)
C24	C25	C26	C21	1.2(8)	P2	C31	C36	C35	-177.7(5)
C26	C21	C22	C23	2.9(8)	P2	C41	C42	C43	179.5(5)
C26	C21	P1	C11	-143.7(4)	P2	C41	C46	C45	-179.0(4)
C26	C21	P1	N1	-28.3(5)	P2	N1	P1	C11	-127.5(2)
C26	C21	P1	P2	10.8(5)	P2	N1	P1	C21	119.7(2)
C26	C21	P1	Tc1	75.1(4)	P2	N1	P1	Tc1	3.01(19)

Table M.6 Hydrogen Atom Coordinates (Å×10^4) and Isotropic Displacement Parameters (Å^2×10^3) for *fac*-[^{99}Tc(Chzyl-4-*p*-tolyl)$(CO)_3$Cl].

Atom	***x***	***y***	***z***	**U(eq)**
H1	9183	8267	8127	42
H2A	7545	9266	6582	67
H2B	8860	10699	6951	67
H3A	7522	9517	8764	112
H3B	7259	10875	8116	112

H4A	9924	12088	9338	117
H4B	9161	11550	10360	117
H5A	10170	9671	10563	81
H5B	11528	11067	10913	81
H6A	11710	10688	8849	51
H6B	11724	9281	9470	51
H12	14060	10276	7139	45
H13	15933	12314	8342	51
H15	12735	14385	7579	60
H16	10819	12341	6401	50
H17A	15656	15687	8369	89
H17B	16822	14798	8987	89
H17C	15797	15121	9745	89
H22	10550	11591	3911	47
H23	8557	12201	2268	53
H25	5437	9084	2832	51
H26	7422	8442	4502	43
H27A	4494	10497	1210	105
H27B	5592	11015	444	105
H27C	5532	12065	1550	105
H32	7076	6753	6138	43
H33	4781	4968	5315	52
H35	7056	2254	4795	60
H36	9375	4064	5605	54
H37A	3585	2366	3380	102
H37B	3505	2310	4816	102
H37C	4347	1359	4330	102
H42	9598	5216	8483	52
H43	11001	4782	10615	63
H45	14880	7340	10556	50
H46	13496	7819	8434	45
H47A	15111	5918	12315	97
H47B	13658	4701	12209	97
H47C	13903	6234	12864	97